Development and Evaluation of Novel Hydrocarbon Stapled Peptidomimetics with Future Application to Bionic Proteins

David James Yeo

Submitted in accordance with the requirements for the degree of
Doctor of Philosophy

University of Leeds

School of Chemistry

June 2014

ii

Intellectual Property and Publication Statements

The candidate confirms that the work submitted is his own, except where work has formed part of jointly-authored publications has been included. The contribution of the candidate and the other authors to this work has been explicitly indicated below. The candidate confirms that appropriate credit has been given within the thesis where reference has been made to the work of others.

The work reported in Chapter 3a formed the basis of a research article published in September 2013: 'Monosubstituted alkenyl amino acids for peptide "stapling" David J. Yeo; Stuart L. Warriner and Andrew J. Wilson, Chemical Communications, 2013, 49, 9131-9133. The contributions of the authors were as follows: DJY (the candidate), SLW and AJW designed the research, DJY (the candidate) performed the research and drafted the manuscript, SLW and AJW edited the manuscript into its present form (see attached copy).

Acknowledgements

Firstly, I would like to thank my formidable panel of supervisors, Dr. Stuart Warriner, Prof. Sheena Radford and Prof. Andy Wilson who have ensured that my project has been an intellectual challenge but were malleable enough to recognise when the project needed to evolve. Moreover, for the advice and balanced guidance throughout my PhD that'll be retained during my career development. I also want to extend my gratitude to Dr. Julie Fisher, who was instrumental in helping me turn things around at the 21 month nadir. Also, Sri, who has feigned interest at the appropriate moments to keep me motivated.

This project has been a collaborative effort and would not have been anywhere near as successful without the help of several people from Chemistry and Astbury. The technical staff, Tanya Marinko-Covell (MS), Simon Barrett (NMR), Iain Manfield (ITC), Chris Empson (FAA) and particularly Martin Huscroft (HPLC) have been wonderfully tolerant of me over the last four years. A special thanks to Nasir Khan (CD) who gave me the first hope with the circular dichroism results of the BID peptide series and to Lynette Steele and Jane Levesley at LIMM for the cell work. Dr. Jen Miles, Dr. Alice Bartlett, Hannah Kyle and Dr. Thomas Edwards have also been helpful in either providing me with protein for testing and for teaching me how to express it myself, especially Jen and Ed, whose crystal trials have been of the upmost importance.

Right then. Sentiments. ~~You can all assume how much you've meant to me.~~ Job satisfaction is partly down to the description, but mostly down to the *environment*. The people who I've worked with, from supervisors to placement students have been a drive of my PhD when things have been at their worst. The Radford and Edwards groups have been supportive into my forays into biology and biophysics and have been wonderful people to interact with. The first six months of the PhD have been the most memorable, thanks to the people in 1.32 and the inorganic corridor. Similarly, the people in the Warriner/Turnbull/Webb groups who've cheerfully welcomed my presence in their labs, in addition to the Marsden group who helped clear the blue air during the upscaling attempts. To keep me away from descending into

chemistry madness, the footballers, volleyballers, squash players and grappler have been dear to me.

The Wilson Group. So many thanks to the group members who welcomed me when I first started and got me settled into my first forays into scientific research. Then, to the 2013/2014 Wilson group. I feel that I'm leaving the group at the wrong time. You are all wonderful, wonderful people who should never doubt their scientific abilities or personalities. The sweetness of the submission of this thesis will never be balanced by the bitterness of leaving you all. Jayapal for an unrepressed spirit; Irène for all of your craziness and massages; Sarah – thank you for the Staircase of Rant and calming me down; Jen for keeping me properly sane; George Burslem, who then undermined that proper sanity; Hannah for being a football and gin outlet; Kérya for the insults; Ludwig it's a crying shame that you didn't join the group earlier - I'll never forget Old Trafford; Silvia for teaching me that sometimes blunt is best; Kelly for teaching me that unreserved loveliness is best mixed with bluntness; Anna - the Lab Mum. Phil Winkworth, it seems appropriate that the first person I met in my PhD programme is at the end of the acknowledgments. Valeria. Nothing ever *ever* changes.

Finally, I want to acknowledge the support and (enthusiastically feigned in some cases) understanding of my families, the Parker family, the Scotland clan a arbennig o Yeo tylwyth; a Mam a Tad. Diolch yn fawr.

The last word, to my fiancée Charlotte, who has put up with being a Chemistry- and Thesis-widow for long enough. Our bright future together starts here.

This thesis is dedicated to the memory of my grandfathers, Neville Yeo and Peter Scotland - who inspired and nurtured my scientific interest from the very beginning. Their passing happened far too soon.

In five years, I hope to reopen this thesis and realise that whatever my next step was after the PhD was both my best decision and my worst mistake.

Abstract

Hydrocarbon stapling is a method of constraining a short polypeptide through the incorporation of alkenyl alanine unnatural amino acids,[1, 2] which are metathesised during peptide synthesis to afford a covalent crosslink on one face of the peptide. The purpose of 'stapling' is to improve the therapeutic properties of a peptide by improving transport properties and resistance to proteolysis.[2, 3] Stapling also reduces the conformational plasticity of a peptide, which in turn, should improve the potency of the crosslinked peptide with its binding partner.

Alkenyl glycine ('monosubstituted') derivatives of amino acids have been previously synthesised, but overlooked for peptide stapling experiments.[4] This project investigated the utility of monosubstituted amino acids as surrogates for hydrocarbon stapling with a therapeutically relevant family of proteins, the apoptosis regulator Bcl-2 family and p53 proteins.[5, 6] This led onto an investigation of the foundations of hydrocarbon stapling, to assess the extent that hydrocarbon stapling modulates potency through various biophysical and structural experiments.

Hydrocarbon stapled peptides are classified as peptidomimetics within the field of foldamers,[7, 8] which aims to construct scaffolds from synthetic oligomers which can replicate the three dimensional topography and functionality of native proteins.[7, 8] Since the *de novo* design of synthetic proteins is out of reach, regions of proteins with distinct architecture have been replaced with mimetics to afford semi-synthetic proteins in a technique described as 'protein prosthesis'.[9, 10]

The project also aimed to chemically synthesise a protein with four distinct helical regions, colicin immunity protein Im7,[11] with the view to replace one of the helical regions with a stapled peptide or an oligobenzamide helix mimetic[12] to afford a semi-synthetic protein to add to the growing field of secondary and tertiary structure mimetics.

Table of Contents

List of Tables

List of Schemes

List of Figures

List of Abbreviations

AA	Generic amino acid residue
Ac	Acyl
Aib	2-aminoisobutyric acid
BAD	Bcl-2 Associated Death promoter protein
BAK	Bcl-2 homologous Antagonist Killer protein
BAX	Bcl-2 Associated X-Protein
Bcl-2	B-Cell Lymphoma-2 anti-apoptotic protein
Bcl-x_L	B-Cell Lymphoma 'extra large' anti-apoptotic protein
BH	Bcl-2 Homologous region
BID	BH3-Interacting Domain death agonist
BIM	Bcl-2 Interacting Mediator of cell death
Bn	Benzyl
Boc	*tert*-butylcarbonate
BODIPY	Boron-dipyrromethene
BPB	(*S*)-2-[*N*-(*N*'-benzylprolyl)amino]-benzophenone
BSA	Bovine Serum Albumin
Bu	Butyl
CD	Circular Dichroism
COSY	Correlation Spectroscopy
d.r.	Diastereometric Ratio
Dbz	diaminobenzoic acid
DEPT	Distortionless Enhancement by Polarisation Transfer
DIPEA	Di*iso*propylethylamine (a.k.a. Hünig's Base)
Dha	Dehydroalanine

DMF   *N,N*-dimethylformamide

dmP   5,5-Dimethyl Proline

DMSO   Dimethylsulfoxide

DNA   Deoxyribonucleic Acid

DTT   Dithiothreitol

e.e.   Enantiomeric Excess

EC$_{50}$ Half maximal effective concentration

EDT   Ethane-1,2dithiol

ER-CoA   Oestrogen Receptor/Coactivator Complex

ESI   Electrospray Ionisation

Et   Ethyl

FITC   Fluorescein Isothiocyanate

Fmoc   9-Fluorenylmethoxycarbonyl

GB1   B1 domain of immunoglobulin G protein

Gn   Guanidinium

HATU   1-[Bis(dimethylamino)methylene]-1*H*-1,2,3-triazolo[4,5-*b*]pyridinium 3-oxid hexafluorophosphate

HBS   Hydrogen Bond Surrogate

HBTU   *O*-(Benzotriazol-1-yl)-*N,N,N′,N′*-tetramethyluronium hexafluorophosphate

HCTU   *O*-(1H-6-Chloro-benzotriazole-1-yl)-1,1,3,3-tetramethyluronium hexafluoro   phosphate

hdCM   heterodimeric chorismate mutase

*h*DM2   Human Double-Minute 2

hIL-8   Human Interleukin 8 protein

HIV   Human Immunodeficiency Virus

HMBC   Heteronuclear Multiple Bond Correlation

HMDS	Hexamethyldisilazane
HMQC	Heteronuclear Multiple Quantum Coherence
HOBt	1-Hydroxybenzotriazole
HPLC	High Pressure Liquid Chromatography
HRMS	High Resolution Mass Spectroscopy
IC_{50}	Half maximum inhibitory concentration
Im7	*E. Coli* Immunity cofactor 7
^{i}Pr	*iso*-propyl
IR	Infrared (spectroscopy)
ITC	Isothermal Titration Calorimetry
K_d	Dissociation Constant
K_i	Inhibition Constant
LCMS	Liquid Chromatography Mass Spectroscopy
m.p.	Melting Point
MBHA	4-Methylbenzhydrylamine Resin
*m*DM2	murine double-minute 2 protein
Me	Methyl
MPAA	4-Mercaptophenyl acetic acid
mRNA	'Messenger' Ribonucleic Acid
Ms	Mesylate
MSH	mesitylenesulfonyl-hydroxylamine
Nbz	*N*-acylbenzimidazolinone
NCL	Native Chemical Ligation
N.D.	Not Determined/Determinable
NMP	*N*-Methylpyrrolidinone
NMR	Nuclear Magnetic Resonance

NOESY	Nuclear Overhauser Effect Spectroscopy
NOP/NOR	Nociceptin opioid receptor
Noxa	Phorbol-12-myristate-13-acetate-induced protein 1 (*Noxa = damage, Latin*)
PDB	Protein Data Bank
Pbf	2,2,4,6,7-pentamethyldihydrobenzofurane
Pd/C	10% Palladium catalyst on Carbon support
PEG	Polyethyleneglycol
Ph	Phenyl
PPI	Protein-Protein Interaction
pTs	*para*-toluenylsulfonate
PyBOP®	(Benzotriazol-1-yloxy)tripyrrolidinophosphonium hexafluorophosphate
SPPS	Solid Phase Peptide Synthesis
R	Generic substituent
Ras/SOS	Rat Sarcoma/Son of Sevenless
RCM	Ring Closing Metathesis
RNase	Ribonuclease
RSV	respiratory syncitial virus
rt	Room Temperature
SPPS	Solid Phase Peptide Synthesis
$t_{1/2}$	Half-life (kinetics)
^{t}Bu	tertiary-Butyl
TCEP	*tris*-2-carboxyethylphosphine
TFA	Trifluoroacetic acid
TFE	Trifluoroethanol
TGR	Rink amide derivative of Novasyn® TG resin

TGT	4-carboxytrityl derivative of Novasyn® TG Resin
THF	Tetrahydrofuran
Thz	L-thiazolidine-4-carboxylic acid
TIPS	Tri*iso*propylsilane
TLC	Thin Layer Chromatography
T_m	Melting Temperature (thermal denaturation)
TMS	Tetramethylsilane
TOF	Time of Flight
Tol	Toluene
tRNA	'Transfer' Ribonucleic Acid
Ts	4-Toluenesulfonyl (synonym of pTs)
Trt	Trityl
UV	Ultraviolet
WT	Wild Type
XRD	X-Ray Diffraction

Amino Acid Abbreviations

A	Ala	Alanine
	Ahx	6-aminohexanoic acid
C	Cys	Cysteine
D	Asp	Aspartic Acid
E	Glu	Glutamic Acid
F	Phe	Phenylalanine
G	Gly	Glycine
H	His	Histidine
hC	hCys	homo-cysteine
I	Ile	Isoleucine
K	Lys	Lysine
L	Leu	Leucine
M	Met	Methionine
N	Asn	Asparagine
N_L	Nle	Norleucine
P	Pro	Proline
Q	Gln	Glutamine
R	Arg	Arginine
S	Ser	Serine
T	Thr	Threonine
V	Val	Valine
W	Trp	Tryptophan
Y	Tyr	Tyrosine

Chapter 1

Introduction

1.1 Protein Prosthesis: Replacing Sections of Native Proteins

1.1.1 Proteins - A definition

Proteins are diverse biological macromolecules that are comprised of a specific sequence of amino acids (*primary* structure), which fold into a three-dimensional structure (known as its native conformation) to govern many intra- and extracellular biological functions.[13] Sections of the polypeptide chain within a protein can adopt architectural features, known as secondary structures, which commonly are α-helices, β-strands, and turns;[14, 15] all of which are stabilised by intramolecular hydrogen bonding networks. The folded, functional protein, which is composed of *secondary* structure is referred to as its *tertiary* structure.[16] Finally, *quaternary* structure comprises multiple subunits of tertiary structure (which are not functional in isolation) that function as a complex. Conversely, with protein-protein interactions,[17, 18] tertiary protein subunits associate to form functional complexes that are more transient in nature.

1.1.2 Protein Synthesis - Biological Machinery

The unique sequences of proteins are genetically encoded within DNA, which commences polypeptide biosynthesis through a regulated pathway (Figure 1.1).[19]
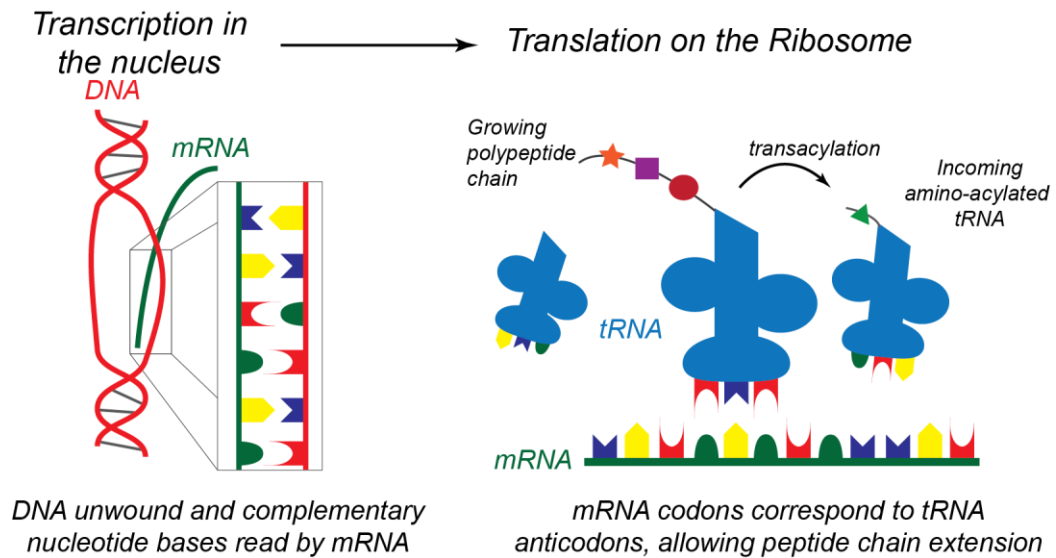
Figure 1.1 - Cartoon representation of the biosynthesis of a protein, demonstrating the key steps of transcription and translation before the full protein detaches from tRNA after a Stop codon is read by tRNA.

The first process, transcription, is the unfolding of the double-helical structure of DNA followed by the recognition of the canonical nuclear bases of DNA by a complementary strand of *'messenger'* RNA (mRNA), which passes into the cellular cytoplasm. During the second process, translation, mRNA is bound to a ribosome complex. Meanwhile, '*transfer'* RNA (tRNA) is specifically acylated with an amino acid. Within the ribosome, translation of mRNA begins at a specific 'start' codon - a unique combination of three ribosomal bases (AUG in eukaryotic cells). The trinucleotide codon is then recognised by a complementary anticodon on amino-acylated tRNA, which has the first amino acid covalently bound to it. The next codon on mRNA is then 'read' by the ribosome, matched with a complementary amino-acetylated tRNA macromolecule and the amino acids translocated to form a dipeptide. This chain elongation continues until a 'stop' codon is reached on the mRNA, whereby the polypeptide detaches from the final tRNA unit and either undergoes posttranslational modification and/or folding into its functional tertiary structure.

Typically, ribosomal protein expression is widely used in biology to synthesise native proteins using an 'overexpression' technique in different types of cells to afford large quantities of proteins for structural and biophysical studies.[20-22]

1.1.3 Modification of proteins - a mutagenesis approach

Site-directed mutagenesis[23] is widely used to mutate the DNA coding and therefore sequence of a protein of interest prior to its overexpression as outlined above (1.1.2). Mutagenesis systematically varies the protein sequence and the changes in the properties of the mutant protein - such as its activity, folding or recognition - are correlated with the changes in the amino acid sequence to identify 'key' residues.[24, 25] Whilst this protein engineering technique is useful for studying mutations between the 20 proteinogenic amino acids, it does not allow the *direct* incorporation of unnatural amino acids in a specific position.

To address this, Schultz and coworkers developed the 'Amber Suppression Method' which can allow the specific incorporation of unnatural amino acids into a polypeptide sequence (Figure 1.2a).[26] The Amber Suppression Method utilises site directed mutagenesis by altering the codon at the desired position to a nonsense 'Amber Stop' codon. This codon recognises a complementary tRNA macromolecule within the ribosome that is aminoacylated with an unnatural amino acid, for its addition into a protein using biological machinery. Indeed, the toolkit of amino acids incorporated (Figure 1.2b)[27] by these means have allowed the sequence specific installation of fluorophores,[28] click handles,[29, 30] biotin tags[31] and photocages.[32]
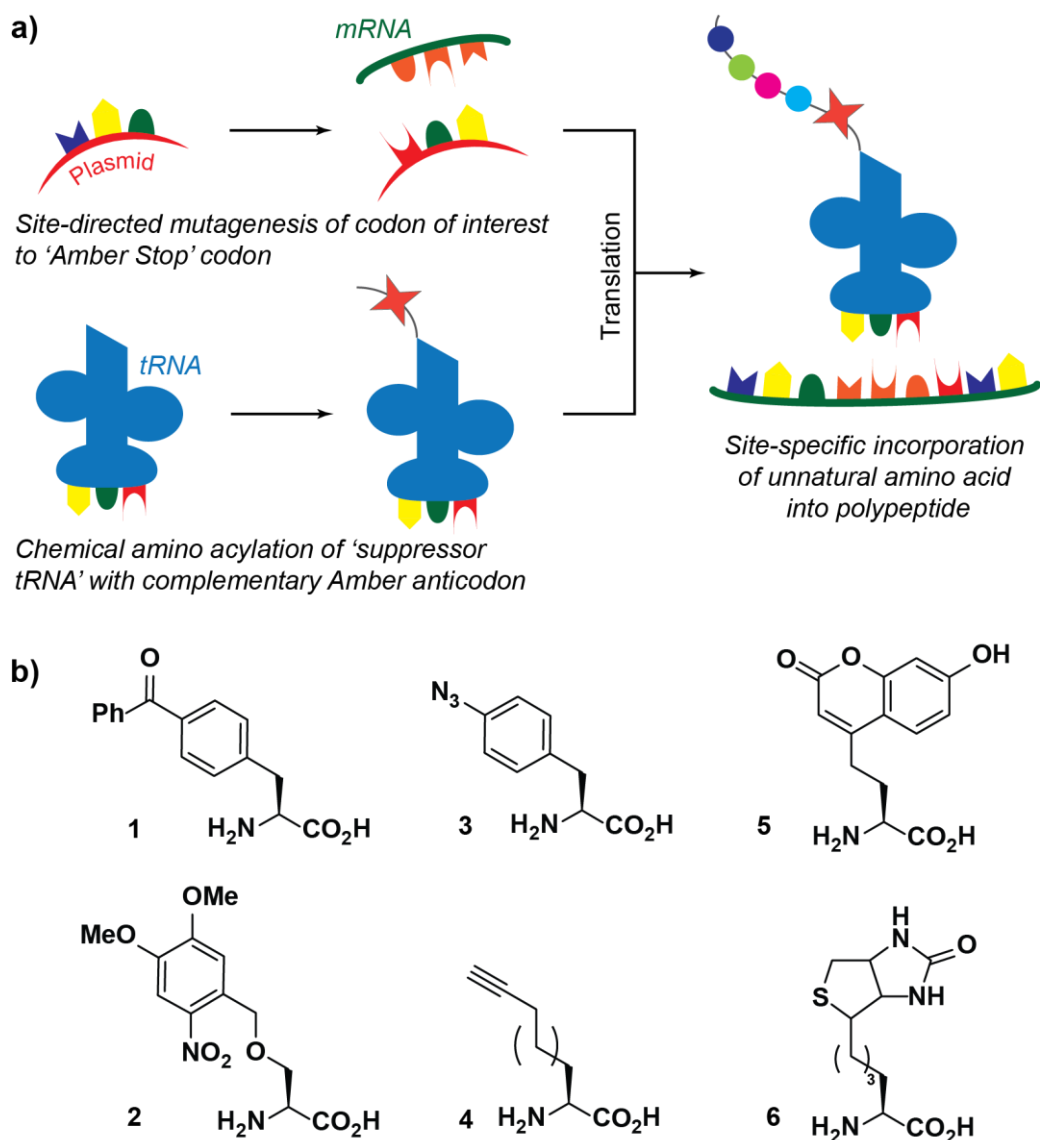
Figure 1.2 - a) Cartoon representation of the Amber Suppression Method, which combines site-directed mutagenesis and chemical tRNA amino acylation to selectively incorporate unnatural amino acids; b) examples of interesting amino acids with light activated functionalities **1**, **2**;[32, 33] click handles **3**, **4**;[30, 33] fluorophores **5**[33] and biotin tags **6**.[31]

Amber Suppression Methods have been recently expanded to allow installation of multiple unnatural amino acids by using other nonsense stop codons[34-36] and expansion of the genetic code to quadruplet recognition.[37] The culmination of the Amber Suppression Method has allowed the introduction of photocages and fluorophores into living cells[32, 38, 39] and finally *in vivo* by fluorescently labelling *Caenorhabditis elegans* nematode worms.[40]

However, there are limitations. Firstly, the fidelity of incorporation decreases as more unnatural residues are installed. Whilst this has been reported to be effective for five individual amino acids,[34] this represents an

outlier. In addition, there are limitations to the use of quadruplet codons to expand the genetic code, whereby ribosomes also require mutagenesis to recognise quadruplet stop codons.[37] Finally, suppression methods do not allow the placement of unnatural residues that are not α-amino acids, since the translocation site of the amino acids in the growing peptide chain are governed by the ribosome. Essentially, β-amino acids (where a methylene unit is added to the amino acid backbone) and other non α-amino acids are too sterically hindered to be effectively accommodated.

1.1.4 Modified Proteins Through Chemical Synthesis

1.1.4.1 Solid Phase Peptide Synthesis (SPPS) Methods

Mutagenesis-based modifications of proteins have become an elegant tool in protein engineering, but to overcome the limitations of the ribosome, synthetic chemistry is required to feasibly exchange any native amino acid, or sections of a protein with no limit to the number of mutations.

Solid Phase Peptide Synthesis, established by Merrifield,[41] allows peptide elongation on resin, where excess reagents are employed in couplings and are washed out after coupling is finished.
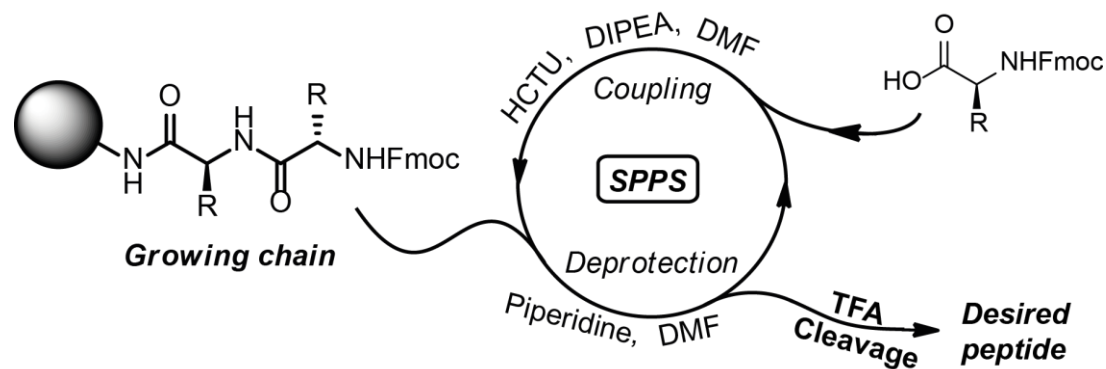
Figure 1.3 - Steps of solid phase peptide synthesis using the Fmoc protection strategy.

The common adaptation of SPPS is the use of Fmoc protecting strategies (Figure 1.3),[42] where amino acid side chains are orthogonally protected by acid-labile protecting groups and peptide elongation is performed under basic conditions. It is using these methods that the majority of unnatural amino acids are incorporated into a polypeptides, but the caveat of SPPS is that coupling efficiency decreases as the peptide chain length increases. Since proteins, with

only a few notable exceptions,[43] are generally accepted to compromise more than 50 residues, stepwise synthesis of a protein is considered inefficient. As a result, a convergent method for the total synthesis of proteins is required.

1.1.4.2 Native Chemical Ligation Approach to Protein Synthesis

Kent and coworkers devised an elegant route to the total chemical synthesis of proteins by their discovery of Native Chemical Ligation (NCL).[44] Essentially, two peptides, one functionalised with a *C*-terminal thioester and the other with an *N*-terminal cysteine can be chemoselectively coupled (Figure 1.4a). Under denaturing buffer with neutral pH, the thiol of cysteine attacks the *C*-terminal thioester prior to an acyl switch to furnish a native peptide bond.[45]

One apparent disadvantage of the NCL method is the requirement of a native cysteine to be present in the peptide sequence, but this can be circumvented by the conversion of Cys to Ala by reduction with Raney Nickel.[46] Elaboration of the NCL pathway to Auxiliary Mediated Ligation obviates the use of cysteine entirely on the *N*-terminus of a peptide (Figure 1.4b & c).

Similarly, methodologies have advanced to allow *C*-terminally activated peptides to be constructed and cleaved on modified resins, which alleviates the requirement for a solution phase chemoselective activation of a *C*-terminal carboxylic acid.[47]
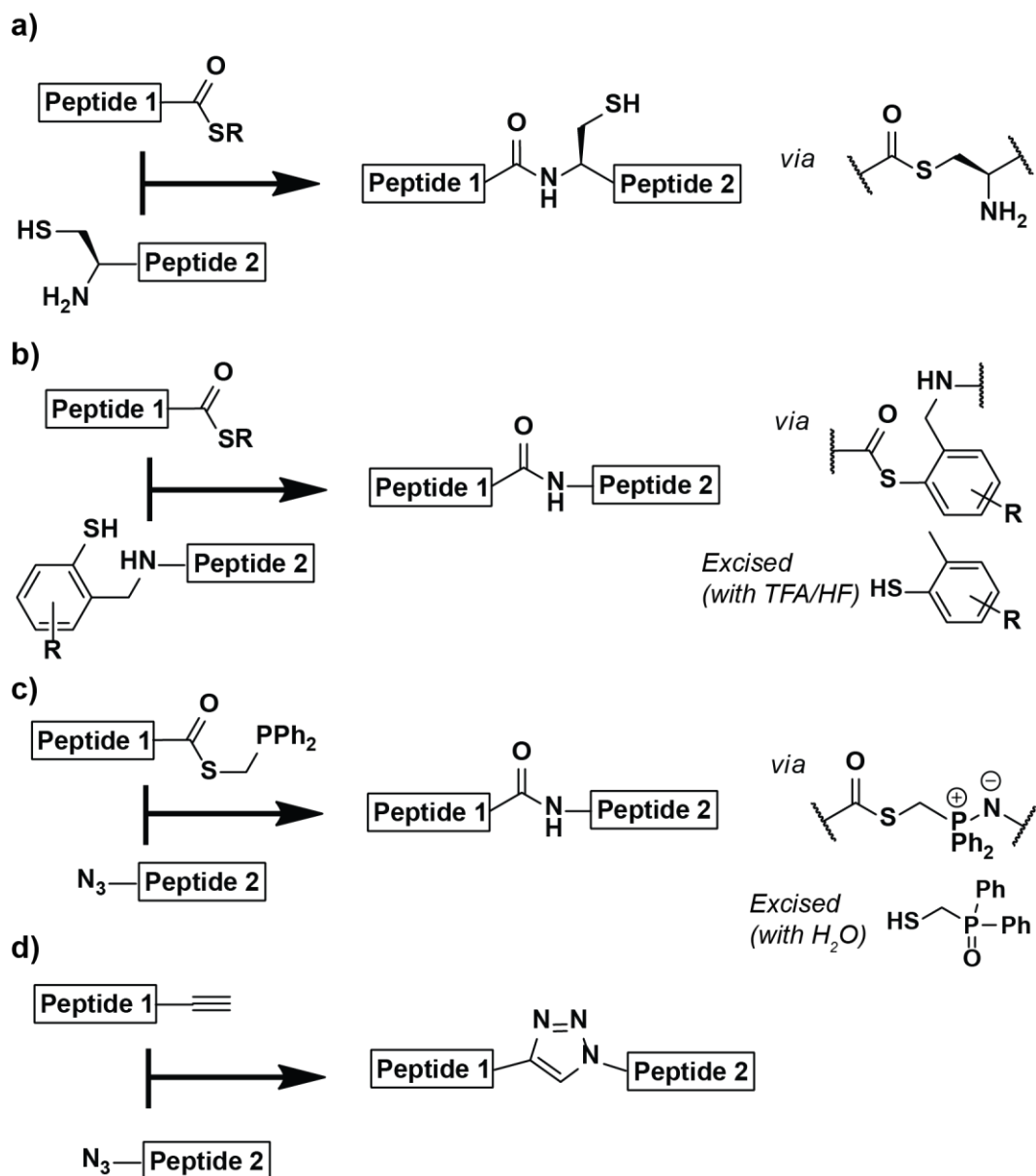
Figure 1.4 - Examples ligation methods after their synthesis. a) is the classic thioester/cysteine native chemical ligation;[45] b) utilises an auxiliary to afford a native peptide bond without cysteine, similar to c) which is the traceless Staudinger reaction;[48-50] d) is the installation of a trizole moitey into a polypeptide from appropriately functionalised fragments.[51]

With NCL being an efficient and convergent pathway, peptides are generally built in sections of less than 30 residues before being ligated together. It is even possible to have a one-pot ligation strategy of more than two fragments by the use of a protected cysteine residue (Figure 1.5 *Ligation 2*),[45, 52] which can be deprotected after the first ligation has completed.
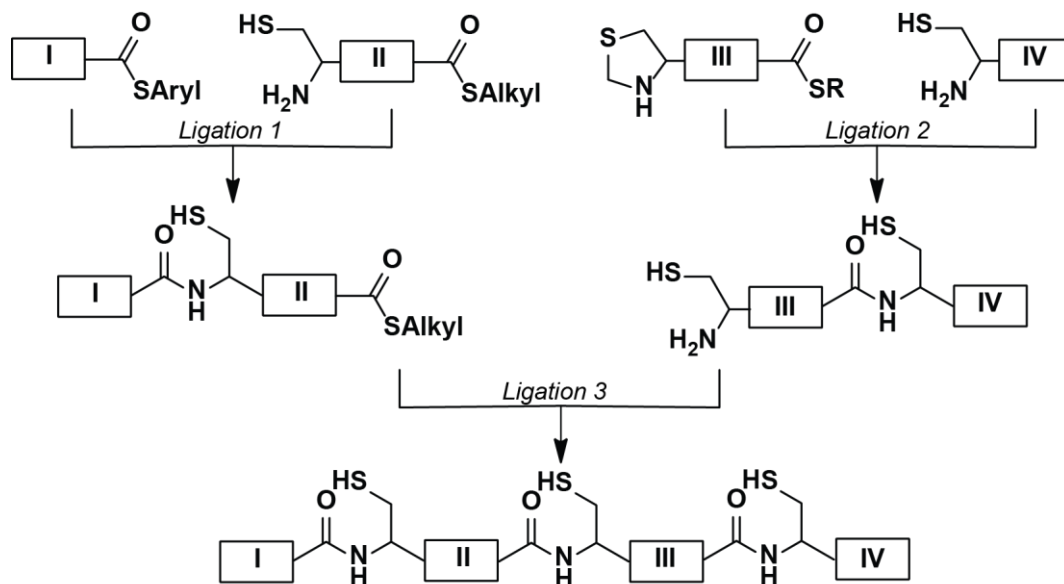
Figure 1.5 - Simplified version of the total chemical synthesis of Sortase A which required several elegant chemoselective steps.[53] Ligation 1 demonstrates the kinetic ligation product of a mixture of aryl and alkyl thioesters. Ligation 2 shows the use of a masked cysteine residue, thiazolidine (Thz), which is deprotected before Ligation 3. Desulfurisation followed ligation 3 to convert all non-endogenous cysteine residues to alanine.

The elegance of NCL has been proven in the total chemical synthesis of several proteins that maintain full enzymatic activity and are of a size that is out of reach by a single step-wise synthesis on solid phase. Of particular interest are proteins that have required four peptide fragments and a succession of native chemical ligations and protection strategies, such as in the total synthesis of HIV-1 protease (203 residues)[54] and Sortase A (148 residues, Figure 1.5).[53] NCL has also been combined with microbial expression, where polypeptide thioesters are expressed and ligated with a chemically synthesised peptide and is termed 'Expressed Protein Ligation'.[55-57] This particular methodology is related to the biochemistry of inteins,[58] which are segments of proteins that undergo self-excision after expression through a related mechanism to native chemical ligation.[59] Over the past 20 years, the range of techniques that are available to chemically synthesise proteins have provoked

studies into the replacement of secondary structure inducing residues or entire sections of proteins.

1.1.5 'Posttranslational' Chemical Modification of Proteins

Following translation on the ribosome, some amino acid residues can be further altered to expand the functionality of the protein.[60] The possible modifications range from oxidation of cysteine residues to disulfides,[61] to the introduction of larger molecules such as carbohydrates and lipids.[62-64] Whilst biological machinery has evolved to efficiently and selectively modify polypeptide residues, replicating this chemically is a challenge.

In addition to using Amber Suppression or total synthesis methods to install modified amino acids, Davis and coworkers have described a 'tag-modify' approach where glycosylation can be chemoselectively introduced into proteins and polypeptides through the appropriate combination of reagents.[65]
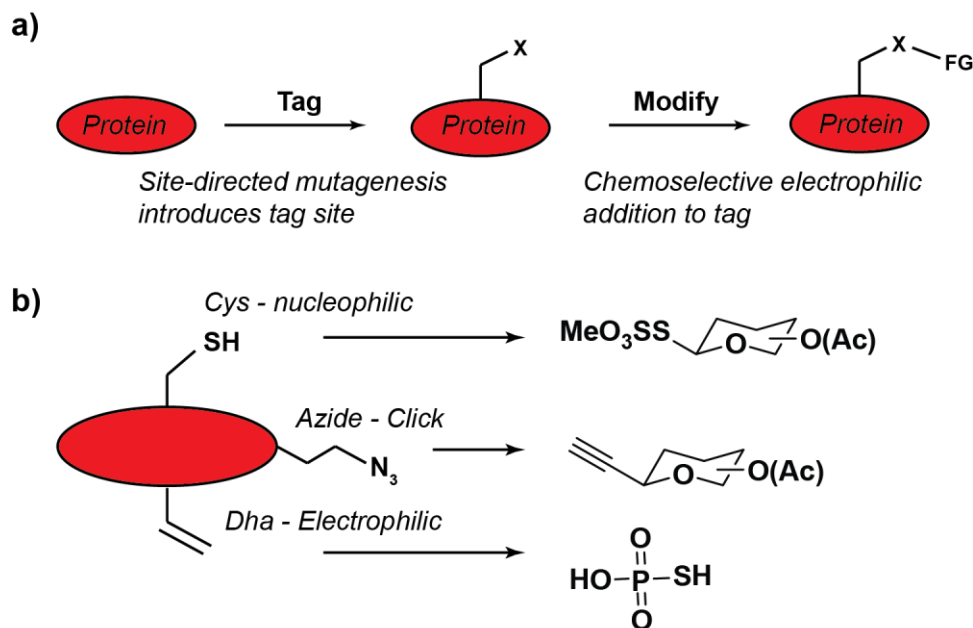
Figure 1.6 - a) Cartoon of the 'tag-modify' approach to the modification of proteins and b) the 'bio-orthogonal' groups[66] that are used in the tag-modify system, with examples of their targets for glycosylation and phosphorylation.

An elegant improvement to the tag-modify system utilises two mutations to install a nucleophilic Cys residue and an azide tag, has been used to chemoselectively add two modifications through nucleophilic attack and

click cycloadditions respectively,[67] which has proven effective for the addition of oligosaccharides and photo-inducible moities.[68]

The final pertinent 'tag-modify' strategy is the chemical conversion of Cys using mesitylenesulfonyl-hydroxylamine (MSH) to dehydroalanine (Dha),[69] which is an electrophilic tag. Dha allows access to phosphorylation and glycosylation by nucelophilic moieties.[69, 70]

Whilst the 'post-translational modification' approach does not lead to the significant alteration of the polypeptide backbone (*vide infra, 1.1.6*), it is nonetheless an essential technique in the biochemist's toolkit for introducing modified residues that cannot be easily installed through orthogonal tRNA or in cases where total protein synthesis is inefficient.

1.1.6 Protein Prosthesis: Combining chemical protein synthesis and unnatural residues

'Protein prosthesis' is the replacement of components of the covalent structure of a protein with a suitable mimetic to afford a semi-synthetic analogue.[9] Typically, the synthetic components are introduced through solid phase synthesis methods (1.1.4) and are designed to recapitulate native secondary structure without perturbing the tertiary structure and function of the protein (Figure 1.7).

Protein Prosthesis 'Top-Down'

Inspired by protein architecture → Develop structure mimetics → Create chimeric proteins

Foldamer 'Bottom-Up'

Inspired by protein architecture → Develop structure mimetics → Create synthetic proteins
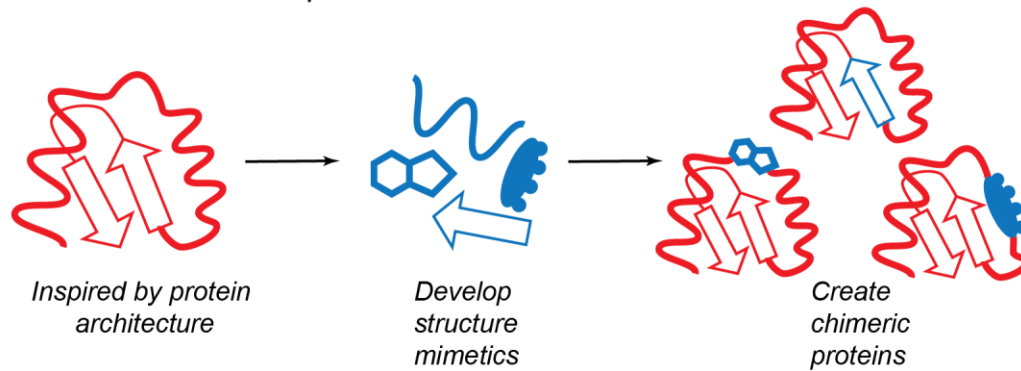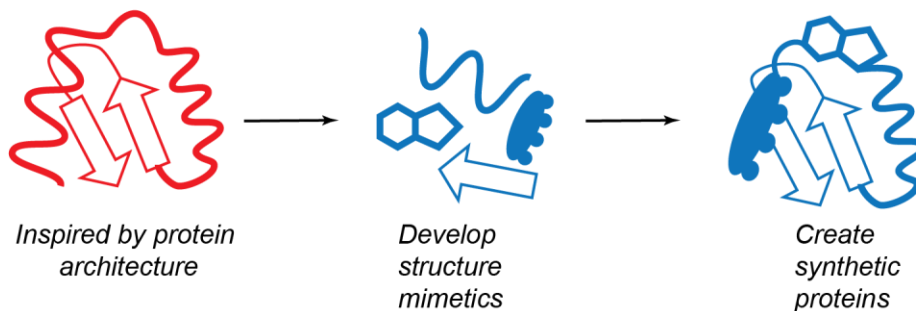
Figure 1.7 - Representation of the two different approaches to the creation of designed proteins with synthetic mimetics.

Protein prosthesis is tangential to the 'foldamer' field of research. Foldamers are unnatural oligomers that are designed to mimic protein structure,[71, 72] with the long term goal of synthesising fully functional, synthetic protein-like scaffolds.[7] Foldamer science is generally observed as designing synthetic scaffolds using a 'bottom-up' approach (Figure 1.7), this is the opposite to protein prosthesis, which replaces secondary protein structure with a mimetic (known as a top-down approach).

A popular choice of protein secondary structure to replace is the β-turn, since β-turns may be induced by amino acids that favour the *cis* conformation, such as proline. Indeed, the introduction of a 5,5-dimethyl proline (dmP) **7** derivative (which exists purely in the *cis* isomer) into [113]NP turn section of RNase A resulted in no loss of catalytic activity and an increase in the conformational stability of the semi-synthetic RNase A (Figure 1.8 a & c).[73]
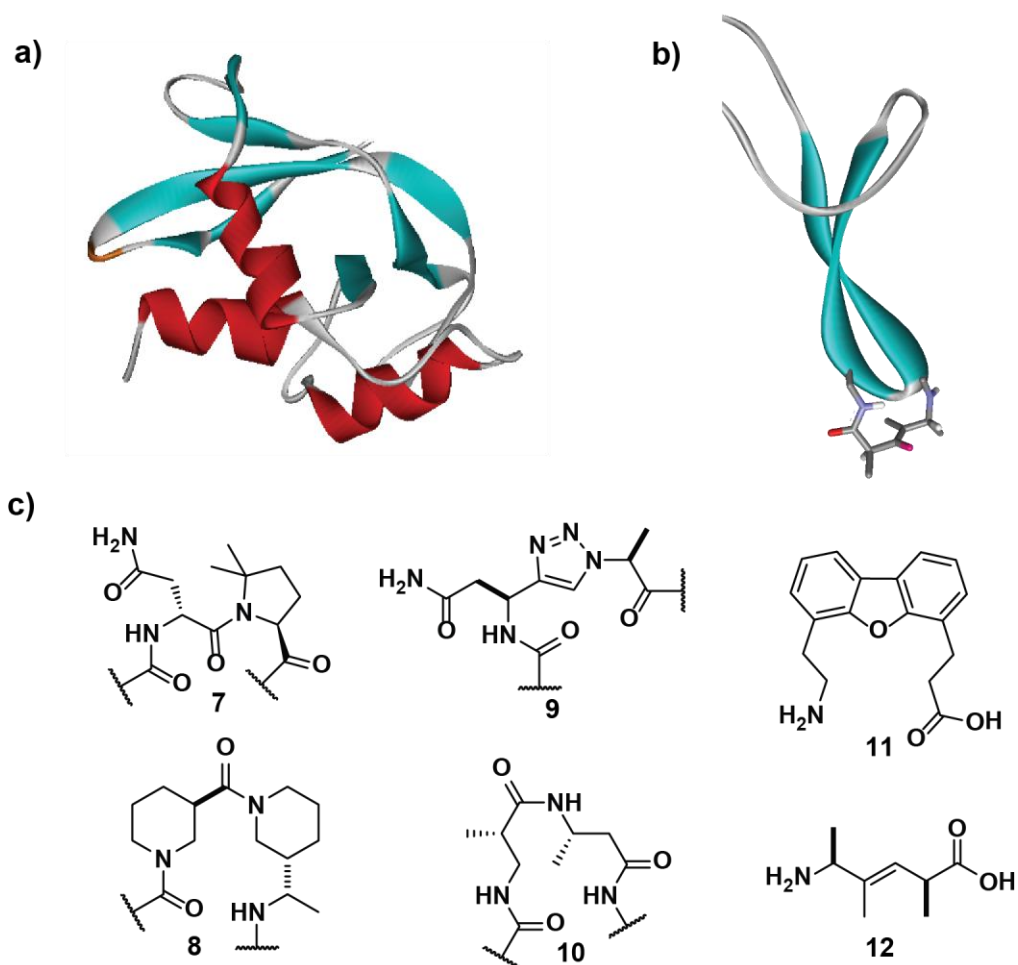
Figure 1.8 - Structures of a) RNase A with the turn and loop regions replaced by β-turn mimetics highlighted in orange (PDB:3I7W); b) the Pin1 WW domain with a β-turn mimetic installed (PDB:2KBU)[74] c) β-turn mimetics incorporated into RNase A **7 - 10** and Pin-1 rotamase **11 & 12.**

The leading research groups in the field of 'protein prosthesis', Kelly and Raines, have identified several candidates for β-turn mimetics based on their intrinsic conformations (Figure 1.8 **7-12**).[9, 73-76] These scaffolds, in turn, have been incorporated into loop regions of Pin-1 rotamase[76] and RNase A,[9, 73] without hindering protein activity. Building from dmP **7**, Raines and coworkers succeeded in the covalent linkage of two polypeptides with 'click' handles to afford a triazole proline mimetic **9** within the RNase A sequence,[77] with no loss in activity compared to the wild type RNaseA. Click ligations have also been demonstrated in the total chemical synthesis of Cystatin A,[51] where the triazole containing semi-synthetic protein did not have a weaker activity compared to the unmodified protein (Figure 1.4d).
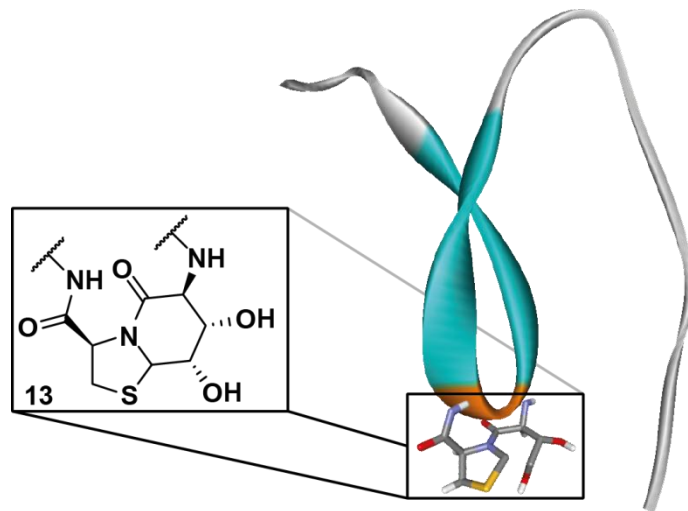
Figure 1.9 – Bicyclic β-turn mimetic Hot=Tap **13** incorporated into the turn region of fibritin foldon (PDB: 2KBL and 2WWL).[78, 79]

A contrast to the previous β-turn mimetics incorporated into proteins came from the laboratory of Geyer.[79] Using a bicyclic 'Hot=Tap' motif **13** promoted the formation of β-turns within a 29 residue miniprotein domain of T4 phage fibritin (Figure 1.9). However, the Hot=Tap molecule includes a pair of hydroxyl groups that are purposefully designed to interact with the tertiary environment of the protein, in contrast to previously examined β-turn mimetics which are designed to avoid disturbing the proximal environment.
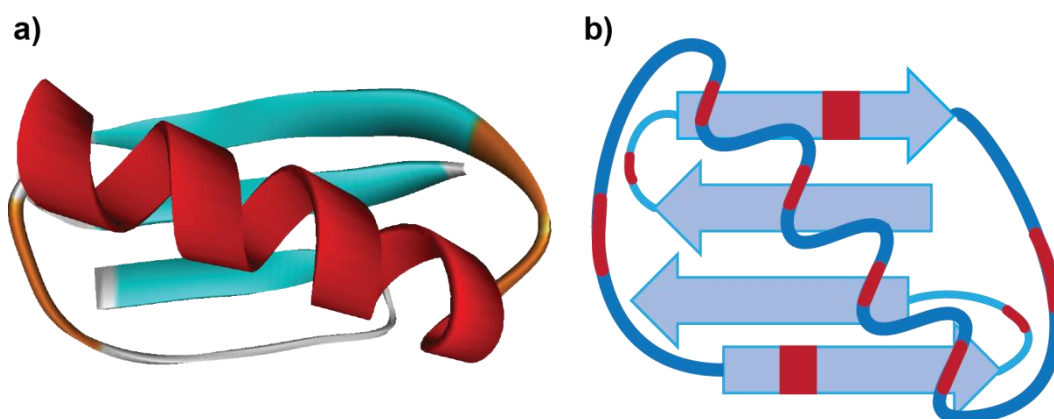
Figure 1.10 - a) Illustration of the loop sections of GB1 replaced by polyethylene glycol chains, highlighted in orange, (PDB: 2QMT)[80] and b) cartoon of the installation of unnatural amino acids (red) in regions of secondary structure.

The overlap between protein prosthesis and foldamer research was made evident by the research of Horne and coworkers.[81, 82] Rather than attempting to rigidify turn regions with a conformationally locked unit, Horne and coworkers introduced a flexible polyethylene glycol (PEG) chain in the

place of three residues within a surface exposed loop section of the B1 domain of immunoglobulin G protein (GB1, 56 residues, Figure 1.10a).[81] Whilst the prosthetic protein maintained the same fully folded architecture and activity of the native protein, the PEG chain decreased the prosthetic protein's folded stability. In another attempt, the same group returned to GB1 to demonstrate the effect of replacing individual amino acids within secondary structure (Figure 1.10b),[82] culminating in a 56-mer protein composing of 20% unnatural residues whilst retaining the folded behaviour of the native protein. Whilst replacing 20% of the native backbone resulted in an unstable protein, it was a rare example of attempting to mimic native tertiary interactions, which has implications in future research into the design of fully functional synthetic tertiary scaffolds. However, the overzealous introduction of artificial building blocks can have a detrimental effect, as found with a prosthetic RNaseA that had its activity reduced to 1% of the wild type.[83] In this instance, native residues in an *N*-terminal helix of RNase A were replaced by peptoids - where the amino acid side chain branches from *N* rather than *C*α - which arrested catalytic activity when 3 out of 13 residues were switched.

An obvious candidate for replacing sections of α-amino acid sequences with unnatural oligomers are β-peptides, which are comprised of repeating units of β-amino acids (α-amino acids with an extra methylene unit within the backbone).[84]
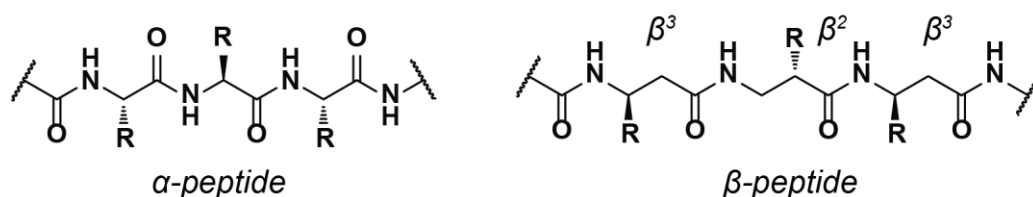
Figure 1.11 - Polypeptides compromised of α- and β- amino acids. β-Amino acids have additional nomenclature, where β³ amino acids have the side chain adjacent to the *N*-terminus and β² have the side chain adjacent to the *C*-terminus.

β-Peptides are of interest in the foldamer research field because of their increased flexibility and improved resistance to proteolytic degradation, in addition to being able to achieve some biomimetic functions.[8, 85] Tailoring an oligomeric chain with different repeating units of α and β amino acids can lead

to mimicry of α-peptide secondary structure, but with different folding and stability properties.[86, 87]

Raines and coworkers recently evaluated and compared the use of a β-dipeptide **10** in the turn region of RNase A (Figure 1.8b), which displayed no pertubation in the function of RNaseA akin to the other β-turn inducing residues that had been previously incorporated.[75]
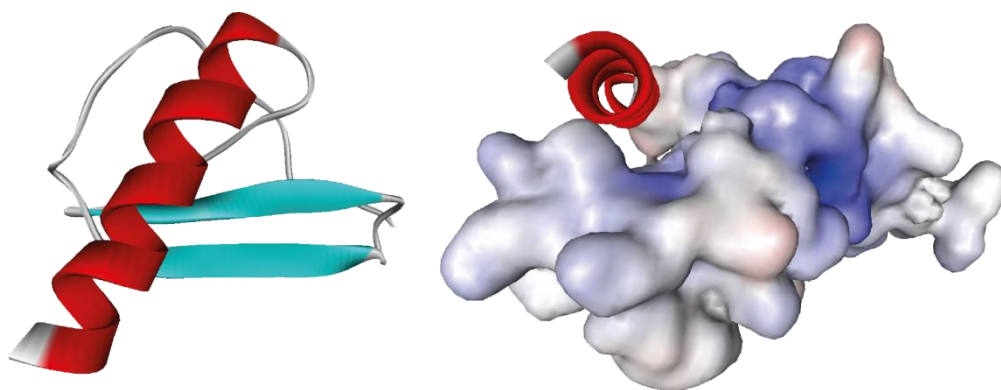
Figure 1.12 – Solution NMR structure of hIL-8, displaying its secondary structure and electrostatic surface. The parent red helix was replaced with a β-peptide, which reversed its handedness. (PDB: 1IL8).[88]

An ambitious introduction of secondary structure mimetics into a protein sequence came from Beck-Sickinger and coworkers.[89] Here, a *C*-terminal α-helix of human interleukin-8 (hIL-8) was replaced by a β-peptide oligomer (Figure 1.12). The extra methylene unit in the β-peptide backbone promoted a 14-helix[90] with opposite handedness to the native hIL-8 α-helix. In spite of this, the functionality of the semi-synthetic protein did not differ from the wild type, since the β-peptide oligomer projected key side chains in the same orientation as the native α-helix.
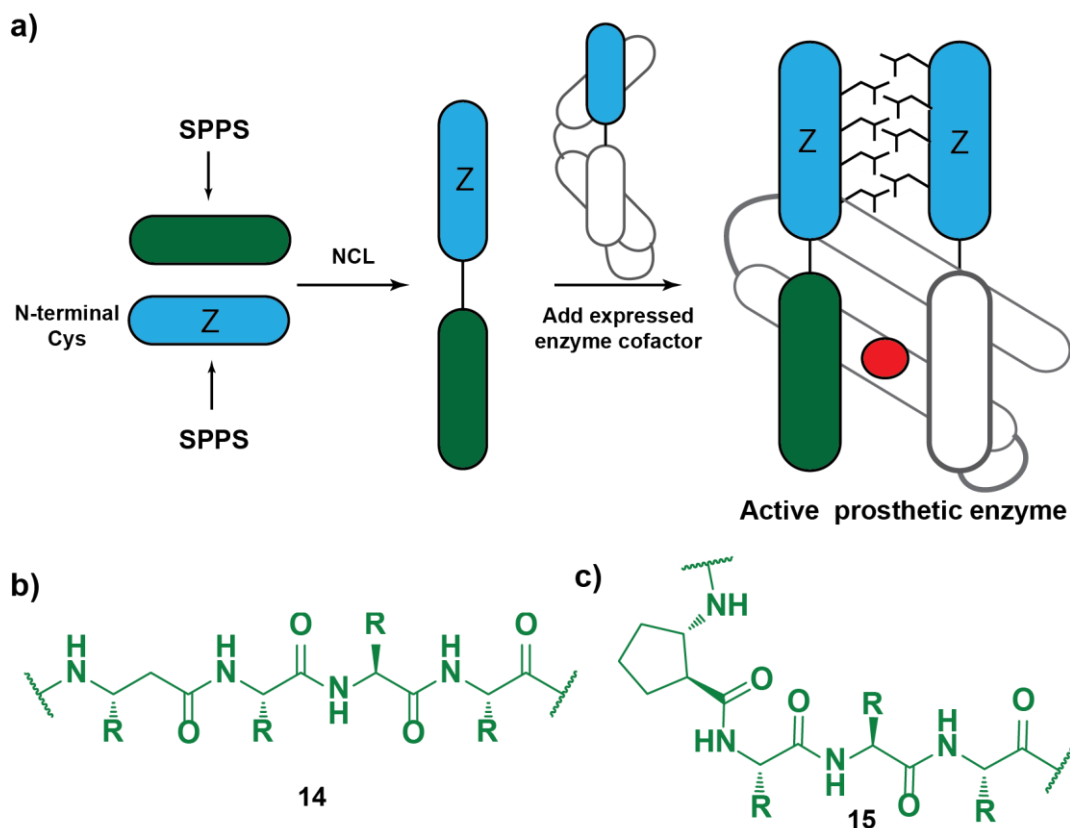
Figure 1.13 - a) Cartoon of the assembly of the hdCM heterodimer. The green helical N1 region was replaced by ααβ peptides b) and c). SPPS and native chemical ligation was performed to furnish the semi-synthetic N1-Z polypeptide, followed by introducing hdCM enzyme cofactor that was microbially expressed. The heterodimeric complex is spontaneously formed and stabilised through a leucine zipper (blue Z ovals), and the red active site arises from the juxtaposition of N1 and three other helices (white ovals).

Recently, Hilvert and coworkers succeeded in building fully functional prosthetic enzymes based on the heterodimeric chorismate mutase (hdCM).[91] Utilising α/β peptides with a repeating unit of ααβ **14**, which have been previously shown as effective α-helix mimetics, an *N*-terminal α-helix was replaced to afford seven prosthetic enzyme sections (Figure 1.13).

The prostheses then formed a heterodimer with another enzyme fragment to form an active site, which allowed the evaluation of the effect of introduction of a foldamer helix on tertiary stucture by observing the loss of enzymatic activity. Of the seven prosthetic enzymes, three demonstrated enzymatic activity close to the wild type, and variants using conformationally locked amino acids **15** abolished activity. This is particularly profound, as this is the first example of a designed foldamer replicating a tertiary environment.

The last 10 years have been fruitful in the development of prosthetic proteins to verify the capability of designed molecules and oligomers to mimic regions of proteins without detriment to activity. The fascinating result with hdCM particularly demonstrates the progress made towards the overall goal of the synthesis of fully functional tertiary structure mimetics.

Aside from the construction of a fully synthetic and functional protein, one the remaining challenges of protein prosthesis methodology is the replacement of α-helical or β-strand architecture that is not located at either terminus. Replacement of internal sections of a native protein could have a greater impact on the stability of a semi-synthetic protein and therefore alter its function. However, with the technology available for protein total synthesis and effective mimetic scaffolds having been identified, this challenge is not out of reach.

1.2   Towards Therapeutic Peptides: Constrained Peptides

The *de novo* design of secondary structure mimetics prior to replacing architecture of a native protein is a difficult challenge in both chemical synthesis and structural biology. However, it is possible to take inspiration from Protein-Protein Interactions (PPIs) that have regions of secondary structure at a binding interface. In mimicking the secondary structure with a synthetic scaffold, foldamer science can diversify into the production of molecules that are capable of recapitulating native protein architecture and inhibit a PPI. Secondary structure mimetics that have demonstrated inhibitory potency could therefore be reconsidered as potential prostheses for its parent protein.

PPIs are ubiquitous in biological systems and are responsible for a variety of signalling and regulation pathways.[85] Unlike an enzyme-substrate interaction, which has a well defined binding cavity (Figure 1.14),[92] PPIs generally form contact over large surface areas (>800 Å^2) which are often hydrophobic in character.[93]
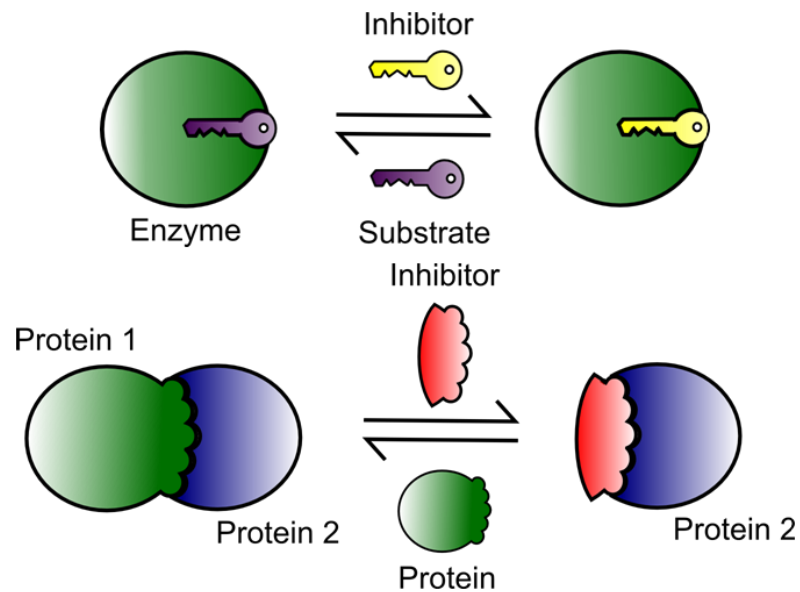
Figure 1.14 - Cartoons of two models in the design of inhibitors for enzyme/substrate (top) and protein-protein interactions (bottom).

Fortunately, a PPI usually involves only a few key residues (known as hot-spots) which contribute to the majority of the binding affinity.[94] Thus, to design inhibitors of PPIs, replication of the projection and proximity of the hot spot residues is critical. One starting point for the design of inhibitors of PPIs is that some have secondary structure on their binding interface, the secondary structure being vital to orienting key binding side chains to interact with a complementary region (Figure 1.15a, b). The full protein can therefore be theoretically reduced to a polypeptide that is involved in the binding interaction, without the hinderance of chain entropy.[93]

One particular class of PPIs that have gathered interest are those mediated by an α-helix at the binding interface, where side chains are projected at the *i*, *i + 4*, *i + 7* (and *i + 11*) positions in the same direction to interact with a complementary (often hydrophobic) groove.[95-97] Foldamer scientists have therefore produced oligomers and small molecules that are capable of recapitulating the spatial orientation of the key binding residues of an α-helix (Figure 1.15c),[95] for the successful inhibition of therapeutically relevant PPIs.
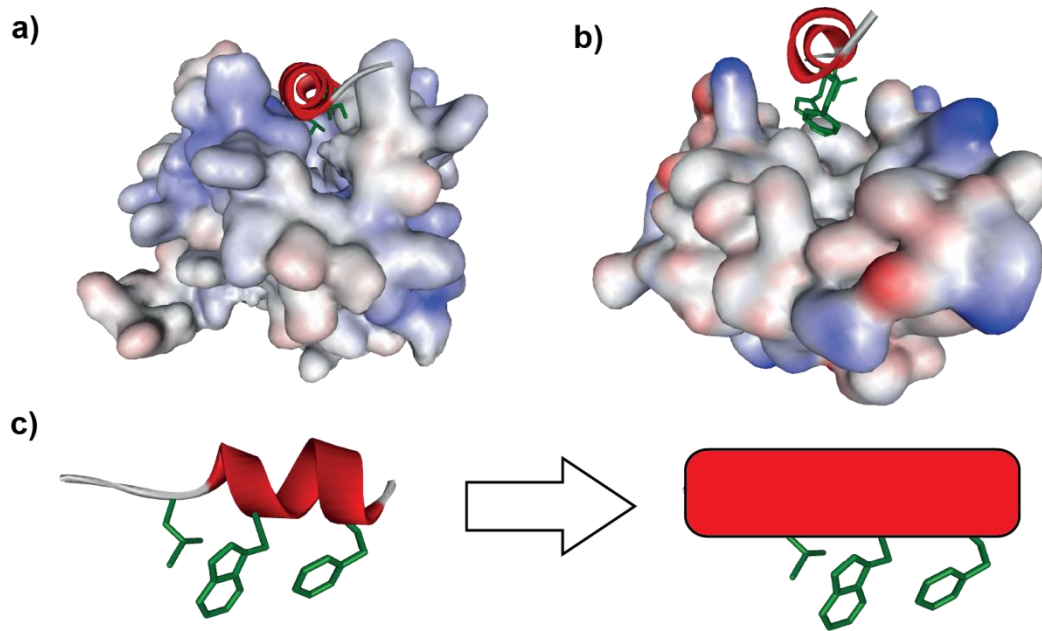
Figure 1.15 - a), b) Examples of protein-protein interactions that are driven by the recognition of an α-helix from one protein into a complementary binding pocket (PDB: a) 2KBW; BID bound to Mcl-1;[98] b) 1YCR; p53 bound to *m*DM2.[99] c) Considering that α-helix mediated PPIs are dependent on a few key side chains, a 'mimetic' strategy replaces the native polypeptide scaffold with one that maintains the orientation of the key side chains.

1.2.1 Constraining Peptides - Rationale

Since the interacting regions of α-helix mediated PPIs are based on a sequence of α-amino acids that are folded in an α-helical conformation, one starting point could be to utilise the peptide sequence in isolation to inhibit the PPI. Unfortunately, short, isolated peptides are therapeutically undesirable due to their lability towards proteases and their poor transport properties.[100, 101] However, small molecules cannot completely recapitulate all of the functions of an active helical peptide, so a compromise is needed to improve the therapeutic potential of peptides.

Small, isolated peptides are generally unstructured, since secondary structure requires the tertiary environment to remain stable.[102] Entropy therefore favours an infinite number of random conformations of a small molecule over a single, organised conformation. Thus, the introduction of synthetic residues to constrain a peptide into one conformation could reduce the entropic penalty of preorganisation prior to binding.[103] This, in turn, should improve the binding affinity of the *peptidomimetic* over an unmodified variant.

1.2.2 Native Peptide Constraints

Constraints can be introduced into a peptide without extensive modification to the native peptide sequence. The simplest constraint can be furnished through the oxidative bridging of cysteine residues (Figure 1.16a),[104] which had been effective for the inhibition of the oestrogen receptor α/co-activator interaction,[105] in spite of the peptide having minimal helical content in an aqueous environment.
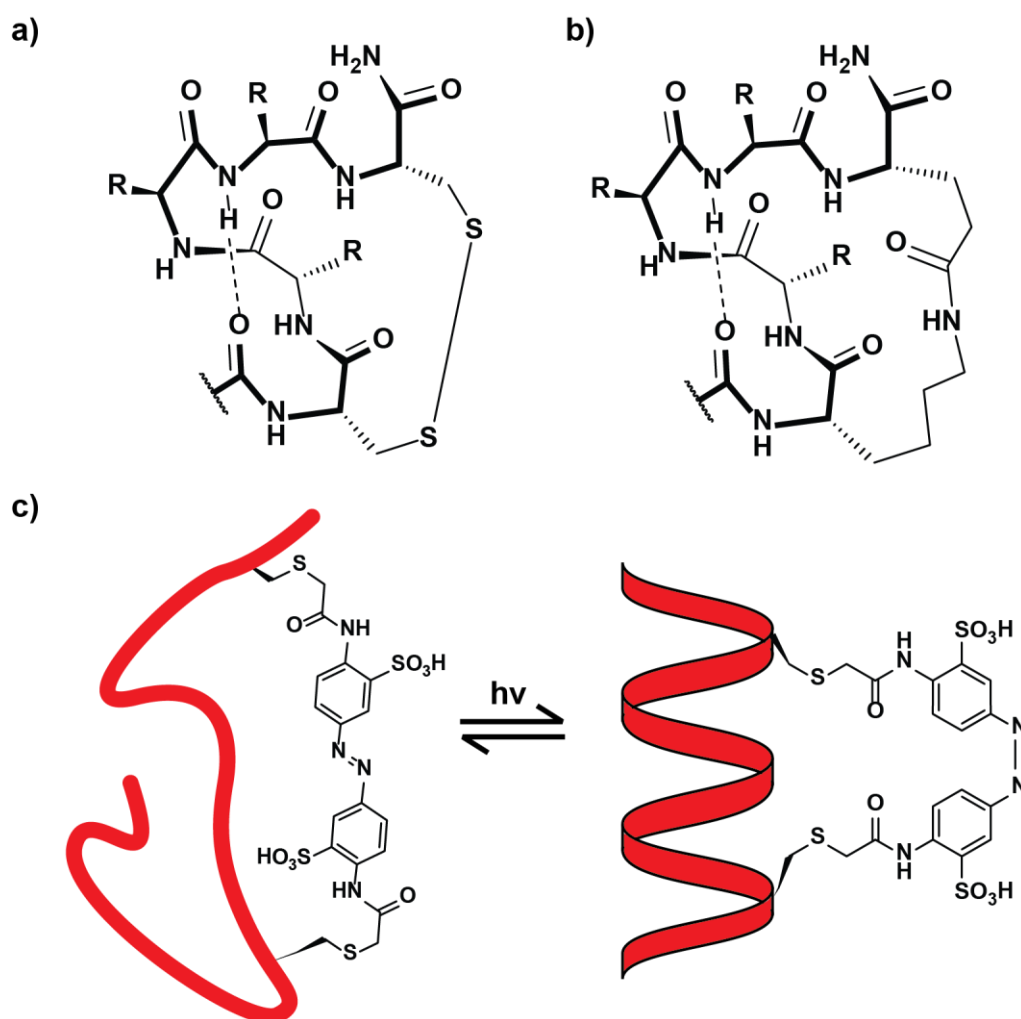
Figure 1.16 -Examples of 'native' constrained peptides: a) Cysteine bridged peptides; b) Lactam bridges formed by the bridging of Asp→Lys; c) Photoinduced constrained peptides using cysteine linked azobenzene moities.

A different measure for controlling the conformation of the peptide *via* cysteine residues was the installation of an azobenzene crosslink, which can undergo a *cis/trans* isomerisation upon irradiation (Figure 1.16c).[106, 107] The upshot was the ability to alter the conformation of a peptide from random coil to stabilised α-helix at will.[108] In addition to this, when incorporated into the *i*,

i + 7 positions, the *cis* isomer stablises a helical conformation, whereas the same isomer *destabilises* the peptide conformation when incorporated at the i, i + 11 position. *In vitro*, stabilised helical peptides (In this case, a BID peptide mimetic) bound to their partner (Bcl-x$_L$, an anti-apoptotic protein) with an improved affinity over their destabilised variants.[106]

A more permanent approach to constraining native residues was initially reported from Rosenblatt and coworkers, who stabilised peptides by forming a lactam bridge between lysine and aspartic acid in the i, i + 4 position (Figure 1.16b). Fairlie and coworkers have since expanded on this methodology by producing a pentapeptide with an [1]Lys→[5]Asp lactam bridge with exceptionally high α-helical content.[109] Using a double lactam bridged peptide maintained high α-helicity in the aqueous environment and furnished inhibitors that surpassed the native affinity for the picomolar inhibition of respiratory syncitial virus (RSV) fusion and picomolar activity of the NOP/NOR nociceptin opioid receptor.[110, 111] Recently, the same group have evaluated different methods for the constraining of pentapeptides, some of which shall be described below.[112]

1.2.3 Hydrogen-Bond Surrogates

Whilst the lactam bridges and the photo-induced constraints have been effective in affording potent inhibitors of protein-protein interactions, one disadvantage is that the constraint interferes with one face of the helix. Hydrogen bond surrogates (HBS) are therefore an attractive method to introduce a covalent constraint to a peptide without blocking any recognition features of the helix (Figure 1.17).[113-115] In addition to an improved α-helical character, HBS endowed a 60-fold proteolytic resistance to a BAK peptide, which bound to Bcl-x$_L$ in the low nanomolar range. HBS peptides have since been applied to p53/*h*DM2,[116] HIF-1α/p300[117] and an *in cellulo* inhibition of Ras/SOS by a cell permeable stabilised α-helix.[118]
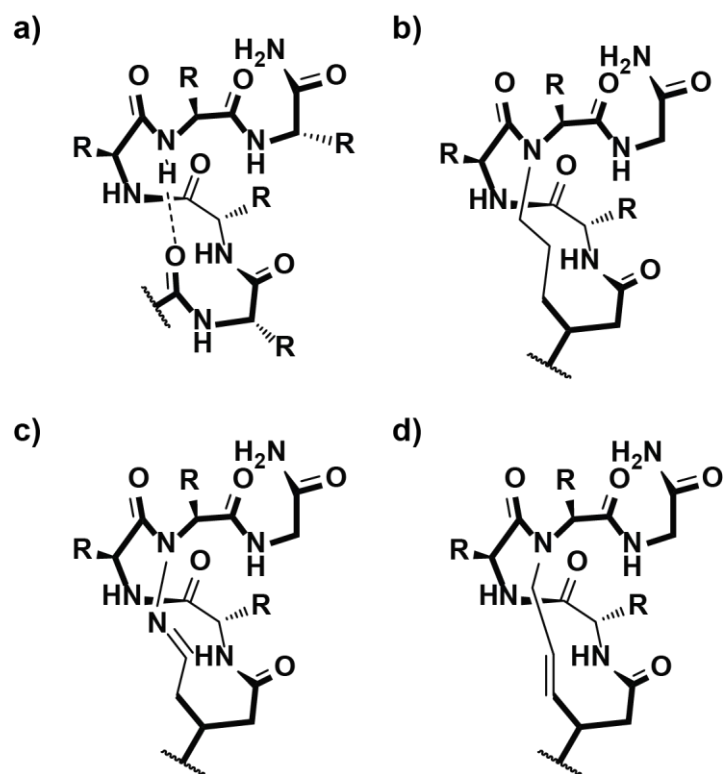
Figure 1.17 - a) Structural represenation of a native peptide α-helix which can be modified by hydrogen-bond surrogate methodologies developed by: b) Alewood;[113] c) Satterthwait[114] and d) Arora.[115]

1.2.4 Hydrocarbon Stapling

The 'hydrocarbon staple' was introduced initially by Grubbs by covalently linking O-allyl serine residues through Grubbs metathesis to afford a permanently linked, constrained peptide.[1] Verdine and coworkers improved on this by the synthesis of an α,α-disubstituted unnatural amino acid with an olefin tether (Figure 1.18).
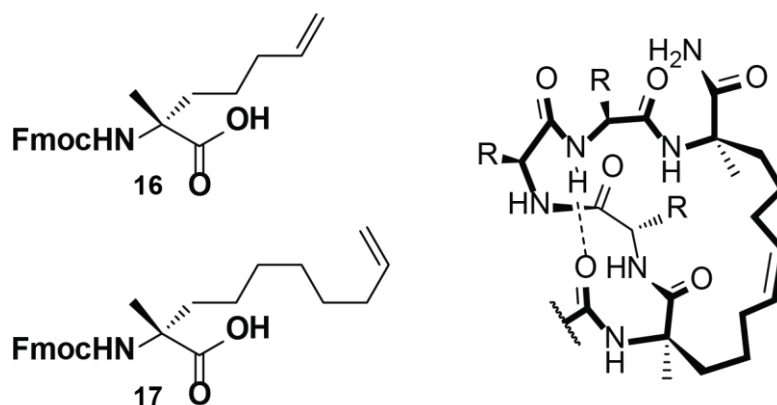
Figure 1.18 - Toolbox of α,α-disubstituted unnatural amino acids that are used for 'hydrocarbon stapling'. Varying the length of the olefin tether allows the crosslink to span between *i, i* + 4 or *i, i* + 7 positions in the peptide.

Using RNase A as a model system, the combination of amino acid stereochemistry and crosslink lengths was assessed to afford peptides with enhanced helical character and proteolytic resistance over the unmodified peptide.[2] The breakthrough in hydrocarbon stapling technology was the synthesis of ligands based on the BID BH3 pro-apoptotic domain, where a stapled BID peptide had demonstrated tumour suppression and regression in leukaemia xenografts.[3] In addition to this, 'stapled' BID BH3 showed 6-fold increase in binding affinity over an unmodified peptide. The Walensky group have since used hydrocarbon stapled peptides to understand the Bcl-2 (B-Cell lymphoma) family and to identify selective binding partners within this family of proteins.[119-122]

The application of hydrocarbon stapling technology has spread to numerous α-helix mediated protein-protein interactions, including the NOTCH pathway,[123] HIV-integrase pathways[124] and hepatitis C membrane fusion inhibitors.[125] Double-stapling of peptides by Walensky and coworkers demonstrated that long peptides can be maintained in a helical conformation, which in turn enhanced antiviral activity against neutralisation resistant HIV-1.[126] Pertinent research into the hydrocarbon stapling of p53 afforded peptides that were capable of activating the tumour suppressor p53 protein *in vivo*.[127] This led to the first reported crystal structure of a hydrocarbon stapled peptide, in this instance stapled p53 bound to *m*DM2 (Figure 1.19a).[128] Crystallographic trials with a stapled oestrogen receptor/coactivator interaction revealed that the hydrocarbon crosslink was responsible for

binding into the hydrophobic pocket and not the key binding side chains on the α-helix (Figure 1.19b,c).[129] This was an important result to prevent the over-interpretation of helicity-potency relationships with stapled peptides.
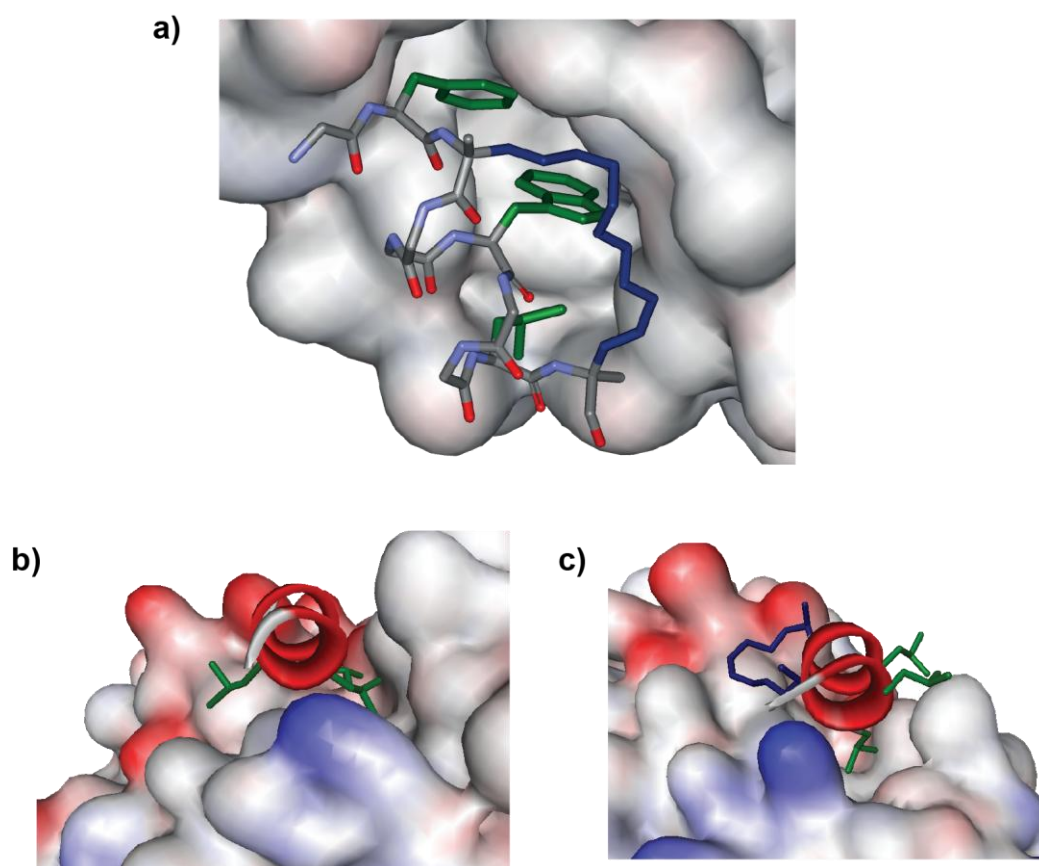
Figure 1.19 – X-Ray crystal structures of a) hydrocarbon stapled p53 bound to *m*DM2 (PDB:3V3B)[128]; b) Wild-type oestrogen receptor/coactivator interaction (PDB: 2QGT)[130] and c) hydrocarbon stapled oestrogen receptor/coactivator interaction (PDB: 2YJD).[129] The key binding side chains are coloured green, and the hydrocarbon staple coloured blue. In c) the staple binds onto the hydrophobic surface of the protein, causing two Leu side chains to move from their binding pocket.

Concerns have been raised through the research of Czabotar and coworkers,[131, 132] who have attempted the hydrocarbon stapling of a BIM peptide in the same sequence position as Walensky[122, 133] but found that there is marginal improvement of helical content and *no* improvement in activity or cellular uptake. The analysis of Czabotar and coworkers into why hydrocarbon stapling affords a less affine ligand rigorously states that interactions of other side chains within the peptidomimetic must not be ignored when designing effective hydrocarbon stapled peptides. Czabotar has therefore highlighted that the rationale behind stapled peptides being improved ligands as a direct consequence of improved α-helicity requires more detailed analysis.

In spite of this, hydrocarbon stapling methodology has been one of the most successful methods for inhibiting α-helix mediated PPIs, culminating in the founding of Aileron Therapeutics, who have entered stapled peptides into Phase I clinical trials.[134, 135]

1.2.5 From Peptidomimetics to Proteomimetics

Peptidomimetics are designed to recapitulate the secondary structure of a section of a protein with the goal of furnishing effective peptide-based therapeutics.[8] On the other hand, proteomimetics are designed to emulate the topography of residues that are essential for recognition and binding.[136] Since proteomimetics consist of synthetic, oligomeric scaffolds, they also belong to the foldamer family but generally deviate from α- and β-amino acid monomers that are utilised in peptidomimetic research.[72, 137]

α-helix proteomimetics are designed to target protein-protein interactions that are driven by key binding side chains residing in an α-helix segment.[95] Oligoamide based α-helix mimetics are currently a popular choice of scaffold,[97] which allows the synthesis of rigid oligomers that are capable of competitively inhibiting protein-protein interactions.
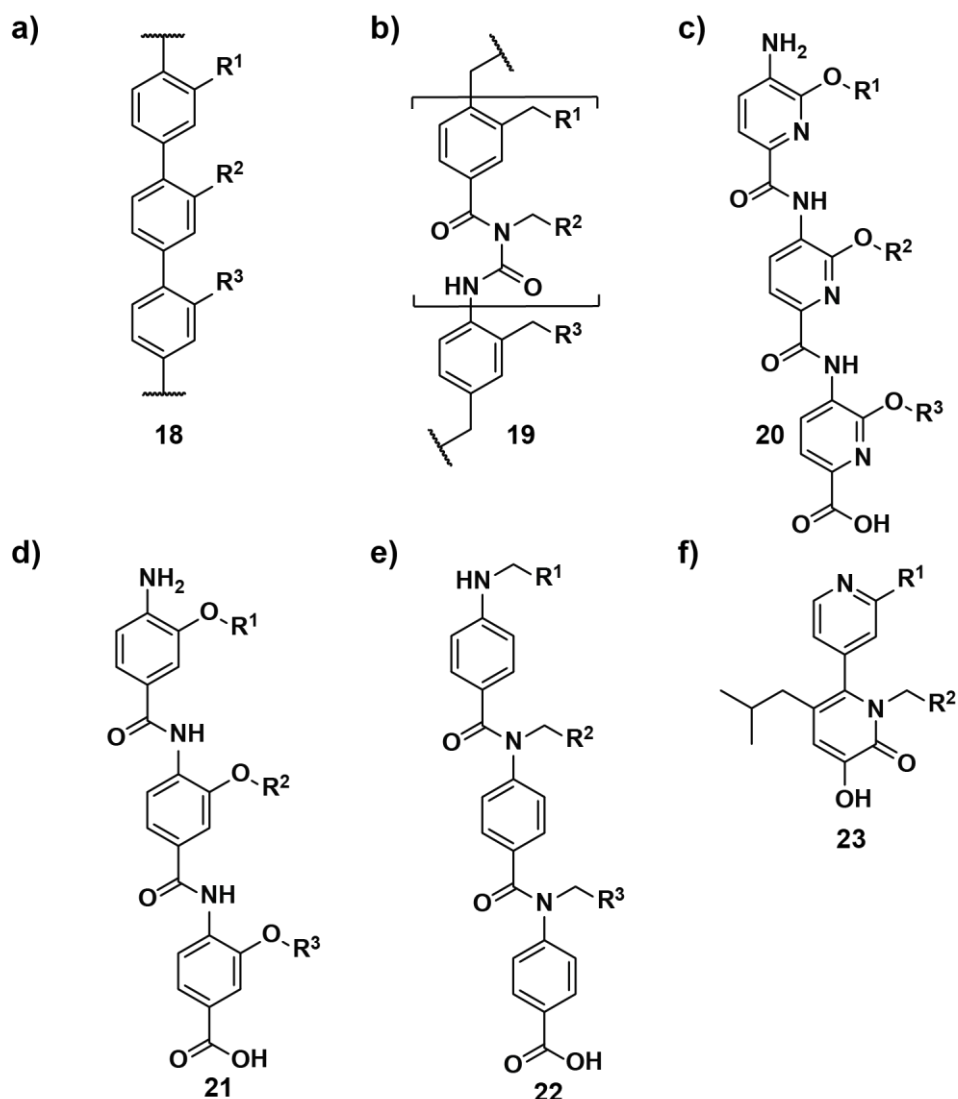
Figure 1.20 - Examples of α-helix proteomimetics from a) terphenyl scaffolds;[138] b) oligourea scaffolds[139, 140]; c) oligopyridylamide[139] and d), e) oligobenzamide scaffolds that are amenable to library generation[12, 141] and f) pyridyl-pyridone scaffold that is capable of mimicking two faces of an α-helix.[142]

From the first reported terphenyl α-helix mimetic **18**,[138] the range of oligoamide scaffolds has developed with variations to the backbone and installation of interacting side-chains **19-22**. Figure 1.20 shows that a rigid backbone, reinforced through restricted rotation, forces side chains to be projected into one face and recapitulate *i, i + 4* and *i + 7* spacings whilst **23** is suitable for mimicking protein-protein interactions that bind through *i, i+3* and *i + 4* recognition.[140] Whilst the above α-helix mimetics have been applied to the inhibition of pertinent protein-protein interactions, such as p53/*h*DM2,[12, 141] the Bcl-2 family[138, 139] and ER-CoA,[142] there is also potential for future

development into the production of semi-synthetic proteins using protein prosthesis methodology.

1.3 Project Aims

The Wilson laboratory has specialised in the design and synthesis of potent oligobenzamide α-helix mimetics capable of inhibiting protein-protein interactions that are relevant to the survival and proliferation of cancerous cells (Figure 1.20 d & e).[12, 141] Allied with the overall goal of producing tertiary structure mimetics, it was envisaged to incorporate hydrocarbon stapled peptides and eventually oligobenzamide α-helix mimetics into a protein, analogous to the research performed by Beck-Sickinger.[89]
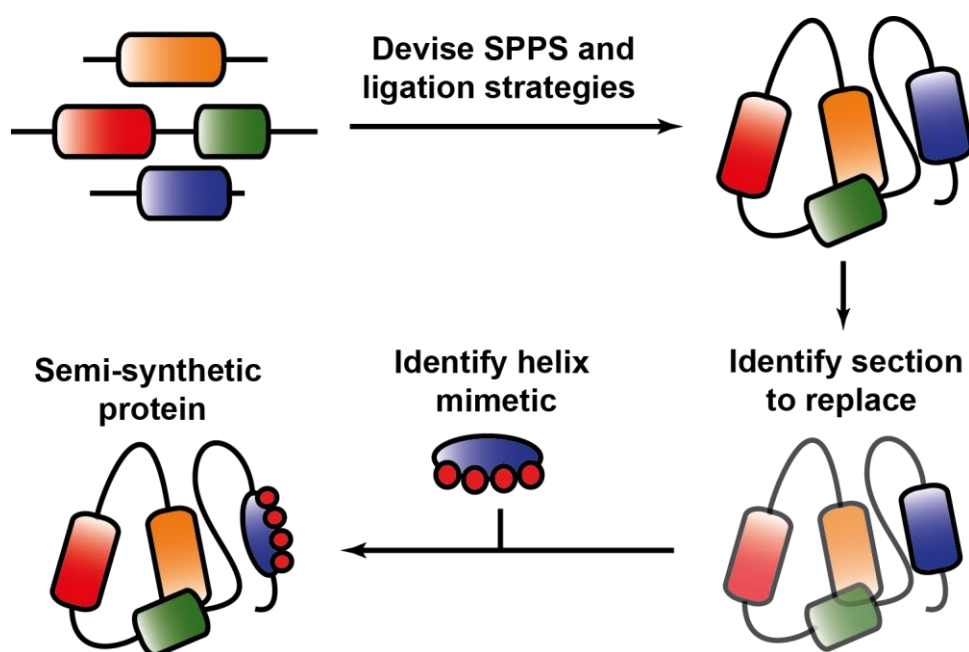
Figure 1.21 – Summary of the aim of the protein prosthesis investigation

The first goal of the project was to design a strategy for the total protein synthesis of a colicin immunity protein, Im7, through an appropriate native chemical ligation strategy (Figure 1.21). Im7 possesses four helical regions, which have the potential for the production of several chimeric Im7 variants. In addition to this, an investigation with stapled peptides was started to expand the Wilson group repertoire of secondary structure mimetics. With the synthesis of the unnatural amino acid for peptide stapling in hand, stapled helical regions of Im7 were to be investigated, before moving onto more dramatic alterations of Im7 with oligobenzamide helix mimetics.
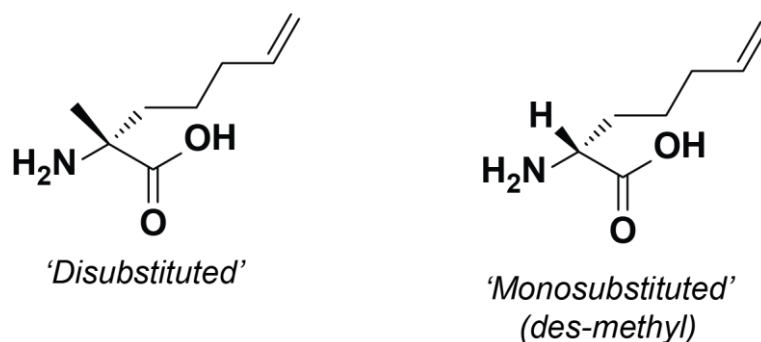
Figure 1.22 - Disubstituted and Monosubstituted unnatural amino acids that are applied to hydrocarbon stapling experiments.

Of particular interest to us was an olefinic amino acid that does not possess the α-methyl group that has been reported by Verdine and Walensky.[2, 3] This *des*-methyl amino acid had been overlooked for investigations with stapled peptides (Figure 1.22), but can be attained by modifying a synthetic approach that has been developed elsewhere in the Wilson group.[143] Thus, we were in a prime position to discover whether *des*-methyl amino acids are suitable surrogates for hydrocarbon stapling and if there is any biophysical contrast between the well characterised and used α,α-disubstituted unnatural amino acid and the overlooked monosubstituted unnatural amino acid.

Chapter 2

Towards the total chemical synthesis of colicin immunity protein Im7

The term 'foldamer' is used to describe a synthetic oligomeric scaffold that has a tendency to adopt specific compact conformations, which assemble through their replication of protein secondary structure.[7, 137] As the field has grown, various oligomers have been characterised to replicate the secondary structure of proteins and have been applied for potential therapeutic strategies.[95] However, foldamers resembling tertiary structure, which rely on folding patterns to provide an active site based on the three-dimensional arrangement of the oligomeric network are currently out of reach. The next milestone in foldamer research is therefore the production of tertiary structure mimetics to furnish fully functional synthetic scaffolds.

There are two possible approaches to the synthesis of effective tertiary structure mimetics. The first is analogous to the design of secondary structure mimetics, through *de novo* design. The second is to replace secondary structure of proteins using characterised secondary structure mimetics to afford semi-synthetic proteins, which would allow the evaluation of secondary structure foldamers within a tertiary protein environment, which is known as the prosthesis approach.[9, 76]

One of the aims of the project was the incorporation of stapled amino acids and oligobenzamide helix mimetics into a protein,[12, 141] replacing an α-helical region, and evaluating the folding properties and activity of the resultant semi-synthetic proteins. Prosthesis has been limited to the replacement of a small number of β-turn inducing residues,[73, 75, 79] with one example of a *C*-terminal α-helix replaced by a β-peptide oligomer.[89] Replacing *internal* protein segments with α-helix mimetics therefore presented a great synthetic challenge.
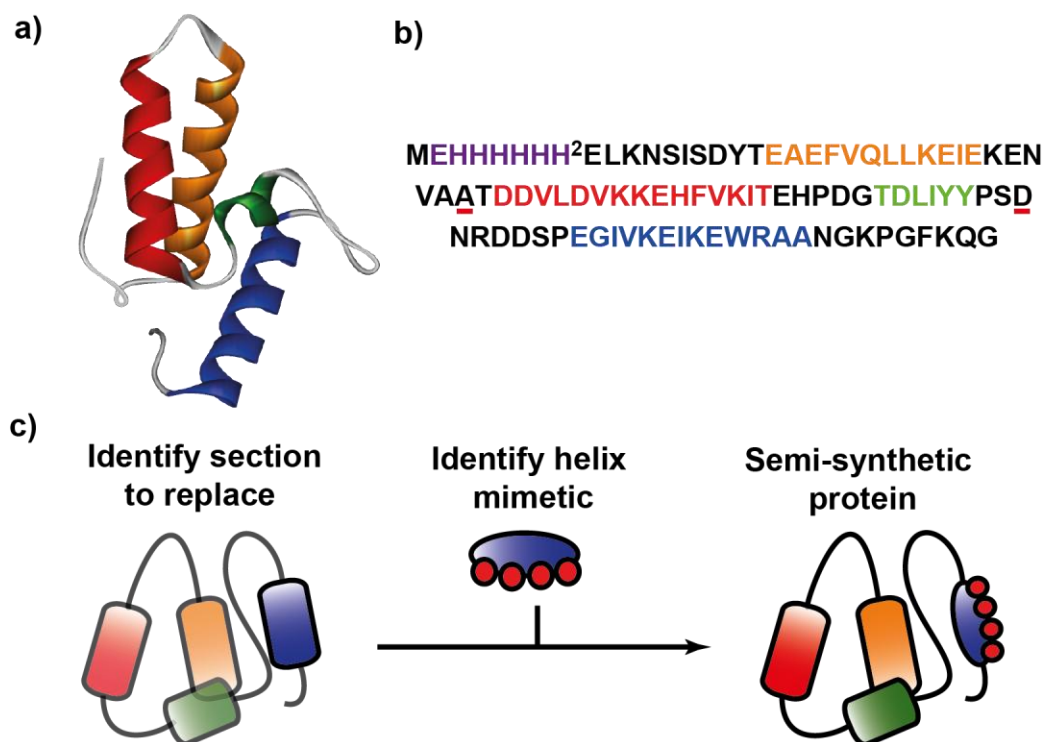
Figure 2.1 – An overview of the 'prosthesis' strategy for the synthesis of tertiary structure mimetics. a) X-Ray structure of Im7 (PDB:1AYI)[144] and b) sequence of Im7 where the native numbering system begins from [2]E, the red underlined [29]A and [59]D are the cysteine mutation points. The coloured regions correspond to Helix 1 (orange), Helix 2 (red), Helix 3 (green), Helix 4 (blue) and the His purification tag is highlighted in purple; c) cartoon of the prosthesis strategy, where a suitable helical region of a native protein is replaced by a secondary structure mimetic to afford a semi-synthetic protein.

The target protein for replacing α-helical segments was colicin immunity protein Im7 (Figure 2.1a), which is responsible for binding with high affinity to a colicin toxin E7.[145] E7 is an indiscriminate toxin which is secreted by an *E. coli* cell to its surroundings; Im7 therefore protects the host cell from its own toxin by neutralising E7.

Im7 was chosen for total chemical synthesis because its folding pathway has been previously characterised at atomic resolution by Radford and coworkers at the University of Leeds,[11, 146-148] thus providing in-house knowledge for comparing semi-synthetic varieties of Im7 with the wild type. Im7 also has the benefit of possessing four α-helical regions, which could all be potential targets of replacement with α-helix mimetics (Figure 2.1c). Im7 has been previously glycosylated at different positions,[148, 149] which required a semi-chemical synthesis approach using intein mediated ligation. In order to

access all helical regions for replacement, a total synthetic strategy was devised.

2.1   Strategy for the total synthesis of Im7

After a bold attempt of the total synthesis of wild type Im7 (93 residues) in one continuous synthesis using the CEM® automated peptide synthesiser was unsuccessful, a total chemical synthesis strategy of Im7 was devised based on previously established methods of Im7 semi-synthesis (Figure 2.2),[148, 149] where the protein was divided into three fragments for two successive native chemical ligation steps.[45] The non-endogenous cysteine residues have also been previously shown to have no effect on the folding characteristics of the protein,[148] and the *N*-terminal His$_6$ tag was included to assist purification. Figure 2.2 represents the ligation methodology for the total chemical synthesis of Im7.
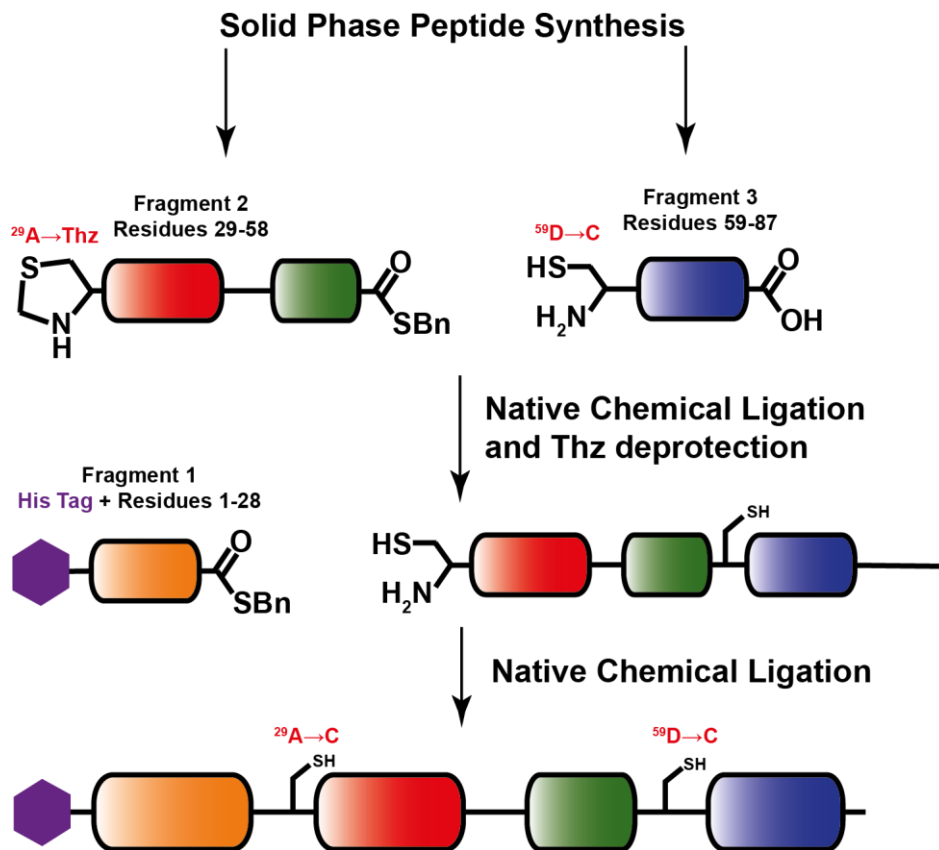
Figure 2.2 – Cartoon representation of the synthetic strategy for Im7, with the coloured ovals representing the helical regions as defined in Figure 2.1. Here, the fragments of Im7 are synthesised using SPPS methods, with Fragment 2 functionalised with a masked cysteine residue and a *C*-terminal thioester. After one native chemical ligation to form Fragment 2-3, deprotection of the Thz group to cysteine precedes the second native chemical ligation to afford complete Im7.

Fragments 1 and 2 required their syntheses to use highly acid labile trityl based resins, which could cleave the peptide from the resin with 0.5 % TFA in CH_2Cl_2 with all of the side chain protecting groups *left intact*. Consequently, the *C*-terminal carboxylic acid of Fragment 2 could then be chemoselectively modified to a thioester, which activates the fragment to native chemical ligation with a peptide that possesses an *N*-terminal cysteine residue. Fragment 2 required an additional protecting group, with its *N*-terminal cysteine protected with a thiazolidine (Thz), which prevents the formation of fragment 2 oligomers during native chemical ligation.

2.1.1   Synthesis of Fragment 3

 ⁵⁹CNRDDSPEGIVKEIKEWRAANGKPGFKQG

Fragment 3, the *C*-terminal fragment was synthesised first, based on there being no requirement for any modifications to its functionalities after cleavage. Table 2.1 summarises the synthetic approaches for Fragment 3.

Entry	Method (mmol scale)	Resin (capacity)	Double couplings	Crude Mass (Theoretical)	Purified Yield
1	Microwave assisted SPPS (0.1)	Novasyn TGR (0.25)	R76 and R61	360 mg (329 mg)	N/A
2	Manual SPPS (0.04)	Novasyn Fmoc-Gly-TGT (0.21)	R61, I68, V69, K70, E71, I72, R76, N79	107 mg (136 mg)	35 mg 25%
3	Manual SPPS (0.08)	Novasyn Fmoc-Gly-Wang (0.79)	I68, V69, E71, I72, N79.	160 mg (255 mg)	48 mg 19%

Table 2.1 – Synthesis attempts of Fragment 3, the capacity of the resin is given as mmol g^{-1}.

The first attempt, using microwave assistance for amino acid couplings and Fmoc deprotections afforded an inseparable mixture of deletion sequence peptides. As a result, the synthesis was performed by manual solid phase peptide synthesis, where each step was monitored by colour tests, at the expense of additional time required for synthesis. In particular, the manual solid phase synthesis allowed periodical LCMS test cleavages to ensure that deletions were avoided, especially in the region of ⁶⁰NRDDSP, which gave ambiguous results to colour tests. The *N*-terminal Cys residue was coupled in a modified manner, using a reduced polarity solvent system (1:1 DMF:CH$_2$Cl$_2$) and 2,4,6 trimethylpyridine to obviate racemisation during the coupling.[150]

Using TGT resin and employing double couplings for residues that failed to couple effectively in the first synthesis attempt, Fragment 3 was effectively synthesised on a 0.04 mmol scale to afford 107 mg of crude peptide (78% crude recovery). Purification of the peptide by reversed phase HPLC did afford 35 mg of Fragment 3 (25% yield).

Since TGT was a low-loading resin, the synthesis of Fragment 3 was attempted using a higher-loading and more versatile resin, with the aim of

affording a higher quantity of Fragment 3. Thus, Fragment 3 was built on Gly-loaded Wang resin on a scale of 0.08 mmol, to afford 48 mg (19% yield) of Fragment 3 after purification by HPLC.

2.1.2 Synthesis and Thioesterification of Fragment 2

Fragment 2 was not previously synthesised in the literature, but required the functionalisation of the *N*-terminus with a thiazolidine protecting group to prevent dimers of Fragment 2 forming during native chemical ligation. The fragment was built using TGT resin, which was necessary to afford a fully protected peptide after cleavage with 0.5% TFA in CH_2Cl_2 followed by the conversion of the *C*-terminus to a thioester.

The fragment was built manually using double couplings for each amino acid in order to provide a suitable quantity of peptide for characterisation free of deletions. Manual SPPS was effective, with a 96% crude recovery (208 mg) of the fully protected peptide on a 0.05 mmol scale, with the identity of the peptide confirmed after a small-scale deprotection, since the fully protected peptide did not ionise effectively during mass spectrometry.

Entry	Method (mmol scale)	Resin (capacity)	Double Couplings	Crude Mass (Theoretical)	Recovery
1	Manual (0.05)	Novasyn Fmoc-Ser-TGT (0.20)	All	208 mg (216 mg)	96%
2	Automated with microwave (0.05)	Novasyn Fmoc-Ser-TGT (0.20)	None	20 mg (216 mg)	9%
3	Automated without microwave (0.05)	Novasyn Fmoc-Ser-TGT (0.20)	F41 & P57	171 mg (216 mg)	79%
4	Automated without microwave (0.1)	Novasyn Fmoc-Ser-TGT (0.20)	F41 & P57	333 mg (432 mg)	77%

Table 2.2 – Summary of the pertinent attempts of the synthesis of Im7 Fragment 2, where 'recovery' means the quantity of crude material obtained after low-acidic cleavage.

Following the success of the manual method, the Fragment synthesis was trialled for automated synthesis using the synthesiser, since double couplings under manual conditions were expensive in terms of time and reagents. The first attempt at automation used microwave irradiation which resulted in no peptide afforded after the synthesis; the frailty of the resin resulted in cleavage of the peptide from the resin at every irradiation step (Table 2.2, Entry 2).

Subsequently, the peptide was synthesised without microwave irradiation on scales of 0.05 mmol, which proved to be effective with the double couplings of [57]Pro and [41]Phe required, since small deletions of these residues had been observed in the first attempt of non-microwave automation. One apparent downside to this was the lower crude recovery of the peptide from the resin, which came from acidic contaminants within the reactor, behaviour that was also observed when the peptide synthesis was scaled up to 0.1 mmol.

2.1.2.1 C-*terminal thioesterification of Fragment 2.*
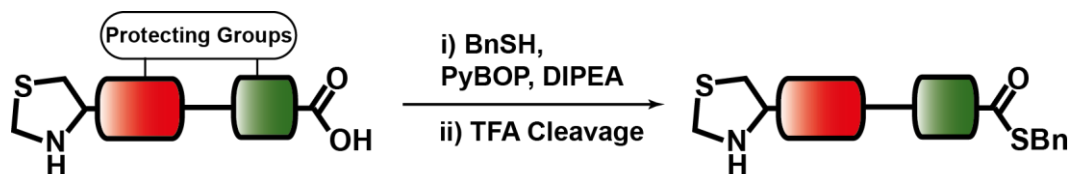
Scheme 2.1 - Scheme for the conversion of the *C*-terminal carboxylic acid of Fragment 2 to a thioester.

Thioesterification of Fragment 2 was carried out by using benzyl mercaptan as the thiol, in the presence of PyBOP as an activator. A particular disadvantage of the thioesterification reaction was that large quantities of protected Fragment 2 were required to monitor the reaction by LCMS, which could only be done by deprotecting the side chains with TFA in order for the peptide to ionise.

The thioesterification required several optimisations (Table 2.3), where appropriate concentration of the solution was essential for the thioesterification to proceed, without the solution emulsifying. The order of the reagent addition was also optimised, where adding additional PyBOP and DIPEA mitigated the loss of PyBOP through its side reactions with benzyl mercaptan.

Entry	Scale (mmol)	Concentration (mM)	Conditions	Outcome
1	0.019	12.6	A	No Reaction
2	0.019	38	A	60% conversion
3	0.027	108	B	100% conversion
4	0.023	115	B	Emulsion, no reaction
5	0.023	58	B	100% conversion

Table 2.3 – Summary of the optimisation of the thioesterification of Fragment 2. Condition A is 20 eq. BnSH, 3 eq. PyBOP, 3 eq. DIPEA under N_2 for 18 h. Condition B is the same as A, but an extra 2 eq. of DIPEA and PyBOP were added after 2 h. The conversion of the thioesterification was determined after global deprotection and was quantified by integration of the LCMS peaks of the starting material *versus* the target peptide.

Optimisation of the reaction conditions did not remove the problem that the peptide required full deprotection with TFA in order to quantify the extent of thioesterification, since mass spectrometry of small aliquots of the reaction

mixture were saturated by PyBOP and its byproducts, which ionised considerably better than that of the full peptide.

Furthermore, purification of Fragment 2 thioester by HPLC was not trivial, since the PyBOP byproducts coeluted with the peptide, but 10 mg (15%) of Fragment 2 was afforded cleanly.

2.1.3 Synthesis and thioesterification of Fragment 1

MEHHHHHH²ELKNSISDYTEAEFVQLLKEIEKENVA

Fragment 1 was synthesised using the same methodology as Fragment 2, utilising TGT resin to afford side-chain protected peptides for thioesterification. The first attempt of peptide synthesis was manual SPPS on a scale of 0.04 mmol with each residue double coupled. Pleasingly, this was effective and afforded 225 mg of peptide (72% recovery) without any deletion sequences (Table 2.4).

Entry	Method (mmol scale)	Resin (capacity)	Double Couplings	Crude Mass (Theoretical)	Recovery
1	Manual (0.04)	Novasyn Fmoc-Ala-TGT (0.21)	All	225 mg (308 mg)	72%
2	Automated without microwave (0.05)	Novasyn Fmoc-Ala-TGT (0.21)	None	N.D.	N.D.
3	Automated without microwave (0.05)	Novasyn Fmoc-Ala-TGT (0.21)	8 N-terminal residues	257 mg (308 mg)	83%

Table 2.4 – Summary of the optimisations of the synthesis of Im7 fragment 1 on TGT resin. Calculation of recovery for Entry 2 was not possible due to a complex mixture of deletion sequence peptides.

The synthesis was then transferred to automated methods without microwave irradiation, where the best results were obtained when double couplings of the His_6 region were carried out, where the possible entanglement of the side chains of the residues made each successive coupling less effective. In spite of this, the crude recovery of the peptide after cleavage was poorer than that of Fragment 2, which suggested that the limit of the peptide was being reached for this particular trityl resin.

With the optimisations of the thioesterification in place using Fragment 2 (2.1.2.1), the *C*-terminal thioesterification of Fragment 1 was attempted. However, no reaction was observed for the optimised conditions, with addition of further reagents, lengthening reaction time and elevating the reaction temperature all ineffective. Considering that thioesterification attempts needed deprotection with TFA to quantify the success of the reaction, the failed attempts could not have been resubmitted to the reaction conditions, which was proving prohibitive in terms of time. As a result, a new method of activation was sought.

2.1.4 Fragment 1 synthesis using Dawson methodology

'Dawson' methodology[47, 50] allows the synthesis of *C*-terminally activated peptides for native chemical ligation with the peptide activated on resin prior to cleavage and deprotection, which avoids the use of the highly labile TGT resin. Dawson resin utilises a diaminobenzoic acid (Dbz) linker that is activated to *N*-acylbenzimidazolinone (Nbz) by *p*-nitrophenyl chloroformate *after* the peptide elongation is complete (Scheme 2.2). The function of the Nbz is to be displaced by thiols in ligation buffer during native chemical ligation, which obviates a functional group transformation that had been arduous in previous Fragment syntheses (2.1.2, 2.1.3).
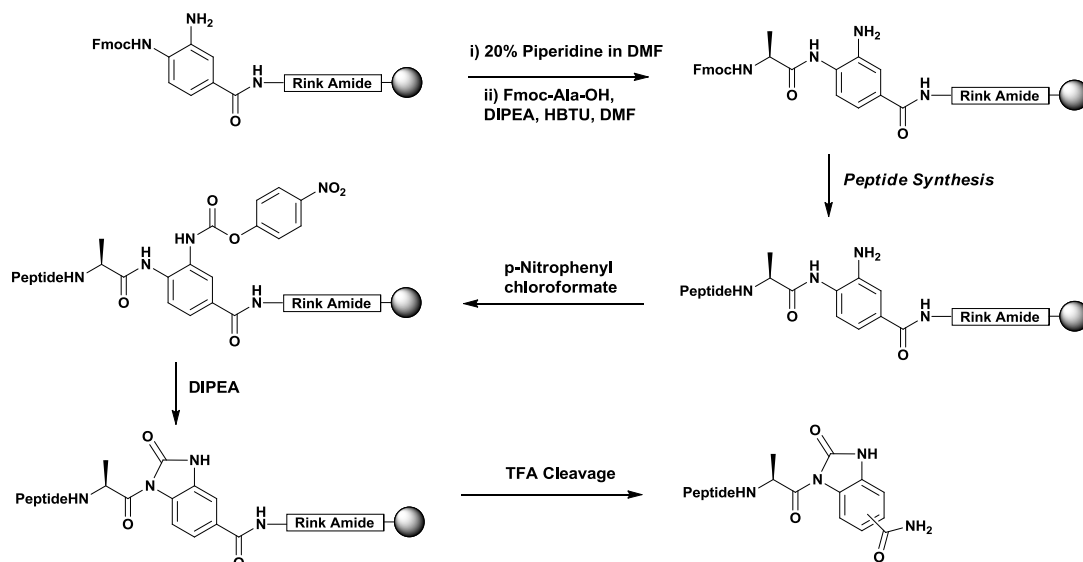
Scheme 2.2 - Scheme for the synthesis and activation of Dawson resin, which starts as a diaminobenzoic acid (Dbz) linker before its activation to *N*-acylbenzimidazolinone (Nbz).

Since Dawson resin was a relatively new innovation, there was no formally established protocol for its use, so the initial coupling of ^{28}Ala was done using several different coupling methods to strike a balance between achieving an effective coupling of the amino acid without overacylation of the Dbz moiety, which would have rendered the Dbz defunct at the end of the synthesis (Table 2.5).

Entry	Activation	Repeats	Outcome
1	HCTU	3	~50% diacylation
2	HBTU	3	~25% diacylation
3	HATU	2	~40% diacylation
4	HBTU/HOBt	2	No diacylation

Table 2.5 – Trials of the loading of the Dawson Dbz resin using 5 eq. of activator, DIPEA and Fmoc-Ala-OH for 1 h.

A double coupling using HBTU and HOBt proved to be effective, since HATU and HCTU promoted some diacylation of Dbz, and resultingly the peptide was synthesised using HBTU and HOBt activation without microwave irradiation.

Some further optimisation was required for the synthesis of the peptide, where couplings were less effective at the His$_6$ region, even with the employment of double couplings and the use of HATU. Finally, the peptide was effectively synthesised using a lower loading variant of the Dawson Resin (which was unavailable for the first attempts), where the complete peptide was

synthesised with no deletions using HBTU/HOBt activation on a 0.05 mmol scale (Table 2.6).

Entry	Coupling Methods	Double Couplings	Outcome
1	HCTU	8 N-terminal residues	Complex mixture, traces of target peptide observed
2	HCTU*	8 N-terminal residues	Complex mixture, traces of target peptide observed
3	HBTU/HOBt	None	Complete peptide, quantitative crude recovery

Table 2.6 – Synthesis attempts of Fragment 1 on Dawson resin after the loading of the first residue with HBTU/HOBt. HCTU* is where the 8 *N*-terminal residues were coupled with HATU. The scale of synthesis was 0.05 mmol for all attempts.

The subsequent activation of the peptide on resin was achieved by spinning the resin in a solution of *p*-nitrophenyl chloroformate overnight, followed by treatment with DIPEA for one hour. The peptide was then cleaved from the resin to provide a quantitative recovery of the peptide in remarkably high purity, surprising considering that the activation method of HBTU/HOBt is milder than that of HATU and HCTU.

Purification by HPLC afforded 10 mg (25% from 40 mg purified) of activated Fragment 1, but evaporation of the eluent had to be performed immediately as hydrolysis of the Nbz moiety to the *C*-terminal carboxylic acid was observed.

2.2 Native Chemical Ligation

With the peptide fragments in hand, native chemical ligation was attempted initially with Fragment 3 and the thioester of Fragment 2. Native chemical ligation (NCL) occurs by the *in situ* activation of a *C*-terminal thioesterified peptides in buffer of neutral pH in the presence of an excess of thiols and reducing agents.

NCL was first attempted using thiophenol and benzyl mercaptan present in buffer, based on the previous Im7 semi synthesis established by Imperiali and coworkers.[149] However, there were only trace amounts of Fragment 2-3 by inspection of LCMS. The ligation may have been arrested by the change of the

pH of the buffer as the partially miscible thiols began to precipitate from the mixture.

To improve on this, the ligation conditions were altered to 6M Guanidinium buffer, which would denature any secondary structure formed by either peptides and improve the rate of reaction. Also, mercaptophenyl acetic acid (MPAA) substituted benzyl mercaptan and thiophenol since its aqueous solubility allowed an improved control of pH.
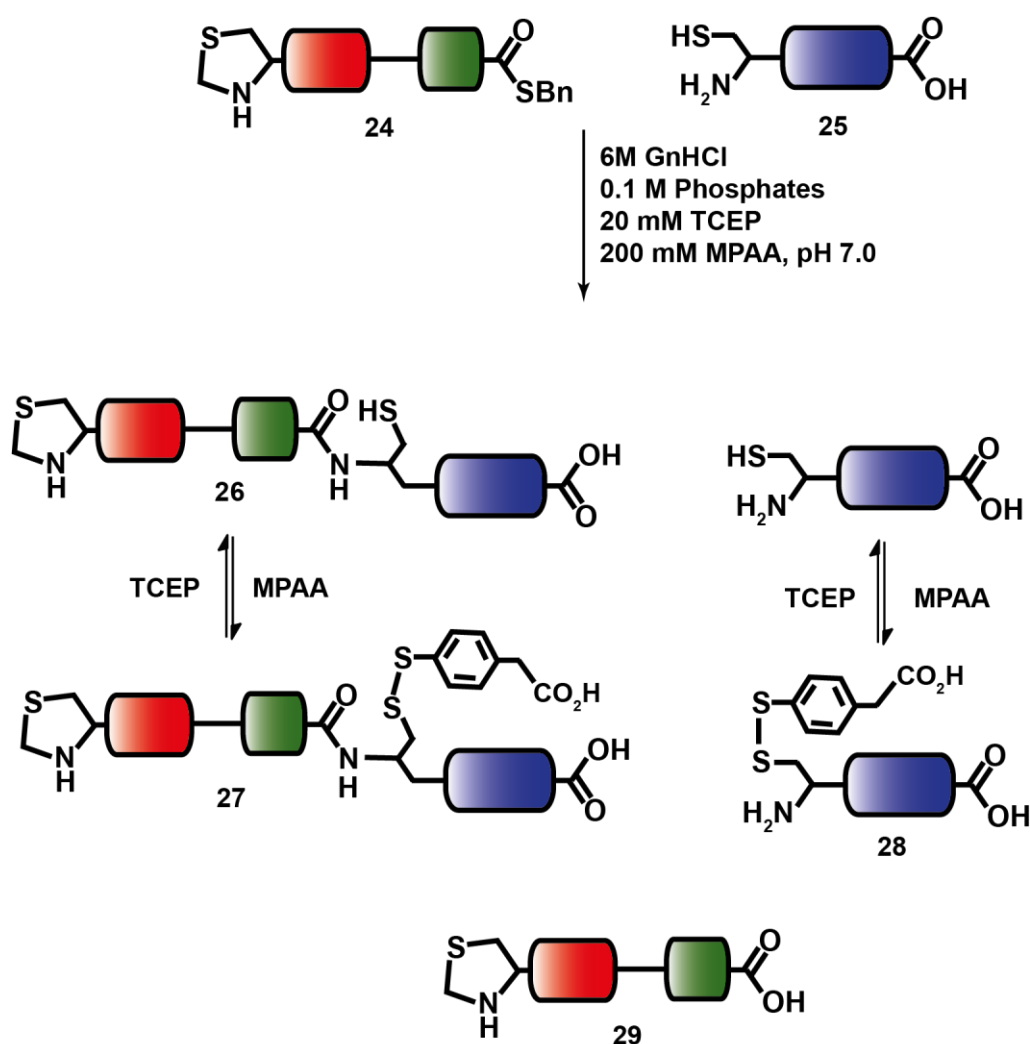
Figure 2.3 - Products from the Native Chemical Ligation of Fragment 2 thioester **24** and Fragment 3 **25**, which afforded ligated peptide Fragment 2-3 **26** and its intermolecular disulfide adduct **27**. Unreacted Fragment 3 **25** also formed intermolecular disulfides **28** and the hydrolysed Fragment 2 **29** was also observed.

Whilst LCMS indicated an improved conversion of Fragments 2 and 3 to the ligated product, hydrolysis of the thioester of Fragment 2 was observed, despite repeating the ligation ensuring that the pH of the fragment solutions was 7.0 prior to their addition. In addition to this, the MPAA formed

intermolecular disulfides with the ligated Fragment 2-3 and unreacted Fragment 3, but this was reversed by adding a further 5 equivalents of TCEP.

Since the native chemical ligation was envisaged to proceed in a one-pot reaction, the Thz protecting group was deprotected using methoxyamine hydrochloride. Initially, the Thz did not deprotect after 3 days which was due to the pH of the buffer being at 7.0. Altering the pH of the buffer to ~3 allowed the complete deprotection of Thz after 48 hours.

Dialysis of the ligation mixture to remove the methoxyamine from the solution followed by the addition of Fragment 1 Nbz moitey for the final ligation was not observed to be successful, since the rate of hydrolysis of the *C*-terminal activating group was faster than that of the rate of acyl transfer.

2.3   Concluding Remarks

The investigation into the total synthesis of Im7 allowed the optimisation of the synthesis of the three polypeptide fragments on solid phase, which could be reproduced for future investigations. The dynamic nature of the study was highlighted through the change of total synthesis strategy, where Dawson activating methodology was investigated in addition to *C*-terminal thioesterification. After trouble-shooting the first couplings onto Dawson resin, the synthesis of 36-mer peptides and on resin activation was more efficient and higher yielding than attempts with thioesterification, which is useful for future work.

The native chemical ligation steps require some optimisation to minimise the hydrolysis of the *C*-terminal activating group of peptides, which can be achieved through altering the activating group or through a judicious control of the ligation buffer pH and components. Whilst time constraints prevented the complete isolation of Im7 and ligation fragments, the attention of the project was shifted to the investigation of the *prostheses*, rather than the methodology of total protein synthesis. Nevertheless, the Im7 total synthesis investigation has substantial foundations laid for future studies.

Chapter 3

Chapter 3a: Investigation of constrained peptides using monosubstituted unnatural amino acids

The work described in this chapter features in the manuscript Yeo, D.J., Warriner S.L., Wilson A.J., *Chemical Communications* **2013**, *49*, 9131.

3.1 Introduction and context

The study of constrained peptides as potential therapeutics has grown rapidly in recent years, with a diverse range of methodologies established to target protein-protein interactions (PPIs).[95] A subset of the constrained peptide family are the hydrocarbon 'stapled' peptides, which furnish an all-hydrocarbon bridge on one face of a helical peptide by incorporation of olefin containing unnatural amino acids and their subsequent metathesis on solid phase (1.2.4).[1, 2] All prior work with respect to hydrocarbon stapling has utilised an α, α-disubstituted unnatural amino acid **16**, which includes a methyl group on the α-carbon in addition to a side chain with a terminal alkene. The length of the side chain can be tailored depending on the chosen positions of unnatural amino acid incorporation, to afford *i*, *i*+4 or *i*, *i*+7 crosslinked peptides, whose utility *in vitro* and *in vivo* has been demonstrated across a range of targets.[3, 4, 119, 120, 122, 124, 127, 151, 152]

It was apparent that a *des*-methyl ('monosubstituted') unnatural amino acid had been overlooked for investigation as a stapling reagent, and it was therefore decided to examine the use of this amino acid crosslink for the inhibition of protein-protein interactions.[12, 141]

Reported syntheses of the required unnatural amino acids have mostly employed a chiral auxiliary, to enable asymmetric installation of the alkenyl side chain. Such auxiliaries include morpholinones,[153, 154] *bis*-lactims,[155 156, 157] oxazolidinones,[124, 151] and transition metal complexes.[158, 159]

The current investigation utilised two different synthetic methods for amino acid synthesis, based on prior research,[154, 160] and utilised two well known α-helix mediated protein-protein interactions; p53/*h*DM2 and the Bcl-2 family,[161, 162] as model systems upon which to evaluate the resulting stapled systems.

3.2   Small molecule chemical synthesis

3.2.1 Synthesis of α,α-disubstituted amino acids

α,α-disubstituted amino acids were synthesised to enable comparison with monosubstituted amino acids. Synthesis proceeded *via* a morpholinone auxiliary **35** as reported by Verdine and coworkers (Scheme 3.1).[2, 3] From benzoin **30**, formation of the oxime **31** and its subsequent reduction to racemic amino alcohol **32** afforded excellent yields (quantitative and 96% respectively). The following step, a chiral resolution with successive recrystallisations with different aqueous ethanol mixtures was abandoned after several attempts. Essentially, the recrystallisation was profligate and the enantiopurity of the resultant amino alcohol **33** and its antipode was not guaranteed, which would have a profound effect on the overall enantiopurity of the amino acid after the synthesis was complete. Therefore, the synthesis was continued using commercially available amino alcohol **33**.
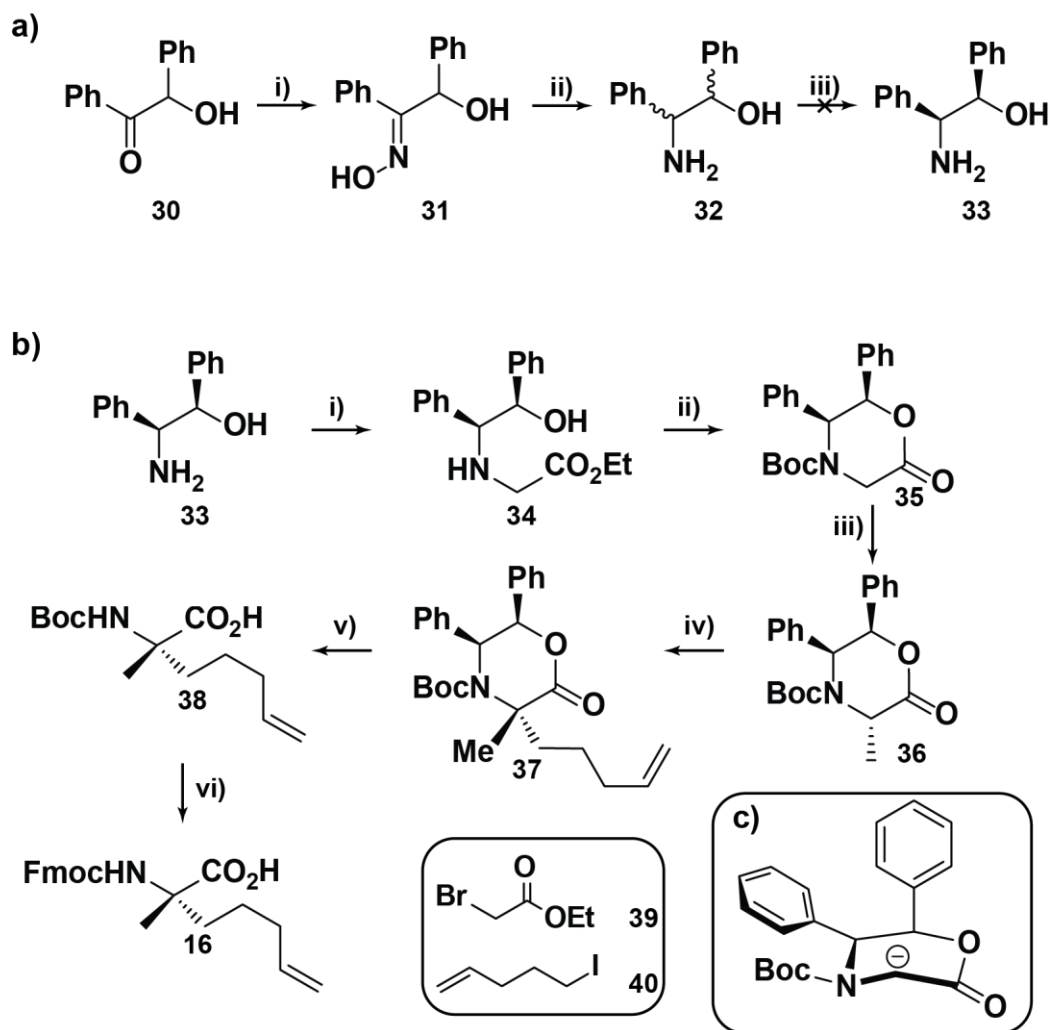
Scheme 3.1 – Synthetic route for the synthesis of α,α-disubstituted unnatural amino acids. a) Synthesis up to the aborted chiral resolution;[163] i) NH$_2$OH·HCl, NaOAc, EtOH:H$_2$O (6:1), Δ, **quant**.; ii) H$_2$ Pd/C, EtOH, 1.5% (v/v) aq.HCl, **96%**; iii) L-Glu, EtOH:H$_2$O. b) Synthesis from (1R, 2S)-1,2-diphenyl-2-aminoethanol **33** to Fmoc-protected (S)-α,α-disubstituted unnatural amino acid **16**;[153] i) **39**, Et$_3$N, THF, Δ, **92%**; ii) Boc$_2$O, Tol., Δ, *then* TsOH, Tol., Δ, **81%**; iii) MeI, NaHMDS, THF, −78 °C, **78% one diasteroisomer**; iv) **40**, KHMDS, THF, −40 °C, **49% one diastereoisomer**; v) Li^0, NH$_3$ (l), −78 °C, **84%**; vi) TFA, CH$_2$Cl$_2$ *then* Fmoc-OSu, NaHCO$_3$, H$_2$O:Acetone (1:1), **62%**. c) Proposed intermediate of the alkylation of **35**.

Formation of the morpholinone auxiliary **35** was straight-forward, where amination to **34** with ethyl bromoacetate afforded only the secondary amine with no evidence of further alkylation. Boc protection and cyclisation to **35** was a one-pot procedure, cyclisation occurred when the reaction temperature was elevated to 120 °C, to afford **35** in reliable yields of 85% after recrystallisation.

The diastereoselective alkylations followed the production of morpholinone **35**, with diastereoselectivity of the alkylations driven by the *syn*

configuration of the two phenyl groups, which block one face of the auxiliary from incoming electrophiles (Scheme 3.1c).[153, 154] The first alkylation with methyl iodide gave only monosubstituted product **36**, which was completely diastereoselective. However, the auxiliary was found to be prone to decomposition during reaction, work-up and purification by flash chromatography. This unwanted decomposition was suitably mitigated by temperature control during the reaction and quenching, followed by altering the published purification to trituration. The second alkylation with 1-iodopent-4-ene **40** was more challenging to initiate and control. After a succession of tests of conditions, whereby the halide, base cation, solvent and temperature were modified, a modest yield of 49% was afforded, and not improved upon. Incidentally, the order of addition of reagents was vital to the reaction proceeding successfully, since the addition of 1-iodopent-4-ene followed by KHMDS gave a successful reaction, but reversal of these additions promoted decomposition of the morpholinone auxiliary. The lower yield of the second alkylation step can be attributed to the weaker acidity of the α-proton of the auxiliary and a competing elimination pathway of the alkyl iodide.

*Di*alkylated auxiliary **37** was cleaved using dissolving metal reduction to afford Boc protected amino acid **38**, which remained Boc-protected after an acidic extraction. Finally, Fmoc-protected α,α-disubstituted amino acid **16** was furnished in yields of 62% after *in situ* Boc deprotection with trifluoroacetic acid, followed by protection with Fmoc-OSu under mildly basic conditions.

3.2.2 Synthesis of α-monosubstituted amino acids

The difficult nature of the synthesis of the α,α-disubstituted unnatural amino acid made the route described in 3.2.1 unsuitable to follow for α-monosubstituted amino acids. Therefore, Schiff-base complex **45**[4, 160] was employed to furnish *des*-methyl amino acid **48** (Scheme 3.2).

To this end, L-proline **41** was converted to *N*-benzyl proline **43** with potassium hydroxide and the dropwise addition of benzyl chloride. It is notable that attempting this reaction using sodiated bases resulted in the reaction mixture emulsifying, and the use of benzyl bromide or benzyl iodide promoted the formation of a mixture of quaternary ammonium salts and benzyl esters.

Any *N*-benzyl proline benzyl ester **42** was extracted with chloroform and hydrogenolysed using a poisoned palladium support to afford *N*-benzyl proline as the free acid. Coupling *N*-benzyl proline **43** with 2-aminobenzophenone **49** required a modification of the published procedure from using thionyl chloride to a dropwise addition of mesyl chloride in the presence of *N*-methyl imidazole, since the former gave no reaction. With (*S*)-*N*-(benzylprolyl)aminobenzophenone (BPB, **44**) in hand, complexation to tetradentate nickel complex **45** with glycine gave excellent yields.
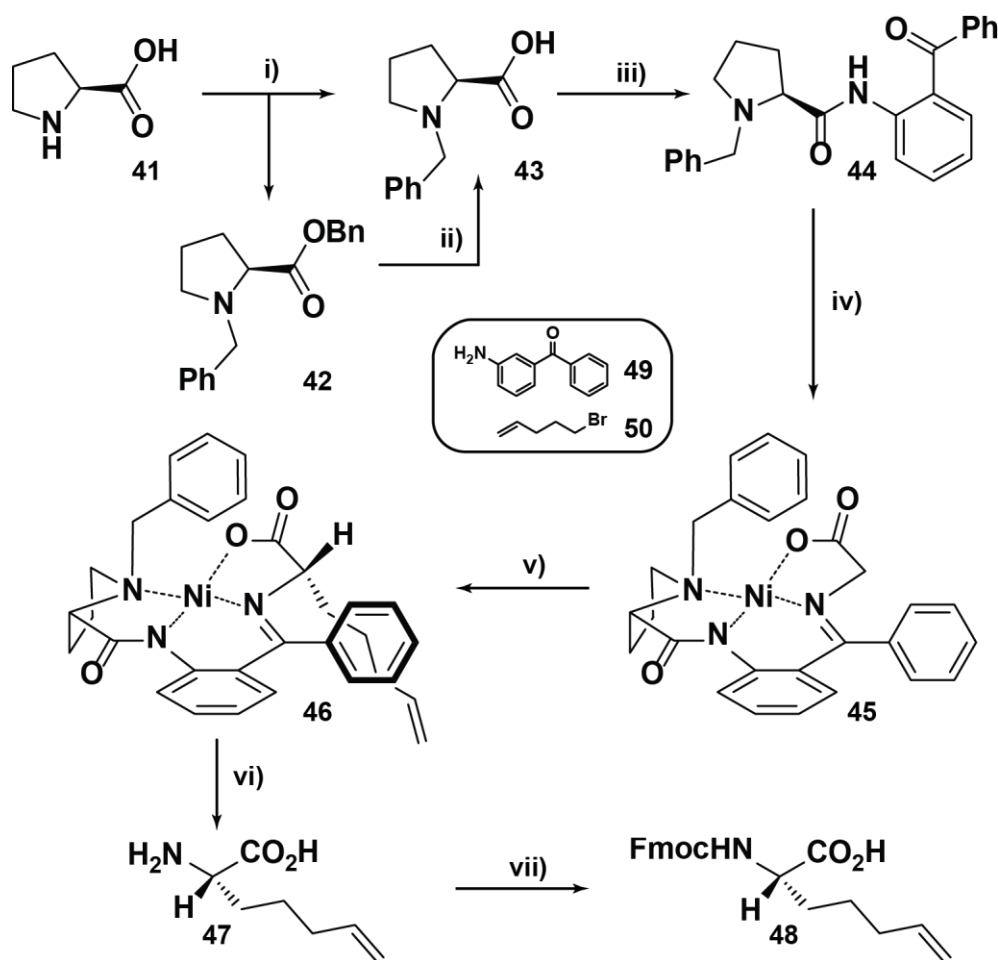
Scheme 3.2 – Reaction scheme of the synthesis of Fmoc-protected monosubstituted unnatural amino acid **48**;[158] i) BnCl, KOH, ^{i}PrOH, **55%**; ii) H_2 Pd/BaSO$_4$, EtOH, **60%**; iii) **49**, MsCl, NMI, CH$_2$Cl$_2$, **86%**; iv) Glycine, NaOMe, Ni(NO$_3$)$_2$·6H$_2$O, **96%**; v) **50**, MeCN, NaOH, –22 °C, **70% one diastereoisomer**; vi) 3M HCl$_{(aq)}$ MeOH, Δ, **95%**; vii) Fmoc-OSu, Na$_2$CO$_3$, H$_2$O:Dioxane (1:1), **53%**.

Alkylation with 1-bromopent-4-ene or 1-iodopent-4-ene gave good yields after optimisation of the reaction conditions, where allowing an extra 24 hours for the reaction to proceed gave a better conversion to the singly alkylated product **46**, with only minimal *di*alkylated complex observed.

Pleasingly, the diastereomeric ratio of the alkylation was at worst 98:2, by inspection of the 1H-NMR spectra and comparison with the literature precedent.[158] The stereochemistry of complex **46** was confirmed in the solution state by extensive NOESY analysis, in conjunction with COSY, HMQC and HMBC data. In addition to this, **46** was crystallised from toluene:pentane and single crystal X-ray diffraction confirmed the absolute stereochemistry in the solid state (Figure 3.1).

Hydrolysis of complex **46** followed by ion-exchange chromatography furnished free amino acid **47** in high yields (>90%), with the additional advantage of the BPB ligand **44** being extracted with chloroform and recycled for further use. Fmoc protection to **48** generally afforded modest yields (50-60%), without racemisation. This synthetic route has been found to be amenable to scale. The initial steps of the production of *N*-benzyl proline **43** and BPB **44** were performed on 50 gram scales, with the complexation to **45** performed on a 22 gram scale.[I] This afforded a total of 6.2 grams of Fmoc amino acid **48**, which has been provided to Sigma-Aldrich; under a commercialisation agreement.
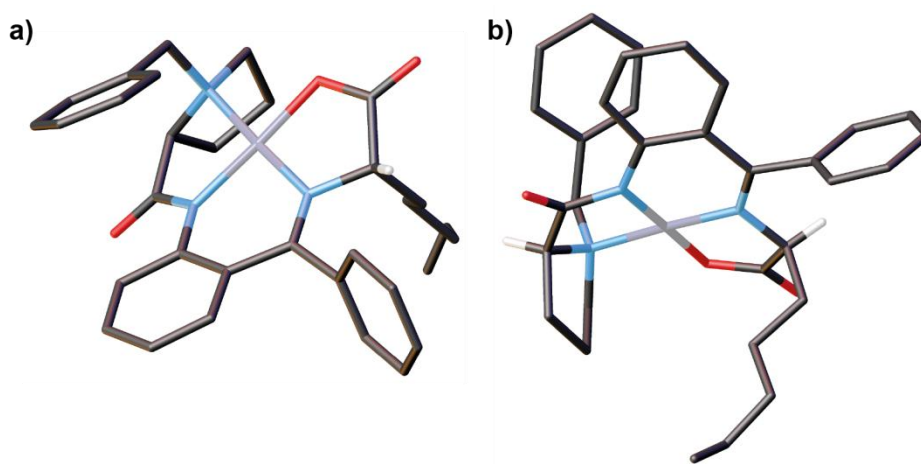
Figure 3.1 – X-ray crystal structure of alkylated complex **46**, confirming the absolute stereochemistry of the alkylation. Hydrogen atoms other than at the α-position have been omitted for clarity. (Colour code: Grey = C, Blue = N, Red = O, Silver = Ni). a) top perspective; b) lower perspective.

[I] It was observed in the up-scaled procedure that significant quantities (~3 g) of Fmoc-β-Alanine was isolated as a side product, from a suspected Lossen rearrangement of OSu under basic conditions.

3.3 Peptide Synthesis

3.3.1 p53/*h*DM2

p53 has a pivotal role in the regulation of cells. It prevents cancer through initiation of DNA repair of damaged cells, cell cycle arrest or through signalling the apoptosis of cells whose DNA cannot be repaired.[5, 164] The binding of p53 to its negative regulators, *h*DM2 and *h*DMX has been well studied and characterised,[5, 99] where the key binding region is an α-helical transactivation domain spanning residues 15-31 (Figure 3.2a, b).
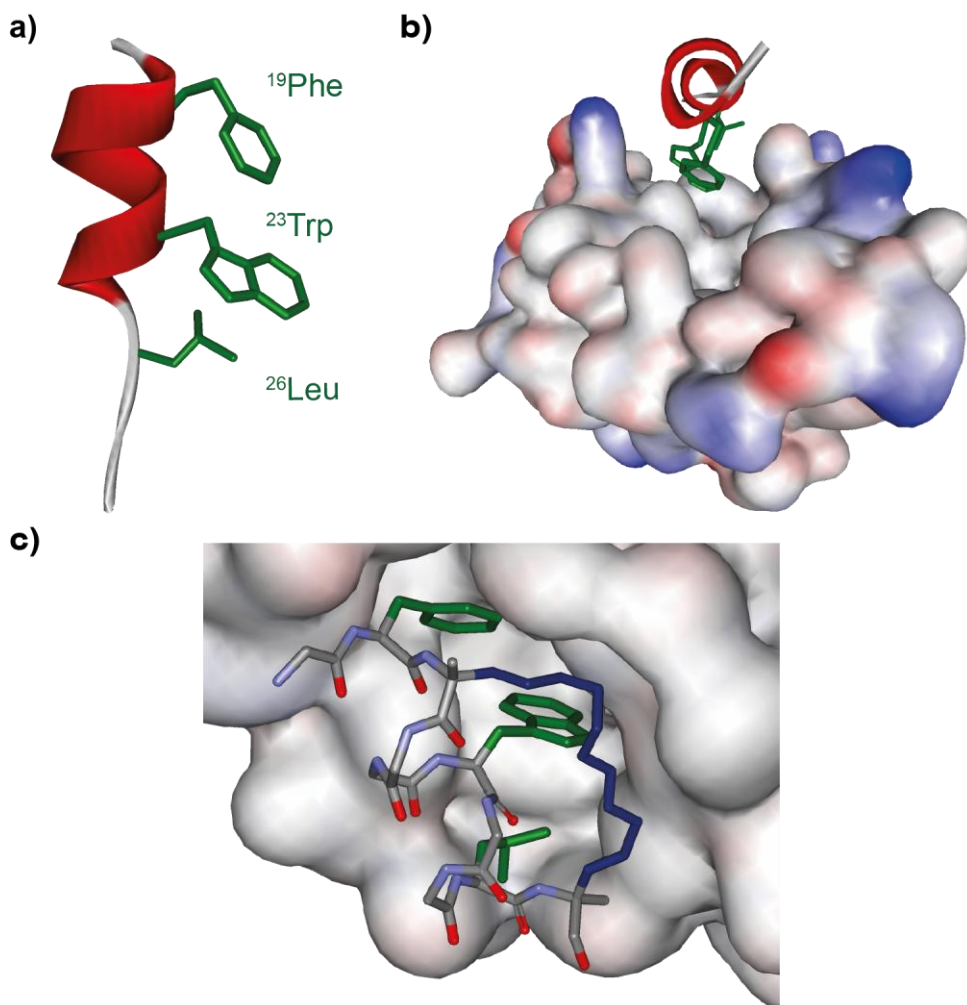
Figure 3.2 – Images of the binding of p53 to *m*DM2; a) The helical region of p53 with the key side chains displayed; b) Visualisation of the transactivation domain of p53 binding into a complementary hydrophobic cleft on *m*DM2 (PDB:1YCR)[99]; c) Crystal structure of a stapled p53 peptide bound to *m*DM2 (PDB:3B3V)[128]

Three hydrophobic side chains, [19]Phe, [23]Trp and [26]Leu, oriented on one face of the α-helix, contribute to the majority of the binding energy by burying into a complementary hydrophobic pocket on the surface of *h*DM2.

Recapitulation of the key side chains has therefore been pivotal for inhibition of p53/hDM2 by small molecules and proteomimetics.[85, 161] Constrained peptides improve affinity by the preorganisation of the peptide into an active conformation that is suitable for binding, with the key side chains oriented correctly for efficient binding to their complementary partner. For the purposes of this investigation, the p53/hDM2 PPI has been targeted in-house,[12, 141] as well as targeted in the field of hydrocarbon stapling by Verdine and coworkers, culminating in a crystal structure of a stapled p53 peptide bound to the murine equivalent, mDM2 (Figure 3.2c).[127, 128]

3.3.2 Nomenclature of p53 peptides

The discussion of the synthesis and biophysical analysis of stapled p53 will use the following abbreviations: p53 WT, p53 MM and p53 MU. Wild type is the unmodified transactivation domain peptide (residues 15-32). p53 MM is **monosubstituted metathesised** (stapled) where monosubstituted amino acid **48** has been incorporated. p53 MU is **monosubstituted unmetathesised** (unstapled).

Figure 3.3 –The synthesised sequences of the p53 transactivation domain. The key hydrophobic binding residues are coloured green, with the chosen sites of incorporation of alkenyl amino acids coloured red. The abbreviations of the peptides are **M**onosubstituted **M**etathesised (MM) and **M**onosubstituted **U**nmetathesised (MU).

3.3.3 Peptide Synthesis of p53

Sites for the incorporation of monosubstituted amino acids within the peptide sequence, were chosen at [18]Thr and [22]Leu (red in Figure 3.3), on the basis that these residues are suitably spaced and modification should not interfere with the orientation of the key hydrophobic side chains.[127] This substitution also does not replace any charged residues that may have implications for solubility or disrupt stabilising salt bridges. The peptides were synthesised on Rink Amide MBHA resin on a 0.05 mmol scale, in order to afford

C-terminally amidated peptides that are equivalent to the transactivation domain of p53.

The synthesis was carried out using well established Fmoc solid phase peptide synthesis (SPPS), with HCTU, HOBt and DIPEA as the activating reagents for peptide elongation.[42] Double couplings were required for the coupling of [29]Asn and [30]Asn, since small scale test cleavages had revealed these couplings to be cumbersome and incomplete after 2 hours. In spite of this, the monosubstituted unnatural amino acid **48** was incorporated completely with no special considerations or modifications, with the Kaiser test[165] being conclusive for their couplings and deprotections.

The alkenyl side chains of the unnatural amino acids were metathesised using the first generation Grubbs catalyst in degassed dichloroethane, which gave >98% conversion of the alkenyl side chains into an 8-carbon crosslink after two treatments with the catalyst. Optimal cleavage and global deprotection of the peptide from the resin was found to require Cleavage Reagent K, which contains ethanedithiol and thioanisole as its scavengers, to prevent disulfide oxidation of [32]Cys and the irreversible alkylation of nucleophilic side chains by *t*Bu cations. Generally, the stapled and unstapled p53 peptides were the dominant species present in the LCMS of the crude precipitate and deletion sequences were not observed. Purification of the stapled and unstapled p53 peptides was performed using reverse phase preparative HPLC, which in spite of using TCEP in the loading solution, gave poor recoveries of 13% and 11% of pure stapled and unstapled p53 based on crudes of 100 mg.

3.4 Biophysical evaluations of the p53 peptides

3.4.1 Circular Dichroism

In order to evaluate the effectiveness of the hydrocarbon crosslink to promote a particular conformation and to reduce conformational plasticity in aqueous solution, circular dichroism was employed to probe the type and

extent of secondary structure of peptides and proteins. CD provides distinct spectral profiles depending on the secondary structure present.[166]
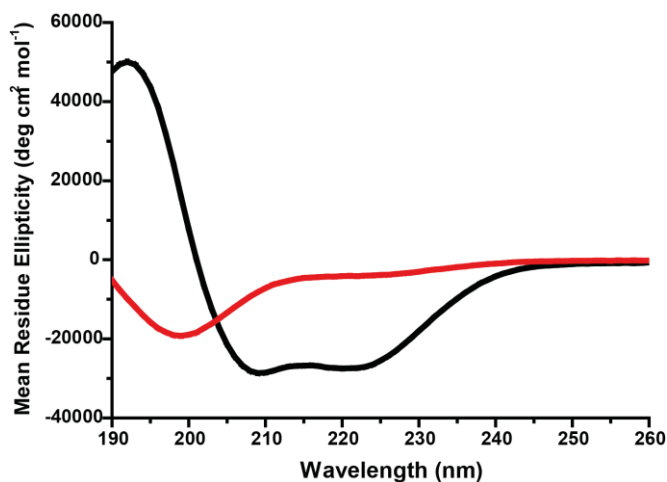
Figure 3.4 – Representative example of circular dichroism spectra for unstructured, random coil peptides (red) and α-helical peptides (black).

In the context of investigating α-helical peptides and peptidomimetics, the amplitude at 222 nm is used to quantify the percentage α-helicity of a polypeptide.[103, 167] CD is therefore a fundamental tool in the design and optimisation of stapled peptides.[1, 2]

3.4.1.1 Circular Dichroism of the Stapled p53 Peptides

The monosubstituted p53 peptides were examined for their helical character using circular dichroism to compare the unstapled and the stapled variants. The peptides were dissolved in an acetonitrile:water solvent mixture - the acetonitrile was necessary to solubilise the peptides and was chosen over DMSO to obviate the strong absorption observed with DMSO below 230 nm.
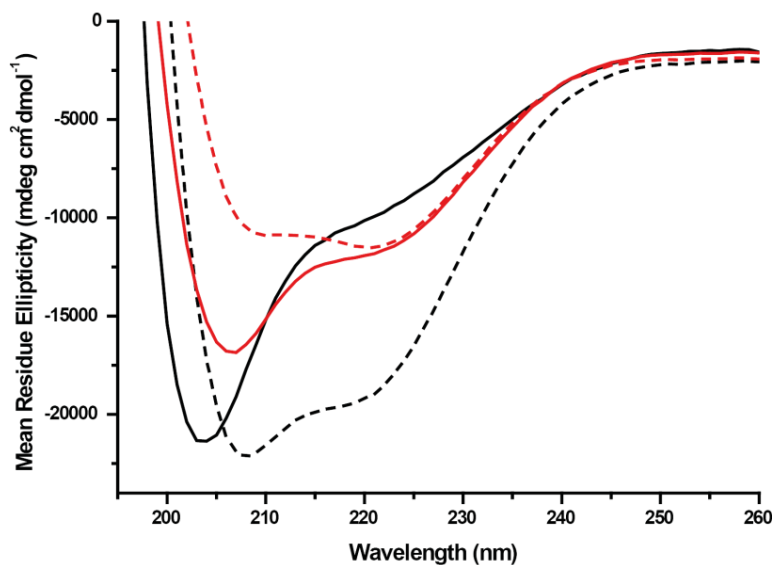
Peptide	% Helicity (no TFE)	% Helicity (TFE)
p53 MU	27%	54%
p53 MM	32%	32%

Figure 3.5 - Expansion of the circular dichroism spectra of p53 MU (black) and p53 MM (red) peptides. Solid lines are spectra of peptides dissolved in acetonitrile:water, with dashed lines the spectra of the peptides dissolved in 3:7 TFE:H_2O. The % helicity of wild type p53 has been reported as 11%.[127]

p53 MM appeared to have a modest increase in its helical character compared to reported wild type values,[127] but its CD profile suggested a predominantly random coil character. Whilst p53 MU had a similar % helicity, its CD profile suggests a greater proportion of random coil character. Employing trifluoroethanol (TFE) in the solvent, which promotes the formation of α-helical structure in short peptides,[168, 169] provided a benchmark for the maximum helicity p53 MU and p53 MM could attain. p53 MU had a dramatic change in its % helicity and its CD profile, which matches an α-helical conformation. Meanwhile, p53 MM also displayed a change in its CD profile, but had no change in its % helicity, which suggests that the hydrocarbon staple greatly reduces the conformational flexibility of the peptide.

3.4.2 Fluorescence Anisotropy

The potency of the p53 peptides was evaluated using fluorescence anisotropy competition assays previously developed within the Wilson laboratory.[12, 141] The principle of fluorescence anisotropy as a measure of potency is underpinned by the binding of a fluorescently labelled tracer to a

larger binding partner. As the concentration of the unlabelled partner, typically a protein, increases, a greater fraction of the tracer is bound. Once the labelled species is bound, the tumbling rate of the complex is reduced and, upon excitation of the fluorophore, an increase of anisotropy signal (r) is observed (Figure 3.6).[II] Plotting the fraction bound of the tracer against the concentration of the unlabelled partner allows the extraction of a K_d value for this interaction.
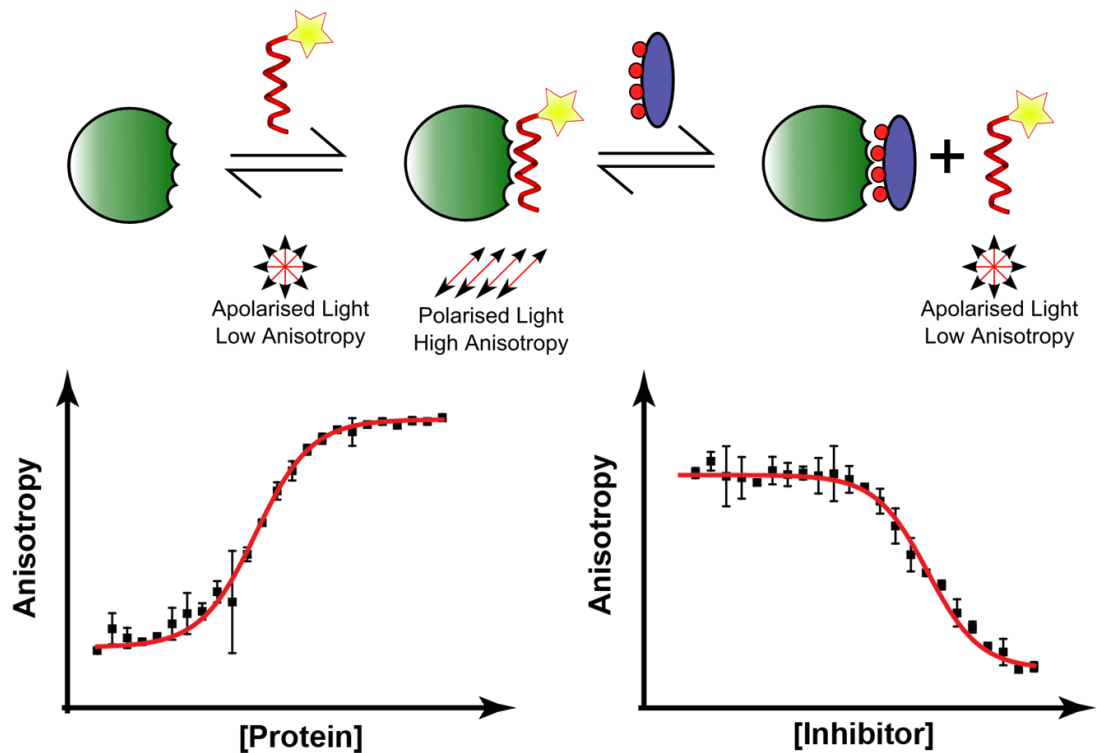
Figure 3.6 – Overview of the fluorescence anisotropy assay, with anisotropy signal increasing as a protein binds to a fluorescently labelled species (left) and the decrease of anisotropy signal (right) as an inhibitor competes out the labelled species.

With the K_d of an interaction of a fluorescently labelled species and its partner established, it is possible to extract information of potencies of inhibitors of the tracer:protein interaction. Fixing the concentration of protein and tracer, and titrating the inhibitor of interest results in the release of the tracer from the protein binding site *in lieu* of the inhibitor. The release of the tracer allows it to tumble freely in solution, causing a decrease in the anisotropy signal. Plotting of anisotropy signal against the concentration of the

---

[II] Anisotropy is inversely proportional to the rate of tumbling of a species compared to its fluorescence lifetime.

inhibitor allows a K_i or IC_{50} to be extracted - the inhibitory equilibrium constant and the half inhibitory concentration point respectively.

3.4.2.1 Fluorescence Anisotropy Competition Assays of Stapled p53 peptides

The stapled and unstapled p53 peptides were evaluated for their potencies against a fluorescein-labelled p53 peptide (p53*), using procedures analogous to those previously reported.[12, 141]

Peptide	IC_{50} (µM)
p53 WT	1.2
p53 MU	**17.8 ± 1.7**
p53 MM	**10.4 ± 1.0**
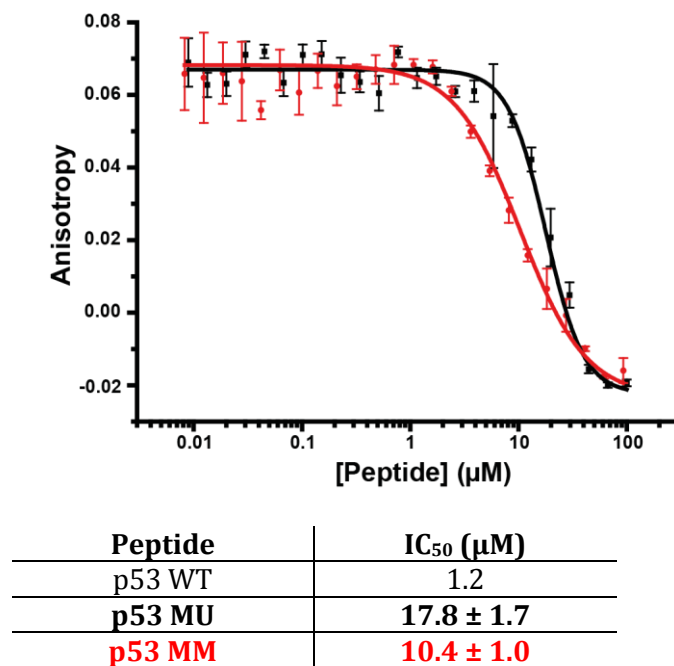
Figure 3.7 – Fluorescence anisotropy competition curves of the inhibition of p53/*h*DM2 using stapled (red) and unstapled (black) p53 peptides.

The results were somewhat disappointing, considering that the IC_{50} of p53 WT has been previously established as 1.2 µM in the Wilson laboratory. Interestingly, there was a marginal improvement of binding affinity between p53 MM and p53 MU, which could lead to the conclusion that restricting the conformation of the peptide mitigated a penalty in the installation of amino acid **48**. Constraining a peptide prevents the entropic penalty of organisation of the peptide into its binding conformation; therefore stapling of this p53 peptide suggests a reduction of the entropic penalty. Nevertheless, the reduced potency relative to the wild type leads to the conclusion that the positioning of this crosslink is not suitable for improvement of helical content or inhibitory potency.

3.4.3 Concluding remarks of the stapling of p53

It was evident that the use of the p53 peptide was not appropriate for the evaluation of *des*-methyl amino acids for peptide stapling. Inspection of the circular dichroism data suggests that, whilst the p53 MM peptide has been conformationally rigidified, the lack of α-helical character suggests that the positions chosen for the incorporation of the amino acids were inappropriate. This hypothesis was further reinforced by the inhibitory potency of p53 MM versus p53 WT, which was lower by an order of magnitude. In spite of the fact that p53 MU was a weaker inhibitor than MM, possibly from the additional entropic penalty of the peptide folding into its active conformation, the position of the crosslink was insufficient to promote improved inhibitory activity.

In some respects this is unsurprising, considering preceding work on the stapling of p53 identified optimal crosslinks to bridge the *i*, *i*+7 positions and using an (*S*)-pentenyl amino acid with an (*R*)-octenyl partner,[127] the latter which had not been synthesised using our current methodology.

It was therefore necessary to explore a different interaction with the monosubstituted stapled peptides, which had precedent with the use of two (*S*)-pentenyl amino acids in an *i*, *i*+4 configuration.

3.5 Investigation with the Bcl-2 family of proteins

The B-Cell Lymphoma (Bcl-2) family of proteins are a series of homologous proteins that regulate the apoptosis of cells through a balance of pro- and anti-apoptotic proteins. After the discovery of the eponymous anti-apoptotic Bcl-2 protein,[170] several family members with homologous sequences have been found, of which some are involved in the promotion of apoptosis.[6, 162, 171-173] The four homologous sequences are all α-helical and are termed as BH (Bcl-2 homologous) regions, which allowed the subdivision of the Bcl-2 family based on the presence of the BH regions and the function of the protein. Anti-apoptotic (Bcl-2, Mcl-1, Bcl-x$_L$) and pro-apoptotic executioner (BAK, BAX) proteins contain *up to four* BH regions, with a third class of 'BH3 only' modulation proteins (BID, BIM, BAD, NoxaB) that contain only the BH3 helical region (Figure 3.8).
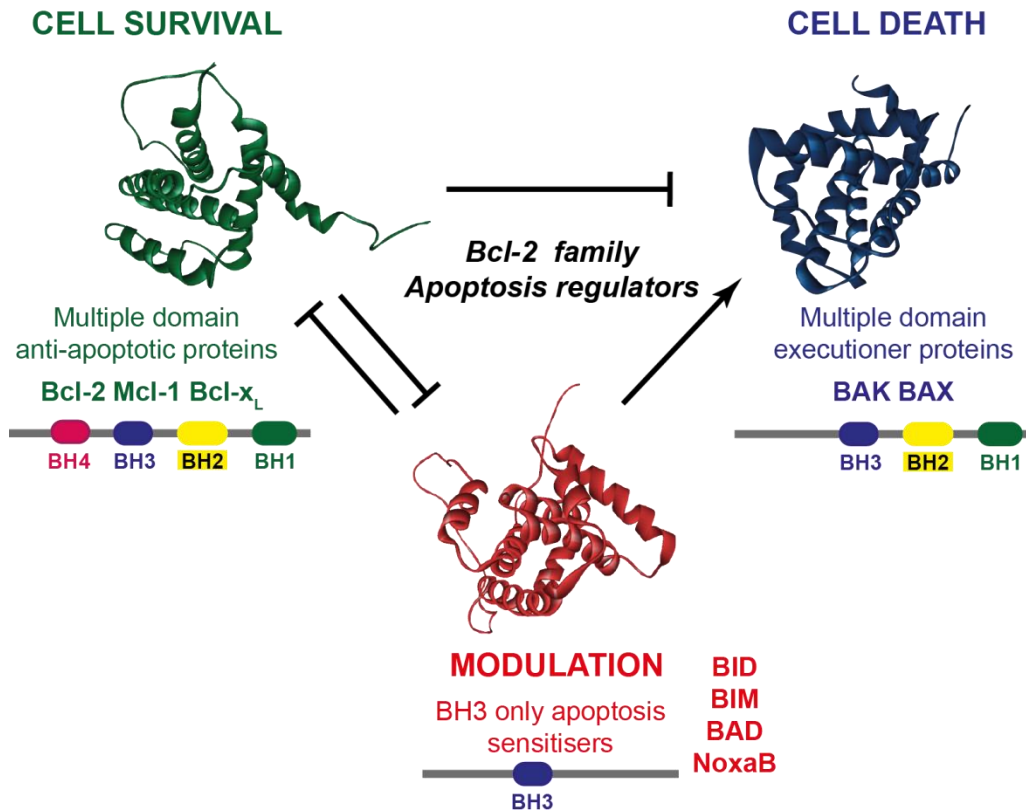
Figure 3.8 – Schematic representation of the three classifications of the Bcl-2 family and their complementary interactions). The illustrated proteins are Bcl-x$_L$ (green, PDB: 1BXL)[174]; BAK (blue, PDB: 2M5B)[175] and BID (red, PDB: 2BID).[98]

Regulation by the Bcl-2 family occurs in the mitochondrial outer membrane where, in healthy cells, anti-apoptotic proteins sequester BAK and BAX.[6, 172] In the event of cellular stress, signalling pathways regulate the expression of the BH-3 only modulation proteins, which in turn relay the pro-apoptotic signals to the multiple domain members (Figure 3.9). Signalling occurs either by the direct activation of BAK or BAX,[176-178] or by sequestering of anti-apoptotic proteins on the mitochondrial membrane by the BH-3 only proteins,[6, 162] resulting in the oligomerisation of BAK or BAX, permeabilisation of the mitochondrial membrane and the release of cytochrome *c*, triggering apoptosis by the caspase cascade (Figure 3.9).[173]
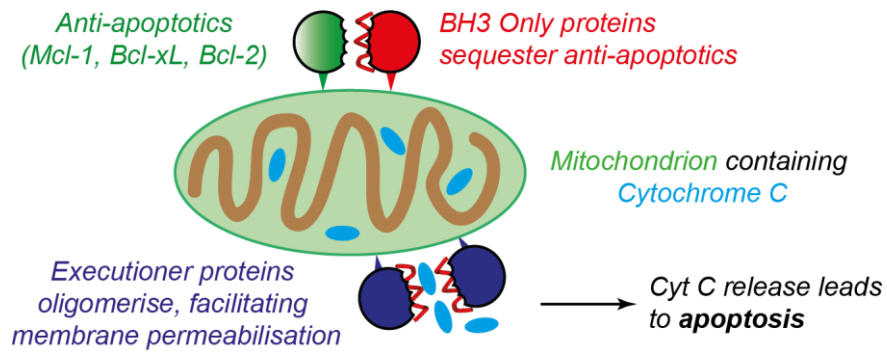
Figure 3.9 – Illustration of the association of proteins within the Bcl-2 family and their roles in triggering apoptosis by the caspase cascade.

The promiscuity of the BH3 'death domain', which binds into the juxtaposition of the BH1, BH2 and BH3 domains of the multiple domain family members has given rise to numerous studies on the use of BH3 peptides as potential therapeutics, notably hydrocarbon stapled BH3 peptides.[3, 119, 120, 133, 178, 179]
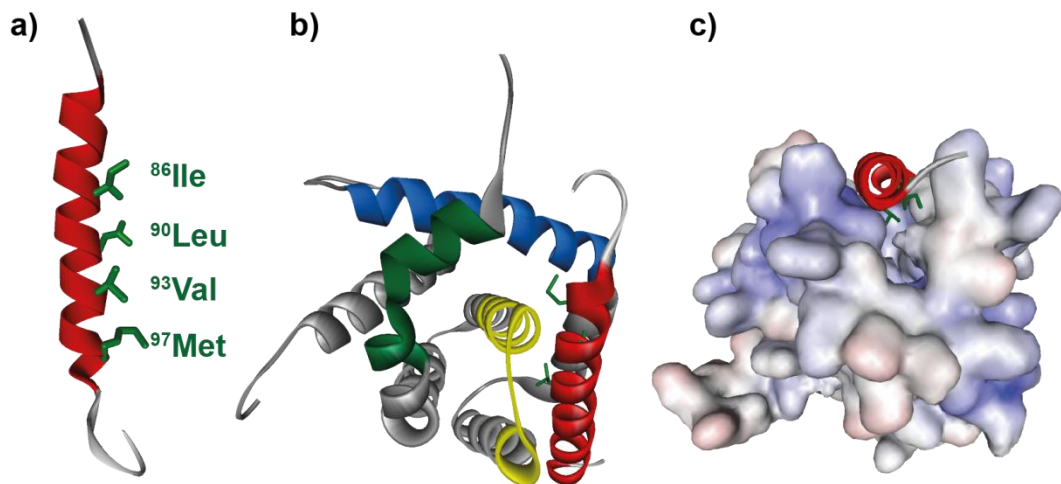
Figure 3.10 – Representations of BID bound to Mcl-1. a) The key side chains within the BH3 region that are essential for binding; b) ribbon diagram of BID BH3 (red helix) and Mcl-1, with the BH1 (yellow), BH2 (green) and BH3 regions of Mcl-1 coloured; c) surface representation of the BID BH3 (red helix) binding into the hydrophobic pocket of Mcl-1, formed by the juxtaposition of BH1, 2 and 3. PDB: 2KBW.

In the context of this investigation, the constrained BID BH3 sequence which has been shown to be effective in killing leukaemia xenografts in mice was used.[3] The BID protein is an indiscriminate binder to all multi-domain proteins and binds into the hydrophobic groove of its partner by projection of [86]Ile, [90]Leu, [93]Val and [97]Met along one face of the α-helical BH3 domain (Figure 3.10). The preceding work provided a foundation for the study of monosubstituted unnatural amino acids as surrogates for stapling, as well as

potential studies on the selectivity of stapled peptides across anti-apoptotic family members.

3.5.1 Peptide synthesis of unlabelled BID peptides

The peptides synthesised for the study of stapled BID peptides encompass the BH3 region of the BID pro-apoptotic protein, utilising the peptide sequence used by Walensky and coworkers (Figure 3.11b, BID-DM).[3] A direct replacement of the disubstituted amino acid positions optimised for the most helical constrained peptide with monosubstituted amino acids allowed a comparison of the two stapling methodologies. In addition, a peptide with 2-aminoisobutyric acid (Aib) was synthesised as a further control, since Aib is known to promote helical character.[180]

The nomenclature of the BID peptide series is similar to that described with the p53 series (3.3.2), with the addition of **disubstituted metathesised** (DM) and **disubstituted unmetathesised** (DU) which used α,α-disubstituted amino acid **16**.

With respect to the modifications of the peptide sequence, tryptophan was added at the *C*-terminus to assist purification and for accurate determination of concentration. In addition, the native methionine residue was exchanged to norleucine which prevents interference of the thioether moiety with Grubbs metathesis.
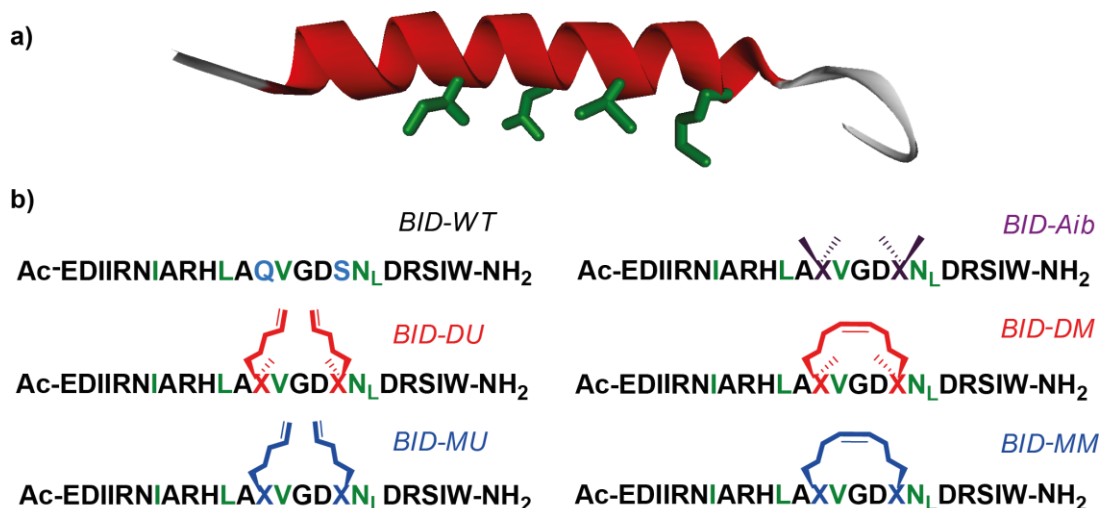
Figure 3.11 – a) The BH3 region of BID (residues 80-102) with the key hydrophobic side chains coloured green; b) sequences of the BID BH3 peptides used in the investigation of mono- and disubstituted unnatural amino acids for peptide stapling. MM and MU retain their definitions from Figure 3.3, and **D**isubstituted **M**etathesised (DM) and **D**isubstituted **U**nmethesised (DU) are also used in further discussions.

BID WT was synthesised on Rink Amide MBHA resin manually on a 0.1 mmol scale to establish which couplings in the sequence were troublesome before using automated peptide synthesis. The first attempt afforded a poor crude recovery of peptide and several deletion sequences in the sterically encumbered [82]IIRN region close to the *N*-terminus. The following repeated synthesis ensured that these residues were double coupled, and the peptide built on a LL (low loading) variant of the resin, which prevented aggregation of the peptide during synthesis and afforded a greater quantity of crude peptide. Purification afforded 24 mg (11%) of pure BID WT, with the low yield attributed to the tendency of the peptide to aggregate during HPLC.

Scale (mmol)	Double Couplings	Crude Yield	Outcome
0.1	None	40%	82IIRN deletions
0.1	82IIRN, 103W	82%	Purified. 11% yield

Table 3.1 - Summary of synthesis attempts of BID WT

Conversely, synthesis of the BID peptide using the unnatural amino acids required several rounds of optimisation before a reliable synthesis and purification was established.

	Peptide	Couplings	Outcome
1	BID DU	A	Deletion of 91A, 95D; acetyl capping
2	BID DU	B	Trace deletion of 91A, 95D; acetyl capping
3	BID DU	C	Successful & purified. 5% yield
4	BID MU	C	Acetyl capping & complete peptide
5	BID MU	C	Successful & purified. 5 % yield

Table 3.2 - Summary of the optimisation of the BID MU and BID DU peptides. Coupling Condition A was double coupling of [82]IIRN and [103]W; B was double couplings of [82]IIRN, [91]A, [95]D and [103]W; C was the same coupling strategy as B, but with 10 equivalents of HATU employed for [91]A and [95]D and with Fmoc deprotection of the unnatural amino acids extending to 30 minutes.

The most common deletion sequences observed for BID DU were [91]A and [95]D, which can be rationalised by the hindered *N*-terminus of a disubstituted amino acid being less efficient during standard coupling conditions. Trial cleavages also identified that the Fmoc protecting group of the disubstituted unnatural amino acid was not fully removed after 10 minutes. Therefore, using HATU as the coupling reagent instead of HCTU and extending the Fmoc deprotection time prevented these deletion sequences from occurring.

Figure 3.12 – Deletion sequences and acetyl capping of the BID DU/MU peptides described in Table 3.2.

Table 3.2 entries 1, 2 and 4 also had unexpected incorporations of an acetyl cap in the sequence. The acetyl capping in the place of the unnatural amino acids in BID DU and BID MU was attributed to traces of acetic acid that were present in the purification of the Fmoc protected monomers. Removal of acetic acid from purification completely eliminated the capping.

On-resin Grubbs metathesis of BID DU and MU was effective, with a >98% conversion in both BID DU and MU to BID DM and BID MM. Cleavage and deprotection using Reagent K afforded respectable crude yields of peptides (typically ~90% for BID DU and MU; ~75% for BID DM and MM), which led to the purification of the stapled BID peptides to afford 7 mg (7%) and 13 mg (10%) of BID DM and BID MM respectively.

The crude peptides typically contained a species with a mass of 44 Da heavier than expected, due to incomplete decarboxylation of the Boc protecting group on [103]W. Decarboxylation was completed by repeated lyophilisation of the crude peptides with 0.1% formic acid added to a mixture of dioxane and water.

The disappointing yields of the purified peptides after HPLC were attributed to the broad UV chromatogram of the crude peptides, which required small injections and shallow solvent gradients to afford peptides of acceptable purity.

Finally, BID Aib was synthesised using a mixture of automated and manual methods, with the region of [91]A(Aib)VGD(Aib)N_L coupled manually with Coupling Strategy C (Table 3.2) and the other residues coupled using automated, non-microwave-assisted conditions. Ultimately, BID Aib was purified to afford 9 mg (10%) on a 0.05 mmol scale.

3.5.2 Protein Expression of Bcl-x$_L$ (no loop)

One of the basic biophysical experiments of the BID BH3 peptide series is calculating inhibitory potency by distrupting a Bcl-x$_L$ PPI. Bcl-x$_L$ 'no loop' is a construct of Bcl-x$_L$ that omits an unstructured region of Bcl-x$_L$ with little effect on its binding potency. Removing the flexible loop region of Bcl-x$_L$ can promote a more crystalline packing behaviour, which would be useful for future structural studies. From a 10 L growth, 19.1 mg of GST–Bcl-x$_L$ was afforded, of which 10 mg of GST–Bcl-x$_L$ was subjected to PreScission Protease to remove the GST tag, which furnished 4.9 mg of Bcl-x$_L$ 'no loop' for binding assays after gel filtration chromatography (4.6 & Appendix IV).

3.6   Biophysical evaluations of BID BH3 peptides

3.6.1 Circular Dichroism of the BID peptides

The secondary structure of BID BH3 peptides was examined in solution by circular dichroism. In order to prevent precipitation and to ensure that the concentration was accurate - an essential factor in circular dichroism - the

peptides were dissolved in 30 % acetonitrile in phosphate buffer (40 mM, pH 7.50).
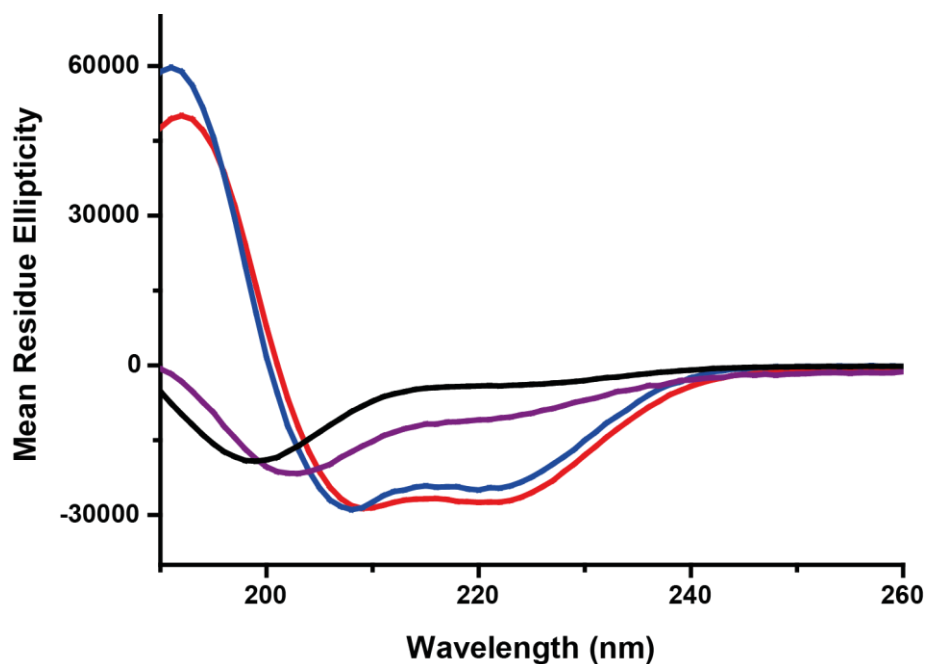
Peptide	% Helicity
BID WT	12
BID MM	73
BID DM	80
BID Aib	31
BID MU	17
BID DU	20

Figure 3.13 – Circular dichroism spectra and the table of % helicities of the BID BH3 peptides investigated. The spectra that have been plotted are emboldened on the table. The normalised ellipticities of the peptides were converted into a percentage of helicity as described by Baldwin and coworkers, and for consistency, by the original stapled BID investigation.[3, 103, 167]

Pleasingly, the DM and MM peptides gave a characteristic α-helix signal, whilst the Aib and wild type peptides displayed minimal helical character. The random coil profile of the wild type peptide confirmed that the quantity of acetonitrile in the buffer was not contributing to promotion of secondary structure. The results are consistent with respect to the DM percentage of helicity (Figure 3.13), but also demonstrated that the monosubsituted amino acid was capable of promoting an α-helical conformation in solution to the same extent. The profiles of the unmetathesised peptides appeared to have a mixture of character - random coil and α-helix - but the amplitude of the signal at 222 nm was insufficient for an α-helical character to dominate (See Appendix

II, 6.1). The exciting CD results provided the first validation of monosubstituted amino acids as hydrocarbon staples, which led into further biophysical investigations.

3.6.2 Enzymatic Degradation

One of the key biophysical markers of the effectiveness of stapled peptides as therapeutic ligands is their resistance to enzymatic degradation. Essentially, the peptide must be unfolded in order to be accommodated into the active site of a protease.[181] Therefore, rigidifying a peptide would decrease its enzymatic lability allowing the peptide to reach its target and perform its function. In order to investigate the effect of the novel monosubstituted amino acid stapling methodology, a degradation study with trypsin was performed. Trypsin selectively digests at the carboxyl side of positively charged residues, such as lysine and arginine.[182] With the BH3 region of BID possessing three arginine residues, trypsin was an ideal protease to monitor the degradation of the peptide by HPLC, and to provide insight on the mechanism of degradation (Figure 3.14).

A suitable ratio of substrate:enzyme of 10,000:1 was established, ensuring that digestion was slow enough to obtain data points over 90 minutes by HPLC. Integration of the UV trace of the undigested peptide and conversion of the area into a fraction undigested allowed calculation of half lives (4.5.1).
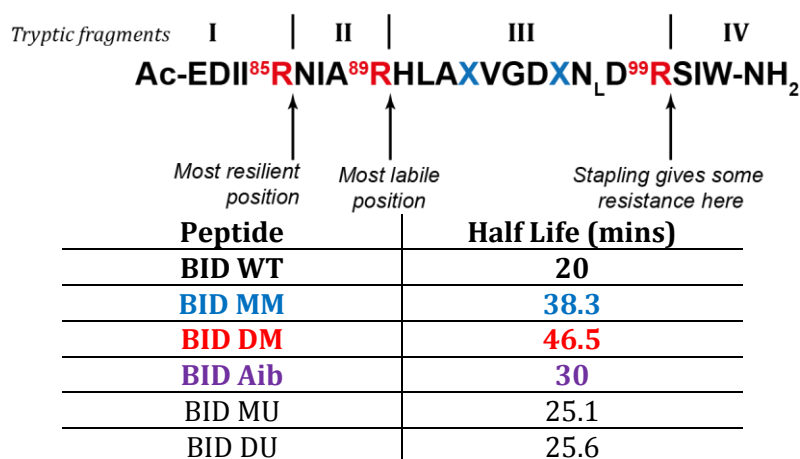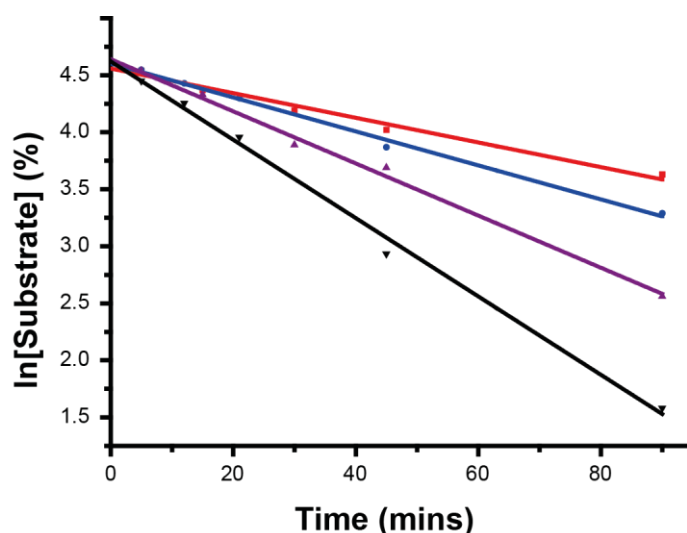
Figure 3.14 – Results of the enzymatic degradation study with BID WT (black), MM (blue), DM (red) and Aib (purple) shown and the cleavage sites of BID when subjected to proteolytic digestion.

It was gratifying that the DM and MM peptides displayed a marked improvement in their protease resistance over the wild type and Aib peptides, but it was also an excellent result that the MM peptide had a half life that was similar to that of the literature DM stapled peptide. The unstapled peptides displayed slight improvements in their resistance over the wild type, which allows the conclusion that constraining the peptide with a hydrocarbon crosslink gives rise to a greater enzymatic resistance for both of the alkenyl amino acids.

HR-LCMS confirmed the mechanism of trypsin digestion of BID BH3 peptides. Regardless of modification, the site at ^{89}R is the most labile position, followed by ^{99}R. Hydrocarbon stapling slows the rate of digestion of the full peptide at all of the positions, but the mechanism of fragmentation is the same

regardless of modification to the peptide. Indeed, the site at [85]R is the least labile site, since the peptide corresponding to Fragments I-II remains after Fragment III-IV has been completely digested.

3.6.3 Fluorescence Anisotropy of BID BH3 peptides

The BID BH3 only proteins are known to bind to all members of the anti-apoptotic Bcl-2 family proteins, as well as to the BAK and BAX effector proteins (Figure 3.15).[6, 172, 183] As such, for assessment of the binding affinity of the BID BH3 peptides using fluorescence anisotropy, the assays with a labelled species and the available protein Bcl-x_L required establishment under direct binding conditions before competition assays could be used.
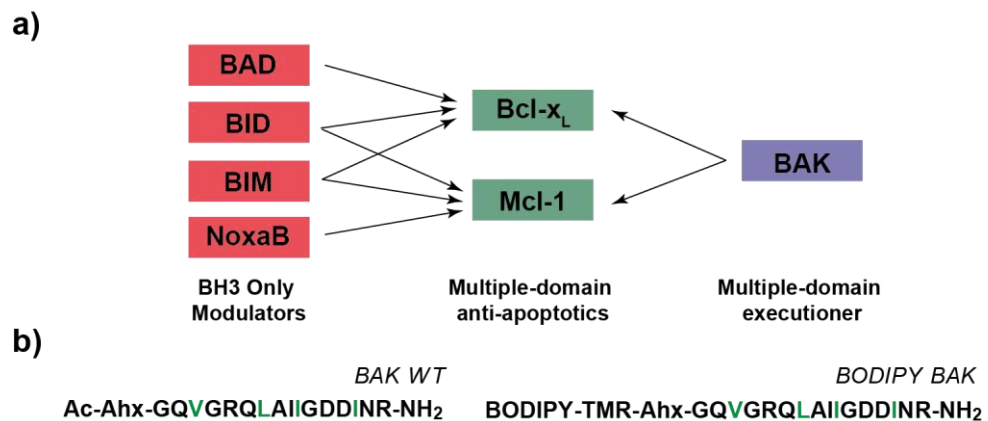
Figure 3.15 –a) Schematic of the binding selectivities of the BH3 only modulator proteins with two of the anti-apoptotic proteins used in the following binding assays; b) sequences of the BAK peptide that was used in the assays for screening of Bcl-x_L inhibitors (synthesised by Dr. P. Prabhakaran).

3.6.3.1 Establishing direct binding Bcl-x_L assays with BODIPY-BAK

The potency studies for BH3 peptides with anti-apoptotic Bcl-x_L were established by utilising the BH3 region of effector protein BAK, which was functionalised with an *N*-terminal BODIPY TMR fluorophore analogous to studies from the laboratory of Gellman (Figure 3.15).[184, 185]

Optimisation of the *protein titration* experiment found that 100 nM of BAK* was required to accelerate equilibration at low protein concentrations. The slow equilibration had been previously observed,[184] and after 20 h, a K_d was calculated to be 4 nM (Figure 3.16) - consistent with that from the literature.[184]
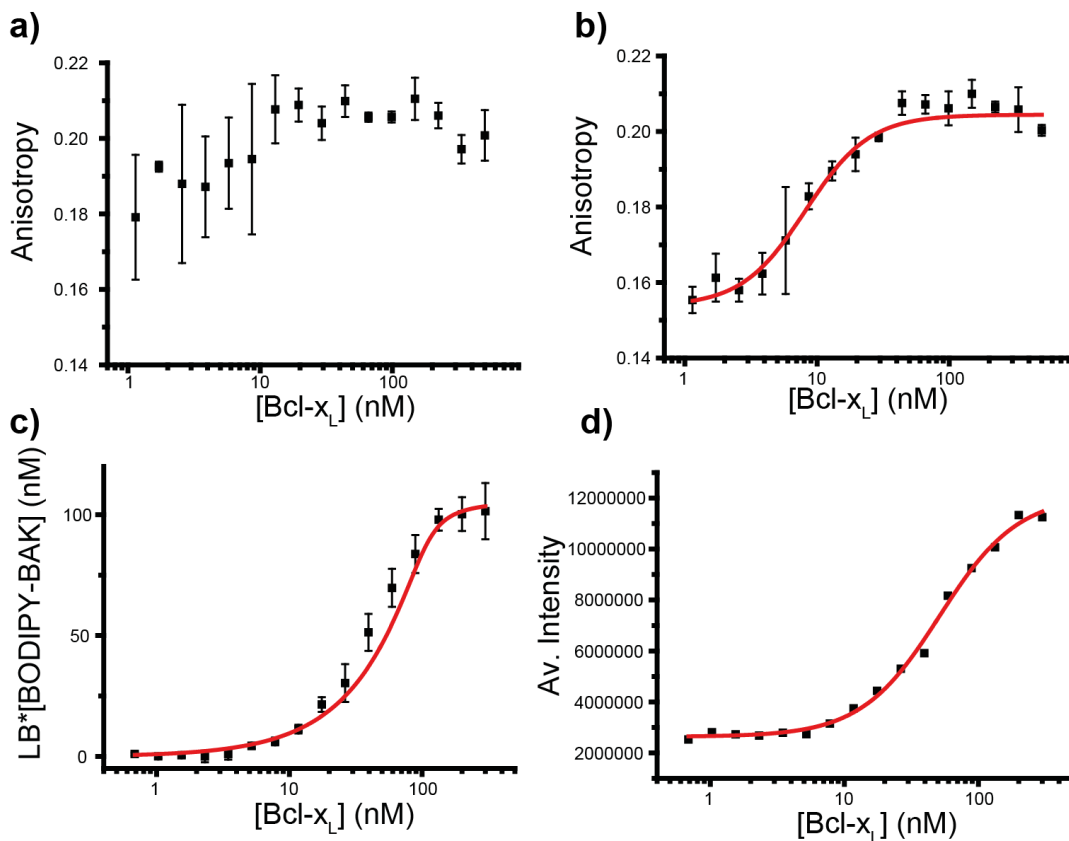
Figure 3.16 – Protein titration of Bcl-x$_L$ with BODIPY-BAK; a) Anisotropy data after 2 h incubation at rt; b) Anisotropy data after 20 h incubation at rt; c) K_d determination of BAK*/Bcl-x$_L$ with [BAK*] set at 100 nM; d) Raw intensity of the data in the direct binding experiment.

It was noticeable that there was a large change in intensity upon binding (Figure 3.16d) which suggests that the fluorophore environment is altered at higher concentrations of Bcl-x$_L$. In addition, the r_{min} value of unbound BAK* was unexpectedly high in the protein titration experiment, which could point to aggregation of BAK*.

To confirm the K_d value from the protein titration, the conditions were reversed and the Bcl-x$_L$ concentration was fixed at 50 nM (henceforth described as a *peptide titration* experiment). This assay gave a lower r_{min} value than that of the protein titration but despite this, a K_d value of 12.5 ± 3.2 nM was extracted (Appendix II, 6.2.3).

3.6.3.2 Competition assays of the Bcl-x$_L$/BAK* interaction

Peptide	IC$_{50}$ (µM)
BID WT	1.44 ± 0.05
BID MM	0.62 ± 0.02
BID DM	1.14 ± 0.04
BID Aib	1.15 ± 0.04
BID MU	2.48 ± 0.11
BID DU	2.94 ± 0.10
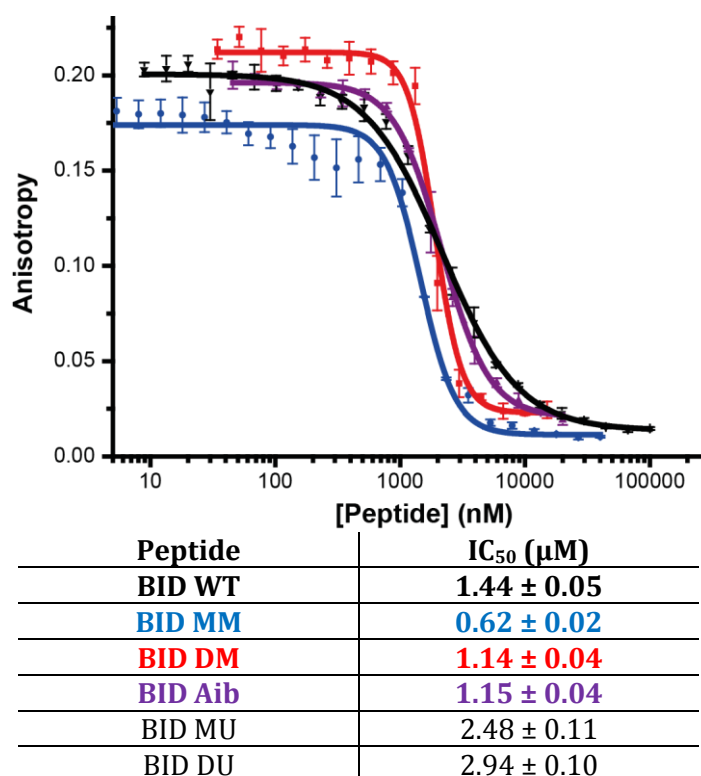
Figure 3.17 – Inhibition curves for a selection of BID BH3 peptides against the Bcl-x$_L$/BAK* interaction, showing BID WT (black), MM (blue), DM (red) and Aib (purple).

With the direct binding assay of Bcl-x$_L$/BAK* established, the competition mode of the assay was set with [Bcl-x$_L$] and [BAK*] at 131 nM and 43 nM respectively. The IC$_{50}$ values calculated for the inhibition of Bcl-x$_L$/BAK* were within a surprisingly narrow range, with the stapled peptides being marginally better inhibitors compared to the wild type peptide. As observed with p53/hDM2, unstapled MU and DU were poorer inhibitors compared to MM and DM, which suggests that the alkenyl amino acid is an unfavourable incorporation, which is mitigated by constraining the peptide. The slopes of the curves were unexpectedly steep, which suggests there may be association of unbound inhibitor and BAK*.

3.7   Discussion and Conclusions

In terms of the synthesis of the different amino acids for peptide stapling, it was found that the route for α,α-disubstituted scaffolds was challenging to optimise, but has the potential for the synthesis of either (*S*) or (*R*) amino acids. In contrast, the nickel complex synthetic route in its current

form only allows access to the (*S*) amino acid since performing two successive alkylations affords racemic amino acids.[158] Whilst the (*S*) amino acid was sufficient for effective crosslinking at *i, i*+4 positions, future investigations with stapling at *i, i* + 7 requires an (*R*) amino acid.[2] One potential future investigation could focus on the use of an analogous complex and stereoselective alkylations mediated through phase transfer catalysis.[159]

Initial studies with the p53 peptide were unfortunately insufficient to provide evidence for whether *des*-methyl amino acids were suitable for use in stapled peptides. The circular dichroism data does not show an effective promotion of a helical structure of the peptide after stapling. The reduced potency of p53 MM compared to p53 WT was also insufficient to demonstrate the utility of monosubstituted amino acids as suitable staples.

The BID BH3 investigation provided conclusive evidence that the *des*-methyl amino acids were capable of recapitulating the results of their widely reported disubstituted analogues, since a direct comparison of BID DM and BID MM peptides was available in this investigation. CD and enzymatic degradation data demonstrated the utility of *des*-methyl amino acids as monomers for hydrocarbon stapling for structural constraint, whilst the slight improvement of $Bcl-x_L$/BAK* inhibition compared to BID WT was pleasing.

Walensky and coworkers have previously reported that BID DM is >10 fold more potent than BID WT in binding studies with homologous Bcl-2.[3] Thus, it would have been expected that BID DM would bind more strongly to **$Bcl-x_L$** than BID WT. Since this was not observed to such a magnitude, an investigation into potential selectivity of stapled peptides against a homologous series of targets could be opened.

Chapter 3b: Investigation into the modulation of potency of hydrocarbon stapled peptides

Chapter 3a proved that *des*-methyl amino acids were suitable as monomers for hydrocarbon stapling, matching the helix promotion and enzymatic resistance characteristics of widely used disubstituted amino acids in a BID BH3 peptide. Interestingly, the IC_{50} values of the inhibition of Bcl-x$_L$/BAK* were similar for constrained and unmodified BID BH3, which appears to counter previous hypotheses that an increase in helical character of a peptide results in an increase of potency of the peptide with its binding partner.[3, 127]

Given the results of the otherwise overlooked monosubstituted stapled peptides, it was necessary that further evaluation of both monosubstituted and disubstituted stapled peptides was required to rigorously challenge the original hypotheses of stapled peptides. The required experiments were to establish a direct binding method for BID BH3 peptides, firstly to directly calculate K_d and secondly to provide a handle on the thermodynamic factors associated with the binding of stapled peptides with their receptors - experiments which are lacking in the literature.

In addition to this, the selectivity of the stapled BID BH3 peptides with the other members of the Bcl-2 family has not been previously examined. BID DM and BID MM would provide further data on whether there is a difference in potency with a homologous anti-apoptotic protein, Mcl-1, in comparison to Bcl-x$_L$ as well as differences in potencies between mono- and disubstituted amino acids.

Furthermore, the monosubstituted amino acids can be applied to other disubstituted stapled peptides in the Bcl-2 family that have already been proven effective ligands, to further assess the application of *des*-methyl amino acids in stapled peptides. Finally, structural and *in cellulo* experiments were required to formally supplement the data obtained from circular dichroism and test the hypothesis that hydrocarbon stapled peptides impart an improvement in cellular uptake over unmodified peptides.

3.8 Peptide synthesis of BIM BH3 and FITC-labelled BID BH3 peptides

3.8.1 FITC-BID Peptide Synthesis

One particular limitation of the fluorescence anisotropy competition assay performed in 3.4.2.1 and 3.6.3 is that a direct inhibition constant (K_i) could not be calculated from the data. This was due to the fluorophore unbound anisotropy plateau in the competition assay being lower than the unbound anisotropy plateau in the direct binding experiment, which may arise from BAK* aggregating with the titrated inhibitor upon displacement (Appendix II, 6.2.1). Therefore, functionalising the BID peptides with a fluorescein label could allow access to direct binding fluorescence anisotropy experiments and thus calculation of K_d.

The sequences of the peptides for labelling are identical to those used in Figure 3.11, with the exception of further functionalisation of the *N*-terminus with either 6-amino hexanoic acid (Ahx, in the case of the wild type)[6] or β-alanine (for MM*, DM* and Aib*)[3] followed by coupling with fluorescein isothiocyanate (FITC). The linkers were chosen based on literature precedent and were necessary to prevent excision of the FITC tag.[186] The abbreviations of the peptides are the same as those used in Figure 3.11 and fluorescently labelled peptides are denoted with an asterisk.

Figure 3.18 – a) Sequences of the FITC labelled stapled peptides, which is the same for MM*, DM* and Aib*. The wild type (WT*) uses a 6-aminohexanoic acid linker. B) Fluorescein isothiocyanate (FITC).

The peptide synthesis, based on all of the optimisations outlined in 3.5.1 used low loading rink amide MBHA resin. In order to prevent any complications between Grubbs' catalyst and the FITC label, the metathesis was performed before the final Fmoc deprotection and coupling of FITC. Cleavage, deprotection

and purification of the peptides was complicated by the hydrophobic nature of the peptide and label to cause streaking during HPLC, but the four peptides were afforded after synthesis on a 0.05 mmol scale with yields of 6.5 mg (7%), 9.9 mg (10%), 23 mg (21%) and 9.25 mg (10%) for WT*, Aib*, MM* and DM* respectively. Whilst the purified yields of these peptides were low, the quantities of peptide that were afforded were sufficient for *in vitro* and preliminary *in cellulo* experiments.

3.8.2 BIM BH3 Peptide Synthesis

After having successfully established the use of *des*-methyl amino acids with the BID BH3 peptide, the methodology was expanded into another area of investigation within the Bcl-2 family of pro-apoptotic proteins to investigate the possibility of selectivity of stapled BH3 ligands with Bcl-2 family proteins.

The BIM BH3 region is analogous to that of BID, matching its binding promiscuity by binding to all of the anti-apoptotic proteins in the Bcl-2 family.[6, 172] Areas of sequence redundancy are evident when comparing the BH3 regions of BID and BIM, with the key binding residues oriented along the *i, i+4, i+7 and i+11* face of the BH3 helix.
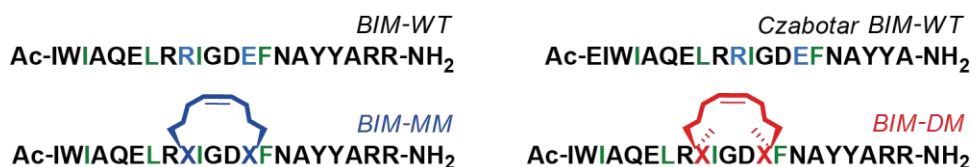
Figure 3.19 – Sequences of the BIM BH3 peptides that have been studied. BIM WT and BIM DM have been previously characterised by Walensky and co-workers.[119] Czabotar and coworkers have studied stapled BIM peptides using the sequence labelled Czabotar BIM-WT,[131] with the substitution positions of the unnatural amino acids the same as BIM-DM. The green residues are the key hydrophobic side chains.

Hydrocarbon stapling of the BIM BH3 region has also been previously examined, with disubstituted amino acids replacing the native [94]Arg and [98]Glu residues.[119, 131] Incidentally, the results of stapling of the BIM BH3 region by two different research groups have provoked a debate into the effectiveness of hydrocarbon stapling as a suitable therapeutic strategy. Walensky and coworkers demonstrated, in accordance with their previous work, that stapling the BH3 region of BIM improves helicity (20% to 81%), potency and cell uptake of the modified peptide.[122] In contrast, the research of Czabotar and coworkers

shows that despite using the same position of the hydrocarbon stapling, a modest increase of helicity is observed (20% to 39%) with binding affinity and cellular uptake not improved.[131]

A recent exchange of publications[122, 131, 132, 187] has hypothesised that the sequence of the peptide is vital to its activity *in vitro* and *in cellulo*, but for the purposes of this investigation, the peptide sequence characterised by Walensky and coworkers was chosen.[122]

The synthesis and purification of the BIM series of peptides was originally carried out by P. Rowell, who was able to effectively synthesise and purify the wild type peptide on a scale of 0.1 mmol with 17 mg of pure peptide obtained (41% crude yield, 6% purified), however, the unnatural variants were not effectively synthesised or purified.

The peptides for hydrocarbon stapling were synthesised on a 0.075 or a 0.1 mmol scale (BIM DM and BIM MM respectively) using analogous procedures to those reported in 3.5.1, where the first 8 residues were built using an automated peptide synthesiser. The unnatural amino acids were subsequently coupled manually, and the remaining 8 residues coupled using automated methods. After on-resin Grubbs' metathesis, the MM and DM BIM peptides were pleasingly obtained in high purity with no observed deletions. Semi-preparative HPLC afforded 21.5 mg of DM BIM (32%) and 9.2 mg of MM BIM (23% based on 40 mg crude purified).

3.9   Circular Dichroism

After the synthesis of the FITC labelled BID BH3 and BIM BH3 peptides, their secondary structure in aqueous solution was assessed to verify whether the FITC tag altered α-helicity of BID BH3 and whether α-helical character of BIM BH3 was improved after stapling.

3.9.1 Circular Dichroism of FITC-BID Peptides

It was confirmed that the FITC labelled peptides had a degree of helicity that was consistent with those observed in 3.6.1, with a slight decrease in % helicity seen for the stapled peptides, but with an increase of 10% of the wild type with respect to its unlabelled analogue (3.6.1). Whilst the CD profiles of

BID WT* and BID Aib* did not show an overriding random coil profile as previously observed, they are similar to those of the BID MU and DU (Appendix II, 6.2.1).
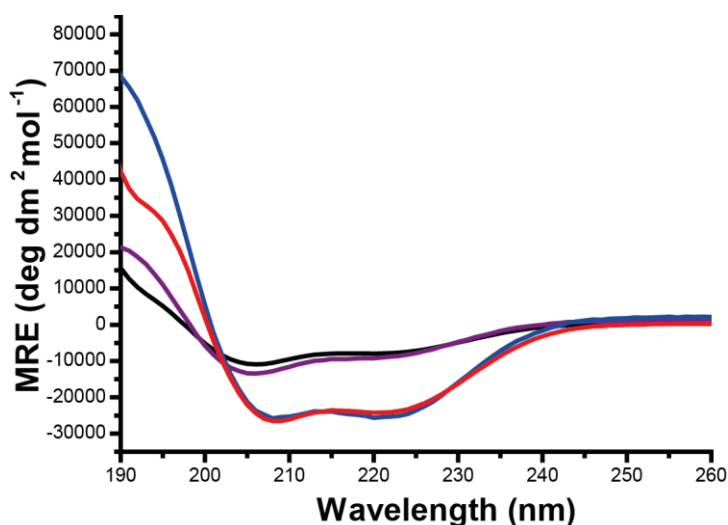
Peptide	% Helicity
BID WT*	23
BID MM*	74
BID DM*	70
BID Aib*	25

Figure 3.20 – Circular dichroism of the FITC labelled peptides including their percentage helicities: BID WT* (black), BID MM* (blue), BID DM* (red) and BID Aib (purple).

The maximum scanned wavelength was also increased to 500 nm, to observe any possible induced circular dichroism[188] of the FITC tag with the BID peptides. The absence of a CD signal at 490 nm demonstrated that there was no induced circular dichroism, which suggested that the fluorophore was capable of moving freely, instead of forming hydrophobic contacts with side chains of the residues.

3.9.2 Circular Dichroism of BIM BH3 Peptides

Previously reported data into the helical content of the stapled BIM BH3 peptides has been contradictory,[119, 122, 131] so the circular dichroism experiment was designed so that the peptides were compared in buffer and buffer containing TFE in order to calculate the 'maximum helicity' of the wild type BIM BH3 peptide and to evaluate the extent to which hydrocarbon stapling introduces helical character.

Peptide	% Helicity (Buffer)	% Helicity (30% TFE)
BIM WT	20	70
BIM MM	57	61
BIM DM	59	62
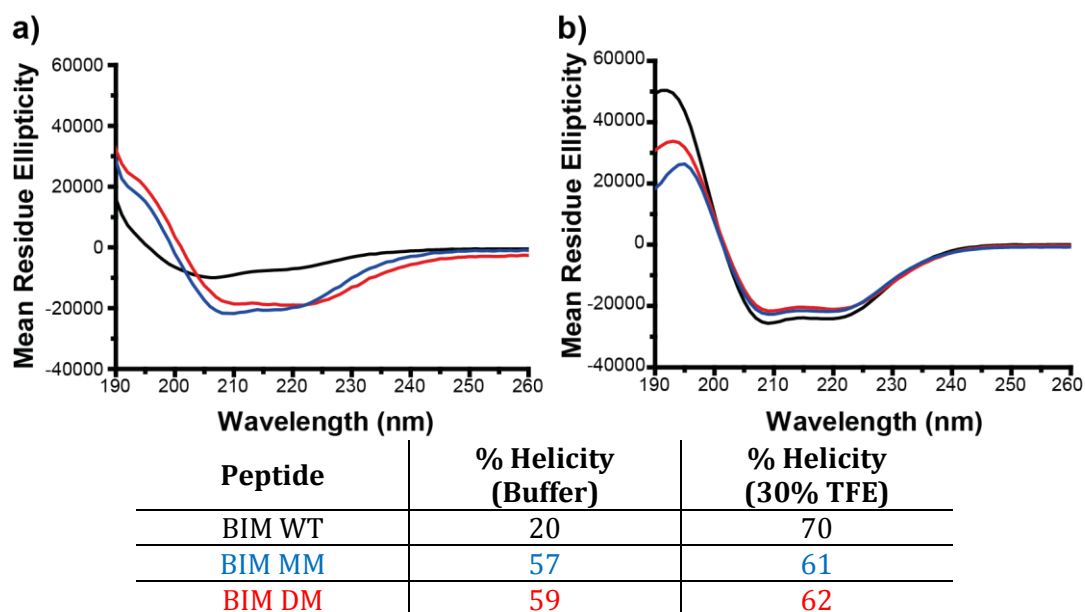
Figure 3.21 – Circular Dichroism spectra of BIM BH3 peptides BIM WT (black), BIM DM (red) and BIM MM (blue) in a) 15% Acetonitrile in 40 mM sodium phosphate buffer and b) with 30% v/v TFE added to the buffer.

The circular dichroism results are consistent in the helical nature of the wild type peptide, showing a random coil profile and a low helical percentage (20%). The two stapled peptides, BIM MM and BIM DM have equivalent helical contents, with 57% and 59% respectively. The addition of the TFE improved the helical content to 70% for the wild type, with a minimal increase of helical character seen for the MM and DM BIM peptides (61% and 62% respectively).

In contrast with precedents,[122] a moderate helicity was seen for both of the stapled peptides, but TFE does not vastly improve their helical contents, which demonstrates that the hydrocarbon staple rigidifies the peptide. Compared to BID, the moderate helicity of BIM DM and MM is somewhat surprising, considering that BID DM and MM possess high helical content in a peptide that is three residues longer (3.6.1). Nevertheless, the *des*-methyl amino acids were capable of matching the helical content of the disubstituted amino acids in this experiment.

3.10 Inhibitor Selectivity Investigations: Competition Assays of Mcl-1/NoxaB*

Stapled BID BH3 peptides were effective inhibitors of the Bcl-x_L/BAK* PPI, but only marginal improvement in inhibitory potency was observed after constraining the peptide, contrary to literature precedent with anti-apoptotic Bcl-2. Therefore, with homologous anti-apoptotic Mcl-1 available,[III] the stapled BID BH3 peptides could be evaluated to provide insight into possible selectivities of a stapled ligand across a family of degenerate proteins. Also, with BIM BH3 in hand, the selectivity profile of different hydrocarbon stapled ligands could be constructed.
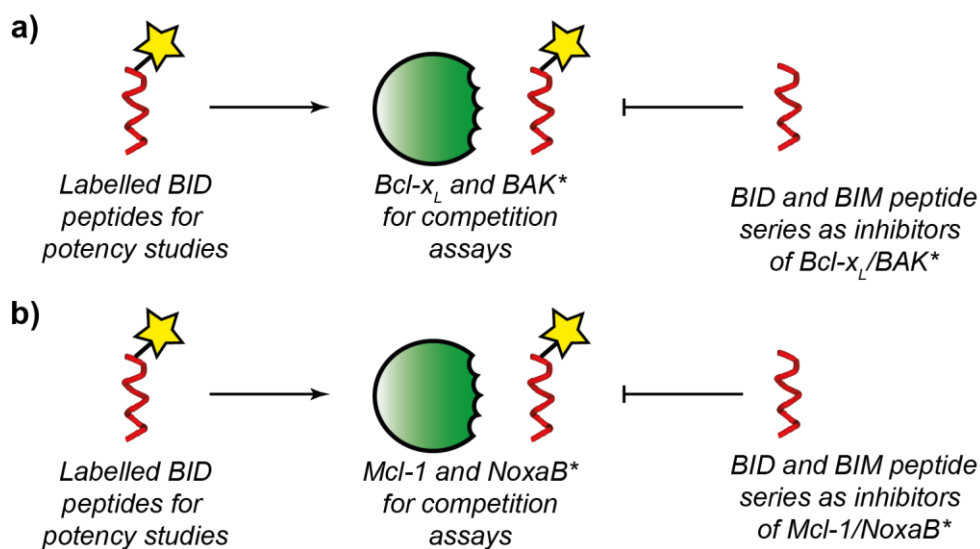
Figure 3.22 – A routemap of the fluorescence anisotropy assays performed with the various members of the Bcl-2 family; a) Using Bcl-x_L as the complete protein and b) Mcl-1 as the complete protein.

Thus, a collaborative effort was made to establish a fluorescence anisotropy assay to test ligands for Mcl-1 affinity. With Dr. K Long and V. Azzarito, an assay with a FITC-labelled NoxaB* peptide (the 16-residue BH3 region of pro-apoptotic NoxaB) was established for the testing of potential Mcl-1 ligands. A K_d of 18.7 ± 0.9 nM was calculated for the direct binding

---

[III] Mcl-1 was expressed by Dr. A. Bartlett or Dr. J. Miles in the laboratory of Dr. T. Edwards (University of Leeds). NoxaB* synthesised by Dr. P. Prabhakaran.

Mcl-1/NoxaB* assay, consistent with literature precedents (assay development is described in Appendix II, 6.2.2).[172, 189]

3.10.1 BID BH3 Inhibitors of Mcl-1/NoxaB*

After optimising the Mcl-1/NoxaB* competition assay conditions to use 150 nM and 50 nM of Mcl-1 and NoxaB* respectively, all of the unlabelled BID BH3 peptides were titrated and afforded an expected decrease in anisotropy as NoxaB* was displaced from Mcl-1. The BID series gave a surprising series of potencies, with the wild type BID being the most potent inhibitor with an IC_{50} of 0.38 μM compared to the IC_{50} values of 0.80 μM and 1.60 μM for DM and MM respectively. Interestingly, the value for the unstapled MU peptide was 2.80 μM, suggesting that the replacement of the native residues with the alkenyl unnatural amino acids is unfavourable to binding, but conformationally rigidifying the peptide provides a compensation in this binding penalty.
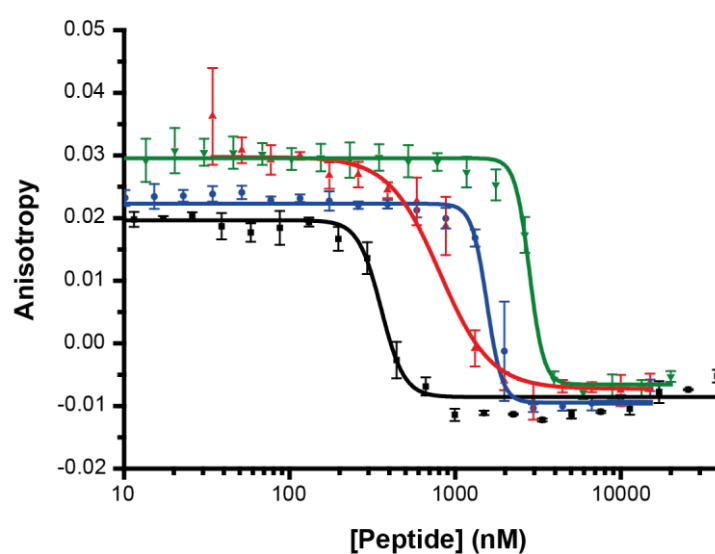
Peptide	IC_{50} (μM)
BID WT	0.39 ± 0.08
BID MM	1.60 ± 0.12
BID DM	0.80 ± 0.07
BID MU	2.80 ± 0.07

Figure 3.23 – Inhibition curves for a selection of the BID BH3 peptides against the Mcl-1/NoxaB* interaction, with BID WT (black), MM (blue), DM (red) and MU (green) illustrated.

The results of the unlabelled BID BH3 peptides suggest there is partial selectivity of stapled peptides, where the constrained peptides are less potent

than unmodified BID WT for inhibiting Mcl-1/NoxaB*, but the potency range across the series is quite narrow.

One caveat of the competition assays is that IC_{50} is more useful for comparing across a family of inhibitors, rather than a family of proteins, since Bcl-x_L/BAK* is more tightly bound than Mcl-1/NoxaB* (3 vs 19 nM respectively). Therefore, direct binding experiments are vital to understanding whether hydrocarbon stapling modulates binding affinity with a family of proteins.

3.10.2   BIM BH3 Inhibitors of Bcl-2 family PPIs

So far, the hydrocarbon stapling of BID BH3 has afforded marginal improvement or diminishment of inhibitory potency of Bcl-2 family protein-protein interactions. With the BIM BH3 stapled peptides in hand, the trends and selectivity of homologous hydrocarbon stapled ligands was open to investigation.

Peptide	IC_{50} vs Mcl-1/NoxaB*	IC_{50} vs Bcl-x_L/BAK*
BIM WT	0.05 ± 0.002 µM	0.32 ± 0.07 µM
BIM MM	1.77 ± 0.25 µM	11.9 ± 3.8 µM
BIM DM	0.89 ± 0.15 µM	4.00 ± 0.62 µM
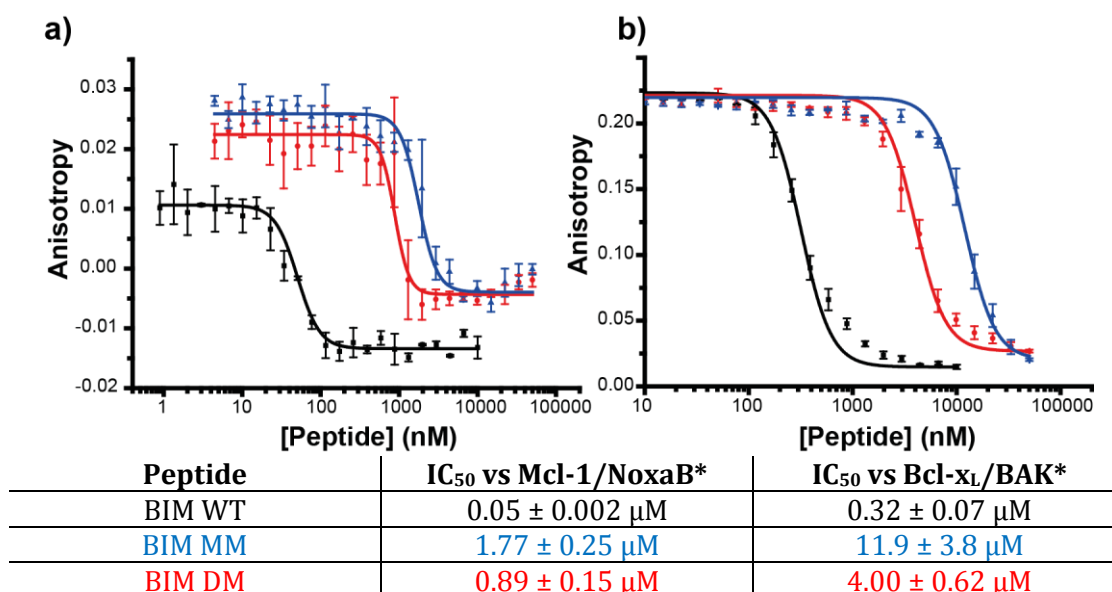
Figure 3.24 - Fluorescence anisotropy competition curves of the BIM BH3 peptides; BIM WT (black), BIM MM (blue) and BIM DM (red) for their inhibition of a) Mcl-1/NoxaB* and b) Bcl-x_L/BAK* (right) protein-protein interactions.

Against Mcl-1, the stapled BIM peptides possess similar IC_{50} values and a similar trend in inhibition (where DM is more potent than MM) compared to their BID BH3 peptides, but these peptides are clearly less potent than the wild type peptide (Figure 3.24a). Indeed, the IC_{50} of the wild type peptide surpasses

that of the wild type BID by an order of magnitude, which is surprising considering that a similar trend to the BID peptides was expected.

Against Bcl-x$_L$, the same trend is also seen, with BIM MM being the weakest peptide, with BIM DM being an order of magnitude weaker as an inhibitor than BIM WT (Figure 3.24b). These results are somewhat alarming, considering that literature precedent states that the BIM DM peptide has a threefold improvement of binding affinity compared to the wild type peptide.[122] But, these results are *consistent* with the observations of Czabotar and co-workers,[131, 132] where stapled BIM DM peptides are weaker ligands towards Mcl-1 and Bcl-x$_L$ (Table 3.3).[131]

	Mcl-1	Bcl-xL
Czabotar BIM DM	K$_i$ 3.4 nM	K$_i$ 300 nM
Czabotar BIM WT	K$_i$ <1.4 nM	K$_i$ 11 nM
Walensky BIM DM	K$_d$ 17 nM	EC$_{50}$ 16.2 nM
Walensky BIM WT	-	EC$_{50}$ 52.0 nM

Table 3.3 - Summary of binding constants of reported BIM peptides against Mcl-1 and Bcl-x$_L$ from Czabotar[131] and Walensky.[119, 120]

However, the difference in the trends that have been observed may arise from the different methods that were used to calculate the K$_d$ of the peptides. Walensky and coworkers calculated their K$_d$ value based on a direct binding assay with FITC-labelled BIM peptides and by using a different Bcl-x$_L$ construct that retains its GST tag in the assay.[119] Whilst it would have been expected to observe an IC$_{50}$ value that is weaker than reported K$_i$ values in the competition assay, considering that the BIM peptides are displacing a fluorophore with a K$_d$ of 4 nM, it was surprising that the stapled peptides - especially in the case of the MM peptide - were considerably weaker than the unmodified control.

BID and BIM BH3 share some sequence redundancies, but the hydrocarbon staple position was in the same location for both peptide series. The significant result from the competition assays - where stapling of BIM BH3 in the investigated positions was detrimental to inhibitory activity - demonstrated that hydrocarbon stapled peptides must be designed on a per-ligand, per-interaction basis, rather than assuming that the best stapling position of one ligand is the same across a homologous series of ligands. Future directions for the BIM peptide series will be the development of an orthogonal

biophysical assay, considering these results are contrary to the majority of published research in hydrocarbon stapling.

3.11 Direct Binding Studies of FITC labelled BID BH3 Peptides

In competition assays, hydrocarbon stapling of BID BH3 peptides with either mono- or disubstituted amino acids had effectively no change of potency for inhibiting Bcl-x$_L$/BAK*; stapled peptides were less potent for inhibiting Mcl-1/NoxaB* compared to unmodified controls. To explore further these findings, FITC-labelled BID BH3 peptides were employed in direct binding fluorescence anisotropy assays with Mcl-1 and Bcl-x$_L$.

3.11.1 Direct Binding of Mcl-1 and FITC-BID BH3 peptides

3.11.1.1 Protein Titration of Mcl-1

The first attempts at direct binding with all of the labelled peptides in the buffer used in all prior fluorescence anisotropy experiments (40 mM sodium phosphate, 200 mM NaCl, 0.02 mg mL^{-1} BSA, pH 7.50) displayed no change in anisotropy across the dilutions of Mcl-1. As a result, the buffer was altered to Tris (50 mM Tris, 140 mM NaCl, pH 7.50) which has been used within the Bcl-2 literature.[3, 119][6, 189] After this modification, there was a clear change in anisotropy detectable for all of the labelled peptides.
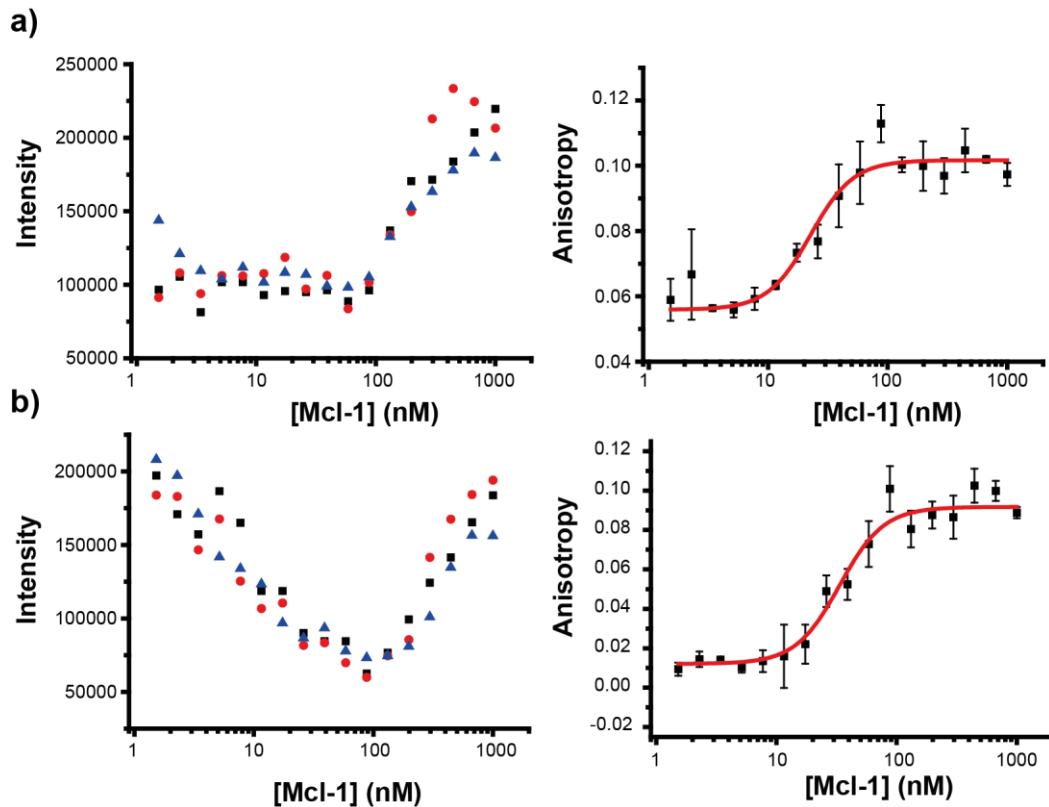
Figure 3.25 – Slow equilibriation of the BID WT* peptide against Mcl-1 a) After 2 hours and b) after 20 hours incubation. It is noticeable that the lower anisotropy plateau settles after 20 h, but the measured intensity increases at lower protein concentrations.

Interestingly, the equilibration of the labelled BID peptides was slower than NoxaB*, where the best results were often obtained after incubation of the plates at room temperature for 18-24 hours, particularly at lower concentrations of the titrated Mcl-1, suggesting that the larger BID peptides had slower binding kinetics than the smaller NoxaB*. It was also noteworthy that, similar to the Bcl-x_L/BAK* titrations, the equilibration of the tracer with the protein (Figure 3.25) was slow, which was not observed with NoxaB*. As the incubation time increased, the lower anisotropy plateau settles, but the intensity began to change in a V-shaped profile. This suggested that the environment of the unbound FITC-labelled peptide was changing during the slow equilibration process.
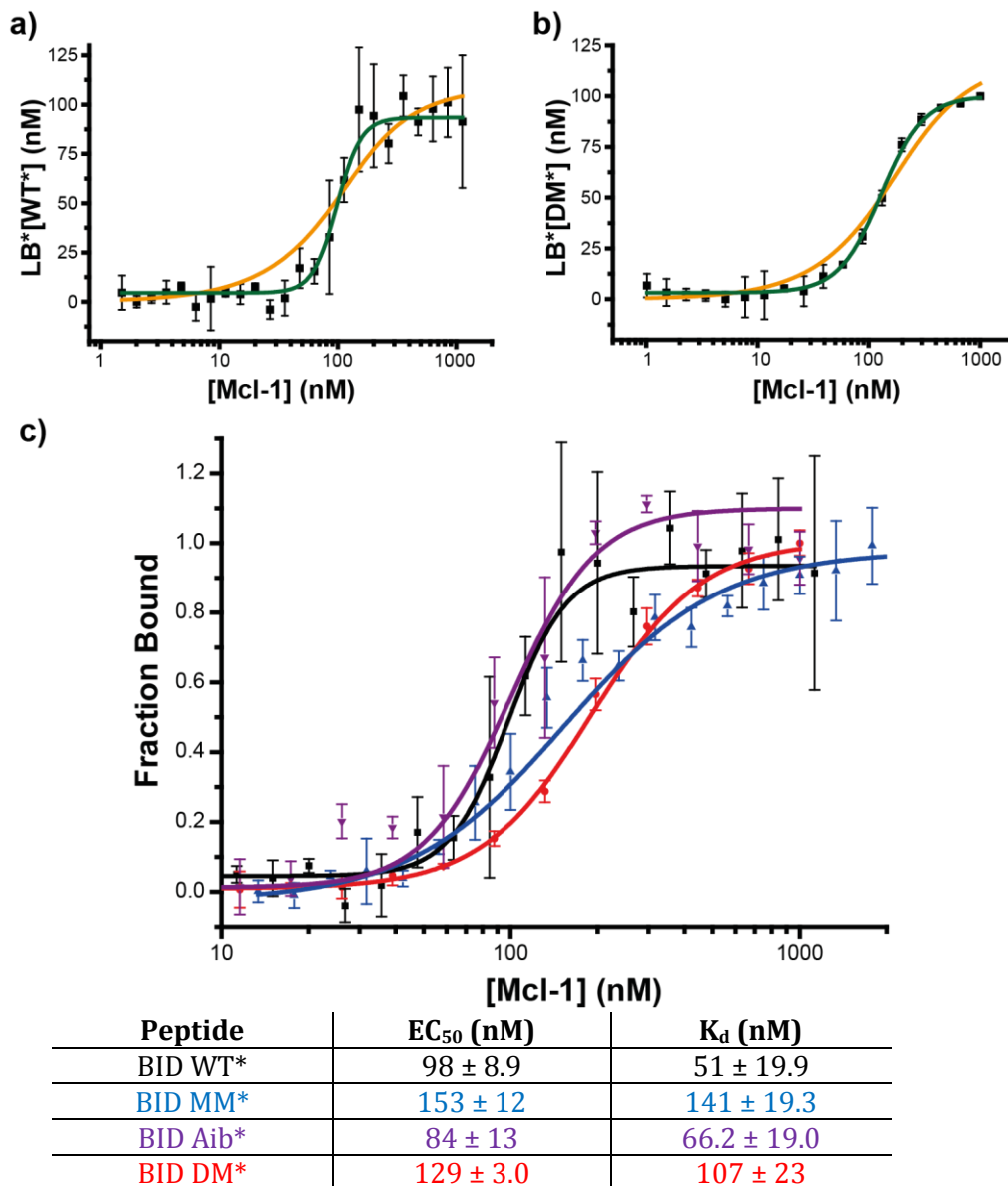
Figure 3.26 – Direct binding curves of FITC BID BH3 peptides with Mcl-1. a) and b) are the curves for BID WT* and BID DM* respectively, fit by the K_d model (orange) and logistic model (green); c) overlaid curves for all of the FITC BID BH3 peptides (100 nM), fitted with the logistic model.

Peptide	EC$_{50}$ (nM)	K$_d$ (nM)
BID WT*	98 ± 8.9	51 ± 19.9
BID MM*	153 ± 12	141 ± 19.3
BID Aib*	84 ± 13	66.2 ± 19.0
BID DM*	129 ± 3.0	107 ± 23

Interestingly, the trend observed in the direct binding studies showed that the K_d and the EC$_{50}$ values of the stapled peptides are twofold weaker than those of the WT* and Aib* peptide, but the marginally more helical DM* peptide has an improved binding affinity compared to MM*. In spite of the weaker binding of the stapled peptides, this is a promising result, since the K_d values are in the same region as those previously reported and that the trend of K_d values match the IC$_{50}$ trend observed in the inhibition of Mcl-1/NoxaB* (3.10.1).[172, 189, 190]

A problem in the calculation of the K_d values of the peptides was the difficult fitting of the data to a 1:1 K_d binding model, which either misinterprets the shape of the curve or overestimates the top plateau of the curve (which represents all of the tracer bound to the protein, and must therefore equal the tracer concentration). The origin of this may arise from non-specific binding or aggregation of the tracer prior to binding to the protein - a reasonable scenario considering the hydrophobic nature of the stapled crosslink and the FITC tag. As a result, EC_{50} values were also considered, which allow the slope of the curve to be accounted for.

3.11.1.2   *Peptide Titration of FITC-labelled peptides with Mcl-1*

In order to corroborate with the K_d values obtained for the protein titration with Mcl-1, the FITC-labelled peptides were titrated against a fixed concentration of Mcl-1 (100 nM). This experiment mirrors the protein titration whereby anisotropy is lower at higher concentrations of FITC labelled peptide.

Peptide	K_d (nM)
BID WT*	70.6 ± 15.0
BID MM*	N.D.
BID Aib*	15.4 ± 2.7
BID DM*	17.2 ± 3.7
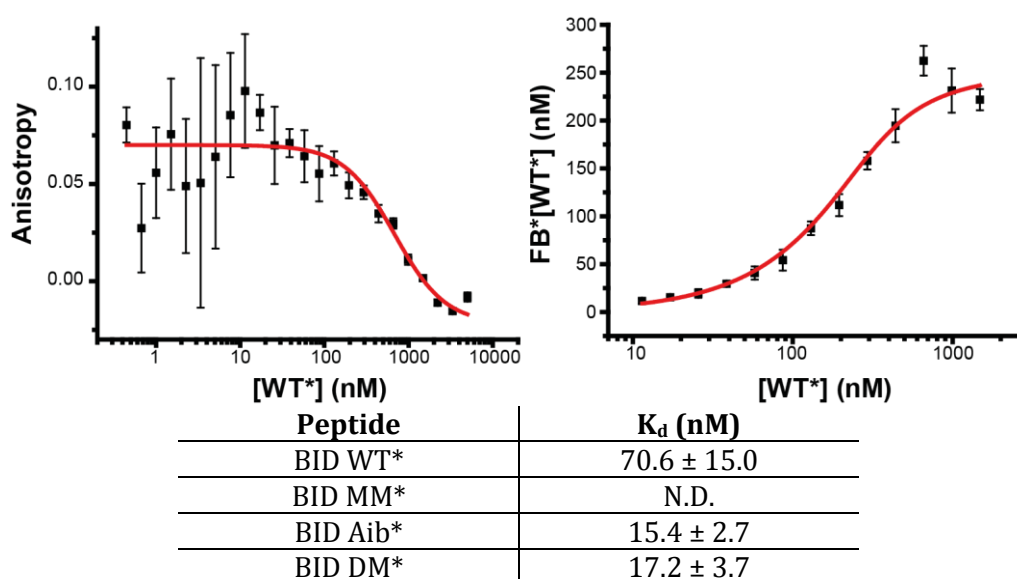
Figure 3.27 – Peptide titration of BID WT* against Mcl-1 and a table of K_d values calculated from the peptide titrations of the other FITC labelled peptides (all curves are presented in Appendix II, 6.2.5). The K_d of MM* was not calculated because a bottom plateau was absent.

The results for the peptide titration do not completely match those of the protein titration, which has been previously observed elsewhere.[12, 141, 191] The titration of the FITC-labelled peptide was hindered by the resolution of the

plate reader. At higher concentrations of the tracer, the decrease in anisotropy can be contributed by an unequal saturation of the polarised emission channels whereas at lower concentrations of the peptide, the poor signal to noise ratio obscured the r_{max} plateau.

3.11.2   Protein titration of FITC-BID peptides with Bcl-x_L.

A protein titration was performed with the FITC-labelled BID peptides and Bcl-x_L in an analogous manner to Mcl-1 to calculate binding affinities of these peptides.
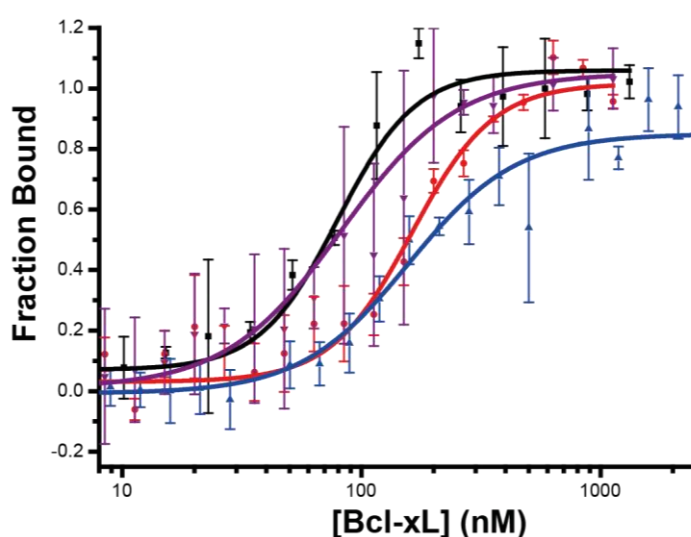
Peptide	EC$_{50}$ (nM)	K$_d$ (nM)
BID WT*	79.3 ± 6.0	20.8 ± 6.6
BID MM*	186 ± 24	246 ± 42
BID Aib*	57 ± 16	59.5 ± 11
BID DM*	159 ± 13	168 ± 19

Figure 3.28 – Direct binding curves and EC$_{50}$/K$_d$ values of the FITC labelled BID peptides (100 nM) against Bcl-x_L.

Similar results were also obtained for Bcl-x_L when compared to Mcl-1, with the unstapled peptides having the strongest affinity compared to the stapled peptides, but, the difference in the K$_d$ values between the stapled peptides and the unmodified peptides against Bcl-x_L is more prominent than those obtained against Mcl-1.

This is not wholly reflected in the IC$_{50}$ values of the unlabelled peptides against Bcl-x_L/BAK*, which were broadly similar across the BID BH3 series. Similar to the direct binding assays with Mcl-1, there are some complications in the fitting of the binding data to a 1:1 binding model. In spite of this, the K$_d$

value of the WT* peptide was consistent with those previously reported.[172] The K_d values obtained here demonstrate that hydrocarbon stapling had an adverse effect on binding affinity, which was not observed in the inhibition of Bcl-x_L/BAK*. Given that Bcl-x_L/BAK* has a K_d of 4 nM, the weaker BID BH3 inhibitors would have a narrow distribution of IC_{50} values. Therefore, the direct binding experiments have been vital to assess how potency of the BID BH3 peptide is modulated by hydrocarbon stapling.

The reverse titration, with the concentration of the labelled peptide varied against a fixed concentration of Bcl-x_L was also attempted for all FITC BID peptides (Appendix II, 6.2.5). However, the errors of fitting, in addition to the experimental restrictions of the peptide titration assay rendered the data unusable for the extraction of $K_{d.}$

3.12 Structural Characterisation of BID BH3

To complement the results from binding studies and to further reinforce the circular dichroism results from 3.6.1, the BID BH3 peptides required further structural characterisation.

3.12.1 X-Ray Crystallography of BID MM and Mcl-1

X-ray crystallography of ligands bound to their targets is seen as a gold standard of characterisation, which allows the confirmation of binding sites and the binding conformation of the ligand. Since BID MM was the weakest peptide in the BID BH3 series in direct binding studies, X-ray crystallography could confirm whether the hydrocarbon crosslink was interfering with the binding site in a similar way to the oestrogen receptor/coactivator interaction.[129]

Dr. J. Miles performed crystal trials with BID MM and Mcl-1 to grow rod-shaped crystals which were fluorescent under UV irradiation. X-ray scattering was performed at Diamond and solved to afford a complex of BID MM with Mcl-1 at a resolution of 1.43 Å.
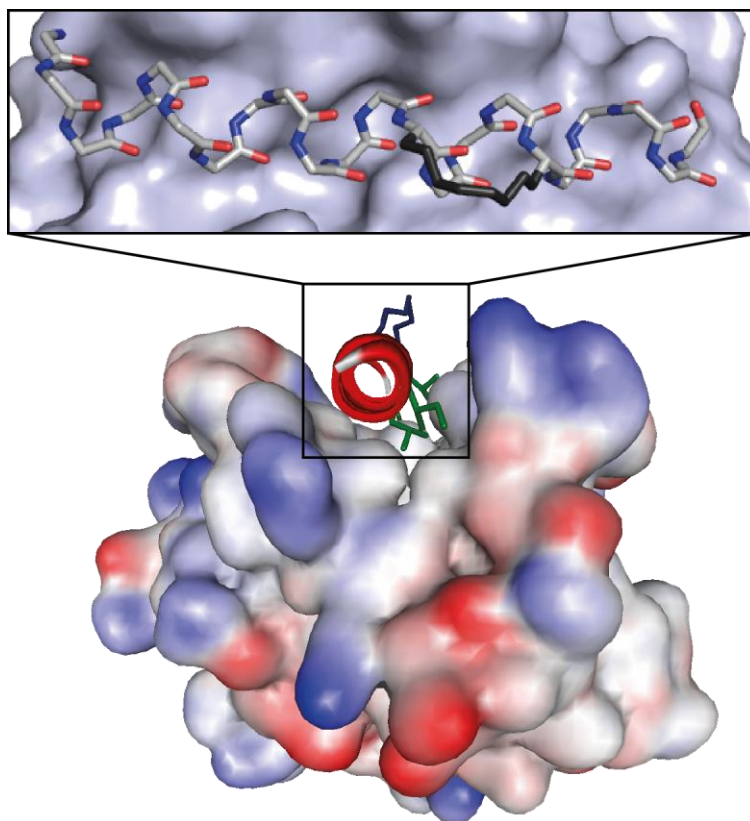
Figure 3.29 – X-ray crystal structure of BID MM bound to Mcl-1 with the hydrocarbon staple coloured blue and the side chains omitted (top); Side-view of the BID BH3 peptide bound to Mcl-1 with the key binding side chains coloured green (bottom).

We were delighted to observe that the BID MM peptide is an α-helix and that the key binding side chains are buried into the hydrophobic pocket of Mcl-1 (Figure 3.29). Also, the hydrocarbon staple does not appear to be in contact with the surface of the protein, residing instead on the solvent exposed face of the BID BH3 peptide. Clearly, the binding conformation of the BID MM peptide is not distorted by the hydrocarbon staple and that helical character is promoted throughout the peptide sequence when bound to Mcl-1.
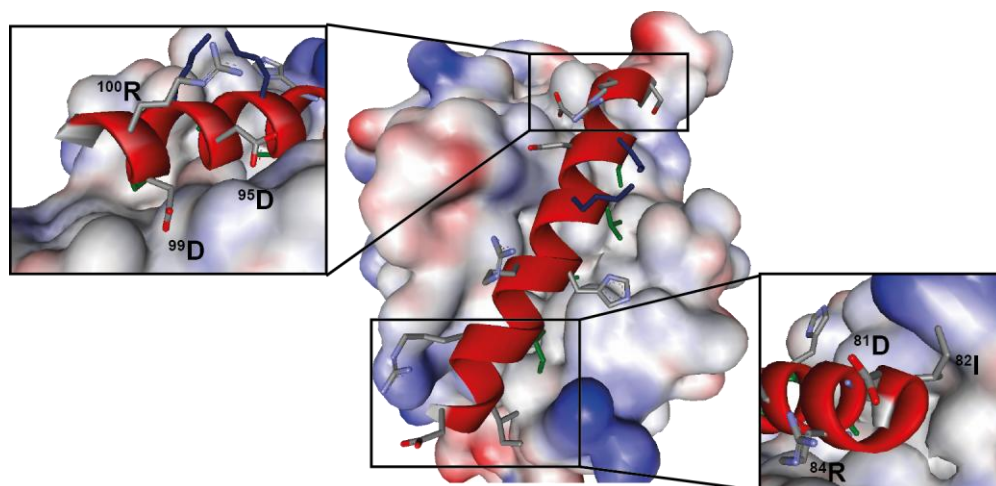
Figure 3.30 – Expansion of the *C*-terminal and *N*-terminal regions of BID MM when bound to Mcl-1

Detailed examination of the crystal structure revealed that the alkene of the hydrocarbon staple was solely in the *cis* configuration. Examination of the remaining side chains revealed the possibility of a salt bridge between [84]R and [81]D at the *N*-terminus, whilst [82]I is forced into a polar surface region of Mcl-1. At the *C*-terminus, [95]D and [99]D both form contacts with basic regions of Mcl-1, whilst [100]R appears to project into the solvent exposed face of the helix, rather than forming salt bridges with the acidic surface at the top edge of the BH3 binding cleft.
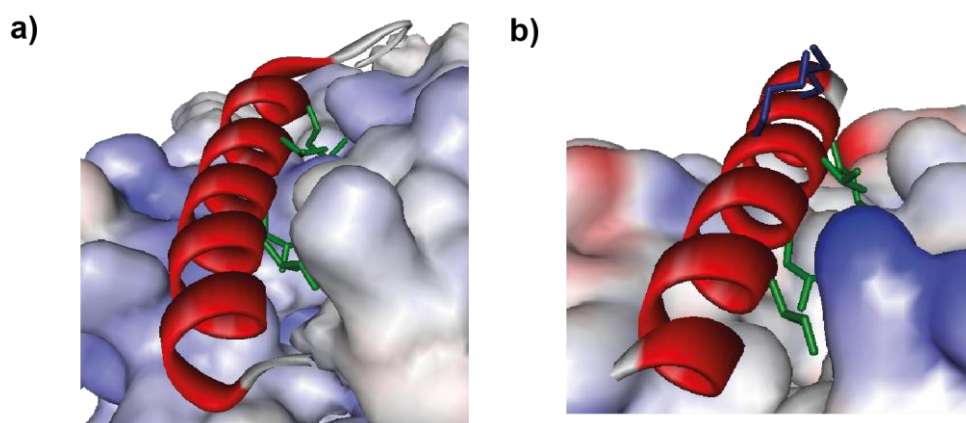
Figure 3.31 – Comparison of a) BID WT (PDB: 2KBW) and b) BID MM with Mcl-1.

Pleasingly, the orientation of the key side chains of BID MM when bound to Mcl-1 is similar to the reported solution state structure of BID WT with Mcl-1 (Figure 3.31). Further crystal trials with BIM MM and BID WT are underway to provide a direct comparison of BH3 ligands bound to Mcl-1 in the solid phase.

3.12.2 Solution Phase Structural Analysis

3.12.2.1 Thermal Unfolding Experiments

Preceding circular dichroism analysis of stapled peptides focused on the calculation of the % helicity of a constrained peptide with no analysis into the extent the peptide maintains its conformation when subjected to denaturation. Considering that stapled peptides are known for their resilience to proteolytic digestion, it was therefore interesting to examine their resistance to denaturation.

The unlabelled BID BH3 peptides were heated in the circular dichroism chamber and scanned in steps of 1 °C and their profiles examined. Initially, it was possible to compare the mean residue ellipticities (MRE) of the stapled peptides against the unfolded wild type at high temperature to evaluate the extent the constraint resists unfolding.

Thermal unfolding of the BID BH3 peptides showed a minimal change in the mean residue ellipticity at 222 nm for the unstapled, Aib and wild type peptides. This is not surprising, since their structures were predominantly random coil (Figure 3.32). Unfolding of the stapled peptides showed that there was a minor transition to a random coil character, based on the change of the signal at 222 nm, and the presence of an isodichroic point at 203 nm. A classic marker for complete unfolding of a peptide to a random coil conformation is the presence of a minimum at 195 nm, which does not appear in the spectra of the stapled peptides because they are not able to completely unfold.

a)

b)

c)
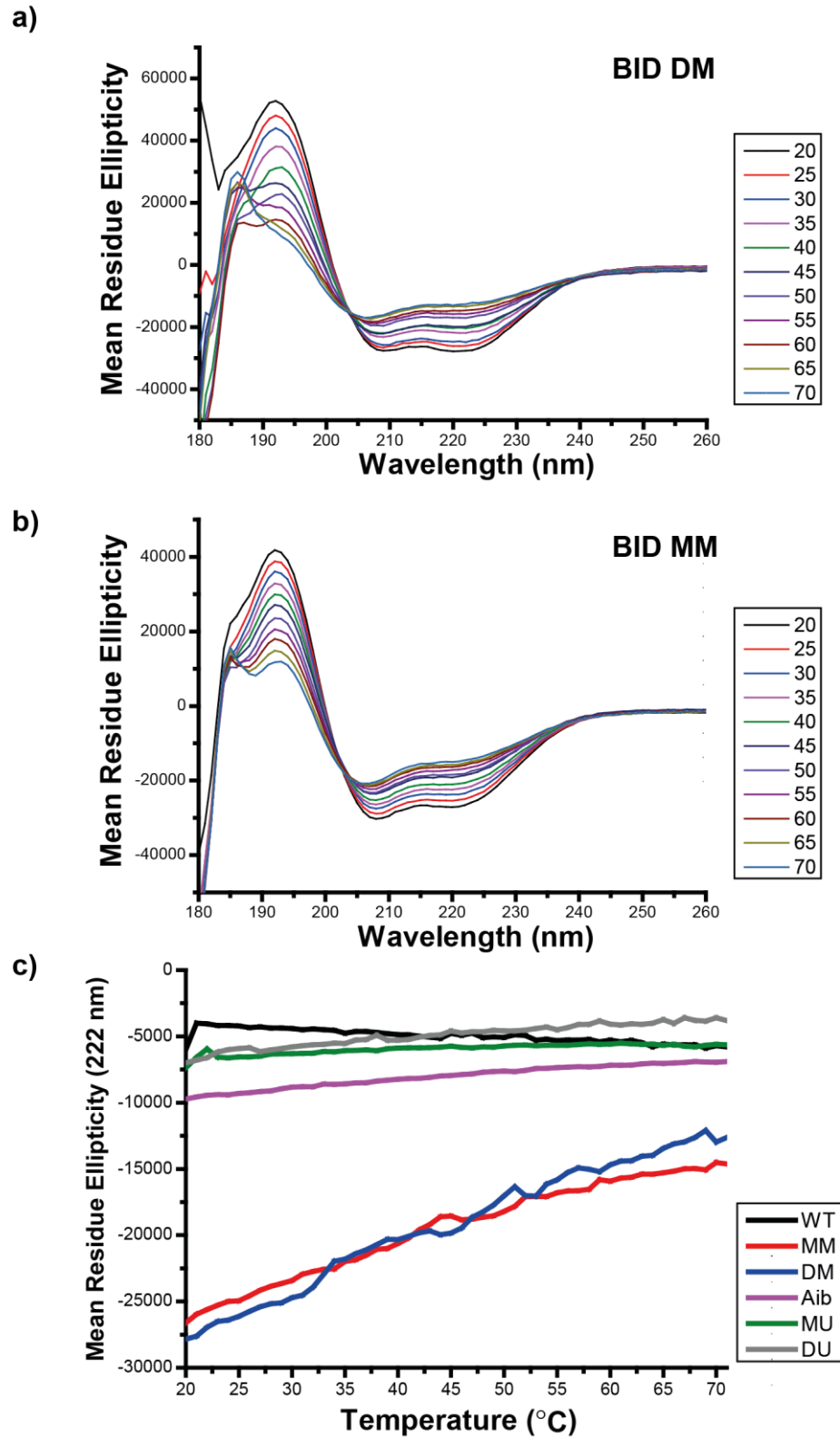
Figure 3.32 – Thermal unfolding circular dichroism spectra for a) BID DM and b) BID MM. The changes in MRE values with increasing temperature of the remaining BID peptides are shown in c).

The stapled peptides both appear to begin forming a plateau in their degradation signal after 65 ℃, where the MRE does not reach the unfolded MRE

of unstapled peptides. Therefore, the hydrocarbon staple prevents complete unfolding of the peptides to a random coil, where the helical character of the peptides is 43% and 37% for MM and DM respectively at the highest temperatures studied.
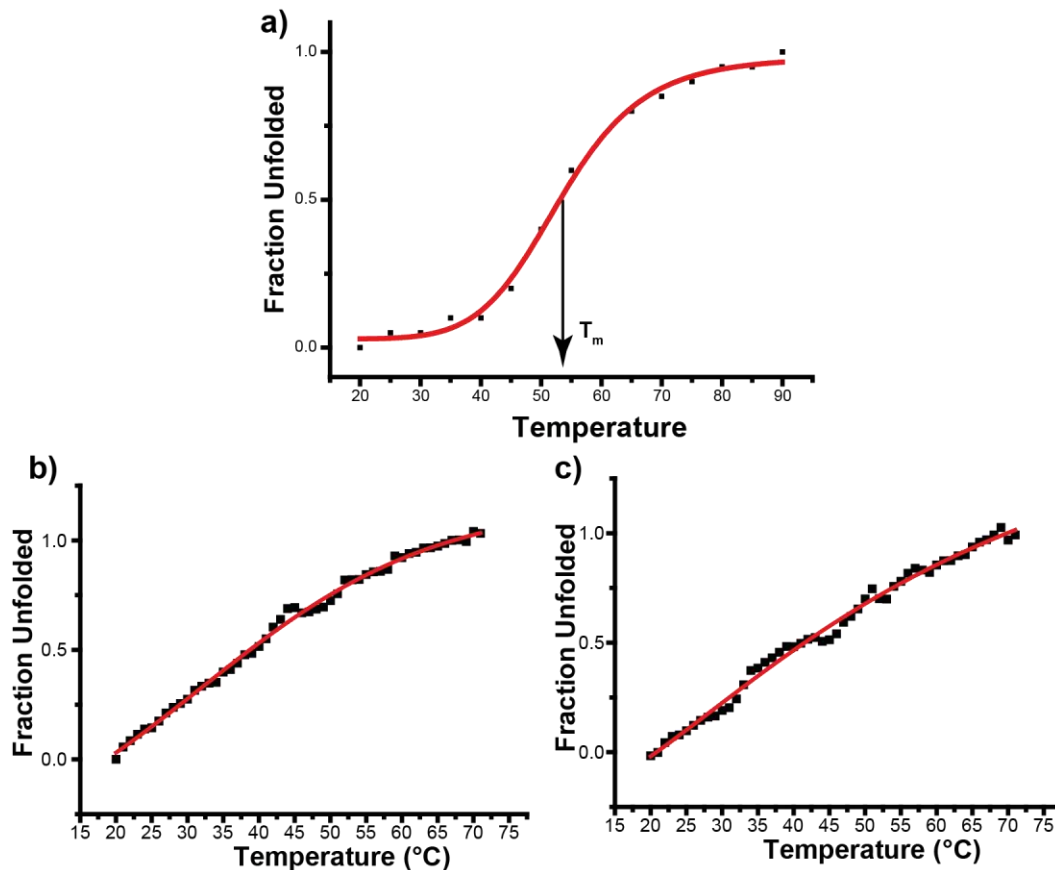
Figure 3.33 – a) An example thermal unfolding curve where a protein unfolds cooperatively upon heating. T_m is the point where the sigmoid inflects, where the fraction unfolded equals 0.5. b) and c) are the unfolding curves of BID DM and BID MM respectively, which do not unfold cooperatively.

To characterise the unfolding thermodynamics of the stapled peptides the fraction unfolded of the peptide was plotted against increasing temperature (Figure 3.33). Cooperative unfolding events are characterised by a sigmoid curve for this plot, whereby the midpoint of the transition is assigned as a melting temperature (T_m). Furthermore, at T_m, the free energy of folding is 0, which can allow the determination of thermodynamic properties of unfolding through Gibbs-Helmholtz and van't Hoff analyses.[167, 192] The indication of a cooperative unfolding event is the presence of pre- and post-transition baselines (the asymptotes in Figure 3.33a).

In contrast, the profile of the plots in Figure 3.33b and Figure 3.33c begin linearly before starting to plateau after 65 °C. The gradual decrease of the amplitude of the trough at 222 nm as temperature increases, suggests that the peptide is unfolding through a non cooperative pathway. Significantly, whilst both of the stapled peptides retained a moderate level of helicity at higher temperatures, re-scanning the peptides at 20 °C after the temperature ramp gave the same MRE value to that at the start of the experiment. The unfolding event of the stapled peptides was therefore a reversible process and the refolding of the peptide into an α-helical enriched conformation was thermodynamically favourable.

In the context of proteins, the stability of the native folded conformation is balanced between chain entropy penalties and stabilisation from non-covalent contacts.[193, 194] However, the overall stability of a folded (globular) protein is marginal, where usually ΔG is in the region of 10 kcal mol^{-1} (to compare, hydrogen bonds contribute around 2 kcal mol^{-1} to enthalpy).[102] As temperature increases, the chain conformational entropy component increases, which leads to protein unfolding. With the stapled BID peptides, it appeared that the hydrocarbon staple maintained helical character by restricting conformational flexibility and preventing the scission of some intramolecular hydrogen bonds. The unfolding mechanism can therefore be envisaged as the termini of the peptide adopting a more random conformation ('fraying'), with the core of the peptide maintaining a rigid, helical conformation.

3.13 Thermodynamic Contributions of Binding of BID BH3 Peptides to Bcl-x$_L$ and Mcl-1

Given that there is a high α-helical character of hydrocarbon stapled BID peptides, it is expected that the entropic penalty of preorganisation is removed from the binding interaction thus improving affinity. Since this is not the case in our studies, understanding the interplay of enthalpy and entropy in the binding interaction would be of use for rationalising the improvement or reduction of binding affinity for hydrocarbon stapled peptides.

3.13.1   Isothermal Titration Calorimetry

Isothermal titration calorimetry (ITC) is a method of studying biomolecular interactions, which involves the measurement of minute heat changes in a cell as one species is titrated into another.[195] As thermal change occurs, the amount of power used to restore cell temperature is measured and is represented in the form of a peak, which reflects the enthalpy change. Over several injections of ligand to macromolecule, the heat change upon binding diminishes as the binding sites of the macromolecule become saturated. This in turn allows the calculation of a K_d, and ΔH, which in turn can be used to determine the thermodynamic contributions of binding events. A particular benefit of ITC is that labels are not required, and since experiments are often two-component systems, complicated equilibria observed in fluorescence anisotropy can be avoided.

3.13.2   Isothermal Titration Calorimetry of BID peptides

The ITC experiments were established by using the BID WT peptide and two of the anti-apoptotic members of the Bcl-2 family; Mcl-1 and Bcl-x_L as used in previous fluorescence anisotropy assays. For Mcl-1, 385 μM of wild type BID was injected into 21.2 μM of Mcl-1, with care taken with the matching of buffers, considering that DMSO was required to solubilise the peptide. BID WT (385 μM) was also injected into Bcl-x_L (25.1 μM).

Protein	N	K_d (μM)	ΔH (cal mol^{-1})	ΔS (cal K^{-1} mol^{-1})
Bcl-xL	0.910 ± 0.03	0.48 ± 0.01	-6041 ± 293	8.66
Mcl-1	1.68 ± 0.04	0.97 ± 0.03	-6586 ± 247	5.42

Table 3.4 - ITC data for the wild type BID peptides and anti-apoptotic members of the Bcl-2 family (Bcl-x_L and Mcl-1).

Pleasingly, clear isotherms were obtained for both of the interactions (Figure 3.34). Whilst the stoichiometry of the Mcl-1 data is wayward for a 1:1 binding model, there are consistencies in the K_d values obtained for the Bcl-x_L and Mcl-1 proteins, since it is reported that BID has a similar potency for both proteins, but the twofold improvement of the binding affinity of Bcl-x_L over Mcl-1 mirrors that of the fluorescence anistropy data. Indeed, isothermal titration calorimetry of a truncated BID peptide with this Mcl-1 construct afforded a K_d value of 0.83 μM.[190] Interestingly, the thermodynamics of the

binding are favourable in both enthalpy and entropy, with a larger entropic contribution in the binding of the BID peptide to Bcl-x$_L$.
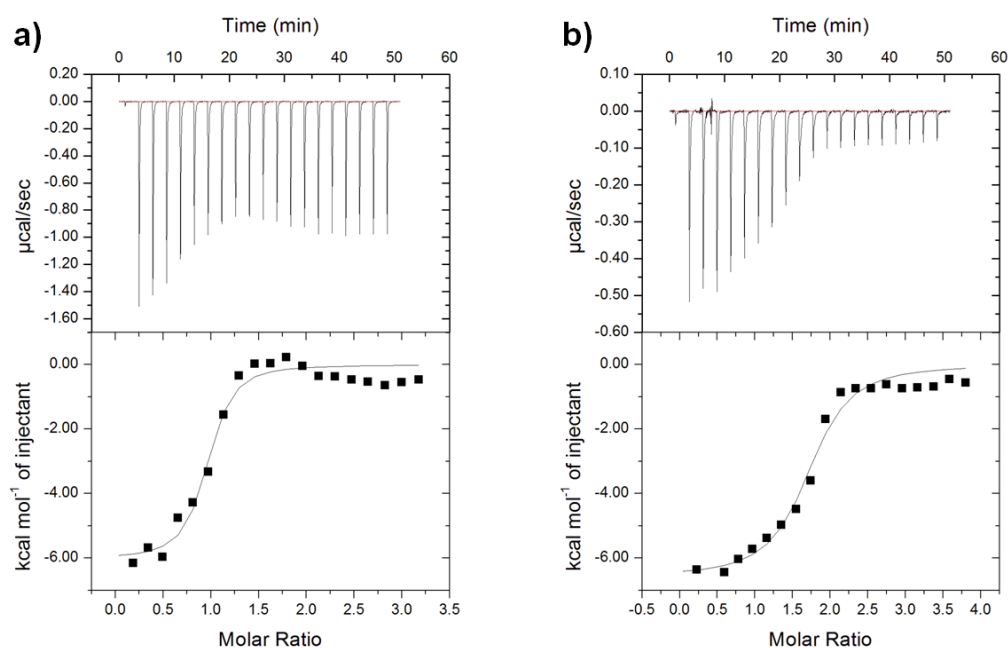
Figure 3.34 – ITC thermograms of the wild type BID peptide against; a) Bcl-x$_L$ and b) Mcl-1.

With these results in hand, ITC was performed with the BID DM and BID MM stapled peptides, with the objective of extracting thermodynamic data of the binding events. Unfortunately, no binding isotherm was detected with either of the stapled peptides (Appendix III), with precipitation observed in the barrel of the ITC syringe after the ITC run. Switching to tris buffer - which provided some successes in the fluorescence anisotropy assays - did not prevent the precipitation of the peptide in either case. Finally, the order of the reagents was reversed, with the smaller concentration of the stapled peptide in the cell and the proteins loaded into the syringe. In spite of this, no binding was observed, and reluctantly further ITC experiments were abandoned due to the uneconomical quantities of reagents that were required for each experiment.

3.13.3   van't Hoff Analyses of the FITC BID Peptides

Considering that isothermal titration calorimetry was unsuccessful for some of the BID peptides, the thermodynamics of the binding interaction of the FITC labelled peptides were extracted using van't Hoff analysis of fluorescence

anisotropy binding assays. The van't Hoff isotherm combines the equilibrium constant with thermodynamic parameters with varying temperature. Therefore, ΔH can be calculated from the gradient of the linear fit and ΔS can be calculated from the intercept of the line with the *y*-axis.

$$lnK = \frac{-\Delta H}{RT} + \frac{\Delta S}{R}$$

As previously shown, the K_d calculation of the labelled peptides was not trivial and the fitting of the curves deviated substantially as the temperature was elevated. As such, the EC_{50} of the binding of the FITC-labelled peptides was considered to provide an indication of the thermodynamics of the binding interactions based on the trends of the change of EC_{50}, for which some limited precedent does exist.[196]
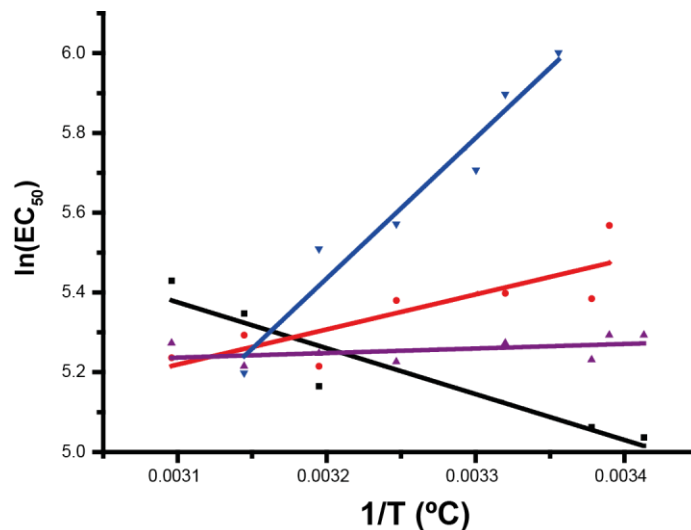
Figure 3.35 – van't Hoff plots of the FITC labelled peptides against Mcl-1: BID WT* (black), BID Aib* (purple), BID DM* (red), BID MM* (blue).

With Mcl-1, it appears that the entropic contributions to the binding are similar across the peptide series, but the intercept of MM* is exaggerated by its first data point. MM*, DM* both appear to have a favourable enthalpic contributions to binding, whilst Aib* appears to have a negligible enthalpic contribution. The surprising result is WT*, which has favourable entropy but appears to have the opposite trend of enthalpy compared to isothermal titration calorimetry. However, ITC used an unlabelled variant of the peptide under different buffer conditions, which complicate a direct comparison.
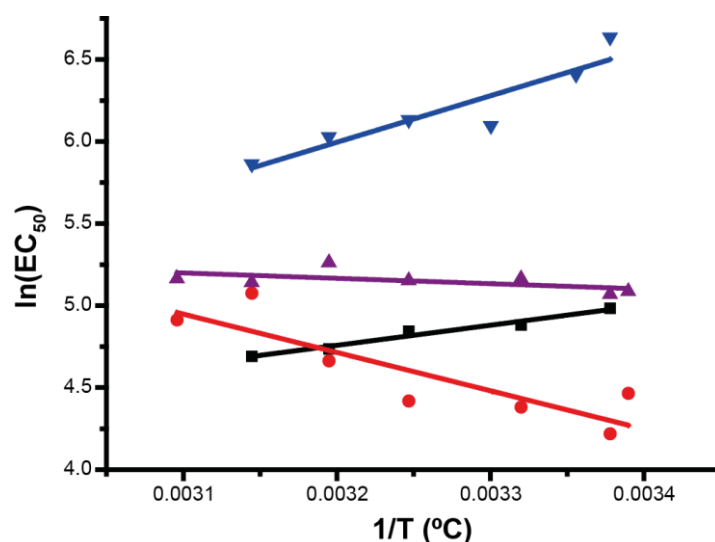
Figure 3.36 – van't Hoff analysis of the FITC BID peptides with Bcl-x$_L$: BID WT* (black), BID Aib* (purple), BID DM* (red), BID MM* (blue).

Against Bcl-x$_L$ (Figure 3.36), entropic contributions to binding were similar across the peptide series, but MM* appeared to have the most favourable entropic component. The surprising trend observed is the apparent disfavoured enthalpic contribution for DM*, whilst WT* and MM* retain their favourable binding enthalpies.

The major caveat in these van't Hoff studies is the use of EC$_{50}$ to indicate binding thermodynamics, rather than K$_d$.[IV] Since fitting the van't Hoff data requires a K$_d$ fitting model that considers non-specific contributions to binding, it is possible that the thermodynamic trends observed may change.

3.14 Preliminary *in cellulo* studies

The *in vitro* binding studies of the BID BH3 stapled peptides suggested that the hydrocarbon staple has no improvement of the potency of the peptide as an inhibitor of two protein-protein interactions. Hydrocarbon stapled peptides have also been hypothesised to improve cell penetration properties from an increased hydrophobic character introduced by the crosslink.[2, 3] With Dr. J Levesley and Dr. L. Steele (Leeds Institute for Molecular Medicine), the BID BH3 peptides were tested *in cellulo* for their ability to penetrate cells, using the

---

[IV] A caveat with van't Hoff analysis is also the assumption that ΔH is constant over the temperature range that is studied.

FITC labelled BID peptides (Figure 3.20), and their ability to promote apoptosis using the unlabelled BID BH3 peptides.

3.14.1 Cellular permeability studies

SF188 paediatric glioblastoma cells were treated with FITC-labelled BID BH3 peptides, whose cell-penetrating properties were examined through FACS analysis, which measures fluorescence intensity of cells by flow cytometry. A fluorescently labelled peptide that is more cell penetrative therefore emits a more intense signal as the cells are passed through the detector. One caveat to FACS analysis is that the fluorescently labelled peptide could be bound to the cell membrane without penetrating it - localisation is therefore confirmed by confocal microscopy.
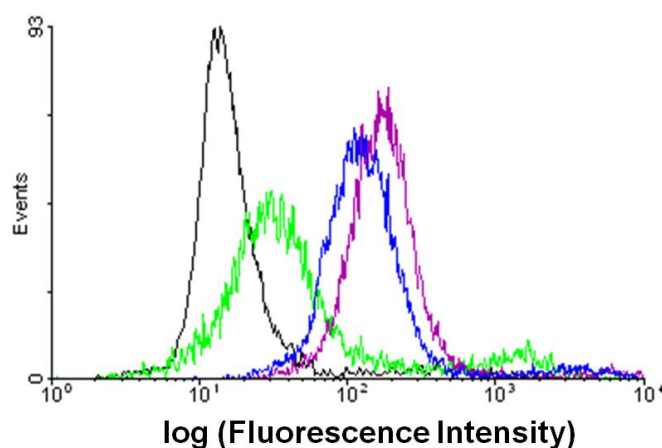
Figure 3.37 – FACS analysis of FITC labelled BID Peptides; BID WT* (Black), BID Aib* (Green); BID MM* (blue) and BID DM* (purple) after 24 h incubation in serum free media. 'Events' on the y-axis refers to the number of fluorescent cells that are counted (Acquired by J. Levesley and L. Steele).

When the fluorescently labelled BID peptides were treated with the cells in serum-free media, which was initially shown to improve the intensity of cellular fluorescence, the stapled BID peptides (DM* and MM*) both had greater fluorescence intensity compared to the Aib* and WT* peptides at concentrations of 10 μM. Whilst all of the peptides had an increased intensity compared to a DMSO control, it was very pleasing that both of the stapled peptides appeared to be more penetrative and that the MM* appeared to be as effective as the DM* stapled peptide. The next requirement is confocal microscopy, which would confirm that the stapled peptides are localising

within the cell. Nevertheless, the preliminary *in cellulo* results are very promising.

3.14.2 Apoptosis studies

The second *in cellulo* study was to examine the ability of the unlabelled BID peptides to induce apoptosis in SF188 pediatric glioblastoma cells, by the use of an MTT assay which quantifies cell death. In the case of a successful apoptosis initiator, the cell membrane begins to permeabilise and allows the uptake and enzymatic processing of MTT, which is measured using a spectrometer.
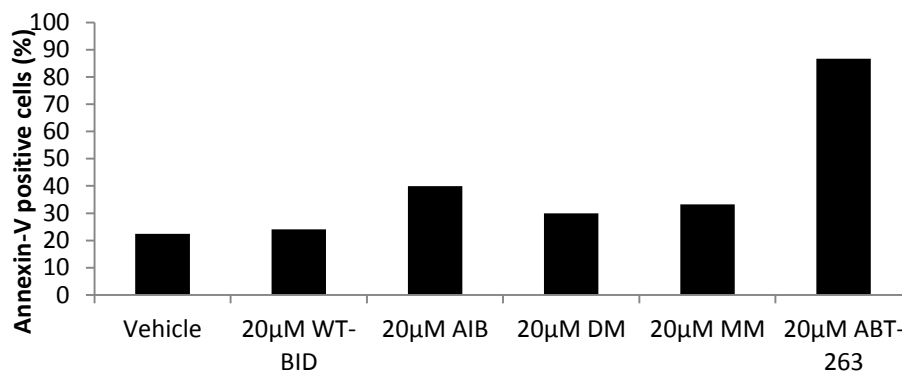
Figure 3.38 – Apoptosis studies of 20 µM quantities of unlabelled BID BH3 peptides and ABT-263 after 72 h incubation in serum free media (acquired by J. Levesley and L. Steele).

Disappointingly, the unlabelled BID peptides did not appear to promote any significant apoptosis of the cells up to a concentration of 20 µM in serum-free conditions after 72 hours. To verify the sensitivity of the cell line to known inhibitors, ABT-263 (Navitoclax) was employed as a positive control as it is a known inhibitor of Bcl-2 and Bcl-x$_L$.[197-199] ABT-263 was capable of inducing apoptosis after 24 hours at concentrations of 20 µM, unlike all of the BID peptides which were unable to induce apoptosis at the same concentration.

The *in cellulo* studies have provided an interesting insight into to biological capabilities of the stapled BID BH3 peptides. Whilst it was pleasing that stapling the peptides appears to improve penetration, it was surprising that apoptosis was not induced in statistically significant quantities *in this cell*

line. Future studies could use the Jurkat T-Cell Leukaemia cell lines that have been previously used for BID DM.[3]

3.15 Discussions and Conclusions

The investigation into peptides functionalised with monosubstituted hydrocarbon staples revealed that, for the BID BH3 series, α-helical character was promoted and proved through crystallographic studies. In addition to this, monosubstituted stapled peptides demonstrated cell penetration properties similar to disubstituted stapled peptides, even if apoptosis was not induced by any of the BID BH3 peptides in SF188 cell lines.

In the BID BH3 series, direct binding studies to Bcl-x_L and Mcl-1 demonstrated a moderate decrease in binding affinity for the stapled BID peptides compared to unmodified BID peptides. However, there appears to be no *selectivity* of stapled BID BH3 peptides for Bcl-x_L over Mcl-1, given that the EC_{50} values for BID DM and BID MM are in the same region for both proteins.

An attempt to understand the thermodynamics of the binding interaction of BID BH3 with Bcl-x_L and Mcl-1 was undermined by practical complications with ITC and complex binding in fluorescence anisotropy. In spite of this, some preliminary conclusions can be made from van't Hoff analysis. BID MM* binds to Mcl-1 and Bcl-x_L with favourable enthalpy, but BID DM* does not have a favourable enthalpic contribution for Mcl-1; entropy appears to be a larger driving force to binding.

Given that stapling BID BH3 modulated potency and not selectivity across family members, transferring stapling methodology to another BH3 ligand (BIM BH3) assessed how transferrable stapling is across a ligand series with sequence degeneracy. Inhibition assays with BIM BH3 demonstrated that stapled BIM peptides are dramatically weaker ligands compared to BIM WT and BID BH3.

Based on this investigation, we can conclude that the original dogma of stapled peptides needs to be rigorously challenged. Whilst hydrocarbon constraints improve helical character when positioned correctly, this does not necessarily lead to an improved binding affinity. Clearly, there are

thermodynamic factors involved in the binding interaction as well as the entropic penalty of organising a ligand into an active conformation. For instance, the enthalpic benefit of forming a hydrogen bonded network as the peptide folds to an α-helix is overlooked in the original methodology.[2] Also, non-covalent interactions within the peptide ligand and between the ligand and protein have only been considered in the instances where potency has fallen after hydrocarbon stapling.[131]

We have found that hydrocarbon stapling cannot be used as a generic therapeutic strategy for a family of redundant proteins. Firstly, for the interactions we studied, whilst the proteolytic resistance and cell penetration properties were improved with hydrocarbon stapling, binding affinity and selectivity was not. Secondly, using the same staple position in a related ligand diminished binding affinity, so hydrocarbon stapling must be optimised for each ligand and thus for each target.

To build on this work, an orthogonal binding assay would be necessary to quantify K_d of the BIM and BID BH3 series. Surface Plasmon Resonance spectroscopy (SPR) provides the kinetic parameters of the binding interaction, and has been previously used in hydrocarbon stapling to justify K_d observed for BIM BH3.[131] Also, further structural studies of BIM BH3 and BID BH3 with Bcl-x_L and Mcl-1 would be indispensable to our understanding of the binding mode of the stapled peptides to further quantify our observed binding affinities. Detailed *in cellulo* experiments, particularly confocal microscopy would also be useful to determine whether the more penetrative stapled peptides localise to mitochondria, where the Bcl-2 family function.

Chapter 3c - Investigation of a new scaffold of stapled peptides

Hydrocarbon stapling methodology furnishes a permanent covalent crosslink into a peptide with the aim of improving its biophysical properties. Reversible constraining methods, through non-covalent crosslinking, which stabilise a peptide through unnatural host-guest moieties,[200] coordinative[201, 202] or π-π stacking[203] of side chains has also been effective in reinforcing helical structure of polypeptides. However, non-covalent constraints generally require carefully balanced (or metal enriched) conditions that are not applicable to living systems.

Reversible covalent crosslinking has already been described, through the stabilisation of peptides with intramolecular cystine dimers (1.2.2). We sought a reversible method of constraining peptides that was analogous to the research performed with the hydrocarbon staples (3.5).

3.16 Synthesis of hCys- and Maleimide- constrained BID

Baker and coworkers have described an effective protocol for the introduction of a maleimide linker into a peptide that contains native cysteine residues. The maleimide unit can then be functionalised to provide a handle for drug delivery, either through intramolecular cysteine residues (Figure 3.39)[204] or through intermolecular linkages of two peptides. [205]
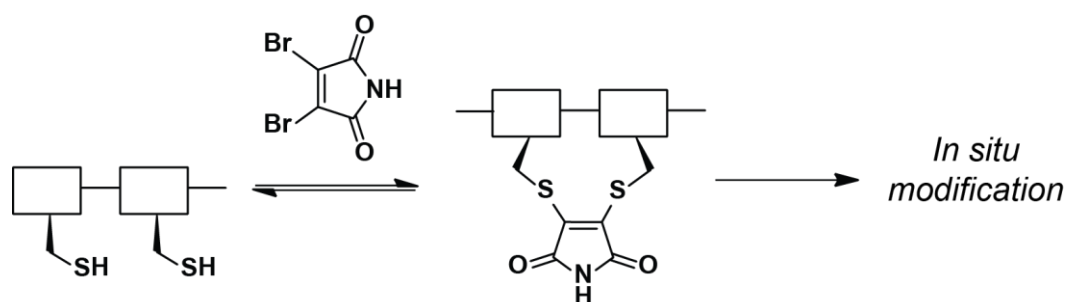
Figure 3.39 - Maleimide bridging methodology used by Baker and coworkers for the *in situ* modification of the maleimide nitrogen of an intramolecular crosslink.[204]

The maleimide-bridged peptide has been overlooked as a potential candidate for covalently constrained peptides and was worthy of further investigation alongside the hydrocarbon stapled BID BH3 peptide. Installing homo-cysteine (cysteine with an additional methylene unit in the side chain) in the same positions as the olefinic amino acids previously studied, followed by bridging with 2,3-dibromomaleimide would afford an 8-atom crosslink that is

regioisomeric with the hydrocarbon stapled peptide. In addition to this, homo cysteine (hCys) analogues of the BID BH3 peptide provide access to investigations into the oxidised and reduced forms of hCys BID, to determine if conformation and binding affinities are changed under reversible oxidation conditions.

Figure 3.40 - Peptide sequences of the homo cysteine (hCys) variants of the BID BH3 peptide.

The synthesis of BID hCys was performed according to the same methods previously described, on a 0.1 mmol scale. After the cleavage and deprotection of the peptide, it was found that significant ^{91}A and ^{95}D deletion sequences were present. These deletions had come from the inefficiency of the Fmoc deprotection of the hCys residue prior to coupling, rather than the inefficiency of the coupling of ^{91}A or ^{95}D. In addition to this, fragmentations occurred during cleavage and deprotection to afford several other peptides that were not identified. Nevertheless, after rounds of purification, 6 mg (5 %) of hCys peptide was afforded.

To perform the maleimide bridging, the hCys peptide was dissolved in 40% acetonitrile:phosphate buffer and 5 equivalents of TCEP and 2,3-dibromomaleimide was added. Pleasingly, the bridging reaction was complete after 4 hours with no evidence of intermolecularly bridged peptides observed, but attempts to purify the bridged peptide were unsuccessful.

To circumvent the problem of two successive purifications, the maleimide-bridging reaction was performed using the crude BID hCys peptide after cleavage from resin. After 6 hours, the bridging was complete, but reduction of the maleimide to succinimide was observed and confirmed by

HRMS. Purification of the succinimide bridged BID hCys SUC peptide afforded 4.1 mg (11% yield) of material.

3.17 Biophysical analyses of hCys BID peptide series

3.17.1   Circular Dichroism

Ahead of circular dichroism, BID hCys OX was fully reduced to BID hCys RED by the addition of 5 equivalents of dithiothreitol (DTT) instead of TCEP, which absorbs strongly below 230 nm. 5 equivalents of diamide (1,1′-azobis(N,N-dimethylformamide) were employed to accelerate the slow oxidative conversion of BID hCys RED to BID hCys OX.
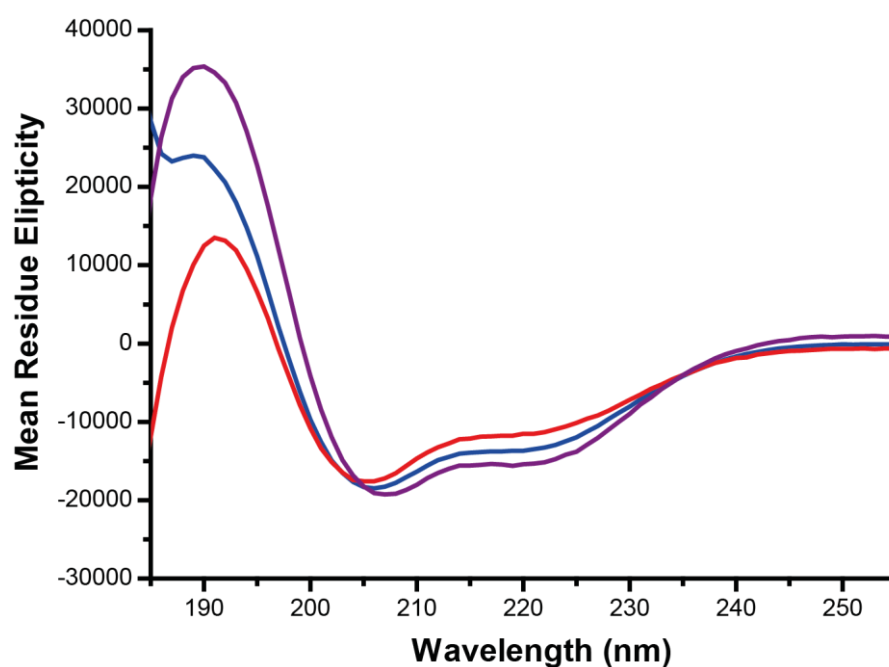
Peptide	% Helicity
BID hCys OX	39
BID hCys RED	33
BID hCys SUC	45

Figure 3.41 – CD spectra of BID hCys OX (blue), RED (red) and SUC (purple).

Pleasingly, there were marginal increases in helicity of the peptide after constraint with a disulfide and succinimide linker. In addition to this, the curve profile changes between RED, OX and SUC, where the minimum at 203 nm of RED moves to 208 nm for SUC. Crosslinking with cysteine and succinimide methodology appears to promote moderate helicity, compared to the high

helical content observed with the hydrocarbon stapled peptides (BID DM = 81%).

3.17.2   Fluorescence Anisotropy Competition Assays

In fluorescence anisotropy control experiments, diamide interfered with the assay, so BID hCys OX was afforded by air oxidation and confirmed by HRMS before starting the assays. TCEP did not interfere with the assay, so it was employed in the assay buffer to ensure that there was no oxidation of the peptide during incubation.

Peptide	IC$_{50}$ Bcl-x$_L$	IC$_{50}$ Mcl-1
BID hCys OX	1.30 ± 0.07 µM	232 ± 17 nM
BID hCys RED	5.42 ± 1.1 µM	268 ± 14 nM
BID hCys SUC	0.34 ± 0.01 µM	186 ± 40 nM
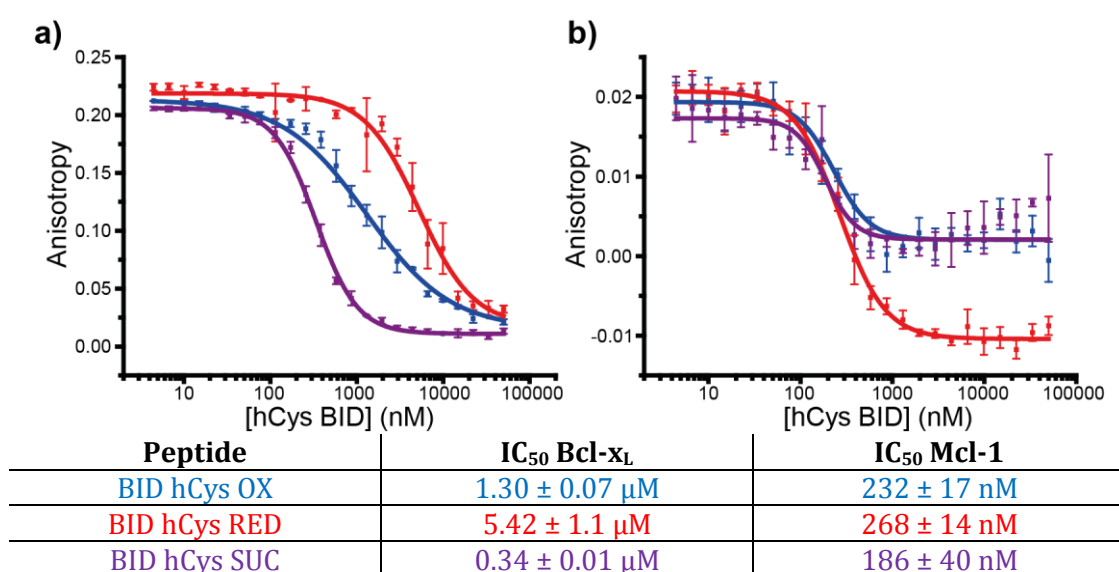
Figure 3.42 – Fluorescence anisotropy competition assays of a) Bcl-x$_L$/BAK* and b) Mcl-1/NoxaB* with BID hCys OX (blue), BID hCys RED (red) and BID hCys BR (purple) employed as inhibitors.

The competition assays yielded some interesting results for the hCys series of peptides. Against Bcl-x$_L$/BAK*, there is a notable increase in potency for the bridged peptides over the reduced peptides – especially for the covalently bridged BID hCys SUC peptide. In contrast, against Mcl-1/NoxaB*, there is only a marginal difference in potencies across the series. In comparison to the hydrocarbon stapled BID BH3 peptides, constrained peptides have a slight improvement of potency over the wild type and unstapled peptides, but the order of magnitude difference between hCys SUC and hCys RED is the largest observed in our potency studies.

3.17.3   Preliminary BID hCys conclusions

The inhibition results of the hCys BID peptides were particularly interesting, where covalently constrained BID hCys SUC outperformed reversibly constrained BID hCys OX and unconstrained BID hCys RED with the inhibition of Bcl-x$_L$/BAK*. SUC and OX also possessed IC$_{50}$ values that outperformed BID WT, in a similar result to the BID hydrocarbon stapled peptide series (3.6.3). It would appear that incorporating hCys into BID proved unfavourable for the inhibition of Bcl-x$_L$/BAK*, but this was mitigated by constraint. Improvement of binding affinity through the SUC constraint was not transferred to the inhibition of Mcl-1/NoxaB*, echoing previous results with hydrocarbon stapling of BID.

Whilst the reduction of BID hCys MAL to BID hCys SUC was unexpected, the results have been particularly fascinating and future investigation is worthwhile. Future expansion in this field shall focus on why the reduction occurred during bridging, followed by investigation of the reversibility of the maleimide crosslinking.

Conclusions and Future Goals

The original goals of the project had been changed as the project evolved through some of the difficulties encountered with the chemical synthesis of unnatural amino acids. Having found the synthesis of disubstituted olefinic amino acids for hydrocarbon stapling challenging, changing to a synthetic route for an overlooked monosubstituted amino acid opened a new avenue of research to expand the repertoire of secondary structure mimetics within the Wilson laboratory.

Indeed, the overlooked monosubstituted unnatural amino acid was shown to be as effective as a surrogate for hydrocarbon stapling as disubstituted unnatural amino acids against two therapeutically relevant protein-protein interactions. The decreased potency of our hydrocarbon stapled peptides therefore triggered an investigation into why binding affinity was not improved after constraining the peptide into a biologically active helical conformation. The culmination of this investigation led to the quantification of the structure of hydrocarbon stapled peptides through solid and solution state techniques, but also provided insights into the selectivity of hydrocarbon stapled ligands within a degenerate family of proteins.

Our findings into selectivity revealed that one stapled ligand (BID BH3) was unselective for Mcl-1 over Bcl-x_L, but transferring the stapling methodology to a similar ligand, BIM BH3 resulted in a dramatic fall in potency. The main result here is that hydrocarbon stapling cannot be used as a generic therapeutic approach for reactivating apoptosis pathways in cells, since the appropriate hydrocarbon-stapled ligand requires specific design for one particular interaction.

The hypothesis that hydrocarbon-stapled peptides are more potent ligands as a result of their increased α-helical character and reduced conformational flexibility has been challenged. Our thermodynamic studies suggest that there must be other thermodynamic penalties with binding to account for stapled peptides possessing a weaker K_d compared to unstapled peptides.

Future work with the stapled peptides would include orthogonal binding assays to reinforce K_d obtained from fluorescence anisotropy, particularly through the investigation of the kinetic parameters of binding (analogous to the on/off rate experiments performed by Czabotar and coworkers).[131]

The stapled peptides investigation can be applied to future protein prosthesis studies, by replacing a helical section of a protein with a stapled peptidomimetic. Whilst the total synthesis of Im7 was not completed due to time constraints, the methodology has been established for future completion.

Based on the deviation of the original project goals, the project has demonstrated that research evolves equally from design and serendipity. The research into the stapled peptides in particular, could have implications for the entire field of constrained peptides. As momentum has gathered with stapled peptides entering clinical trials, gathering an understanding into why the hydrocarbon stapling methodology is effective is a vital stage to the future design of therapeutically active stapled peptides.

Chapter 4

Experimental

4.1   Small Molecule Synthesis

4.1.1 General Considerations

Non-aqueous reactions were carried out in washed and oven-dried glassware. Solvents and reagents were used as received from major suppliers without prior purification unless stated. Anhydrous tetrahydrofuran, acetonitrile, dichloromethane and diethyl ether were obtained from the in-house solvent purification system from Innovative Technology Inc. PureSolv®. Anhydrous dimethyl formamide, methanol and chloroform were obtained from major chemical suppliers equipped with a SureSeal™ (or equivalent). For reactions under non-anhydrous conditions, the solvents used were of HPLC quality and provided by Fisher or Sigma-Aldrich. Water in aqueous solutions and used for quenching was deionised, and water used for buffers and HPLC was ultra-pure 18 MΩ from an ELGA Purelab system. Mixtures of solvents are quoted as ratios and correspond to a volume:volume ratio. Drying of organic extracts was performed using sodium sulfate.

Thin layer chromatography was performed on Merck Kieselgel 60 F_{254} 0.25 mm precoated aluminium plates. Product spots were visualised under UV light (λ_{max} = 254 nm) and/or by staining with basic potassium permanganate. If any other TLC dip was used, it is stated under the specific experimental procedure of a molecule. Flash chromatography was performed using silica gel 60 (0.043 – 0.063 mm VWR) using pressure by means of head bellows.

^{1}H NMR spectra were recorded on Bruker DPX 300 (300 MHz) or Avance 500 (500 MHz) spectrometers and referenced to either residual non-deuterated solvent peaks or tetramethylsilane. ^{13}C spectra were recorded on a Bruker Avance 500 (126 MHz) and referenced to the solvent peak. ^{1}H spectra

are reported as follows: δ_H (*spectrometer frequency, solvent*): *ppm to two decimal places (number of protons, multiplicity, J coupling constant in hertz, assignment)*. Chemical shifts are quoted in ppm with signal splitting recorded as singlet (s), doublet (d), triplet (t), quartet (q), quintet (quin.) multiplet (m), broad (br) and apparent (app.). Coupling constants, *J*, are measured to the nearest 0.1 Hz. Similarly, ^{13}C spectra are reported as follows: δ_C (*spectrometer frequency, solvent*): *ppm to one decimal place* (*assignment*). Assignments of spectra were assisted by the results of DEPT, COSY, HMQC and HMBC experiments.

Infrared spectra were recorded on a Perkin Elmer Fourier-Transfer spectrometer. Spectra were analysed neat and only structurally important absorptions are quoted. Absorption maxima (ν_{max}) are quoted in wavenumbers (cm^{-1}).

HPLC/MS were recorded on a Bruker HCT ultra under the conditions of electrospray ionisation (ESI). HPLC separation was performed on an Agilent 1200 series instrument equipped with a Phenomenex C18 column (50 × 2 mm) using acetonitrile:water as the eluent for positive ion spectra. Values are reported as a ratio of mass to charge. Nominal mass spectra and accurate (4 d.p.) mass spectra were recorded on a Bruker Daltonics micrOTOF Premier Mass Spectrometer, or using a Bruker MaXisImpact Spectrometer under positive ESI conditions unless otherwise stated.

Optical rotations were recorded on an Optical Activity AA-10 polarimeter using the sodium D line (589 nm). $[\alpha]_D^T$ are reported in units of $10^{-1} \deg dm^2 g^{-1}$.

Melting points were determined on an Electrothermal digital melting point apparatus and are uncorrected. Microanalysis was performed by the School of Chemistry service, utilising a Carlo Erba 1108 Elemental Analyser.

4.1.2 Procedures and data for monosubstituted unnatural amino acid synthesis

(*S*)-*N*-benzyl Proline **43**
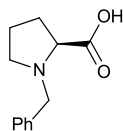
(S)-Proline **41** (20.0 g, 174 mmol) and potassium hydroxide (19.5 g, 348 mmol) were dissolved in 2-propanol (150 mL) and heated to 40 °C. Benzyl chloride (21 mL, 183 mmol) was added dropwise over 2 h at 40 °C. After 6 h, the suspension was diluted with aqueous hydrochloric acid (1M) to attain a pH of 5 (pH paper) and extracted with chloroform (3 × 200 mL). The aqueous suspension was filtered, washed with acetone (200 mL) and the combined organic fractions concentrated *in vacuo*. The colourless precipitate was found to be (S)-N-benzyl proline **43** (19.9 g, 97.5 mmol, 55%) that was used without further purification. The concentrated organic layers afforded (S)-N-benzyl proline benzyl ester **42** as a thin orange oil.[v] (S)-N-benzyl proline **43** m.p. 165-166 °C (Lit: 167 °C)[158]; δ_H (500 MHz, DMSO-d$_6$) 1.74-1.83 (1H, m, Pro-γH), 1.89-1.97 (2H, m, Pro-βH and Pro-γ'H), 2.24-2.32 (1H, m, Pro-β'H), 2.96-3.03 (1H, m, Pro-δH), 3.25-3.31 (1H, m, Pro-δ'H), 3.90 (1H, dd, J = 9.6, J = 6.8, Pro-αH), 4.10 (1H, d, J = 12.8, NC*H*HPh), 4.32 (1H, d, J = 12.8, NCH*H*Ph), 7.36-7.42 (3H, m, ArC*H*), 7.45-7.49 (2H, m, ArC*H*); δ_C (125 MHz) 22.3, 28.2, 53.6, 57.3, 65.7, 128.6, 128.8, 130.2, 132.9, 170.8; ESI-HRMS found *m/z* 228.0991 [M+Na]$^+$, C$_{12}$H$_{15}$NO$_2$Na requires 228.0994; $[\alpha]_D^{25}$ (DMSO, c = 0.5) −28.1 (Lit: −28.4; MeOH, c = 1).[158]

Hydrogenolysis of (S)-N-benzyl proline benzyl ester **42**
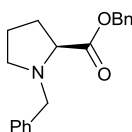
The (S)-N-benzyl proline benzyl ester **42** mixture (35.0 g, 118 mmol) was dissolved in degassed ethanol (250 mL) and 15% Palladium on Barium Sulfate (150 mg) was added. The reaction was left under positive pressure of hydrogen for 24 h, filtered through Celite® and washed with ethanol (400 mL). The ethanol was concentrated *in vacuo* and the residue of **43** washed with

---

[v] This also contained quaternary benzyl ammonium proline that was carried through to the hydrogenolysis step

acetone, dried *in vacuo* and used without further purification (16.0 g, 78.4 mmol, 60%).

(*S*)-2-[*N*-(*N'*-benzylprolyl)amino]-benzophenone **44**
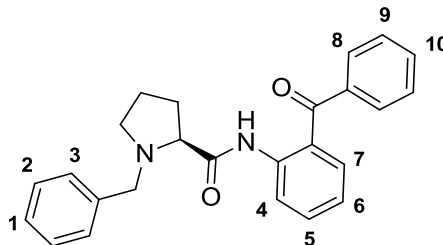
(*S*)-*N*-benzyl Proline **43** (5.0 g, 24.5 mmol) was dissolved in dichloromethane (50 mL) under a nitrogen atmosphere. *N*-methyl imidazole (4.27 mL, 53.9 mmol) was then added dropwise, followed by the cooling of the reaction mixture to 0 °C and the addition of mesyl chloride (1.92 mL, 24.5 mmol) over 2 h. The mixture was warmed to rt, and 2-aminobenzophenone **49** (4.35 g, 22.1 mmol) dissolved in dichloromethane (40 mL) was added dropwise and the reaction heated to 40 °C for a further 12 h. The reaction was quenched with saturated ammonium chloride (200 mL) and extracted with dichloromethane (3 × 200 mL). The combined organic layers were concentrated *in vacuo* to afford (*S*)-2-[*N*-(*N'*-benzylprolyl)amino]-benzophenone **44** as an amorphous, colourless solid (7.29g, 18.9 mmol, 86%). R_f = 0.8 (Chloroform:Acetone 5:1); δ_H (500 MHz, CDCl$_3$): 1.77-1.89 (2H, m, Pro-γH and γ'H), 1.96-2.04 (1H, m, Pro-βH), 2.24-2.34 (1H, m, Pro-β'H), 2.44 (1H, td, *J* = 9.6, 6.9, Pro-δH), 3.22-3.27 (1H, m, Pro-δ'H), 3.35 (1H, dd, *J* = 10.1, *J* = 5.0, Pro-αH), 3.63 (1H, d, *J* = 12.8, NC*H*HPh), 3.95 (1H, d, *J* = 12.8, NCH*H*Ph), 7.12 (1H, t, *J* = 8.0, ArH-6), 7.15-7.20 (3H, m, ArH-7, ArH-2, ArH-2'), 7.39-7.43 (2H, m, ArH-1, ArH-1'), 7.50-7.59 (4H, m, ArH-1, ArH-5, ArH-9, ArH-9'), 7.64 (1H, t, *J* = 7.3, ArH-10), 7.81 (2H, d, *J* = 6.8, ArH-8, ArH-8'), 8.61, (1H, d, *J* = 8.2, ArH-4), 11.5 (1H, br s, N*H*); δ_C (125 MHz, CDCl$_3$): 24.2, 31.0, 53.9, 59.9, 68.3, 121.5, 122.2, 125.3, 127.1, 128.2, 128.3, 129.1, 130.1, 132.5, 132.6, 133.4, 138.2, 138.6, 139.2, 174.7, 197.9; ESI-HRMS found *m/z* 407.1729 [M+Na]$^+$ C$_{24}$H$_{25}$N$_2$O$_2$Na requires 407.1729; [α]$_D^{25}$ (CHCl$_3$ c = 0.5) −130.5 (Lit: −132.2, MeOH, *c* = 1).[158]

(*S*)-Gly-Ni-BPB Schiff Base **45**
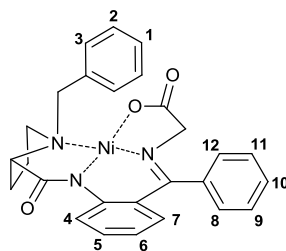
(*S*)-2-[*N*-(*N*'-benzylprolyl)amino]-benzophenone **44** (1000 mg, 2.61 mmol), Nickel (II) nitrate hexahydrate (908 mg, 3.13 mmol) and glycine (390 mg, 5.22 mmol) were dissolved in anhydrous methanol (8 mL) and heated to 55 °C. 25% w/v sodium methoxide in methanol (6.26 mL, 22.9 mmol) was added and the reaction diluted to 30 mL by the addition of anhydrous methanol. After 1h, the solution was cooled to rt and acetic acid (1.7 mL, 29.6 mmol) was added, followed by dilution with water (100 mL). The solution was extracted with chloroform (3 × 50 mL), dried and concentrated *in vacuo*. Purification by silica gel chromatography (Chloroform:Acetone 5:1) afforded Gly-Ni-BPB **45** as a scarlet, glassy solid (1.25 g, 2.51 mmol, 96%): m.p. 211-213 °C (Lit: 208-209 °C)[158]; R_f = 0.2 (Chloroform:Acetone 5:1); δ_H (500 MHz, CDCl$_3$): 2.02-2.10 (1H, m, Pro-γH), 2.12-2.18 (1H, m, Pro-δH), 2.36-2.47 (1H, m, Pro-βH), 2.53-2.63 (1H, m, Pro-βH), 3.29-3.39 (1H, m, Pro-δH), 3.46 (1H, dd, *J* = 10.7, *J* = 5.6, Pro-αH), 3.64-3.74 (4H, m, Pro-γH, Gly-αH, NC*H*HPh, 4.48 (1H, d, *J* = 12.7, NCH*H*Ph), 6.70 (1H, t, *J* = 7.2, ArH-6), 6.79 (1H, dd, *J* = 7.9, *J* = 1.6, ArH-7), 6.96-7.00 (1H, m, ArH-8), 7.10 (1H, d, *J* = 7.2, ArH-12), 7.20 (1H, td, *J* = 8.7, *J* = 1.6, ArH-*5*), 7.30 (1H, t, *J* = 7.2, ArH-1), 7.42 (2H, t, *J* = 7.6, ArH-2, ArH-2'), 7.48-7.56 (4H, m, ArH-9, ArH-10, ArH-11), 8.07 (2H, d, *J* = 7.6, ArH-3, ArH-3'), 8.29 (1H, d, *J* = 8.3, ArH-4). ESI-HRMS found *m/z* 520.1159 [M+Na]$^+$, C$_{27}$H$_{25}$N$_3$NiO$_3$ requires 520.1142.

(*S*)-Pent-4-enyl-gly-Ni-BPB **46**
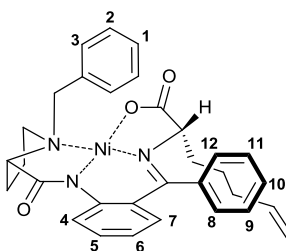
Under an atmosphere of N$_2$, Gly-Ni-BPB **45** (500 mg, 1 mmol) and 1-bromopent-4-ene (151 mg, 0.77 mmol) was suspended in acetonitrile (15 mL) and powdered sodium hydroxide (168 mg, 4.19 mmol) at −22 °C

(Methanol–Ice). The reaction was gradually raised to rt and stirred for 20 h, before the addition of water (30 mL) and acetic acid (1 mL), and the solution extracted with chloroform (3 × 30 mL). The combined organic fractions were concentrated *in vacuo* and purified by silica gel chromatography (chloroform:acetone 8:1) to afford (*S*)-pent-4-enyl-gly-Ni-BPB **46** (392 mg, 0.69 mmol, 69%) as a glassy, scarlet solid. R_f = 0.3 (chloroform:acetone 5:1); δ_H (500 MHz, CDCl$_3$): 1.57-1.75 (2H, m, alkyl), 1.87-2.28 (6H, m, alkyl, Pro-γH), 2.41-2.59 (1H, m, Pro-βH), 2.69-2.83 (1H, m, Pro-βH), 3.43-3.62 (4H, m, Pro-δH, NC*H*HPh, Gly-αH), 3.91 (1H, dd, *J* = 8.1, *J* = 3.3, Pro-αH), 4.44 (1H, d, *J* = 12.9, NCH*H*Ph), 4.93-5.03 (2H, m, *H*$_2$C=C), 5.64-5.79 (1H, m, H$_2$C=C*H*), 6.61-6.69 (2H, m, ArH-8, ArH-12), 6.92 (1H, d, *J* = 8.1, ArH-7), 7.11-7.22 (3H, m, ArH-5, ArH-9, ArH-11), 7.35 (2H, t, *J* = 7.6, ArH-2, ArH-2'), 7.44-7.51 (3H, m, ArH-1, ArH-6, ArH-10 8.04 (2H, d, *J* = 7.2, ArH-3, ArH-3'), 8.12 (1H, d, *J* = 8.6, ArH-4). δ_C (126 MHz, CDCl$_3$): 23.6, 24.6, 30.8, 33.3, 34.8, 57.0, 63.1, 70.3, 70.4, 115.3, 120.8, 123.7, 126.5, 127.2, 127.6, 128.9, 128.9, 129.7, 131.6, 132.1, 133.2, 133.8, 137.8, 142.3, 142.3, 170.4, 179.4, 180.4; ESI-HRMS found *m/z* 566.1926 [M+H]$^+$; C$_{32}$H$_{34}$O$_3$N$_3$Ni requires 566.1948; [α]$_D^{25}$ (CHCl$_3$, *c* = 0.03) +2533 (Lit: CHCl$_3$ *c* = 0.033, +2560).[4]

(*S*)-2-amino-hept-6-enoic acid
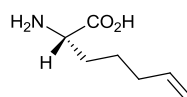
(*S*)-pent-4-enyl-gly-Ni-BPB **47** (492 mg, 0.87 mmol) was dissolved in methanol (25 mL), which was added dropwise to a solution of aqueous hydrochloric acid (3 M, 7 mL) and heated to 50 °C until a colour change from scarlet to yellow/green was observed (after 15 min) when cooling to rt was followed by the evaporation of the solvent *in vacuo*. The resulting yellow/white residue was extracted with chloroform (3 x 25 mL) to remove the BPB ligand **44** for re-use (**44** was purified as described above). The aqueous fraction was loaded on a Dowex 50X2 100 H$^+$ column (prewashed with H$_2$O to pH 7), which was rinsed with methanol (50 mL) and water (50 mL) to remove residual nickel, amino acid **47** was then eluted with 20% ammonium hydroxide:ethanol 1:1, where fractions containing **47** were identified by ninhydrin staining. Concentration of the fractions *in vacuo* afforded (*S*)-2-amino-hept-6-enoic acid

47 (118 mg, 95%) as a white, amorphous solid. m.p. 224-225 °C (Lit: 225 °C)[4]; δ_H (500 MHz, D_2O): 1.31-1.43 (2H, m, H3), 1.71-1.83 (2H, m, H4), 1.97-2.05 (2H, m, H5), 3.64 (1H, t, J = 5.9, H2), 4.94 (1H, d, J = 10.3, H7 *cis*), 4.99 (1H, d, J = 17.5, H7 *trans*), 5.74-5.84 (1H, m, H6). δ_C (125 MHz, D_2O): 23.5, 29.9, 32.5, 54.7, 115.0, 138.6, 174.9. ESI-HRMS found 144.1044; $C_7H_{14}NO_2$ [M-H]$^-$ requires 144.1019, $[\alpha]_D^{26}$ (H_2O c = 0.5) +9.5, Lit (H_2O, c = 1.2) +10.0.[4]

(*S*)-2-((((9H-fluoren-9-yl)methoxy)carbonyl)amino)hept-6-enoic acid **48**
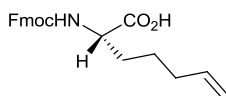
(*S*)-2-amino-hept-6-eneoic acid **47** (186 mg, 1.30 mmol) and sodium carbonate (273 mg, 2.59 mmol) were dissolved in water (4 mL) and cooled to 4 °C. 9-Fluorenylmethyl succinimidyl carbonate (657 mg, 1.95 mmol) was dissolved in 1,4 dioxane (8 mL) at 4 °C and added dropwise to the amino acid aqueous solution. After 1 h, the reaction was warmed to rt and allowed to continue for a further 14 h. The reaction suspension was diluted with water (15 mL) and extracted with ethyl acetate (2 × 25 mL). The organic layers were back-extracted with saturated sodium hydrogen carbonate solution (20 mL), with the combined aqueous fractions acidified to pH 1 with 3M hydrochloric acid and extracted further with ethyl acetate (3 × 35 mL). The combined organic fractions were dried and concentrated *in vacuo* to afford a pale yellow oil. Purification by flash chromatography (Dichloromethane:toluene:methanol 85:10:5) afforded (*S*)-2-((((9H-fluoren-9-yl)methoxy)carbonyl)amino)hept-6-enoic acid **48** as a viscous, straw coloured oil (260 mg, 0.69 mmol, 53%). R_f = 0.2 (Dichloromethane:methanol:acetic acid 95:4:1, visualised by ninhydrin (violet spot) and permanganate), δ_H (500 MHz, MeOD) 1.47 – 1.58 (2H, m, H3), 1.67 – 1.76 (1H, m, H4), 1.84 – 1.92 (1H, m, H4), 2.09 – 2.15 (2H, m, H5), 4.17 (1H, dd, J = 9.1, 4.8, H2), 4.26 (1H, t, J = 7.2, H10), 4.38 (2H, d, J = 7.2, H9), 4.99 (1H, d, J = 9.9, H7 *cis*), 5.05 (1H, d, J = 17.1, H7 *trans*), 5.78 – 5.88 (1H, m, H6), 7.33 (2H, t, J = 7.6, ArC*H*), 7.41 (2H, t, J = 7.6, ArC*H*), 7.65 – 7.72 (2H, m, ArC*H*), 7.82 (2H, d, J = 7.6, ArC*H*); δ_C (125 MHz, MeOD): 26.3, 32.3, 34.3, 35.5, 48.3 (*identified by HMQC)*, 55.3, 68.0, 115.6, 121.0, 126.3, 128.2, 128.8, 139.4, 142.6,

145.1, 145.4, 158.7, 175.5; ESI-HRMS found 364.1590 [M-H]$^-$; $C_{22}H_{22}NO_4$ requires 364.1554; $[\alpha]_D^{22.4}$ (CHCl$_3$, c = 1) +3.1.

4.1.3 Procedures and Data for Disubstituted Unnatural Amino Acid Synthesis

α-Benzoin oxime 31[153, 163]
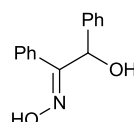
Benzoin **30** (20.0 g, 94.3 mmol) and sodium acetate (19.3 g, 235 mmol) were dissolved in ethanol (320 mL). Hydroxylamine hydrochloride (15.9 g, 230 mmol) and water (60 mL) were added and the reaction heated to 75 °C to dissolve all of the solid. After 30 mins, the solution was cooled to rt and diluted with water (200 mL). The solution was extracted with dichloromethane (3 × 200 mL) and the combined organic layers washed with saturated sodium bicarbonate (2 × 150 mL) and water (200 mL). The organic solution was dried (Na$_2$SO$_4$) and concentrated *in vacuo* to afford α-benzoin oxime **31** as a colourless, sticky solid (21.9 g, 94.3 mmol, quant.): m.p. 151 – 152 °C (From H$_2$O as pale yellow needles); (Lit 153 – 155 °C)[153]; δ$_H$ (500 MHz, CDCl$_3$): 3.85-3.52 (1H, br s, OH), 5.59 (0.5H, s, *E* isomer), 6.24 (0.5H, s, *Z* isomer), 7.52-7.13 (10 H, m, ArC*H*).

2-amino-1,2-diphenylethanol 32[153, 163]
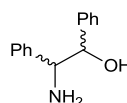
Palladium on carbon (50 mg) was added to a solution of α-benzoin oxime **31** (1.00 g, 4.44 mmol) in degassed ethanol (30 mL) and concentrated hydrochloric acid (0.4 mL). The solution was stirred under a positive pressure of H$_2$ for 7 h at rt. The suspension was filtered through Celite® and washed with methanol (100 mL). The solution was then concentrated *in vacuo* and the residue dissolved in dichloromethane (150 mL) and washed with saturated sodium bicarbonate (200 mL) to remove the hydrochloride salt. The organic layer was dried and then concentrated *in vacuo* to afford 2-amino-1,2-

diphenylethanol **32** as a colourless, amorphous solid (900 mg, 4.26 mmol, 96%). m.p. 145-146 °C (Recrystallised from H_2O as colourless, stubby needles) (Lit: 142-145 °C)[163]; Found C 78.60%, H 7.10%, N 6.65%; $C_{14}H_{15}NO$ requires C 78.84%, H 7.09%, N 6.59%; δ_H (500 MHz, $CDCl_3$): 2.40 – 1.60 (3H, br s, NH_2 & OH), 4.17 (1H, d, J = 5.9, CHNH$_2$), 4.75 (1H, d, J = 5.9, CHOH), 7.38 – 7.20 (10 H, m, ArH).

(1*S*, 2*R*)-Ethyl-*N*-(1,2-diphenyl-2-hydroxyethyl)glycinate **34**
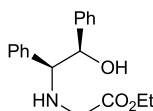
(1*R*, 2*S*)-2-amino-1,2-diphenylethanol **33** (1000 mg, 4.76 mmol) was dissolved in anhydrous tetrahydrofuran (25 mL) at rt. Ethyl bromoacetate (760 μL, 7.1 mmol) and triethylamine (1.32 mL, 9.5 mmol) were then added dropwise to the solution. After 18 h, the suspension was passed through a sintered funnel to remove the precipitated triethylammonium bromide salt and the filtrate concentrated *in vacuo* to afford an off-white, amorphous solid. The solid was recrystallised from ethanol (15 mL) to afford (1*S*, 2*R*)-ethyl *N*-(1,2-diphenyl-2-hydroxyethyl)glycinate **34** (1400 mg, 4.66 mmol, 98%) as white needles; m.p. 125-126 °C (Lit: 126-127 °C);[206] Found C 71.85%, H 6.95%, N 4.50; $C_{18}H_{21}NO_3$ requires C 72.22%, H 7.07%, N 4.68%; δ_H (500 MHz, $CDCl_3$): 1.20 (3H, t, J = 7.2, CH$_2$CH_3), 1.90 (1H, br s, NH), 2.84 (1H, br s, OH), 3.15 (1H, d, J = 17.5, NHCHH'CO$_2$Et), 3.28 (1H, d, J = 17.5, NHCHH'CO$_2$Et), 3.95 (1H, d, J = 6.0, OHCH), 4.11 (2H, q, J = 7.2, CH_2CH$_3$), 4.80 (1H, d, J = 6.0, NHCH), 7.16-7.22 (4H, m, ArCH), 7.23-7.31 (6H, m, ArCH); δ_C (126 MHz, $CDCl_3$): 14.2, 48.4, 60.7, 68.3, 126.9, 127.8, 127.9, 128.1, 128.3, 128.4, 128.4, 138.5, 140.2, 172.2; ESI-HRMS found *m/z* 300.1590 [M+H]$^+$; $C_{18}H_{22}NO_3$ requires 300.1594; $[\alpha]_D^{24}$ ($CHCl_3$, *c* = 0.7) +23.7 (Lit: CH_2Cl_2, *c* = 1) +24.2.[206]

(5*S*, 6*R*)-4-(*t*-Butoxycarbonyl)-5,6-diphenylmorpholin-2-one **35**
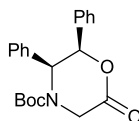
(1*S*, 2*R*)-Ethyl *N*-(1,2-diphenyl-2-hydroxyethyl)glycinate **35** (1310 mg, 4.38 mmol) was dissolved in toluene (20 mL) and heated to 110 °C. Di-*tert-*

butyl dicarbonate (1300 mg, 5.96 mmol) was added slowly as a solution in toluene (10 mL) to the reaction mixture over 1 h. After 12 h, 10 mL of toluene was distilled from the reaction at 130 °C at atmospheric pressure to remove any residual water. Fresh toluene (10 mL) and *p*-toluenesulfonic acid monohydrate (83 mg, 0.438 mmol) were added to the reaction mixture, which was heated at 110 °C for 1 h. 20 mL of toluene was then distilled from the reaction mixture over 2 h, followed by cooling to rt. The resulting solid was filtered and crystallised from hot ethanol to afford two rotamers (confirmed as rotamers by VT-NMR) of (5*S*, 6*R*)-4-(*t*-butoxycarbonyl)-5,6-diphenylmorpholin-2-one **35** (1315 mg, 3.72 mmol, 85%) as colourless, fine needles. m.p. 204-205 °C (Lit: 207 °C)[206]; Found C 71.30%, H 6.55%, N 3.90%; $C_{21}H_{23}NO_4$ requires C 71.37%, H 6.56%, N 3.96%; δ_H (500 MHz, CDCl$_3$) 1.18 (5H, s, ^tBu), 1.44 (4H, s, ^tBu), 4.31 (0.55 H, d, *J* = 18.2, H3), 4.45 (0.45H, d, *J* = 17.9, H3), 4.60 (0.45H, d, *J* = 17.9, H3'), 4.86 (0.55H, d, *J* = 18.2, H3'), 5.03 (0.55H, s, H5), 5.36 (0.45H, s, H5), 5.85 (1H, br s, H6). 6.62-6.80 (2H, m, ArC*H*), 6.96-7.30 (8H, m, ArC*H*); δ_C (75 MHz, CDCl$_3$) 27.9, 28.3, 44.8, 45.7, 58.7, 60.8, 80.4, 81.1, 81.4, 81.8, 126.3, 126.4, 127.7, 127.8, 128.0, 128.2, 128.6, 134.0, 134.3, 135.0, 136.0, 153.2, 153.5, 167.6, 168.0; ν_{max} (neat) 3041, 2974, 2914, 1741, 1687, 1604, 1455, 1432, 1362, 1343, 1273, 1240, 1196; ESI-HRMS found *m/z* 376.1474 [M+Na]$^+$, $C_{21}H_{23}NO_4Na$ requires 376.1441. $[\alpha]_D^{27}$ (CHCl$_3$, *c* = 0.7) -92.0, Lit: (CH$_2$Cl$_2$, *c* = 0.2) -87.3.[206]

(3*S*, 5*S*, 6*R*)-3-Methyl-4-(*t*-butoxycarbonyl)-5,6-diphenylmorpholin-2-one **36**
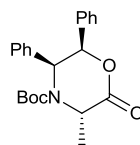
(5*S*, 6*R*)-4-(*t*-Butoxycarbonyl)-5,6-diphenylmorpholin-2-one **35** (2.57 g, 7.28 mmol) was dissolved in tetrahydrofuran (50 mL) and cooled to –78 °C. Sodium *bis*-(trimethylsilyl)amide (7.78 mL, 7.74 mmol, 1M solution in tetrahydrofuran) was added dropwise to the reaction mixture. After 35 min, methyl iodide (4.66 mL, 75 mmol) was added dropwise at –78 °C. After 90 min, the reaction mixture was poured into water (150 mL) and the aqueous layer extracted with ethyl acetate (3 × 120 mL). The combined organic layers were

dried and concentrated *in vacuo* to afford an orange oil. Purification by flash chromatography (Chloroform:methanol 99:1) afforded two rotamers of (3*S*, 5*S*, 6*R*)-3-methyl-4-(*t*-butoxycarbonyl)-5,6-diphenyl-morpholin-2-one **36** (2.09 g, 5.68 mmol, 78%) as brown, stubby needles (after crystallisation from hot ethanol). R_f = 0.4 (Hexane:ethyl acetate 2:1); m.p. 198-200 °C; Found C 71.15%, H 6.85%, N 3.60%; $C_{22}H_{25}NO_4$ requires C 71.91%, H 6.86%, N 3.81%; δ_H (500 MHz, DMSO-d_6, 392 K): 1.23 (9H, br s, ^tBu), 1.72 (3H, d, *J* = 7.0, C*H*$_3$), 4.88 (1H, q, *J* = 7.0, H3), 5.17 (1H, d, *J* = 3.1, H5), 6.15 (2H, d, *J* = 3.1, H6), 6.58 – 6.60 (2H, m, ArC*H*), 7.05 – 7.10 (5H, m, ArC*H*), 7.20 – 7.24 (3H, m, ArC*H*); δ_C (75 MHz, CDCl$_3$): 19.4, 28.7, 52.2, 60.3, 80.1, 125.4, 125.6, 126.3, 126.6, 126.7, 126.8, 127.0, 127.1, 127.5, 127.6, 133.0, 135.3, 152.0, 169.7; ESI-HRMS found *m/z* 390.1689 [M+Na]$^+$; $C_{22}H_{25}NO_4Na$ requires 390.1676;[154] $[\alpha]_D^{26}$ (CHCl$_3$, *c* = 0.7) −69.4 Lit: (CH$_2$Cl$_2$, *c* = 0.2) −61. [154]

(3*S*,   5*S*,   6*R*)-*tert*-butyl-3-methyl-2-oxo-3-(pent-4-enyl)-5,6-diphenylmorpholine-4-carboxylate **37**
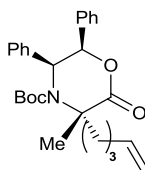
(3*S*, 5*S*, 6*R*)-3-methyl-4-(*t*-butoxycarbonyl)-5,6-diphenylmorpholin-2-one **36** (2100 mg, 5.71 mmol) was dissolved in anhydrous tetrahydrofuran (42 mL) and cooled to −40 °C (Liquid nitrogen in acetonitrile). 1-Iodopent-4-ene (2800 mg, 14.3 mmol) was added dropwise and the mixture was allowed to stir for 30 min. Potassium *bis*-(trimethylsilyl)amide (7.8 mL, 8.57 mmol, 0.91 M in tetrahydrofuran) was added dropwise and the reaction retained at −40 °C. After 1 h, water (50 mL) was added at −40 °C and the suspension was raised to rt and extracted with ethyl acetate (3 × 100 mL). The organic layers were dried (Na$_2$SO$_4$) and concentrated *in vacuo* to afford an orange, amorphous solid. Purification by flash chromatography (Chloroform:acetone 99:1) afforded (3*S*, 5*S*, 6*R*)-*tert*-butyl-3-methyl-2-oxo-3-(pent-4-enyl)-5,6-diphenylmorpholine-4-carboxylate **37** as a colourless, amorphous solid (970 mg, 2.80 mmol, 49%). R_f = 0.6 (Hexane:ethyl acetate 2:1), δ_H (500 MHz, DMSO-d_6, 392 K): 1.40 (9H, br s, ^tBu), 1.69 (3H, s, C*H*$_3$), 1.45 – 1.57 (2H, m, CH$_2$C*H*$_2$CH$_2$), 2.09 (2H, app q,

J = 7.3, CH_2CH=CH$_2$), 2.21 – 2.28 (1H, m, C(Me)CH_2CH$_2$), 2.43 – 2.45 (1H, m, C(Me)CH_2CH$_2$), 4.95 – 4.99 (1H, m, CH=CH_2 *cis*), 5.03 (1H, dq, J = 17.2, 2.1, CH=CH_2 *trans*), 5.57 (1H, d, J = 3.6, H5), 5.78 – 5.89 (1H, m, H4), 6.13 (1H, d, J = 3.6, H6), 6.94 – 6.97 (2H, d, ArCH), 7.12 – 7.14 (3H, m, ArCH) 7.19 – 7.24 (5H, m, ArCH); δ_c (125 MHz, CDCl$_3$): 24.1, 24.3, 25.2, 28.5, 33.6, 33.7, 57.6, 64.0, 67.3, 80.5, 114.3, 115.4, 125.8, 127.8, 127.9, 128.1, 128.2, 128.3, 129.0, 129.9, 135.4, 135.7, 135.9, 137.9, 172.5, 173.0; $\nu_{(max)}$ 3066, 3034, 2976, 2931, 1747, 1694, 1641, 1498, 1454; ESI-HRMS found 458.2303 [M+Na]$^+$; C$_{27}$H$_{33}$NO$_4$Na requires 458.2302, $[\alpha]_D^{23.3}$ (CHCl$_3$, c = 1) +29.9.

(*S*)-2-(*tert*-butoxycarbonyl)amido-2-methylhept-6-enoic acid **38**
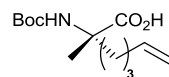
(3*S*, 5*S*, 6*R*)-*tert*-butyl-3-methyl-2-oxo-3-(pent-4-enyl)-5,6-diphenylmorpholine-4-carboxylate **37** (950 mg, 2.18 mmol) was dissolved in anhydrous tetrahydrofuran (25 mL) and anhydrous ethanol (2 mL) and transferred *via cannula* to liquid ammonia (~50 mL) at –78 °C. Lithium wire (301 mg, 43.7 mmol) was washed in hexane and added to the reaction mixture in several portions. After the blue colour dissipated (15 min), saturated ammonium chloride was added dropwise, and the temperature allowed to rise to rt overnight, to ensure evaporation of ammonia gas. The aqueous solution was extracted with ether (2 × 50 mL), acidified to pH 2 with 1M hydrochloric acid and extracted further with ethyl acetate (3 × 50 mL). The organic layers were combined, dried and concentrated *in vacuo* to afford a colourless solid. Purification by flash chromatography (dichloromethane : methanol 95:5) afforded (*S*)-2-(*tert*-butoxycarbonyl)amido-2-methylhept-6-enoic acid **38** as a colourless, amorphous solid (468 mg, 1.83 mmol, 84%). m.p. 230 °C (decomposes); R_f = 0.2 (dichloromethane:methanol 95:5, stained with ninhydrin (scarlet spot) and permanganate); δ_H (500 MHz, MeOD) 1.25 – 1.41 (3H, m, H3 & H4), 1.45 & 1.46 (12H, 2 × br s, ^{t}Bu & CH_3), 1.75 – 1.85 (1H, m, H3), 4.93 (1H, *fine splitting obscured by residual peaks*, H7), 4.98 (1H, d, J = 17.0, H7 *trans*), 5.75 –5.95 (1H, m, H6); δ_C (125 MHz, MeOD) 24.3, 25.0, 28.9, 35.0, 37.3, 61.0, 79.7, 115.0, 139.9, 156.4, 181.2; $\nu_{(max)}$ 3411, 3355, 1667, 1620, 1485,

1454, 1405, 1367, 1170; ESI-HRMS found 280.1507 [M+Na]$^+$; $C_{13}H_{23}NO_4Na$ requires 280.1519, $[\alpha]_D^{24.7}$ (MeOH, *c* = 1) +16.0.

(*S*)-2-((((9H-fluoren-9-yl)methoxy)carbonyl)amino)-2-methylhept-6-enoic acid **16**
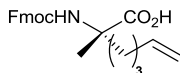
(*S*)-2-(*tert*-butoxycarbonyl)amido-2-methylhept-6-enoic acid **38** (468 mg, 1.82 mmol) was suspended in dichloromethane (6 mL) and trifluoroacetic acid (6 mL) was added slowly (2 mL/min) at rt. After 30 min, the solvents were removed *in vacuo* and dried on the high vacuum manifold until less than 2 equivalents of trifluoroacetic acid remained by weight. The residue was then dissolved in water:acetone (1:1, 10 mL), cooled to 0 °C and then sodium carbonate (963 mg, 9.10 mmol) and 9-fluorenylmethyl succinimidyl carbonate (644 mg, 1.90 mmol) were added. After 1 h, the suspension was acidified to pH 3 with 1M hydrochloric acid and extracted with ethyl acetate (3 × 120 mL). The combined organic layers were combined, dried and concentrated *in vacuo* to afford a yellow residue. Purification by flash chromatography (dry loaded, and eluted with 85:10:5 dichloromethane:toluene:methanol) afforded (*S*)-2-((((9H-fluoren-9-yl)methoxy)carbonyl)amino)-2-methylhept-6-enoic acid **16** as a pale yellow oil (430 mg, 1.13 mmol, 62%). R_f = 0.2 (94:5:1 dichloromethane:methanol:acetic acid), stained with ninhydrin (violet)), δ_H (500 MHz, MeOD) 1.29 – 1.42 (5H, m, C*H*$_3$ and H3), 1.81 – 1.93 (2H, m, H4), 2.00 – 2.08 (2H, m, H5), 4.19 (1H, t, *J* = 6.8, H10), 4.28 – 4.35 (2H, m, C*H*$_2$O), 4.93 (1H, d, *J* = 10.7, H7 *cis*), 4.99 (1H, d, *J* = 17.1, H7 *trans*), 5.71 – 5.89 (1H, m, H6), 7.29 (2H, t, *J* = 7.3, ArC*H*), 7.36 (2H, t, *J* = 7.3 ArC*H*), 7.60 – 7.67 (2H, m, ArC*H*), 7.77 (2H, d, *J* = 7.7, ArC*H*); δ_C (125 MHz, MeOD): 24.4, 34.8, 37.6, 49.6 (*identified by HMQC)*, 60.8, 67.5, 115.2, 120.9, 126.2, 126.3, 128.2, 128.8, 139.6, 142.6, 145.3, 158.1, 178.0; ν_{max} 3331 (br), 3029, 2956, 1950, 1913, 1680, 1615, 1535, 1421; ESI-HRMS found 402.1687 [M+Na]$^+$; $C_{23}H_{25}NO_4Na$ requires 402.1676. $[\alpha]_D^{21.1}$ (CHCl$_3$, *c* = 0.3) + 6.5.

1-iodopent-4-ene **40**
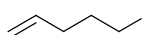
4-Penten-1-ol (200 mg, 2.32 mmol), triphenyl phosphine (728 mg, 2.78 mmol) and imidazole (237 mg, 3.48 mmol) were dissolved in dichloromethane (5 mL) at 0 °C. Iodine (703 mg, 2.78 mmol) was added and the solution allowed to stir at 0 °C for 1 h. The solution was allowed to warm to rt and quenched with saturated NH_4Cl (15 ml) and extracted with dichloromethane (3 × 10 mL). The combined organic layers were washed with brine (20 mL), dried and concentrated *in vacuo* to afford a thin, colourless oil. Purification by silica gel chromatography (Ethyl acetate:hexane, 1:19) afforded 1-iodopent-4-ene **40** as a thin, volatile oil (270 mg, 1.40 mmol, 60%): R_f = 0.9 (Ethyl acetate:hexane 1:19); δ_H (500 MHz, $CDCl_3$): 1.92 (2H, quin, *J* 6.8, H2), 2.17 (2H, q, *J* 6.8, H3), 3.20 (2H, t, *J* 6.8, H1), 5.02 (1H, d, *J* 10.3 H5 *cis*), 5.09 (1H, d, *J* 17.1, H5 *trans*), 5.80 – 5.70 (1H, m, H4). δ_C (126 MHz, $CDCl_3$): 6.7, 32.8, 34.7, 116.3, 137.0.

4.2 Procedures regarding the synthesis of peptides

4.2.1 General Regards

All amino acids and resins were purchased from either Novasyn (Merck) or Sigma-Aldrich. All amino acids were *N*-Fmoc protected and side chains were protected with Boc (Lys, Trp); *O*^tBu (Asp, Glu, Ser, Thr); Trt (Cys, Asn, Gln); Pbf (Arg). Synthesis of peptides was performed either manually using vaculate reservoirs and draining from a water aspirator or by the use of a microwave assisted automated peptide synthesiser (CEM Liberty). DMF used in peptide synthesis was of ACS grade from Sigma-Aldrich. Peptide identities were confirmed by the LCMS and HRMS machines stated in 4.1.1. Multiple charge states were used to reinforce the assignment of species observed by LCMS, and the monoisotopic mass used in 4 d.p. analysis.

4.2.2 Methods for Manual Fmoc Solid Phase Peptide Synthesis

Method A: Resin Swelling

The required quantity of resin was placed in a vaculate reservoir and CH_2Cl_2 (2 ml) was added and the resin was agitated on a blood spinner for 2 h to allow swelling of the resin.

Method B: Deprotection of *N*-Fmoc protecting groups

N-terminal Fmoc protecting groups were removed by the addition of 20% piperidine:DMF (5 × 2 mL × 2 min), followed by rinsing the resin with DMF (5 × 2 mL × 2 min). Successful deprotection was determined by a positive colour test (Methods C & D).

Method C: Kaiser Test[165]

The Kaiser Test was employed for the determination of the successful coupling or deprotection for most of the residues. A small number of resin beads were rinsed in ethanol and placed in a vial, followed by the addition of two drops of each of the three solutions in the following order:

1) Ninhydrin (5% w/v) in ethanol;

2) Phenol (80% w/v) in ethanol;

3) 1 mM $KCN_{(aq.)}$ in pyridine (2% v/v).

The solution was then heated to ca. 150 °C for 1 min. A successful coupling gave no change in the colour of the beads, whereas bright blue beads illustrate a successful deprotection. This colour test was useful for the identification of free primary amines, however inconclusive results are obtained for Asp, Ser, Pro and Asn residues.

Method D: Chloranil Test[207]

The chloranil test was also employed for the determination of successful couplings or deprotections of some residues. A small number of beads were rinsed in ethanol and placed in a vial, followed by the addition of two drops of each of the two solutions in the following order:

1) Acetaldehyde (2% v/v) in DMF;

2) *p*-Chloranil (2% w/v) in DMF.

The solution was left at rt for 5 min. No change in colour of the beads showed a negative result, whereas the change of bead colour to pale green/bright blue illustrated a successful deprotection. This test was especially useful for Pro residues, where the bead colour became a very bright blue (often after 10 seconds) to show a free secondary amine. However, the length of time (often ~10 min for a primary amine) for the colour change made this colour

test less useful than the Kaiser test for the determination of free primary amines.

Method E: Coupling of Amino Acids with Uronium Coupling Reagents

The desired amino acid (5 equiv.), DIPEA (5 equiv.), HOBt (5 equiv.) and Uronium coupling reagent (Either HATU, HBTU or HCTU) (5 equiv.) were dissolved in DMF (2 mL) and added to the resin, followed by agitation for 1 h (2 h for unnatural amino acids). For double couplings, this step was repeated. After draining the reagents, the resin was washed with DMF (3 × 2 mL × 2 min) and the success of coupling determined by a negative colour test (Methods C & D). Deprotection of the Fmoc-protected *N*-terminus then followed (Method B).

Method F: Coupling of Cysteine and Thiazolidine (Thz)

The desired amino acid (5 equiv.), 2,4,6-trimethylpyridine (5 equiv.) and HCTU (5 equiv.) were dissolved in   1:1 CH_2Cl_2:DMF (2 mL) and added to the resin, followed by agitation for 1 h. After draining the reagents, the resin was washed with DMF (3 × 2 mL × 2 min) and the success of coupling determined by a negative colour test (Methods C & D).

Method G: *N*-terminal acetylation

Acetic anhydride (10 equiv.) and DIPEA (10 equiv.) were dissolved in DMF (2 mL) and the solution was transferred to the resin. After 2 h, the resin was drained, washed with DMF (3 × 2 mL × 2 min) and successful capping determined by a negative colour test (Methods C & D).

Method H: *N*-terminal FITC labelling[172]

Fluorescein isothiocyanate (1.2 equiv.) was dissolved in 12:8:5 Pyridine:DMF:CH_2Cl_2 (2 mL) and the solution transferred to the resin in the dark. After 18 h, the resin was washed with DMF (5 × 2 mL × 2 min) ahead of cleavage and deprotection (Method K). The solvents were of anhydrous grade and the pyridine distilled prior to use.

Method J: On-Resin Olefin Metathesis

After the completed peptide elongation and *N*-terminal acetylation, on-resin olefin metathesis was completed by the preparation of a 10 mM solution of Grubbs First Generation Catalyst in degassed dichloroethane (2 mL), which

was added to the resin beads and allowed to agitate gently for 2 h, after which time the metathesis procedure was repeated for another 2 h. *N*-terminally acetylated peptides were then cleaved from the resin (Method K). For FITC labelled peptides, metathesis was performed before labelling (Method H).

Method K: Cleavage and deprotection of Rink Amide MBHA and Wang resins

After elongation and *N*-terminal acetylation was complete, the resin was washed with DMF (5 × 2 mL × 2 min), CH_2Cl_2 (5 × 2 mL × 2 min) and then Et_2O (3 × 2 mL × 2 min). Peptides were then simultaneously cleaved and side-chain deprotected with cleavage 'Reagent K' TFA:EDT:Thioanisole:Phenol:H_2O, 82:3:5:5:5 (3 × 2 mL × 1 h). The resin was washed with fresh TFA (2 mL × 2 min) and the solution concentrated *in vacuo*.

The resulting oil was precipitated with ice-cold ether (10 mL) and placed in a centrifuge (3000 rpm × 0.5 min). The supernatants were removed, the precipitate rinsed with ice-cold ether (3 × 10 mL) and dried *in vacuo*.

Method L: Cleavage of TGT Resins to Afford Side-chain Protected Peptides

After rinsing with DMF (5 × 2 mL × 2 min), CH_2Cl_2 (5 × 2 mL × 2 min) and then Et_2O (3 × 2 mL × 2 min), the peptides were cleaved from the resin with a cleavage cocktail of TFA:CH_2Cl_2, 1:199 (2 × 2 mL × 1 h). The resin was rinsed with fresh cleavage cocktail (2 × 2 mL × 2 min) and the solution concentrated *in vacuo*.

Method M: *C*-terminal thioesterification of protected peptides

The side-chain protected peptide was dissolved in anhydrous DMF (to a concentration of 0.0575 M) under N_2, and BnSH (20 equiv.) was added at rt. After 30 mins, PyBOP (2 equiv.) was added, followed by DIPEA (2 equiv.) after a further 15 min. After 2 h, PyBOP (2 equiv.) and DIPEA (2 equiv.) was added. The reaction was monitored by LCMS by removing an aliquot of the reaction mixture and adding TFA:TIPS:H_2O (92.5:2.5:5) deprotected the side chains to allow the peptide to ionise. After 15 h, the solvent was evaporated *in vacuo* and the peptidyl thioester globally deprotected using 'Reagent K' 82:3:5:5:5 TFA:EDT:Phenol:Thioanisole:H_2O (5 mL) under N_2 for 2 h. The solution was

concentrated *in vacuo* and the peptide precipitated with ice cold ether (10 mL) and placed in a centrifuge (3000 rpm × 0.5 min). The supernatants were removed, the precipitate rinsed with ice-cold ether (10 × 10 mL) and dried under a nitrogen jet.

Method N: Peptide Purification

Peptides were purified by preparative scale HPLC using a Jupiter Proteo preparative column (reversed phase) on an increasing gradient of acetonitrile to water (plus 0.1% formic acid v/v in both solvents) at a flow rate of 20 mL min^{-1}. Crude peptides were suspended in either dimethylsulfoxide or 1:1 acetonitrile:water at an approximate concentration of 15 - 20 mg mL^{-1}. Purification runs injected a maximum of 2.5 mL of crude peptide solution and were allowed to run for 35 min, with acetonitrile increasing from 5 to 95%, and the eluent scanned with a diode array at 220, 254, 280 and 490 nm. Fractions were checked by LCMS, concentrated *in vacuo* and lyophilised. For semi-preparative purification, a Jupiter Proteo Semi-Preparative (reversed phase) column was used, with the injection reduced to 250 μL and the flow rate reduced to 3 mL min^{-1}. For peptides with crude UV traces that were unsuitable for collection by chromatogram, purification was performed on a semi-preparative scale using a mass directed chromatography software Masshunter by ChemStation (Agilent). Mass directed chromatography allows the collection of the desired peptide by mass, with the eluent split into an Agilent 6120 Quadrupole LCMS which triggers collection of eluent at a programmed m/z. The column used with this apparatus is an Agilent XBridge 5 μM 10×50 mm C$_{18}$ semi preparative column. Injections were 250 μL and flow rate 5 mL min^{-1}.

4.2.3 Cycles for automated peptide synthesis

Peptides that were built on the microwave assisted Liberty CEM Peptide Synthesiser followed this cycle:

Resin Loading

Clean reaction vessel; wash with DMF; wash with CH$_2$Cl$_2$; transfer resin to reaction vessel; wash with DMF; wash with CH$_2$Cl$_2$; transfer resin to reaction vessel; wash with DMF; wash with CH$_2$Cl$_2$; vessel draining.

Deprotection and coupling

Clean resin dip tube, wash with DMF (15 mL), add 20% piperidine in DMF (6 mL), microwave method (30 sec), wash with DMF (15 mL), add 20% piperidine in DMF (6 mL), microwave method (30 sec), wash with DMF (15 mL), clean resin dip tube, wash with DMF (15 mL), add amino acid (2.5 mL), add coupling reagent (1 mL), add activator base (0.5 mL), microwave method (5 min), wash with DMF (15 mL), drain.

For methods that ***did not*** use microwave assistance, the reaction cycle was the same, except the microwave method for deprotection and coupling was replaced by agitation of the resin at rt for 10 min and 90 min respectively.

After the final residue, the resin is ejected from the reaction vessel and cleavage/deprotection was performed manually using Methods K-M.

4.2.4 Specific protocols for the use of Dawson resin

Method O: Loading of Dawson Resin

After swelling of the resin (4.2.2, Method A) and deprotection of the Fmoc-Dbz group (4.2.2, Method B), the first coupling was done by the addition of Fmoc-Ala-OH (5 equiv.), HBTU (5 equiv.), HOBt (5 equiv.) and DIPEA (10 equiv.) in DMF (2 mL) and the resin agitated for 1.5 h. The resin was drained, and the coupling repeated. After the first residue was successfully coupled by determination from LCMS, the following residues were deprotected and coupled by the methods described above (4.2.2, Methods B & F).

Method P: The final coupling of Dawson resin

Boc-Met-OH (5 equiv.), HBTU (5 equiv.), HOBt (5 equiv.) and DIPEA (5 equiv.) was dissolved in DMF (2 mL) and agitated at rt for 1 h. After determination of a successful coupling (4.2.2, Method D), the resin was washed with DMF (5 × 2 mL × 2 min) and CH_2Cl_2 (5 × 2 mL × 2 min).

Method Q: Activation of Dawson resins to *C*-terminal *N*-acylbenzimidazolinone

After purging the resin beads with a stream of N_2, *p*-nitrophenylchloroformate (5 equiv.) was dissolved in anhydrous CH_2Cl_2 (2 ml)

and agitated at rt, sealed under N_2 for 2 h. The resin was drained, and DIPEA (10 equiv.) in DMF (2 mL) was added and the resin agitated for a further 60 min. After confirming the completion of the activation by LCMS, the peptide was cleaved from the resin using 'Reagent K'; (82:3:5:5:5 TFA:EDT:Phenol:Thioanisole:H_2O) for 2 × 2 h. The peptidyl solution was concentrated *in vacuo* and precipitated with ice cold ether (10 mL) and placed in a centrifuge (3000 rpm × 0.5 min). The supernatants were removed, the precipitate rinsed with ice cold ether (3 × 10 mL) and dried *in vacuo*.

4.2.5 Native Chemical Ligation

Fragment 3 and Fragment 2 were separately dissolved in freshly prepared, degassed ligation buffer (6M guanidinium hydrochloride, 0.1 M sodium phosphate, 200 mM 4-mercaptophenyl acetic acid, 20 mM tris(2-carboxyethyl) phosphine, pH 7.0) to a concentration of ~ 2 mM. The peptidyl solutions were centrifuged (10000 rpm × 2 min) and the concentration of the supernatant verified by UV-Vis spectroscopy. The supernatants were then mixed to equimolar concentrations of Fragment 3 and 2 under nitrogen and the ligation monitored by LCMS.

The *N*-terminal Thz residue on the ligated Fragment 2-3 was deprotected by the addition of 200 mM methoxyamine hydrochloride and 20 mM tris(2-carboxyethyl) phosphine (TCEP) and the pH adjusted to ~4. The deprotection was monitored by LCMS.

Fragment 1 Nbz was then dissolved in ligation buffer to a concentration of ~2 mM and centrifuged (10000 rpm × 2 min). The supernatant was then added to the Fragment 2-3 ligation mixture to have an equimolar mixture of Fragment 1 and Fragment 2-3, with the ligation monitored by LCMS.

4.2.6 Maleimide Bridging of hCys BID peptides

hCys BID was dissolved to a 200 μM concentration in degassed bridging buffer (2.5:37.5:60 dimethylformamide:acetonitrile: 40 mM phosphate buffer) with 5 eq. TCEP and 5 eq. dibromomaleimide added and the pH adjusted to ~6.5. After 12 h, the reaction mixture was washed with ethyl acetate and the concentrated *in vacuo*.

4.3 Specific Peptide Synthesis Procedures - p53 and Bcl-2 family

4.3.1 p53 peptide series

The p53 series of peptides (p53 MM and p53 MU) were built on Rink Amide MHBA Resin (Capacity 0.79 mmol g^{-1}) on a scale of 0.05 mmol, using Methods A-G, J and K. The coupling reagent was HCTU and double couplings were employed for ^{29}Asn and ^{30}Asn. Purification of the peptides using preparative HPLC (Jupiter Proteo Preparative column) on a gradient of 20-60% acetonitrile over 20 mins afforded 7 mg (13%) and 6 mg (11%) of p53 MM and p53 MU respectively.

4.3.2 Unlabelled BID peptides

The unlabelled BID series (BID WT, BID MM, BID MU, BID DM, BID DU and BID Aib) were synthesised on Rink Amide MBHA LL Resin (Capacity ~0.45 mmol g^{-1}) on a 0.1 mmol scale using manual and automated SPPS methods. Residues ^{91}AXVGDX were coupled manually, with the surrounding residues coupled using non-microwave assisted automated synthesis. The coupling conditions followed Method E with HCTU as the coupling reagent, with the following residues double-coupled with HCTU: ^{82}I, ^{83}I, ^{84}R, ^{85}N and ^{103}W. The Fmoc groups of ^{92}X and ^{96}X were deprotected as in Method B, but with each deprotection lasting 5 min. ^{91}A and ^{95}D were double coupled using 10 equivalents of HATU, with the first coupling proceeding for 1 h and the second coupled overnight. For the synthesis of BID MM and BID DM, the peptide was divided into two halves, with one cleaved (Method K) to afford BID MU or DU, and the other half metathesised (Method J) before cleavage (Method K) to afford BID MM or DM.

Purification was performed using a Jupiter Proteo semi-preparative column outlined in Method N. The employed gradient was 0-40-60-95% acetonitrile with 0.1% formic acid at times 0-5-25-30 mins with the elution between 17-19 minutes for WT BID and Aib BID peptides and 19-21 minutes for MM, MU, DM and DU BID. The purified yields of peptides were: BID WT 24.1

mg (11%); BID MM 13.1 mg (10%); BID MU 3.9 mg (4%); BID DM 7.2 mg (7%); BID DU 4.7 mg (5%); BID Aib 9.1 mg (10%).

4.3.3 FITC Labelled BID Peptides

FITC labelled BID peptides (BID WT*, BID Aib*, BID MM* and BID DM*) were synthesised on a 0.05 mmol scale in the same manner described in 4.3.2. The *N*-termini were functionalised with 6-aminohexanoic acid (BID WT*) or β-alanine (BID Aib*, MM*, DM*) which were coupled using Method E with HCTU as the activator. Then, on-resin Grubbs metathesis (Method J) was done for BID MM* and BID DM* before Fmoc deprotection (Method B) and labelling with FITC (Method H). Cleavage and deprotection was performed as Method K, with the exception of the peptide being kept in the dark to prevent photobleaching of the FITC tag.

Purification of the BID WT*, MM* and DM* peptides was performed by semi-preparative HPLC (Method N) using a Jupiter Proteo semi-preparative column with a gradient of 5-40-60-95% acetonitrile (with 0.1% formic acid) at time 0-5-25-30 mins. The peptides generally eluted between 20-22 minutes. BID Aib* was purified using the mass-directed semi-preparative method (Method N) on an Agilent XBridge column, using a gradient of 40-60% acetonitrile (with 0.1 % formic acid) over 20 minutes. BID Aib* eluted at 6 minutes. The purified yields of the peptides were: WT* 6.5 mg (7%); Aib* 9. 9 mg (10 %), MM* 23 mg (21 %) and DM* 9.25 mg (10%).

4.3.4 hCys BID

hCys BID was synthesised on Rink Amide MBHA LL Resin (Capacity 0.36 mmol g^{-1}) on a 0.05 mmol scale, following the same procedure as outlined in 4.3.2, but without the double couplings of ^{82}I, ^{83}I, ^{84}R and ^{85}N.

Purification was performed using semi-preparative HPLC using an Agilent XBridge column using a gradient of 30-50% acetonitrile (with 0.1% formic acid) over 25 minutes. The peptide eluted at 17-18.5 minutes to afford 6 mg (5 %) of pure hCys BID.

4.3.5 hCys BID MAL and hCys BID SUC

hCys BID was converted into hCys BID SUC using the protocol described in 4.2.6. 30 mg of crude hCys BID (cleaved from the resin) was reacted and purified using semi-preparative HPLC using an Agilent XBridge column using a gradient of 35-55% acetonitrile (with 0.1% formic acid) over 25 minutes. The peptide eluted at 7.0-8.5 minutes to afford 4.1 mg (11%) of hCys BID SUC. hCys BID MAL was identified as being present in the reaction mixture and as a shoulder in some HPLC fractions, but was not isolated.

4.3.6 BIM Peptide Series

The BIM series of peptides (BIM MM and BIM DM) were synthesised on Rink Amide MBHA LL resin (Capacity 0.36 mmol g^{-1}) on a scale of 0.1 (BIM MM) and 0.075 (BIM DM) following Methods A-E, with HCTU employed as the coupling reagent. The peptide was synthesised on the automated peptide synthesiser without microwave assistance, except for the residues encompassing ^{152}RXIGDX which were coupled manually. The Fmoc groups of ^{153}X and ^{157}X were deprotected as Method B, but with each deprotection lasting 5 min. ^{152}R and ^{158}D were double coupled using 10 equivalents of HATU, with the first coupling proceeding for 1 h and the second coupled overnight. On-resin Grubbs metathesis followed Method J prior to cleavage and deprotection (Method K).

Purification was performed using semi-preparative HPLC with a Jupiter Proteo semi-preparative column on a gradient of 0-35-52-95% acetonitrile (with 0.1% formic acid) at times 0-7-27-31 mins with BIM DM and MM eluting at 16-18 minutes. The purified yields of peptides were: BIM MM 9.2 mg (23% based on 40 mg purified) and BIM DM 21.6 mg (32% of 0.038 mmol purified).

4.3.7 Im7 Fragment 3

Im7 Fragment 3 was synthesised on Fmoc-Gly-Wang resin (Capacity 0.79 mmol g^{-1}) on a 0.08 mmol scale, using manual SPPS synthesis (Methods A-F) and HCTU as the activator in Method F. Residues ^{68}I, ^{69}V, ^{71}E, ^{72}I and ^{79}N were double coupled before cleavage and deprotection was done following Method K.

Purification of Im7 Fragment 3 was done using a Jupiter Proteo preparative HPLC column on a gradient of 5-40-60-95% acetonitrile at time 0-10-30-35 mins with the peptide eluting at 18-19 mins. The purified yield was 48 mg (19%).

4.3.8 Im7 Fragment 2

Im7 Fragment 2 was synthesised on a scale of 0.1 mmol on Fmoc-Ser NovaSyn TGT resin (Capacity 0.20 mmol g^{-1}) using automated non-microwave assisted synthesis following Methods A-F, with HCTU as the coupling reagent. Residues ^{41}F and ^{57}P were double coupled and the *N*-terminal ^{29}Thz residue was coupled manually (Method F). Cleavage followed Method L to afford 333 mg (77%) of the crude side-chain protected peptide, which was thioesterified on its *C*-terminus (Method M). Global deprotection of the side chain protecting groups then followed Method K.

Purification was done using semi-preparative HPLC using an Agilent XBridge column (Method N), on a gradient of 35-50% acetonitrile (with 0.1% formic acid) over 20 minutes. The peptide eluted between 12-14 minutes. The purified yield was 10 mg (15%).

4.3.9 Im7 Fragment 1 (*C*-terminal Acid)

Im7 Fragment 1 was built on a 0.05 mmol scale on Fmoc-Ala NovaSyn TGT resin (Capacity 0.21 mmol g^{-1}), with the automated non-microwave assisted synthesis performed for all of the peptide couplings (Methods B & F) and HCTU used as the coupling reagent. The eight *N*-terminal residues were double coupled (Method E) before cleavage from the resin (Method L) to afford the crude side-chain protected peptide (257 mg, 83% crude).

4.3.10   Im7 Fragment 1 (*C*-terminal Nbz)

Im7 fragment 1 with *C*-terminal Nbz group was built on a 0.1 mmol scale on Dawson Dbz TGR resin (Capacity 0.22 mmol g^{-1}) following Methods O, F and P with HBTU used as the coupling agent. After peptide elongation was complete, activation of the resin (Method Q) was followed by cleavage and deprotection of the peptide (Method K).

Purification of the peptide was performed by semi-preparative HPLC using a Jupiter Proteo column (Method N) on a gradient of 5-25-45-95% acetonitrile (with 0.1% formic acid) at times 0-5-25-30 minutes. The peptide eluted between 18-20 minutes and required *immediate* evaporation of the solvent to prevent hydrolysis of the Nbz activating group. The purified yield was 10 mg (25%).

4.4 Peptide Data

4.4.1 High Resolution Mass Spectrometry Data

Below is a tabulation of the HRMS data of the peptides that have been synthesised. Peptide identity was confirmed by the inspection of multiple charge states and are quoted as the *monoisotopic* peak for the Expected (Exp[d]) and Observed (Obs[d]) masses.

4.4.1.1 p53

Peptide	[M+H+Na]$^{2+}$Obs[d]	[M+H+Na]$^{2+}$Exp[d]
p53 U	1111.5335	1111.5318
p53 M	1097.5137	1097.5135

4.4.1.2 Unlabelled BID peptides

Peptide	[M+2H]$^{2+}$ Obs[d]	[M+2H]$^{2+}$ Exp[d]	[M+3H]$^{3+}$ Obs[d]	[M+3H]$^{3+}$ Exp[d]
BID WT	1359.7318	1359.7253	906.8313	906.8193
BID-Aib	1337.2347	1337.2328	891.8258	891.8243
BID-DU	1391.2777	1391.2798	927.8572	927.8556
BID-DM	1377.2529	1377.2641	918.5114	918.5118
BID-MU	1377.2619	1377.2641	918.5161	918.5161
BID-MM	1363.2338	1363.2485	909.1673	909.1673

4.4.1.3 hCys BID

Homocysteine BID peptides were oxidised to an intramolecular disulfide in the presence of Diamide (5 equiv.) or reduced to the free thiols by TCEP (5 equiv.).

Peptide	[M+3H]$^{3+}$ Obs[d]	[M+3H]$^{3+}$ Exp[d]	[M+4H]$^{4+}$ Obs[d]	[M+4H]$^{4+}$ Exp[d]
BID hCys OX	912.4684	912.4677	684.6083	684.6028
BID hCys RED	913.1407	913.1396	685.1077	685.1067
BID hCys MAL	944.1281	944.1341	708.3517	708.3524

| BID hCys SUC | 944.8036 | 944.8046 | 708.8556 | 708.8563 |

4.4.1.4 FITC labelled BID peptides

Peptide	[M+4H]⁴⁺ Obs^d	[M+4H]⁴⁺ Exp^d	[M+5H]⁵⁺ Obs^d	[M+5H]⁵⁺ Exp^d
BID WT*	795.3939	795.3942	636.5157	636.5169
BID Aib*	773.6356	773.6362	619.1093	619.1105
BID DM*	793.6513	793.6518	635.1209	635.1230
BID MM*	786.6422	786.6440	629.5143	629.5166

4.4.1.5 BIM BH3 peptides

Peptide	[M+3H]³⁺ Obs^d	[M+3H]³⁺ Exp^d	[M+4H]⁴⁺ Obs^d	[M+4H]⁴⁺ Exp^d
BIM WT	894.4736	894.4735	671.1072	671.1069
BIM DM	882.8175	882.8150	662.3624	662.3662

Peptide	[M+3H]³⁺ Obs^d	[M+3H]³⁺ Exp^d	[M+2H]²⁺ Obs^d	[M+2H]²⁺ Exp^d
BIM MM	873.4713	873.4712	1309.7027	1309.7032

4.4.1.6 Im7 peptides

Peptide	[M+3H]³⁺ Obs^d	[M+3H]³⁺ Exp^d	[M+4H]⁴⁺ Obs^d	[M+4H]⁴⁺ Exp^d
Fragment 3	1077.2106	1077.2168	808.1551	808.1597

Peptide	[M+3H]³⁺ Obs^d	[M+3H]³⁺ Exp^d	[M+4H]⁴⁺ Obs^d	[M+4H]⁴⁺ Exp^d
Fragment 2 Acid	1154.2286	1154.2233	-	-
Fragment 2 Thioester	1189.2355	1189.2351	892.1781	892.1793

Peptide	[M+3H]³⁺ Obs^d	[M+3H]³⁺ Exp^d	[M+4H]⁴⁺ Obs^d	[M+4H]⁴⁺ Exp^d
Fragment 1 Acid	1408.0194	1408.0186	1056.2665	1056.2656

Peptide	[M+6H]⁶⁺ Obs^d	[M+6H]⁶⁺ Exp^d	[M+5H]⁵⁺ Obs^d	[M+4H]⁴⁺ Exp^d
Fragment 1 Nbz	731.0200	731.0201	877.0232	877.0227

4.5   Biophysical Analysis Protocols

4.5.1 Enzymatic Degradation

Peptides were dissolved in PBS Buffer (0.01 M, pH 7.47) at concentrations of 200 μM, from the dilution of a main stock of the peptide in

DMSO (typically 1-5 mM). Trypsin (Promega, Sequencing Grade) was made into a 0.01 nM stock. 60 μL of each stock were added and mixed and the digestion monitored by HPLC at 25 °C, with aliquots removed after 0, 5, 12, 21, 45 and 90 minutes and the digestion quantified by the integration of the peak at 220 nm corresponding to undigested peptide. The HPLC used an Ascentis Analytical Peptide Column (20 μL injection, 0.5 mL min^{-1} flow rate, 5-95% acetonitrile:water gradient, 5.5 min run time). Experiments were done in duplicate, and assume first order kinetics. The HPLC time points were converted into a percentage of the original substrate (S), and plotted as a natural logarithm (lnS) against time (t) in minutes. Half lives ($t_{1/2}$) were calculated by dividing –ln(2) by the slope of the graph, plotted in Origin 8.

$$\ln[S] = -kt + \ln[S]_{t=0}$$

$$t_{\frac{1}{2}} = \frac{-ln2}{k}$$

4.5.2 Circular Dichroism

4.5.2.1 Fixed temperature CD

Circular Dichroism was performed on an Applied Photophysics ChiraScan Apparatus and Software. For each scan, the following parameters were used: 180-260 nm range; point time 1 s; 1 nm per point; step = 1; bandwidth 5 nm; path length 10 mm; temperature 20 °C. Scans were done in triplicate. Samples were dissolved in 1:4 acetonitrile:50 mM sodium phosphate buffer pH 7.50 to concentrations between 5 - 20 μM. DMSO stocks of peptides were not used for CD due to its high absorbance below 230 nm. The raw circular dichroism data obtained for the peptides was processed by the subtraction of the solvent signal and converted into a mean residue ellipticity:

$$[\theta] = \frac{\theta}{10 \times c \times l}$$

$$[\theta]_{MRE} = \frac{[\theta]}{(R - 1)}$$

Where θ = circular dichroism at a given wavelength, c = molar concentration, l = path length in cm, R = number of residues in the peptide sequence.

Calculation of % Helicity was performed by the following equation:[167]

$$\Theta = \left(\Theta(0) + \left(\frac{\partial\Theta}{\partial T}\right)T\right) \cdot (1 - \frac{x}{Nr}))$$

Where: Θ = Theoretical MRE for 100% helicity at 222 nm, $\Theta(0)$ = Theoretical MRE for 100% helicity at 222 nm at 0 °C = -44000, $(\partial\Theta/\partial T)$ = temperature dependence of infinite helix = +250, T = temperature in °C, x = 3, N_r = number of residues in a peptide.

Peptide	MRE 100% Helicity
Ac-BID	−33913
FITC-BID	−34125
Ac-BIM	−33429
p53	−32500

4.5.2.2 Temperature ramped CD

The apparatus and settings were the same as those in 4.5.2.1, except for the temperature, which increased in steps of 1 °C, with an equilibration time of 3 minutes between the rising of the temperature to the reading of the spectrum. The temperature was increased to a maximum of 72 °C with a final reading taken after the chamber had cooled to 20 °C to verify the reversibility of the unfolding. The data was processed into mean residue ellipticity as described in 4.5.2.1, with the following additions for the calculations of the fraction of the unfolded peptide:

$$\alpha = \frac{\Theta(T) - \Theta_f}{\Theta_u - \Theta_f}$$

Where α = Fraction Unfolded; Θ_f = MRE at T = 20 °C; Θ_u = MRE at T = 72 °C.

4.5.3 Fluorescence Anisotropy

4.5.3.1 General regards

The buffers used for fluorescence anisotropy were either phosphate buffer (40 mM sodium phosphate, 200 mM sodium chloride, 0.02 mg ml^{-1} bovine serum albumin, pH 7.50) or Tris buffer (50 mM Tris, 140 mM sodium chloride, pH 7.50). Phosphate buffer was used for all competition assays and the direct binding assays for NoxaB*/Mcl-1, BAK*/Bcl-x$_L$ and p53*/*h*DM2. Tris buffer was used for all FITC labelled BID peptides in direct binding experiments with Mcl-1 and Bcl-x$_L$.

Assays were run in 96 or 384 well Optiplates and were scanned using a Perkin Elmer EnVision™ 2103 MultiLabel plate reader. Fluorescein labelled peptides used an excitation and emission wavelength of 490 nm and 535 nm respectively whilst BODIPY labelled peptides used an excitation and emission wavelength of 531 nm and 595 nm respectively, with a bandwidth of 5 nm.

4.5.3.2 96 well plate competition assay protocol

For competition assays using 96 well plates and a 2/3 dilution regime, solutions were added into 6 rows, 3 assay and 3 control wells:

1) 50 μL buffer added to all wells

2) 100 μL of inhibitor added to the first well of a row and 100 μL mixed and transferred to the adjacent well to achieve a serial dilution

3) 50 μL of fluorescently labelled peptide to each of the 'assay' wells

4) 50 μL of buffer to the 'control' wells

5) 50 μL of protein to *every* well.

4.5.3.3 384 well plate direct binding assay protocol

For a 2/3 dilution regime of a direct binding assay in 384 well plates, the following volumes of solutions were added to 3 'assay' rows and 3 'control' rows.

1) 20 μL buffer added to all wells

2) 40 μL of titrant added to the first well of a row, with 40 μL transferred down the row to achieve a serial dilution.

3) 20 μL of fixed component to each of the 'assay' wells

4) 20 μL of buffer to the 'control' wells

In 'protein titrations' the protein is the titrant, with the fluorescently labelled peptide the fixed component in the assay. These roles are reversed in a 'peptide titration'. For a 3/4 dilution regime, which was employed in some of the FITC BID assays, 60 μL of titrant was added and serially diluted.

4.5.3.4 384 well plate competition assay protocol

For competition assays using 384 well plates and a 2/3 dilution regime, solutions were added into 6 rows, 3 'assay' and 3 'control' wells:

1) 20 μL buffer added to all wells

2) 60 μL of inhibitor added to the first well of a row and 60 μL mixed and transferred to the adjacent well to achieve a serial dilution

3) 20 μL of fluorescently labelled peptide to each of the 'assay' wells

4) 20 μL of buffer to the 'control' wells

5) 20 μL of protein to *every* well.

4.5.3.5 Processing of fluorescence anisotropy data

After reading the plates, the fluorescence anisotropy data was processed using Microsoft Excel to calculate intensity, anisotropy and fraction bound:

$$I = 2PG + S$$

$$r = \frac{S - PG}{I}$$

$$L_b = \frac{(r - r_{min})}{(\lambda(r_{max} - r) + r - r_{min})}$$

r = anisotropy, I = total intensity, P = perpendicular intensity, S = parallel intensity, L_b = fraction ligand bound, $\lambda = I_{bound}/I_{unbound}$, G = 1= instrumental factor.

This data was then transferred into Origin 8 which could fit the data to either a logisitic model (for the calculation of IC_{50} and EC_{50}) or to the K_d model for the extraction of K_d values:

$$y = r_{min} + \frac{r_{max} - r_{min}}{1 + 10^{(x - logx_o)}}$$

$$y = \frac{\{(K + x + [FL]) - \sqrt{\{(K + x + [FL])^2 - 4x[FL]\}}\}}{2}$$

Where for the logisitic model; y = r = anisotropy, x_o = mid-point of the curve between the r_{max} and r_{min} plateaux.

For the K_d model; y = L_b*[FL], K = K_d, [FL] = Concentration of fluorescent ligand.

4.5.3.6 van't Hoff analysis of fluorescence anisotropy data

The van't Hoff analysis of the fluorescently labelled BID peptides was done by following the protocol outlined in 4.5.4.4. After incubation of the plates until the lower anisotropy plateau had equilibrated (between 4-24 hours), the plates were scanned at 20 °C, then the temperature in the plate reader increased in steps of 5 °C, with a 5 minute equilibration time before the plate was read at each increasing temperature. Between 45 and 50 °C, the plate reader was at its limit for heating, therefore the plate was read at the maximum temperature that the plate reader could reach after 15 minutes, to reduce the evaporation of the buffer in the wells.

The data was processed as described in 4.5.3.5 and plotted as its EC_{50} against 1/T.

4.5.4 Specific protocols for fluorescence anisotropy assays

4.5.4.1 p53*/hDM2 competition assays

p53*/hDM2 competition assays were performed in 96 well plates as outlined in 4.5.3.2 in phosphate buffer. The concentration of the inhibitor started at 100 μM and was diluted over 24 wells to a final concentration of 10 nM, with the maximum concentration of hDM2 and p53* being 162 nM and 54 nM respectively in individual wells. Plates were read after 1 h of incubation.

4.5.4.2 NoxaB*/Mcl-1 direct binding assays

NoxaB*/Mcl-1 direct binding assays were performed in 96 well plates as outlined in 4.5.3.2 in phosphate buffer. In protein titrations, [Mcl-1] started from 10 μM and was diluted over 24 wells, with [NoxaB*] fixed at 25 nM. In

peptide titrations, [NoxaB*] started at 5 µM and was diluted over 24 wells with [Mcl-1] fixed at 25 nM. Plates were read after 1 h of incubation.

4.5.4.3 BAK*/Bcl-x$_L$ direct binding assays

BAK*/Bcl-x$_L$ direct binding assays were performed in phosphate buffer in 384 well plates (4.5.3.3). In the protein titration, [Bcl-x$_L$] started from 3 µM and was diluted over 24 points with [BAK*] fixed at 25 nM. In the peptide titration, [BAK*] started at 3 µM and was diluted over 24 points with [Bcl-x$_L$] fixed at 25 nM. Plates were read after 4 hours of incubation.

4.5.4.4 BID*/Mcl-1 and BID*/Bcl-x$_L$ direct binding assays

For all variants of the labelled BID peptides (WT*, MM*, DM* and Aib*), the direct binding assays were performed in Tris Buffer in 384 well plates as described in 4.5.3.3. In protein titrations, the protein concentration started from between 1-10 µM and was diluted over 24 points in a 3/4 dilution regime, with the concentration of the labelled peptide fixed at 25-100 nM. In the peptide titrations, the concentration of the labelled peptides started from 5 µM and were diluted in a 2/3 regime over 24 points, with the concentration of the protein fixed at 50 nM. Plates were read after 2 hours of incubation, and read again after 4 and 18 hours to ensure complete equilibration.

4.5.4.5 NoxaB*/Mcl-1 competition assays

NoxaB*/Mcl-1 competition assays were performed in either 96 well plates (4.5.3.2) or 384 well plates (4.5.3.4) in phosphate buffer, with the concentration of the inhibitor typically starting from 5-100 µM, diluted over 24 points in a 2/3 regime and with [NoxaB*] and [Mcl-1] fixed at 50 nM and 150 nM respectively. Plates were read after 1 h.

4.5.4.6 BAK*/Bcl-x$_L$ competition assays

BAK*/Bcl-x$_L$ competition assays were performed in 384 well plates in phosphate buffer (4.5.3.4) with the concentration of the inhibitor typically starting from 5-50 µM, diluted over 24 points in a 2/3 regime with [BAK*] and [Bcl-x$_L$] fixed at 43 nM and 131 nM respectively. Plates were read after 1 h of incubation.

4.5.5 Isothermal Titration Calorimetry

Mcl-1 or Bcl-x_L were dialysed in phosphate buffer containing DMSO (40 mM sodium phosphate, 200 mM sodium chloride, 1% v/v DMSO, pH 7.50) and the BID peptides were dialysed in the same buffer at a concentration ~15× higher than that of the protein. Dialysis was performed at 4 °C overnight, and the final concentration of the protein and peptides verified by UV-Vis Spectrophotometry. A calorimetric run was performed with one injection of 0.5 μL after 90 seconds, followed by twenty injections of 2 μL and a 120 second gap between injections against water as a reference at 25 °C with the cell contents were stirred at 1000 rpm. 60 μL of peptide solution was prepared in the syringe, with 200 μL of protein solution in the cell. ITC experiments also included a control of peptide being injected into phosphate buffer to account for heat changes associated with dilution. Measurements were done on a micro-iTC 200 from Microcal (GE Healthcare) provided by the Wellcome Trust. The thermodynamic calculations and curve fitting was done using ITC-Origin software.

4.6   Protein Expression of Bcl-x_L

The pGEX Bcl-x_L 'no loop' construct was kindly provided by Prof W. D. Fairlie (The Walter and Eliza Hall Institute for Medical Research, Victoria, Australia). The pGEX Bcl-x_L 'no loop' construct was over-expressed in the *E.coli* strain Rosetta 2. 15 ml of overnight starter culture was used to inoculate 1 L 2 xYT containing 100 μg mL^{-1} Ampicillin. Cultures were grown at 37 °C plus shaking until OD$_{600}$ ~ 0.6 – 0.8, the temperature was then switched to 18 °C and protein expression induced by the addition of 0.8 mM IPTG. Induced cultures were grown at 18 °C plus shaking overnight before harvesting by centrifugation. Cells were resuspended in 20 mM sodium phosphate, 140 mM NaCl, pH 7.5 containing 0.1% Triton X-100 and lysed by sonication in the presence of 10 μL of 1 U.ml^{-1} DNase I per litre of over-expression culture and 5 mM MgCl$_2$. DTT was then added to the lysed cells to give a final concentration of 1 mM. The cell lysate was centrifuged (Beckman JA25.50 rotor, 17000 rpm, 30 min, 4 °C) and the supernatant filtered (0.22 μM syringe filter) before mixing with 5ml of Glutathione Superflow (SuperGlu) resin (Generon) at 4 °C for 1

hour. The resin had previously been equilibrated with 5 column volumes (CV) of 20 mM Sodium Phosphate pH 7.5, 140 mM NaCl, 1 mM DTT (low salt buffer). The cleared cell lysate was then allowed to flow through the SuperGlu resin under gravity flow. The resin was then washed with 5 CV of low salt buffer followed by 7 CV of 20 mM sodium phosphate pH 7.5, 1 M NaCl, 1 mM DTT (high salt buffer) and a further 7 CV of low salt buffer.

One half of the fusion protein was retained for future experiments and the remaining GST-Bcl-x$_L$ fusion protein was cleaved on the resin. 10 ml of low salt buffer was added to the resin along with 3 x 100 µL aliquots of PreScission protease (prepared by H. Kyle). The resin was mixed gently at 4 °C overnight. To remove any cleaved Bcl-x$_L$ 'no loop' protein the column was washed with 6 CV followed by 5 CV of low salt buffer. The resin was then washed with 6 CV of 20 mM sodium phosphate pH 7.5, 140 mM NaCl, 20 mM reduced glutathione to remove the GST tag. The eluent from each step was collected and samples run on a 15% SDS-PAGE gel.

The eluent fraction containing cleaved Bcl-x$_L$ 'no loop' was concentrated (Amicon Ultra centrifugal filter, MWCO 3500) to approximately 5 ml. The sample was then filtered before being loaded onto a Superdex 75 column (GE healthcare) equilibrated in 40 mM sodium phosphate, 140 mM NaCl, 5% glycerol, 1 mM DTT, pH 7.5. The purified Bcl-x$_L$ 'no loop' was concentrated to and stored at – 80 °C. From a 10 L growth, 9.1 mg of GST-Bcl-x$_L$ 'no loop' and 4.9 mg of Bcl-x$_L$ 'no loop' was afforded.

4.7   X-Ray Crystallography

4.7.1   Alkylated Ni-Gly-BPB Complex 46

Diffraction and solving was performed by Dr. C. Pask at the School of Chemistry XRD service at the University of Leeds. Measurements were carried out at 100K on an Agilent Supernova diffractometer equipped with an Atlas CCD detector and connected to an Oxford Cryostream low temperature device using graphite monochromated Cu K$_\alpha$ radiation (λ = 1.54184 Å) from a Microfocus Nova X-ray source. The structure was solved by direct methods using SHELXS[208] and refined using SHELX97.

The compound crystallised as orange plates in a monoclinic cell and was solved in the $P2_1$ space group, with two molecules in the asymmetric unit. Most non-hydrogen atoms were located in the Fourier Map and refined anisotropically. There was disorder around the aromatic ring of one of the benzyl groups (C34 to C39). This was refined as two rings each with 50% occupancy. C34, C35A to C39A and C35B to C39B were refined isotropically. All hydrogen atoms were placed in calculated positions and refined isotropically using a "riding model".

During the data collection and reduction, Friedel pairs were unmerged, allowing determination of the stereochemistry of the complex. The Flack parameter,[209] -0.005(12) indicates the correct stereochemistry has been determined.

Chapter 5

References

1. H. E. Blackwell and R. H. Grubbs, *Angew. Chem. Int. Ed.*, 1998, **37**, 3281-3284.
2. C. E. Schafmeister, J. Po and G. L. Verdine, *J. Am. Chem. Soc.*, 2000, **122**, 5891-5892.
3. L. D. Walensky, A. L. Kung, I. Escher, T. J. Malia, S. Barbuto, R. D. Wright, G. Wagner, G. L. Verdine and S. J. Korsmeyer, *Science*, 2004, **305**, 1466-1470.
4. A. D. Bautista, J. S. Appelbaum, C. J. Craig, J. Michel and A. Schepartz, *J. Am. Chem. Soc.*, 2010, **132**, 2904-2906.
5. L. Römer, C. Klein, A. Dehner, H. Kessler and J. Buchner, *Angew. Chem. Int. Ed.*, 2006, **45**, 6440-6460.
6. A. Letai, M. C. Bassik, L. D. Walensky, M. D. Sorcinelli, S. Weiler and S. J. Korsmeyer, *Cancer cell*, 2002, **2**, 183-192.
7. S. H. Gellman, *Acc. Chem. Res.*, 1998, **31**, 173-180.
8. Y.-D. Wu and S. Gellman, *Acc. Chem. Res.*, 2008, **41**, 1231-1232.
9. U. Arnold, M. P. Hinderaker, B. L. Nilsson, B. R. Huck, S. H. Gellman and R. T. Raines, *J. Am. Chem. Soc.*, 2002, **124**, 8522-8523.
10. J. P. Schneider and J. W. Kelly, *Chem. Rev.*, 1995, **95**, 2169-2187.
11. C. T. Friel, D. Alastair Smith, M. Vendruscolo, J. Gsponer and S. E. Radford, *Nat. Struct. Mol. Biol.*, 2009, **16**, 318-324.
12. J. P. Plante, T. Burnley, B. Malkova, M. E. Webb, S. L. Warriner, T. A. Edwards and A. J. Wilson, *Chem. Commun.*, 2009, 5091-5093.
13. L. Stryer, in *Biochemistry 3rd Edition*, 3 edn., 1988, pp. 14-42.
14. W. Kabsch and C. Sander, *Biopolymers*, 1983, **22**, 2577-2637.
15. F. M. Richards and C. E. Kundrot, *Proteins: Structure, Function, and Bioinformatics*, 1988, **3**, 71-84.
16. G. P. Moss, in *Pure and Applied Chemistry*, 1996, vol. 68, p. 2193.
17. S. Jones and J. M. Thornton, *Proc. Natl. Acad. Sci.*, 1996, **93**, 13-20.
18. E. M. Phizicky and S. Fields, *Microbiological Reviews*, 1995, **59**, 94-123.
19. L. Stryer, in *Biochemistry*, 3 edn., 1988, pp. 92-116.
20. F. Baneyx, *Current Opinion in Biotechnology*, 1999, **10**, 411-421.
21. N. Malys, J. A. Wishart, S. G. Oliver and J. E. G. McCarthy, in *Methods in Enzymology*, eds. M. V. Daniel Jameson and V. W. Hans, Academic Press, 2011, vol. Volume 500, pp. 197-212.
22. T. A. Kost, J. P. Condreay and D. L. Jarvis, *Nat Biotech*, 2005, **23**, 567-575.
23. C. A. Hutchison, S. Phillips, M. H. Edgell, S. Gillam, P. Jahnke and M. Smith, *J. Biol. Chem.*, 1978, **253**, 6551-6560.
24. J. A. Brannigan and A. J. Wilkinson, *Nat Rev Mol Cell Biol*, 2002, **3**, 964-970.
25. W. V. Shaw, *Biochem. J.*, 1987, **246**, 1-17.

26. C. J. Noren, S. J. Anthony-Cahill, M. C. Griffith and P. G. Schultz, *Science*, 1989, **244**, 182-188.
27. J. Xie and P. G. Schultz, *Nat. Rev. Mol. Cell. Biol.*, 2006, **7**, 775-782.
28. M. Taki, T. Hohsaka, H. Murakami, K. Taira and M. Sisido, *FEBS Letters*, 2001, **507**, 35-38.
29. A. Deiters, T. A. Cropp, M. Mukherji, J. W. Chin, J. C. Anderson and P. G. Schultz, *J. Am. Chem. Soc.*, 2003, **125**, 11782-11783.
30. J. W. Chin, S. W. Santoro, A. B. Martin, D. S. King, L. Wang and P. G. Schultz, *J. Am. Chem. Soc.*, 2002, **124**, 9026-9027.
31. L. Wang, Z. Zhang, A. Brock and P. G. Schultz, *Proc. Natl. Acad. Sci.*, 2003, **100**, 56-61.
32. E. A. Lemke, D. Summerer, B. H. Geierstanger, S. M. Brittain and P. G. Schultz, *Nat Chem Biol*, 2007, **3**, 769-772.
33. J. Guo, C. E. Melançon, H. S. Lee, D. Groff and P. G. Schultz, *Angew. Chem. Int. Ed.*, 2009, **48**, 9148-9151.
34. J. W. Chin, T. A. Cropp, J. C. Anderson, M. Mukherji, Z. Zhang and P. G. Schultz, *Science*, 2003, **301**, 964-967.
35. S. Brenner, A. O. W. Stretton and S. Kaplan, *Nature*, 1965, **206**, 994-998.
36. S. Brenner, L. Barnett, E. R. Katz and F. H. C. Crick, *Nature*, 1967, **213**, 449-450.
37. H. Neumann, K. Wang, L. Davis, M. Garcia-Alai and J. W. Chin, *Nature*, 2010, **464**, 441-444.
38. A. Gautier, D. P. Nguyen, H. Lusic, W. An, A. Deiters and J. W. Chin, *J. Am. Chem. Soc.*, 2010, **132**, 4086-4088.
39. A. Gautier, A. Deiters and J. W. Chin, *J. Am. Chem. Soc.*, 2011, **133**, 2124-2127.
40. S. Greiss and J. W. Chin, *J. Am. Chem. Soc.*, 2011, **133**, 14196-14199.
41. R. B. Merrifield, *J. Am. Chem. Soc.*, 1963, **85**, 2149-2154.
42. W. C. Chan and P. D. White, *Fmoc Solid Phase Peptide Synthesis*, Oxford University Press, 2000.
43. J. W. Neidigh, R. M. Fesinmeyer and N. H. Andersen, *Nat. Struct. Mol. Biol.*, 2002, **9**, 425-430.
44. P. E. Dawson, T. W. Muir, I. Clark-Lewis and S. B. Kent, *Science*, 1994, **266**, 776-779.
45. S. B. H. Kent, *Chem. Soc. Rev.*, 2009, **38**, 338-351.
46. L. Z. Yan and P. E. Dawson, *J. Am. Chem. Soc.*, 2001, **123**, 526-533.
47. J. B. Blanco-Canosa and P. E. Dawson, *Angew. Chem. Int. Ed.*, 2008, **47**, 6851-6855.
48. E. Saxon and C. R. Bertozzi, *Science*, 2000, **287**, 2007-2010.
49. J. Offer and P. E. Dawson, *Org. Lett.*, 1999, **2**, 23-26.
50. J. Offer, C. N. C. Boddy and P. E. Dawson, *J. Am. Chem. Soc.*, 2002, **124**, 4642-4646.
51. I. E. Valverde, F. Lecaille, G. Lalmanach, V. Aucagne and A. F. Delmas, *Angew. Chem. Int. Ed.*, 2012, **51**, 718-722.
52. D. Bang, G. I. Makhatadze, V. Tereshko, A. A. Kossiakoff and S. B. Kent, *Angew. Chem. Int. Ed.*, 2005, **44**, 3852-3856.
53. F.-K. Deng, L. Zhang, Y.-T. Wang, O. Schneewind and S. B. H. Kent, *Angew. Chem. Int. Ed.*, 2014, **53**, 4662-4666.
54. V. Y. Torbeev and S. B. H. Kent, *Angew. Chem. Int. Ed.*, 2007, **46**, 1667-1670.

55. T. W. Muir, D. Sondhi and P. A. Cole, *Proc. Natl. Acad. Sci.*, 1998, **95**, 6705-6710.
56. M. Vila-Perelló, Z. Liu, N. H. Shah, J. A. Willis, J. Idoyaga and T. W. Muir, *J. Am. Chem. Soc.*, 2012, **135**, 286-292.
57. R. David, M. P. O. Richter and A. G. Beck-Sickinger, *Eur. J. Biochem.*, 2004, **271**, 663-677.
58. Y. Anraku, R. Mizutani and Y. Satow, *IUBMB Life*, 2005, **57**, 563-574.
59. C. J. Noren, J. Wang and F. B. Perler, *Angew. Chem. Int. Ed.*, 2000, **39**, 450-466.
60. F. Wold, *Annual Review of Biochemistry*, 1981, **50**, 783-814.
61. C. Jacob, E. Battaglia, T. Burkholz, D. Peng, D. Bagrel and M. Montenarh, *Chemical Research in Toxicology*, 2011, **25**, 588-604.
62. J. E. Smotrys and M. E. Linder, *Annual Review of Biochemistry*, 2004, **73**, 559-587.
63. M. Wright, W. Heal, D. Mann and E. Tate, *J. Chem. Biol.*, 2010, **3**, 19-35.
64. M. E. Taylor and K. Drickamer, *Introduction to Glycobiology*, Oxford University Press, Incorporated, 2006.
65. B. G. Davis, R. C. Lloyd and J. B. Jones, *J. Org. Chem.*, 1998, **63**, 9614-9615.
66. R. K. V. Lim and Q. Lin, *Chem. Commun.*, 2010, **46**, 1589-1600.
67. S. I. van Kasteren, H. B. Kramer, H. H. Jensen, S. J. Campbell, J. Kirkpatrick, N. J. Oldham, D. C. Anthony and B. G. Davis, *Nature*, 2007, **446**, 1105-1109.
68. Z. Yu, L. Y. Ho and Q. Lin, *J. Am. Chem. Soc.*, 2011, **133**, 11912-11915.
69. G. J. L. Bernardes, J. M. Chalker, J. C. Errey and B. G. Davis, *J. Am. Chem. Soc.*, 2008, **130**, 5052-5053.
70. M. D. Simon, F. Chu, L. R. Racki, C. C. de la Cruz, A. L. Burlingame, B. Panning, G. J. Narlikar and K. M. Shokat, *Cell*, 2007, **128**, 1003-1012.
71. S. Hecht and I. Huc, *Foldamers: Structure, Properties and Applications*, Wiley, 2007.
72. D. J. Hill, M. J. Mio, R. B. Prince, T. S. Hughes and J. S. Moore, *Chem. Rev.*, 2001, **101**, 3893-4012.
73. U. Arnold, M. P. Hinderaker, J. Koditz, R. Golbik, R. Ulbrich-Hofmann and R. T. Raines, *J. Am. Chem. Soc.*, 2003, **125**, 7500-7501.
74. A. A. Fuller, D. Du, F. Liu, J. E. Davoren, G. Bhabha, G. Kroon, D. A. Case, H. J. Dyson, E. T. Powers, P. Wipf, M. Gruebele and J. W. Kelly, *Proc. Natl. Acad. Sci.*, 2009, **106**, 11067-11072.
75. U. Arnold, B. R. Huck, S. H. Gellman and R. T. Raines, *Protein Science*, 2013, **22**, 274-279.
76. R. Kaul, A. R. Angeles, M. Jager, E. T. Powers and J. W. Kelly, *J. Am. Chem. Soc.*, 2001, **123**, 5206-5212.
77. A. Tam, U. Arnold, M. B. Soellner and R. T. Raines, *J. Am. Chem. Soc.*, 2007, **129**, 12670-12671.
78. J. Habazettl, A. Reiner and T. Kiefhaber, *J. Mol. Biol.*, 2009, **389**, 103-114.
79. B. Eckhardt, W. Grosse, L.-O. Essen and A. Geyer, *Proc. Natl. Acad. Sci.*, 2010, **107**, 18336-18341.
80. H. L. Frericks Schmidt, L. J. Sperling, Y. G. Gao, B. J. Wylie, J. M. Boettcher, S. R. Wilson and C. M. Rienstra, *The Journal of Physical Chemistry B*, 2007, **111**, 14362-14369.
81. Z. E. Reinert, E. D. Musselman, A. H. Elcock and W. S. Horne, *ChemBioChem*, 2012, **13**, 1107-1111.

82. Z. E. Reinert, G. A. Lengyel and W. S. Horne, *J. Am. Chem. Soc.*, 2013, **135**, 12528-12531.
83. B.-C. Lee and R. N. Zuckermann, *ACS Chemical Biology*, 2011, **6**, 1367-1374.
84. R. P. Cheng, S. H. Gellman and W. F. DeGrado, *Chem. Rev.*, 2001, **101**, 3219-3232.
85. A. J. Wilson, *Chem. Soc. Rev.*, 2009, **38**, 3289-3300.
86. M. D. Boersma, H. S. Haase, K. J. Peterson-Kaufman, E. F. Lee, O. B. Clarke, P. M. Colman, B. J. Smith, W. S. Horne, W. D. Fairlie and S. H. Gellman, *J. Am. Chem. Soc.*, 2011, **134**, 315-323.
87. D. Seebach and J. L. Matthews, *Chem. Commun.*, 1997, 2015-2022.
88. G. M. Clore, E. Appella, M. Yamada, K. Matsushima and A. M. Gronenborn, *Biochemistry*, 1990, **29**, 1689-1696.
89. R. David, R. Gunther, L. Baumann, T. Luhmann, D. Seebach, H.-J. r. Hofmann and A. G. Beck-Sickinger, *J. Am. Chem. Soc.*, 2008, **130**, 15311-15317.
90. D. H. Appella, L. A. Christianson, I. L. Karle, D. R. Powell and S. H. Gellman, *J. Am. Chem. Soc.*, 1996, **118**, 13071-13072.
91. C. Mayer, M. M. Müller, S. H. Gellman and D. Hilvert, in *Angew. Chem. Int. Ed.*, WILEY-VCH Verlag, 2014, p. 10.1002/anie.201400945.
92. R. E. Babine and S. L. Bender, *Chem. Rev.*, 1997, **97**, 1359-1472.
93. W. E. Stites, *Chem. Rev.*, 1997, **97**, 1233-1250.
94. T. Clackson and J. Wells, *Science*, 1995, **267**, 383-386.
95. V. Azzarito, K. Long, N. S. Murphy and A. J. Wilson, *Nat. Chem.*, 2013, **5**, 161-173.
96. B. N. Bullock, A. L. Jochim and P. S. Arora, *J. Am. Chem. Soc.*, 2011, **133**, 14220-14223.
97. T. Edwards and A. Wilson, *Amino Acids*, 2011, **41**, 743-754.
98. J. J. Chou, H. Li, G. S. Salvesen, J. Yuan and G. Wagner, *Cell*, 1999, **96**, 615-624.
99. P. H. Kussie, S. Gorina, V. Marechal, B. Elenbaas, J. Moreau, A. J. Levine and N. P. Pavletich, *Science*, 1996, **274**, 948-953.
100. S. A. Marshall, G. A. Lazar, A. J. Chirino and J. R. Desjarlais, *Drug Discovery Today*, 2003, **8**, 212-221.
101. N. E. Shepherd, H. N. Hoang, G. Abbenante and D. P. Fairlie, *J. Am. Chem. Soc.*, 2005, **127**, 2974-2983.
102. C. N. Pace, B. A. Shirley, M. McNutt and K. Gajiwala, *The FASEB Journal*, 1996, **10**, 75-83.
103. J. M. Scholtz and R. L. Baldwin, *Annual Review of Biophysics and Biomolecular Structure*, 1992, **21**, 95-118.
104. M. Pellegrini, M. Royo, M. Chorev and D. F. Mierke, *The Journal of Peptide Research*, 1997, **49**, 404-414.
105. A. K. Galande, K. S. Bramlett, J. O. Trent, T. P. Burris, J. L. Wittliff and A. F. Spatola, *ChemBioChem*, 2005, **6**, 1991-1998.
106. S. Kneissl, E. J. Loveridge, C. Williams, M. P. Crump and R. K. Allemann, *ChemBioChem*, 2008, **9**, 3046-3054.
107. J. R. Kumita, O. S. Smart and G. A. Woolley, *Proc. Natl. Acad. Sci.*, 2000, **97**, 3803-3808.
108. L. Guerrero, O. S. Smart, G. A. Woolley and R. K. Allemann, *J. Am. Chem. Soc.*, 2005, **127**, 15624-15629.

109. R. S. Harrison, N. E. Shepherd, H. N. Hoang, G. Ruiz-Gómez, T. A. Hill, R. W. Driver, V. S. Desai, P. R. Young, G. Abbenante and D. P. Fairlie, *Proc. Natl. Acad. Sci.*, 2010, **107**, 11686-11691.
110. N. E. Shepherd, H. N. Hoang, V. S. Desai, E. Letouze, P. R. Young and D. P. Fairlie, *J. Am. Chem. Soc.*, 2006, **128**, 13284-13289.
111. R. S. Harrison, G. Ruiz-Gómez, T. A. Hill, S. Y. Chow, N. E. Shepherd, R.-J. Lohman, G. Abbenante, H. N. Hoang and D. P. Fairlie, *J. Med. Chem.*, 2010, **53**, 8400-8408.
112. A. D. de Araujo, H. N. Hoang, W. M. Kok, F. Diness, P. Gupta, T. A. Hill, R. W. Driver, D. A. Price, S. Liras and D. P. Fairlie, *Angew. Chem. Int. Ed.*, 2014, **53**, 6965-6969.
113. A. J. Vernall, P. Cassidy and P. F. Alewood, *Angew. Chem. Int. Ed.*, 2009, **48**, 5675-5678.
114. E. Cabezas and A. C. Satterthwait, *J. Am. Chem. Soc.*, 1999, **121**, 3862-3875.
115. R. N. Chapman, G. Dimartino and P. S. Arora, *J. Am. Chem. Soc.*, 2004, **126**, 12252-12253.
116. L. K. Henchey, J. R. Porter, I. Ghosh and P. S. Arora, *ChemBioChem*, 2010, **11**, 2104-2107.
117. L. K. Henchey, S. Kushal, R. Dubey, R. N. Chapman, B. Z. Olenyuk and P. S. Arora, *J. Am. Chem. Soc.*, 2009, **132**, 941-943.
118. A. Patgiri, K. K. Yadav, P. S. Arora and D. Bar-Sagi, *Nat Chem Biol*, 2011, **7**, 585-587.
119. L. D. Walensky, K. Pitter, J. Morash, K. J. Oh, S. Barbuto, J. Fisher, E. Smith, G. L. Verdine and S. J. Korsmeyer, *Molecular cell*, 2006, **24**, 199-210.
120. M. L. Stewart, E. Fire, A. E. Keating and L. D. Walensky, *Nat Chem Biol*, 2010, **6**, 595-601.
121. A. L. Edwards, E. Gavathiotis, J. L. LaBelle, C. R. Braun, K. Opoku-Nsiah, G. H. Bird and L. D. Walensky, *Cancer Res.*, 2013, **73**.
122. G. H. Bird, E. Gavathiotis, J. L. LaBelle, S. G. Katz and L. D. Walensky, *ACS Chemical Biology*, 2013.
123. R. E. Moellering, M. Cornejo, T. N. Davis, C. D. Bianco, J. C. Aster, S. C. Blacklow, A. L. Kung, D. G. Gilliland, G. L. Verdine and J. E. Bradner, *Nature*, 2009, **462**, 182-188.
124. Y.-Q. Long, S.-X. Huang, Z. Zawahir, Z.-L. Xu, H. Li, T. W. Sanchez, Y. Zhi, S. De Houwer, F. Christ, Z. Debyser and N. Neamati, *J. Med. Chem.*, 2013, **56**, 5601-5612.
125. H.-K. Cui, J. Qing, Y. Guo, Y.-J. Wang, L.-J. Cui, T.-H. He, L. Zhang and L. Liu, *Bioorg. Med. Chem.*, 2013, **21**, 3547-3554.
126. G. H. Bird, N. Madani, A. F. Perry, A. M. Princiotto, J. G. Supko, X. He, E. Gavathiotis, J. G. Sodroski and L. D. Walensky, *Proc. Natl. Acad. Sci.*, 2010, **107**, 14093-14098.
127. F. Bernal, A. F. Tyler, S. J. Korsmeyer, L. D. Walensky and G. L. Verdine, *J. Am. Chem. Soc.*, 2007, **129**, 2456-2457.
128. S. Baek, P. S. Kutchukian, G. L. Verdine, R. Huber, T. A. Holak, K. W. Lee and G. M. Popowicz, *J. Am. Chem. Soc.*, 2011, **134**, 103-106.
129. C. Phillips, L. R. Roberts, M. Schade, R. Bazin, A. Bent, N. L. Davies, R. Moore, A. D. Pannifer, A. R. Pickford, S. H. Prior, C. M. Read, A. Scott, D. G. Brown, B. Xu and S. L. Irving, *J. Am. Chem. Soc.*, 2011, **133**, 9696-9699.

130. K. W. Nettles, J. B. Bruning, G. Gil, J. Nowak, S. K. Sharma, J. B. Hahm, K. Kulp, R. B. Hochberg, H. Zhou, J. A. Katzenellenbogen, B. S. Katzenellenbogen, Y. Kim, A. Joachimiak and G. L. Greene, *Nat Chem Biol*, 2008, **4**, 241-247.

131. T. Okamoto, K. Zobel, A. Fedorova, C. Quan, H. Yang, W. J. Fairbrother, D. C. S. Huang, B. J. Smith, K. Deshayes and P. E. Czabotar, *ACS Chemical Biology*, 2012, **8**, 297-302.

132. T. Okamoto, D. Segal, K. Zobel, A. Fedorova, H. Yang, W. J. Fairbrother, D. C. S. Huang, B. J. Smith, K. Deshayes and P. E. Czabotar, *ACS Chemical Biology*, 2014, **9**, 838-839.

133. J. L. LaBelle, S. G. Katz, G. H. Bird, E. Gavathiotis, M. L. Stewart, C. Lawrence, J. K. Fisher, M. Godes, K. Pitter, A. L. Kung and L. D. Walensky, *J. Clin. Invest.*, 2012, **122**, 2018-2031.

134. W. Wolfson, *Chem. Biol.*, 2009, **16**, 910-912.

135. D. Seiffert, in *Boston Business Journal*, 2013.

136. A. S. Ripka and D. H. Rich, *Curr. Op. Chem. Biol.*, 1998, **2**, 441-452.

137. C. M. Goodman, S. Choi, S. Shandler and W. F. DeGrado, *Nat. Chem. Biol.*, 2007, **3**, 252-262.

138. B. P. Orner, J. T. Ernst and A. D. Hamilton, *J. Am. Chem. Soc.*, 2001, **123**, 5382-5383.

139. J. T. Ernst, J. Becerril, H. S. Park, H. Yin and A. D. Hamilton, *Angew. Chem. Int. Ed.*, 2003, **42**, 535-539.

140. J. M. Rodriguez and A. D. Hamilton, *Angew. Chem. Int. Ed.*, 2007, **46**, 8614-8617.

141. F. Campbell, J. P. Plante, T. A. Edwards, S. L. Warriner and A. J. Wilson, *Org. Biomol. Chem.*, 2010, **8**, 2344-2351.

142. J. Becerril and A. D. Hamilton, *Angew. Chem. Int. Ed.*, 2007, **46**, 4471-4473.

143. G. W. Preston, S. E. Radford, A. E. Ashcroft and A. J. Wilson, *ACS Chemical Biology*, 2013, **9**, 761-768.

144. C. A. Dennis, H. Videler, R. A. Pauptit, R. Wallis, R. James, G. R. Moore and C. Kleanthous, *Biochem. J.*, 1998, **333**, 183-191.

145. R. James, C. Kleanthous and G. R. Moore, *Microbiology*, 1996, **142**, 1569-1580.

146. A. P. Capaldi, C. Kleanthous and S. E. Radford, *Nat. Struct. Mol. Biol.*, 2002, **9**, 209-216.

147. G. R. Spence, A. P. Capaldi and S. E. Radford, *J. Mol. Biol.*, 2004, **341**, 215-226.

148. M. M. Chen, A. I. Bartlett, P. S. Nerenberg, C. T. Friel, C. P. R. Hackenberger, C. M. Stultz, S. E. Radford and B. Imperiali, *Proc. Natl. Acad. Sci.*, 2010, **107**, 22528-22533.

149. C. P. R. Hackenberger, C. T. Friel, S. E. Radford and B. Imperiali, *J. Am. Chem. Soc.*, 2005, **127**, 12882-12889.

150. Y. Han, F. Albericio and G. Barany, *J. Org. Chem.*, 1997, **62**, 4307-4312.

151. K. L. Huber, S. Ghosh and J. A. Hardy, *Peptide Science*, 2012, **98**, 451-465.

152. J. Spiegel, P. M. Cromm, A. Itzen, R. S. Goody, T. N. Grossmann and H. Waldmann, *Angew. Chem. Int. Ed.*, 2014, **53**, 2498-2503.

153. R. M. Williams, P. J. Sinclair, D. Zhai and D. Chen, *J. Am. Chem. Soc.*, 1988, **110**, 1547-1557.

154. R. M. Williams and M. N. Im, *J. Am. Chem. Soc.*, 1991, **113**, 9276-9286.

155. P. J. M. Taylor and S. D. Bull, *Tet. Asymm.*, 2006, **17**, 1170-1178.
156. S. Neelamkavil, B. P. Mowery, E. R. Thornton, A. B. Smith and R. Hirschmann, *The Journal of Peptide Research*, 2005, **65**, 139-142.
157. U. Schöllkopf, *Tetrahedron*, 1983, **39**, 2085-2091.
158. Y. N. Belokon, V. I. Tararov, V. I. Maleev, T. F. Savel'eva and M. G. Ryzhov, *Tet. Asymm.*, 1998, **9**, 4249-4252.
159. Y. N. Belokon, N. B. Bespalova, T. D. Churkina, I. Cisarova, M. G. Ezernitskaya, S. R. Harutyunyan, R. Hrdina, H. B. Kagan, P. Kocovsky, K. A. Kochetkov, O. V. Larionov, K. A. Lyssenko, M. North, M. Polasek, A. S. Peregudov, V. V. Prisyazhnyuk and S. Vyskocil, *J. Am. Chem. Soc.*, 2003, **125**, 12860-12871.
160. Y. N. Belokon, A. G. Bulychev, S. V. Vitt, Y. T. Struchkov, A. S. Batsanov, T. V. Timofeeva, V. A. Tsyryapkin, M. G. Ryzhov and L. A. Lysova, *J. Am. Chem. Soc.*, 1985, **107**, 4252-4259.
161. L. T. Vassilev, B. T. Vu, B. Graves, D. Carvajal, F. Podlaski, Z. Filipovic, N. Kong, U. Kammlott, C. Lukacs, C. Klein, N. Fotouhi and E. A. Liu, *Science*, 2004, **303**, 844-848.
162. S. N. Willis and J. M. Adams, *Current Opinion in Cell Biology*, 2005, **17**, 617-625.
163. J. Weijlard, K. Pfister, E. F. Swanezy, C. A. Robinson and M. Tishler, *J. Am. Chem. Soc.*, 1951, **73**, 1216-1218.
164. B. Vogelstein, D. Lane and A. J. Levine, *Nature*, 2000, **408**, 307-310.
165. E. Kaiser, R. L. Colescott, C. D. Bossinger and P. I. Cook, *Anal. Biochem.*, 1970, **34**, 595-598.
166. N. Sreerama and R. W. Woody, in *Methods in Enzymology*, eds. B. Ludwig and L. J. Michael, Academic Press, 2004, vol. Volume 383, pp. 318-351.
167. P. Luo and R. L. Baldwin, *Biochemistry*, 1997, **36**, 8413-8421.
168. A. Jasanoff and A. R. Fersht, *Biochemistry*, 1994, **33**, 2129-2135.
169. A. Cammers-Goodwin, T. J. Allen, S. L. Oslick, K. F. McClure, J. H. Lee and D. S. Kemp, *J. Am. Chem. Soc.*, 1996, **118**, 3082-3090.
170. Y. Tsujimoto, L. Finger, J. Yunis, P. Nowell and C. Croce, *Science*, 1984, **226**, 1097-1099.
171. T. Oltersdorf, S. W. Elmore, A. R. Shoemaker, R. C. Armstrong, D. J. Augeri, B. A. Belli, M. Bruncko, T. L. Deckwerth, J. Dinges, P. J. Hajduk, M. K. Joseph, S. Kitada, S. J. Korsmeyer, A. R. Kunzer, A. Letai, C. Li, M. J. Mitten, D. G. Nettesheim, S. Ng, P. M. Nimmer, J. M. O'Connor, A. Oleksijew, A. M. Petros, J. C. Reed, W. Shen, S. K. Tahir, C. B. Thompson, K. J. Tomaselli, B. Wang, M. D. Wendt, H. Zhang, S. W. Fesik and S. H. Rosenberg, *Nature*, 2005, **435**, 677-681.
172. M. Certo, V. D. G. Moore, M. Nishino, G. Wei, S. Korsmeyer, S. A. Armstrong and A. Letai, *Cancer cell*, 2006, **9**, 351-365.
173. N. N. Danial and S. J. Korsmeyer, *Cell*, 2004, **116**, 205-219.
174. M. Sattler, H. Liang, D. Nettesheim, R. P. Meadows, J. E. Harlan, M. Eberstadt, H. S. Yoon, S. B. Shuker, B. S. Chang, A. J. Minn, C. B. Thompson and S. W. Fesik, *Science*, 1997, **275**, 983-986.
175. T. Moldoveanu, C. R. Grace, F. Llambi, A. Nourse, P. Fitzgerald, K. Gehring, R. W. Kriwacki and D. R. Green, *Nat. Struct. Mol. Biol.*, 2013, **20**, 589-597.
176. H. Dai, A. Smith, X. W. Meng, P. A. Schneider, Y.-P. Pang and S. H. Kaufmann, *The Journal of Cell Biology*, 2011, **194**, 39-48.

177. Peter E. Czabotar, D. Westphal, G. Dewson, S. Ma, C. Hockings, W. D. Fairlie, Erinna F. Lee, S. Yao, Adeline Y. Robin, Brian J. Smith, David C. S. Huang, Ruth M. Kluck, Jerry M. Adams and Peter M. Colman, *Cell*, 2013, **152**, 519-531.

178. E. S. Leshchiner, C. R. Braun, G. H. Bird and L. D. Walensky, *Proc. Natl. Acad. Sci.*, 2013, **110**, E986–E995.

179. C. R. Braun, J. Mintseris, E. Gavathiotis, G. H. Bird, S. P. Gygi and L. D. Walensky, *Chem. Biol.*, **17**, 1325-1333.

180. Y. Paterson, S. M. Rumsey, E. Benedetti, G. Nemethy and H. A. Scheraga, *J. Am. Chem. Soc.*, 1981, **103**, 2947-2955.

181. D. P. Fairlie, J. D. A. Tyndall, R. C. Reid, A. K. Wong, G. Abbenante, M. J. Scanlon, D. R. March, D. A. Bergman, C. L. L. Chai and B. A. Burkett, *J. Med. Chem.*, 2000, **43**, 1271-1281.

182. J. V. Olsen, S.-E. Ong and M. Mann, *Molecular & Cellular Proteomics*, 2004, **3**, 608-614.

183. L. D. Walensky, *Nat. Struct. Mol. Biol.*, 2013, **20**, 536-538.

184. J. D. Sadowsky, M. A. Schmitt, H.-S. Lee, N. Umezawa, S. Wang, Y. Tomita and S. H. Gellman, *J. Am. Chem. Soc.*, 2005, **127**, 11966-11968.

185. W. S. Horne, M. D. Boersma, M. A. Windsor and S. H. Gellman, *Angew. Chem. Int. Ed.*, 2008, **47**, 2853-2856.

186. M. Jullian, A. Hernandez, A. Maurras, K. Puget, M. Amblard, J. Martinez and G. Subra, *Tet. Lett.*, 2009, **50**, 260-263.

187. L. D. Walensky and G. H. Bird, *J. Med. Chem.*, 2014, **57**, 6275-6288.

188. H. G. Brittain and F. S. Richardson, *The Journal of Physical Chemistry*, 1976, **80**, 2590-2592.

189. L. Chen, S. N. Willis, A. Wei, B. J. Smith, J. I. Fletcher, M. G. Hinds, P. M. Colman, C. L. Day, J. M. Adams and D. C. S. Huang, *Molecular cell*, 2005, **17**, 393-403.

190. Q. Liu, T. Moldoveanu, T. Sprules, E. Matta-Camacho, N. Mansur-Azzam and K. Gehring, *J. Biol. Chem.*, 2010, **285**, 19615-19624.

191. D. J. Yeo, S. L. Warriner and A. J. Wilson, *Chem. Commun.*, 2013, **49**, 9131-9133.

192. N. J. Greenfield, *Nat. Protocols*, 2007, **1**, 2527-2535.

193. K. A. Dill, *Biochemistry*, 1990, **29**, 7133-7155.

194. C. N. Pace, H. Fu, K. L. Fryar, J. Landua, S. R. Trevino, B. A. Shirley, M. M. Hendricks, S. Iimura, K. Gajiwala, J. M. Scholtz and G. R. Grimsley, *J. Mol. Biol.*, 2011, **408**, 514-528.

195. A. Velázquez-Campoy, H. Ohtaka, A. Nezami, S. Muzammil and E. Freire, in *Current Protocols in Cell Biology*, John Wiley & Sons, Inc., 2001.

196. M. Millingen, H. Bridle, A. Jesorka, P. Lincoln and O. Orwar, *Analytical Chemistry*, 2007, **80**, 340-343.

197. L. Gandhi, D. R. Camidge, M. Ribeiro de Oliveira, P. Bonomi, D. Gandara, D. Khaira, C. L. Hann, E. M. McKeegan, E. Litvinovich, P. M. Hemken, C. Dive, S. H. Enschede, C. Nolan, Y.-L. Chiu, T. Busman, H. Xiong, A. P. Krivoshik, R. Humerickhouse, G. I. Shapiro and C. M. Rudin, *Journal of Clinical Oncology*, 2011, **29**, 909-916.

198. C. M. Rudin, C. L. Hann, E. B. Garon, M. Ribeiro de Oliveira, P. D. Bonomi, D. R. Camidge, Q. Chu, G. Giaccone, D. Khaira, S. S. Ramalingam, M. R. Ranson, C. Dive, E. M. McKeegan, B. J. Chyla, B. L. Dowell, A. Chakravartty, C. E. Nolan, N. Rudersdorf, T. A. Busman, M. H. Mabry, A. P. Krivoshik, R.

A. Humerickhouse, G. I. Shapiro and L. Gandhi, *Clinical Cancer Research*, 2012, **18**, 3163-3169.

199. W. H. Wilson, O. A. O'Connor, M. S. Czuczman, A. S. LaCasce, J. F. Gerecitano, J. P. Leonard, A. Tulpule, K. Dunleavy, H. Xiong, Y.-L. Chiu, Y. Cui, T. Busman, S. W. Elmore, S. H. Rosenberg, A. P. Krivoshik, S. H. Enschede and R. A. Humerickhouse, *The Lancet Oncology*, 2010, **11**, 1149-1159.
200. N. Voyer and B. Guérin, *Tetrahedron*, 1994, **50**, 989-1010.
201. M. J. Kelso, R. L. Beyer, H. N. Hoang, A. S. Lakdawala, J. P. Snyder, W. V. Oliver, T. A. Robertson, T. G. Appleton and D. P. Fairlie, *J. Am. Chem. Soc.*, 2004, **126**, 4828-4842.
202. I. Hamachi, R. Eboshi, J.-i. Watanabe and S. Shinkai, *J. Am. Chem. Soc.*, 2000, **122**, 4530-4531.
203. J. S. Albert and A. D. Hamilton, *Biochemistry*, 1995, **34**, 984-990.
204. F. F. Schumacher, M. Nobles, C. P. Ryan, M. E. B. Smith, A. Tinker, S. Caddick and J. R. Baker, *Bioconjugate Chemistry*, 2011, **22**, 132-136.
205. L. Castaneda, A. Maruani, F. F. Schumacher, E. Miranda, V. Chudasama, K. A. Chester, J. R. Baker, M. E. B. Smith and S. Caddick, *Chem. Commun.*, 2013, **49**, 8187-8189.
206. K. A. Dastlik, U. Sundermeier, D. M. Johns, Y. Chen and R. M. Williams, *Synlett*, 2005, **2005**, 693,696.
207. J. Marik, A. Song and K. S. Lam, *Tet. Lett.*, 2003, **44**, 4319-4320.
208. G. Sheldrick, *Acta Crystallographica Section A*, 2008, **64**, 112-122.
209. H. Flack, *Acta Crystallographica Section A*, 1983, **39**, 876-881.

Chapter 6

Appendix I

HPLC and MS Data for all peptides

The mass spectra were obtained from the LCMS facilities described in 4.2.1, where the reported peak is the *most abundant* isotope. In this instance, multiple charge states were used for confirmation of peptide identity.

p53 series

p53 MU
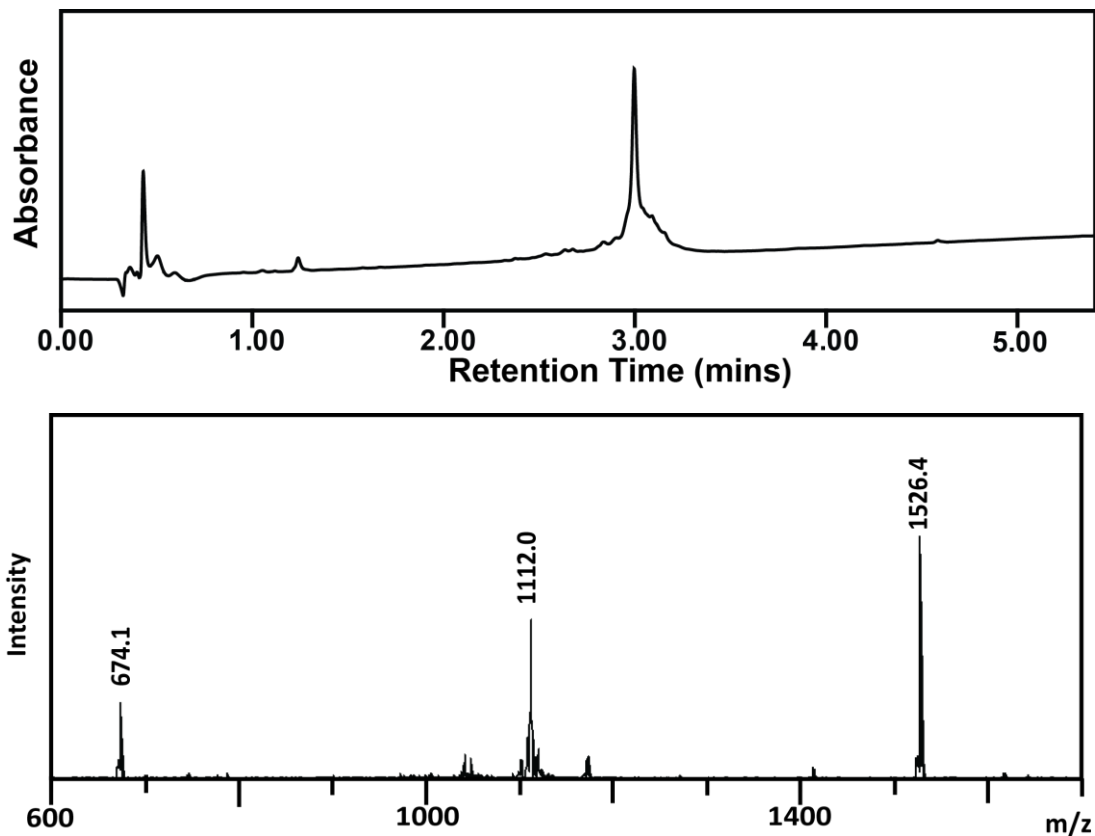
Figure 6.6.1 - MS data shows [M+H+Na]$^{2+}$ at 1112.0. The peaks at 1526.4 and 674.1 are a fragmentation at [27]LP.

p53 MM
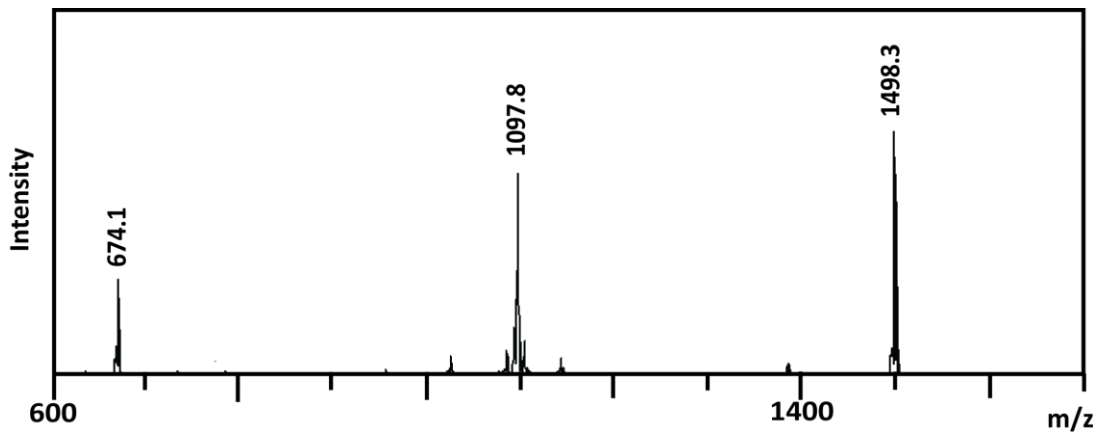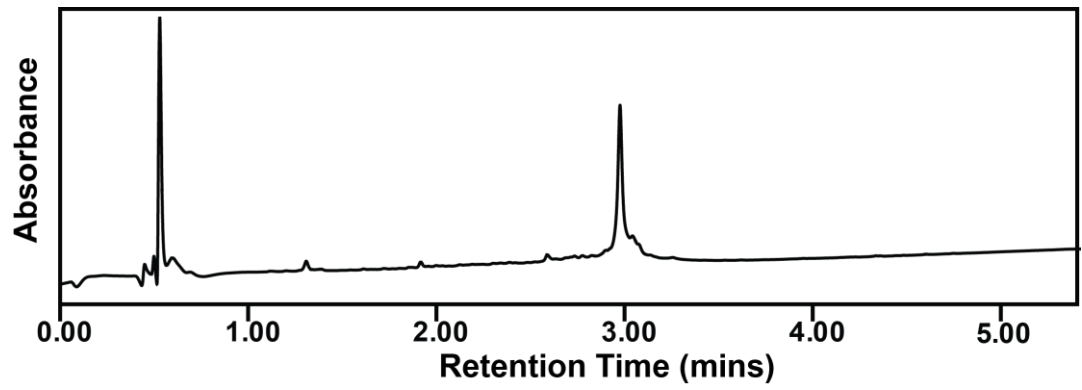
Figure 6.2 - p53MM HPLC and MS data. The MS shows [M+H+Na]²⁺ at 1097.8. The peaks at 1498.3 and 674.1 are a fragmentation at [27]LP.

BID BH3 Series

BID WT
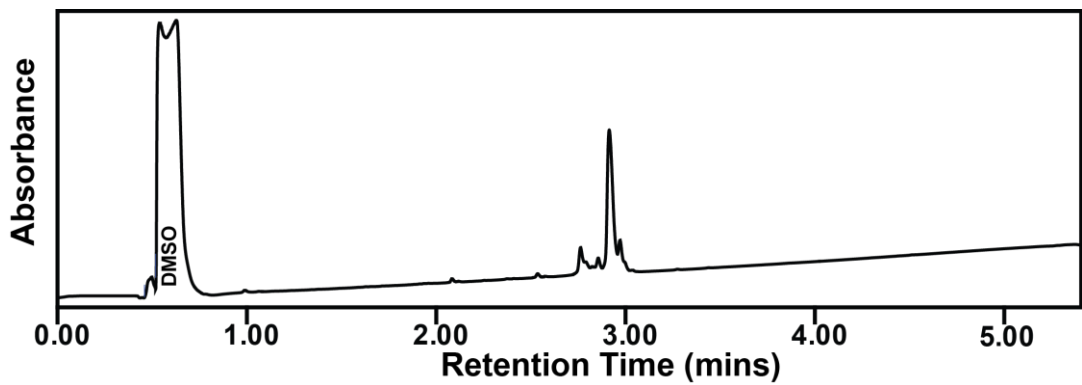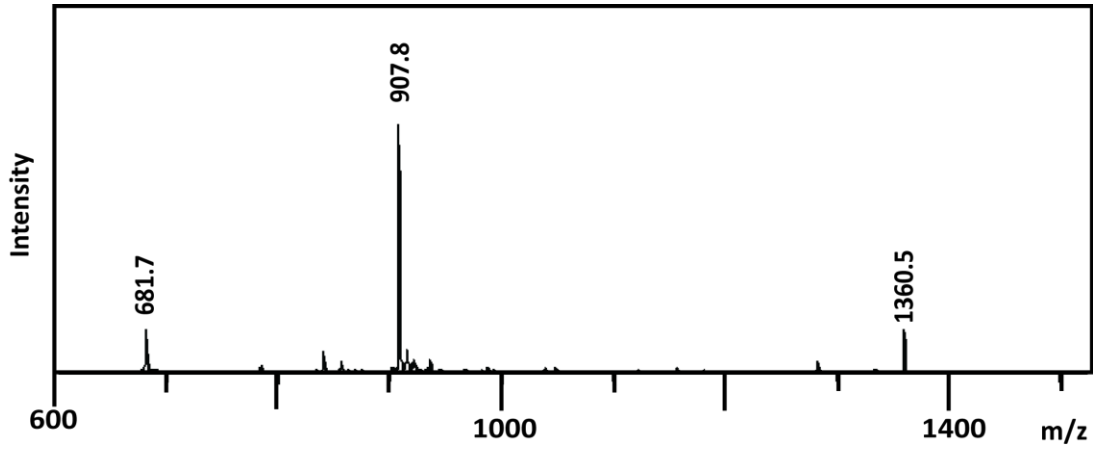
Figure 6.3 -MS data shows [M+4H]⁴⁺ at 681.7, [M+3H]³⁺ at 907.8 and [M+2H]²⁺ at 1360.5.

BID Aib
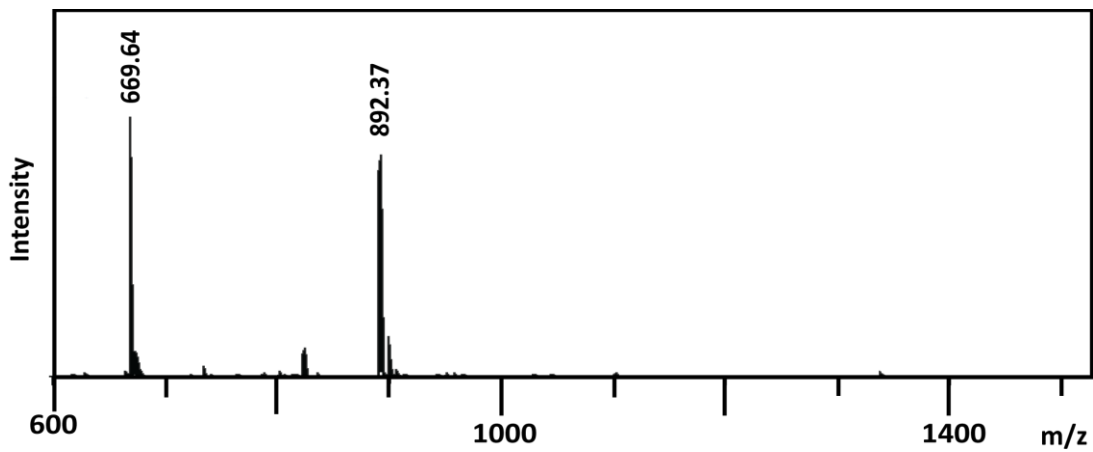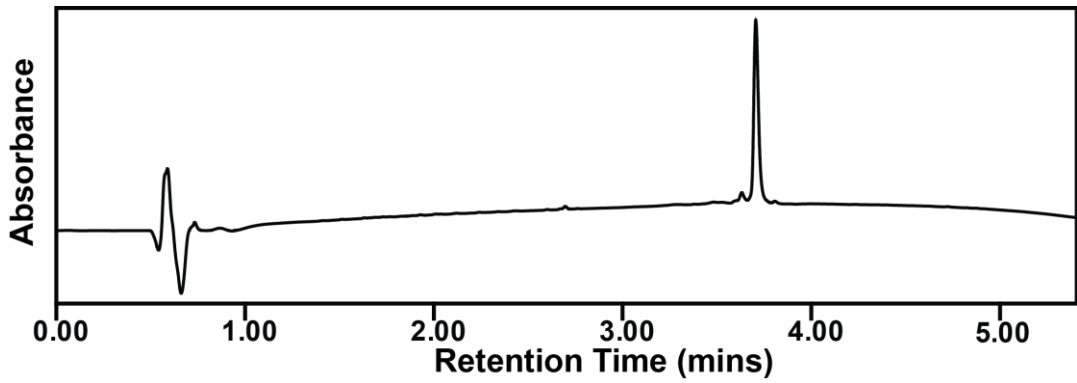
Figure 6.4 - MS data shows [M+4H]⁴⁺ at 669.64 and [M+3H]³⁺ at 892.37.

BID MM
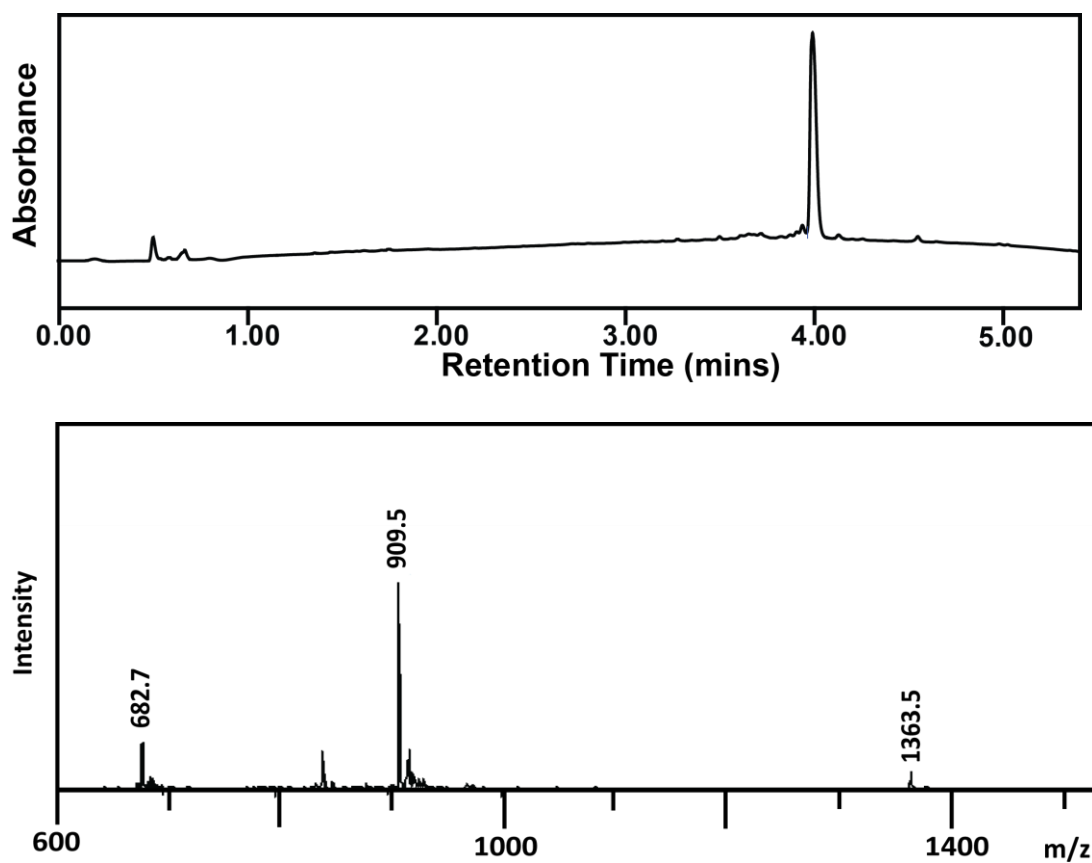
Figure 6.5 - MS data shows [M+4H]⁴⁺ at 682.7 , [M+3H]³⁺ at 909.5 and [M+2H]²⁺ at 1363.5.

BID MU
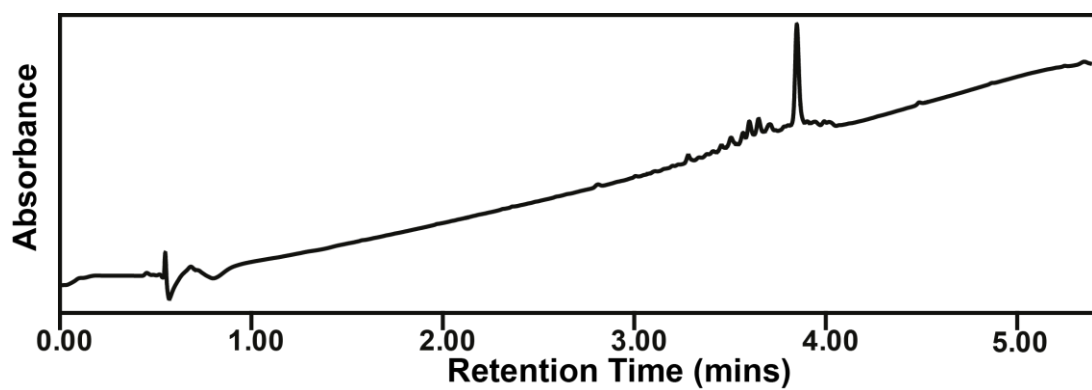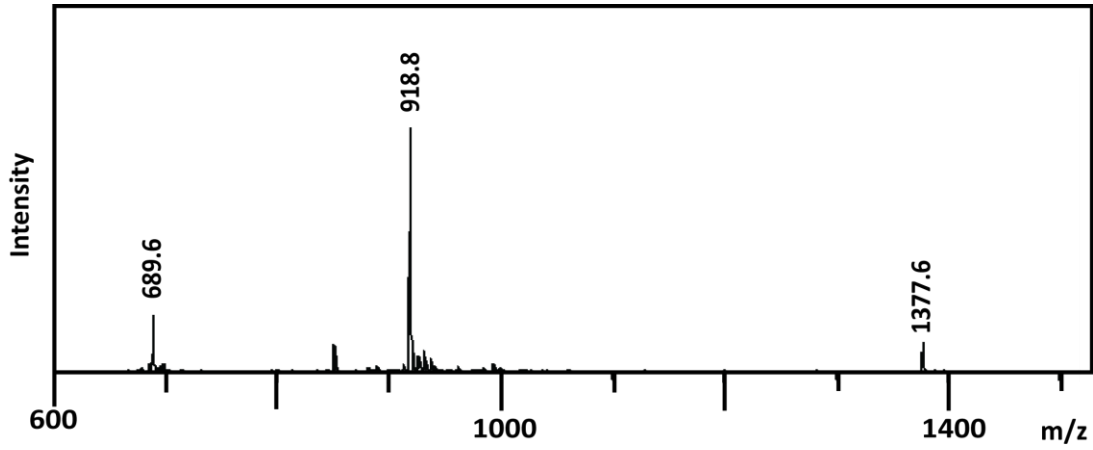
Figure 6.6 - MS data shows $[M+4H]^{4+}$ at 689.6, $[M+3H]^{3+}$ at 918.8 and $[M+2H]^{2+}$ at 1377.6.

BID DM
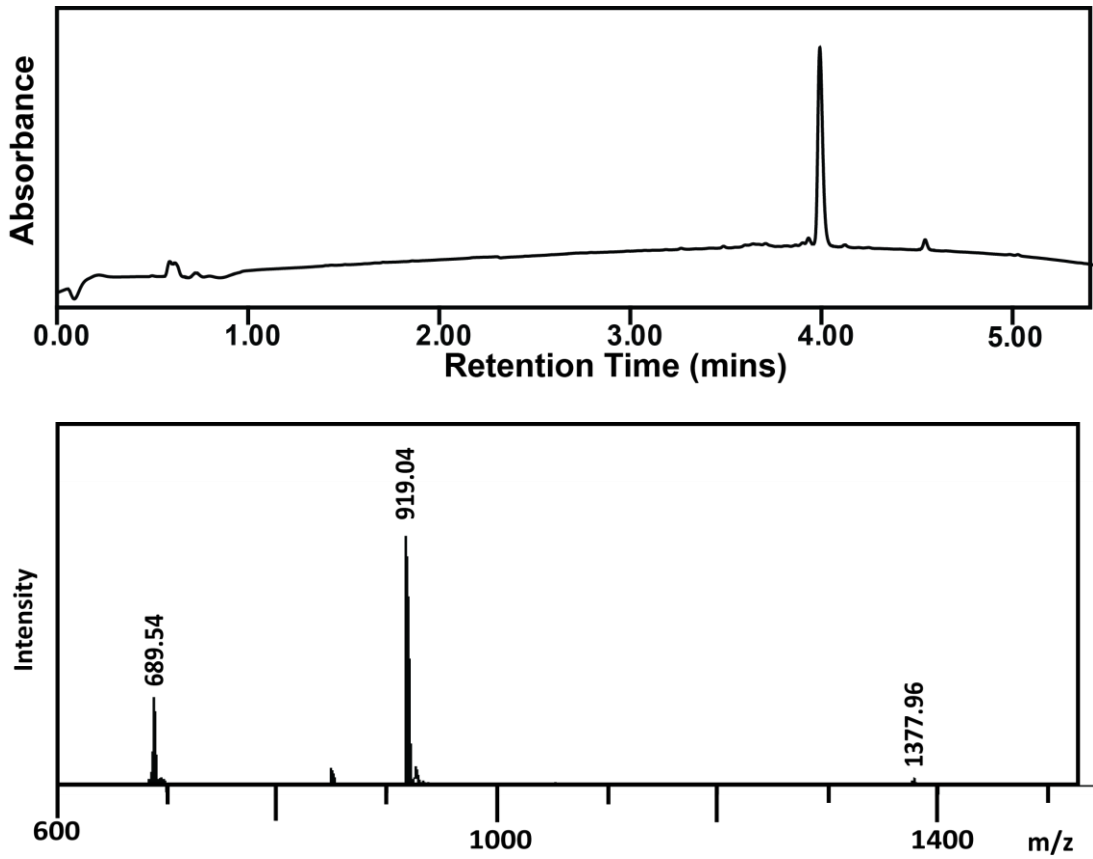
Figure 6.7 - MS data shows $[M+4H]^{4+}$ at 689.54, $[M+3H]^{3+}$ at 919.04 and $[M+2H]^{2+}$ at 1377.96.

BID DU
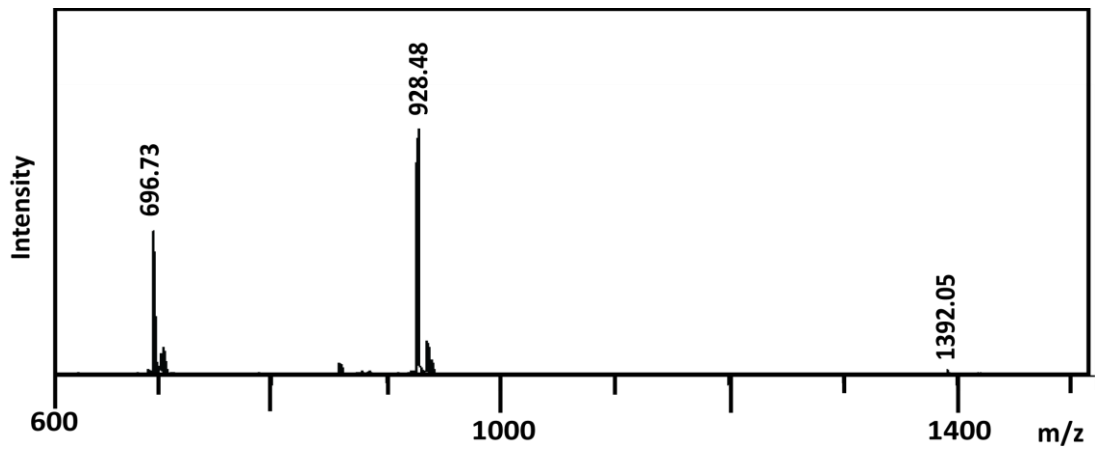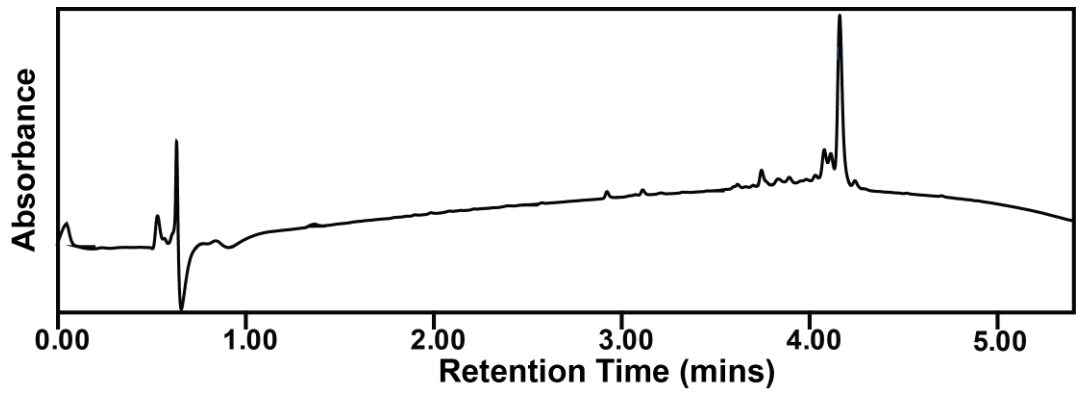
Figure 6.8 - MS data shows [M+4H][4+] at 696.73, [M+3H][3+] at 928.48 and [M+2H][2+] at 1392.05.

FITC Labelled BID Series

BID WT*
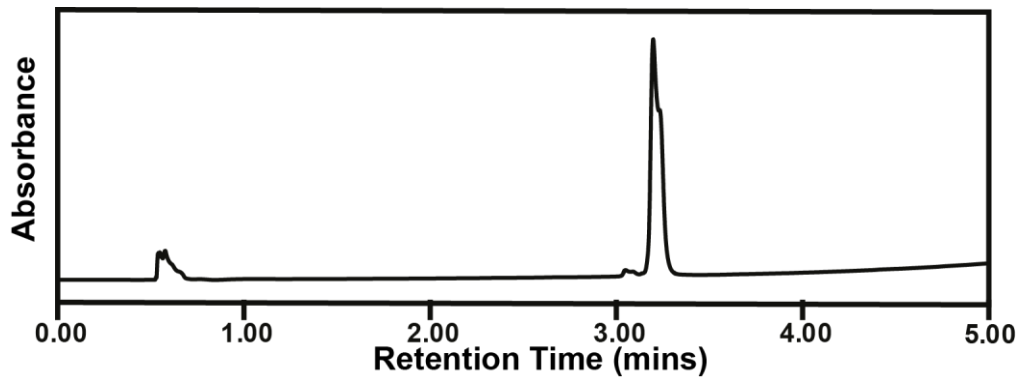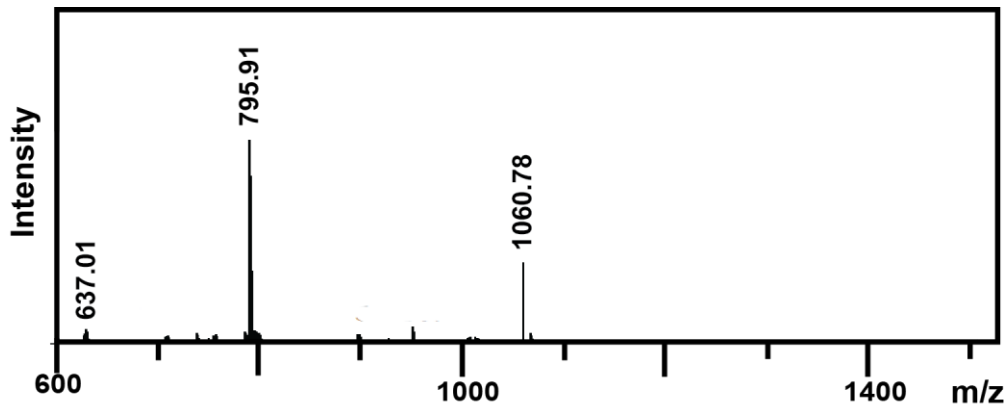
Figure 6.9 - MS data shows [M+4H]$^{4+}$ at 637.01, [M+3H]$^{3+}$ at 795.91 and [M+2H]$^{2+}$ at 1060.78.

BID Aib*
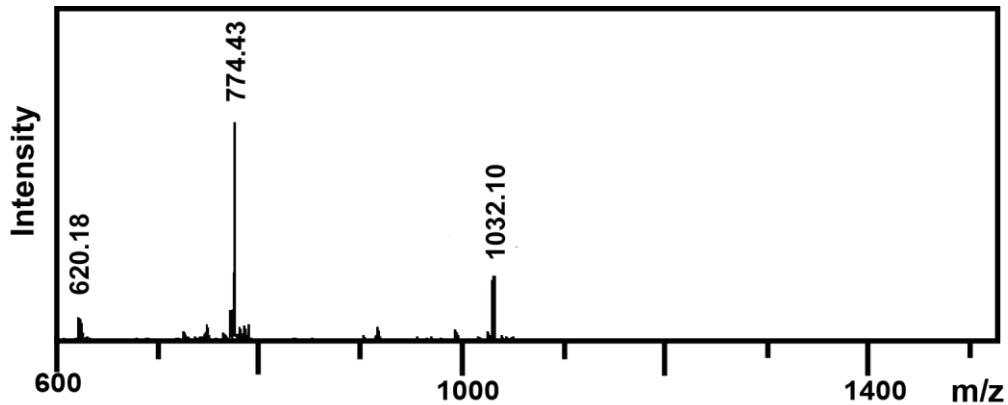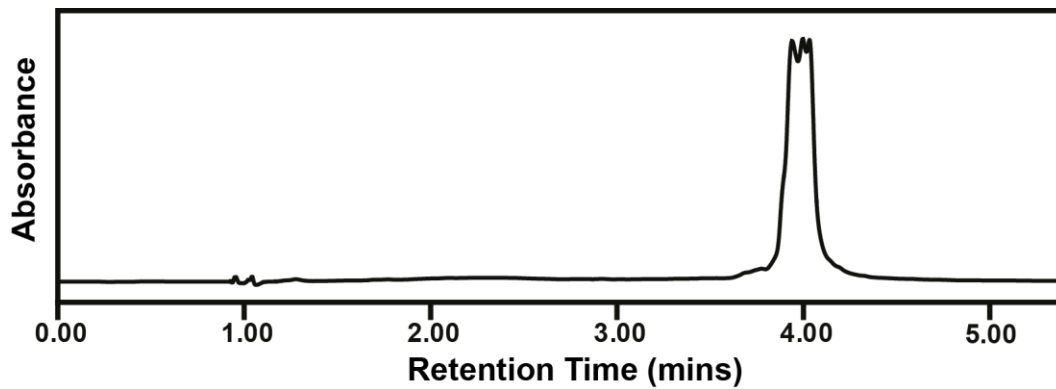
Figure 6.10 - The HPLC trace has been broadened and appears to have breaks in the peak, which may have arisen from the use of mixed isomers of FITC for this peptide. MS data shows [M+4H]$^{4+}$ at 620.18, [M+3H]$^{3+}$ at 774.43 and [M+2H]$^{2+}$ at 1032.10.

BID MM*
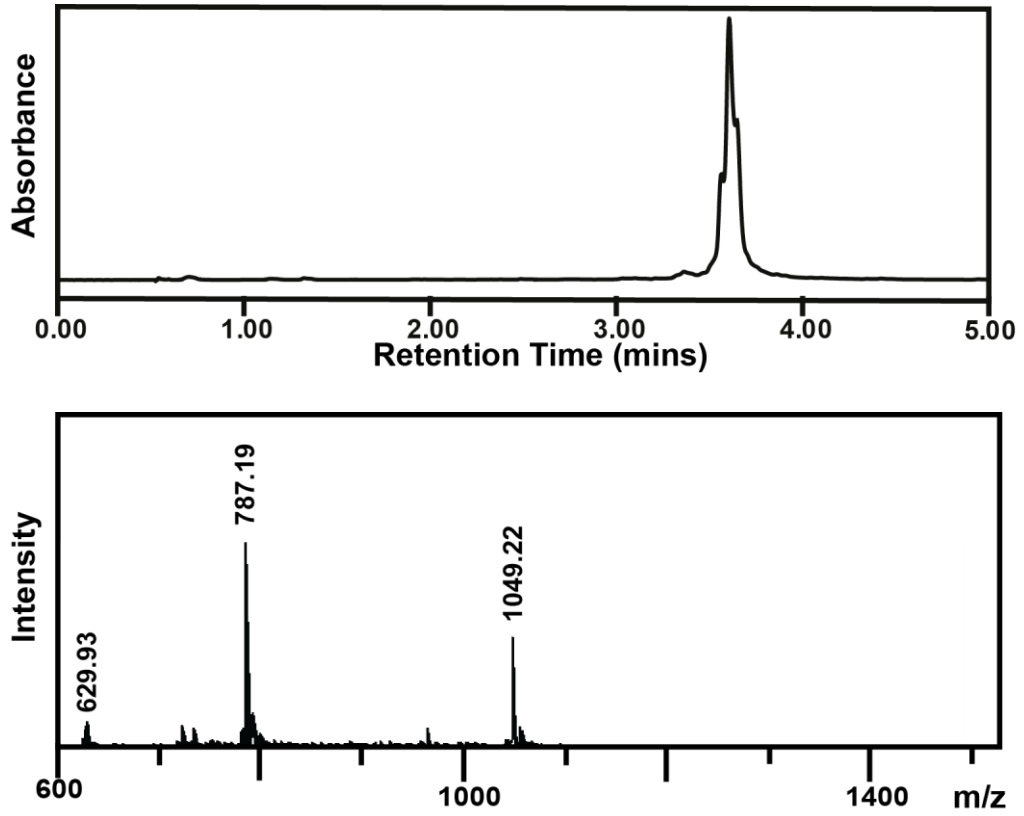
Figure 6.11 - MS data shows the [M+4H]⁴⁺ at 629.93, [M+3H]³⁺ at 787.19 and [M+2H]²⁺ at 1049.22.

BID DM*
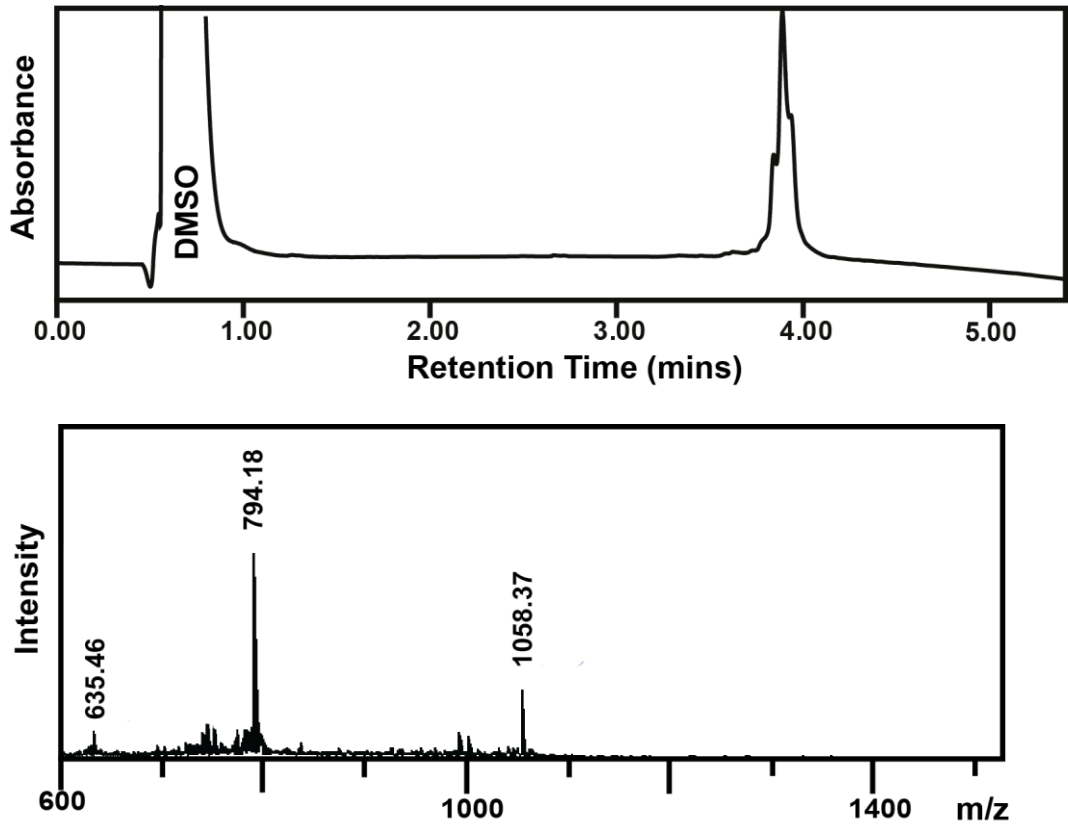
Figure 6.12 - MS data shows the [M+4H][4+] at 635.46, [M+3H][3+] at 794.18 and [M+2H][2+] at 1058.37.

hCys BID Series

BID hCys OX
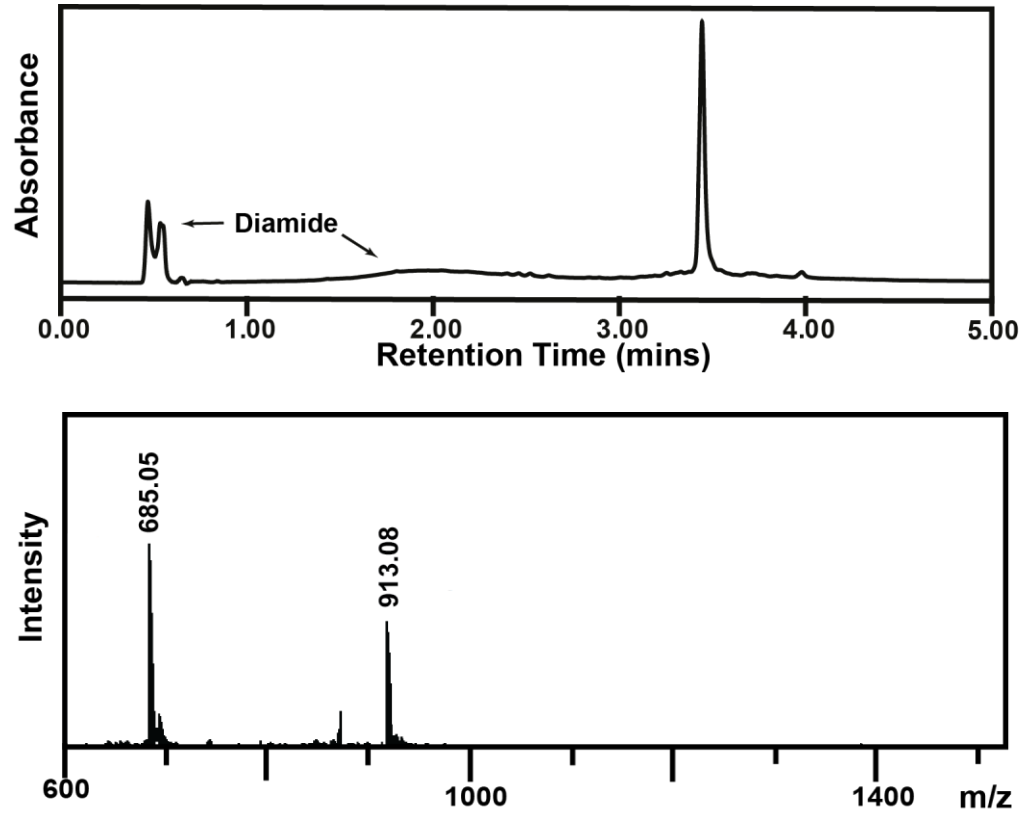
Figure 6.13 - MS data shows [M+4H][4+] at 685.05 and [M+3H][3+] at 913.08.

BID hCys RED
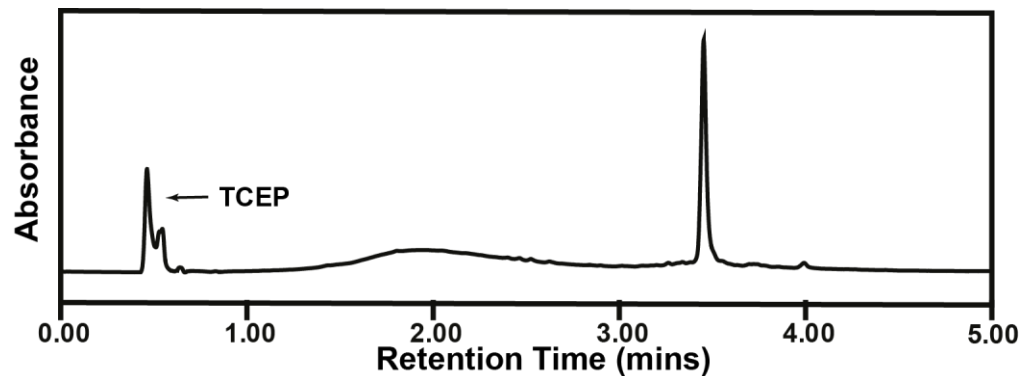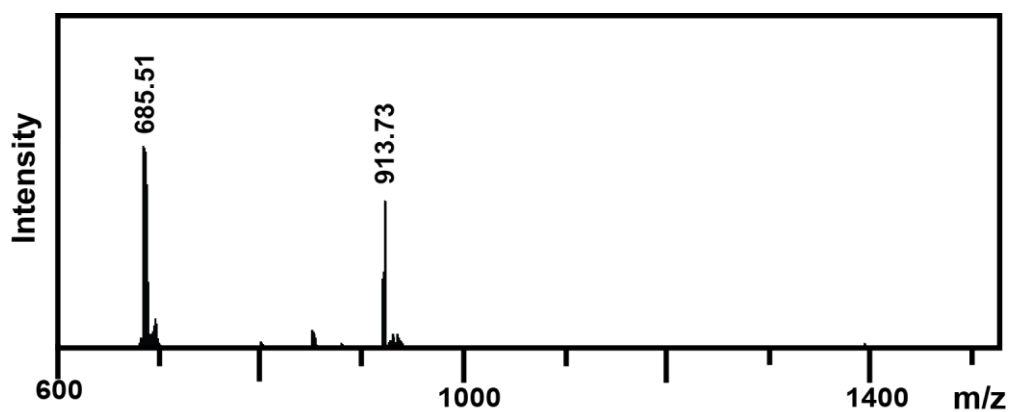
Figure 6.14 - MS data shows [M+4H][4+] at 685.51 and [M+3H][3+] at 913.73.

BID hCys SUC
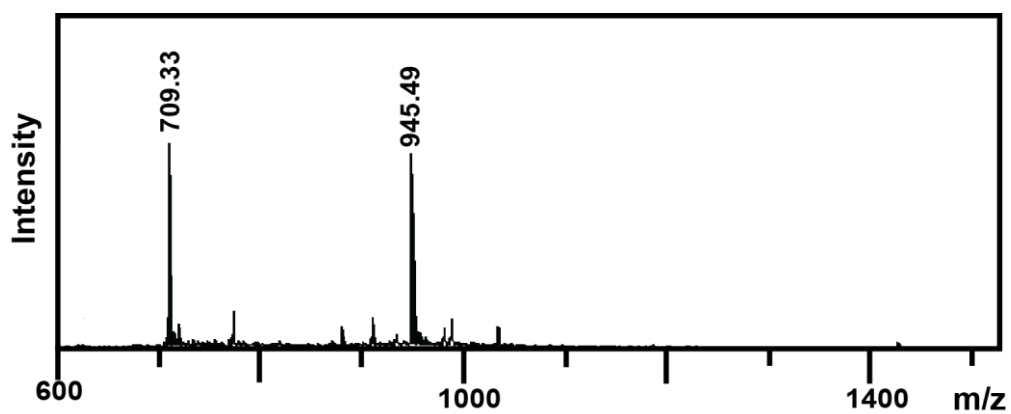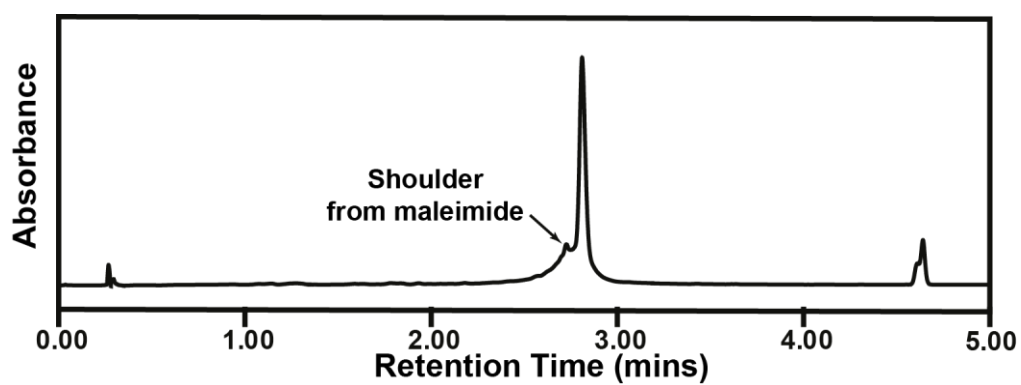
Figure 6.15 - MS data shows [M+4H][4+] at 709.33 and [M+3H][3+] at 945.49.

BID hCys MAL
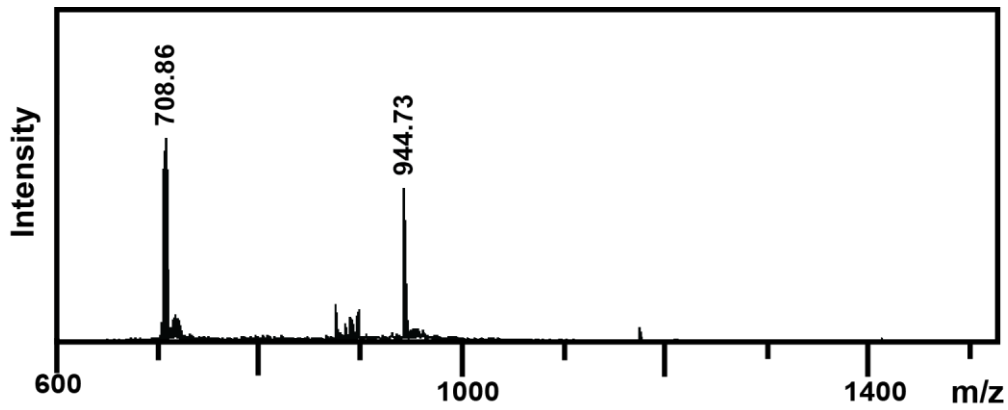
Figure 6.16 -MS data of isolated BID hCys MAL, but the purity of the peptide was insufficient for complete characterisation. Data shows [M+4H]$^{4+}$ at 708.86 and [M+3H]$^{3+}$ at 944.73.

BIM Peptide Series

BIM WT
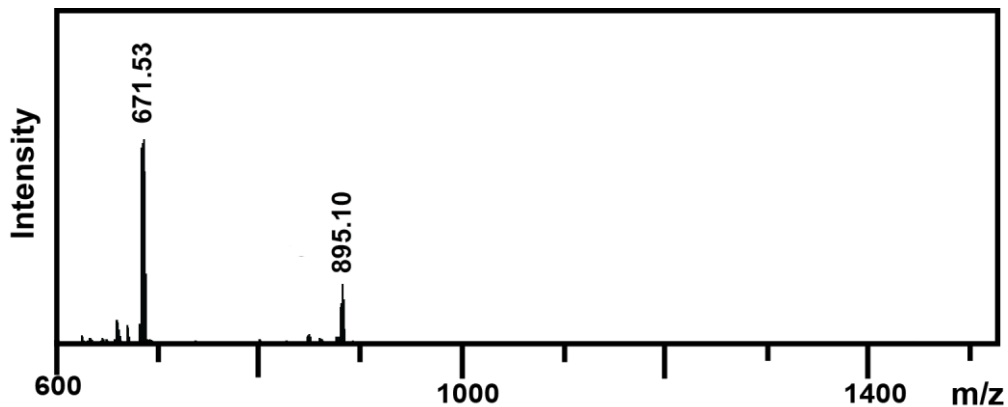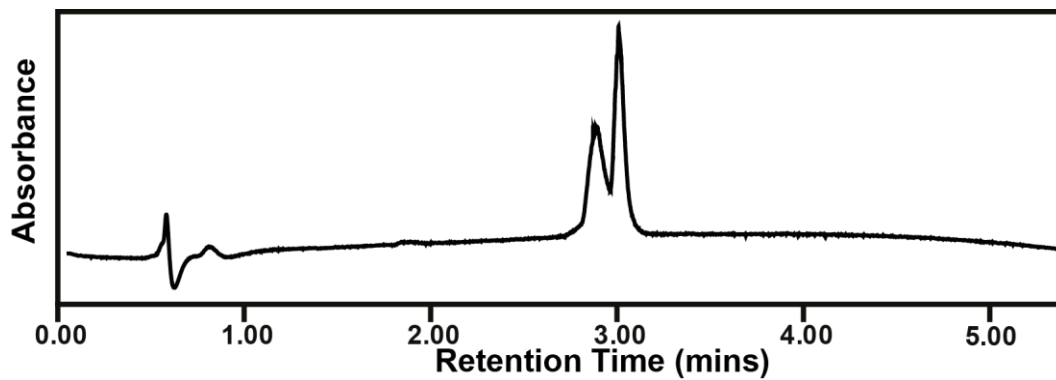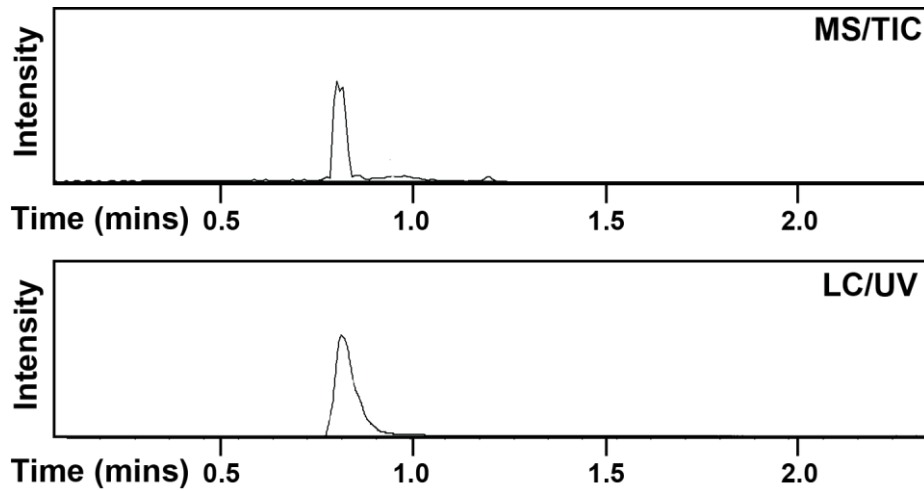
Figure 6.17 -On Analytical HPLC, BIM WT appeared to have two UV peaks, but further analysis with LCMS and altering the HPLC gradient did not separate these peaks out further. Using Loop and LCMS identified only the target peptide with no other species ionising. The MS chromatogram shows $[M+4H]^{4+}$ at 671.53 and $[M+3H]^{3+}$ at 895.10.

BIM MM
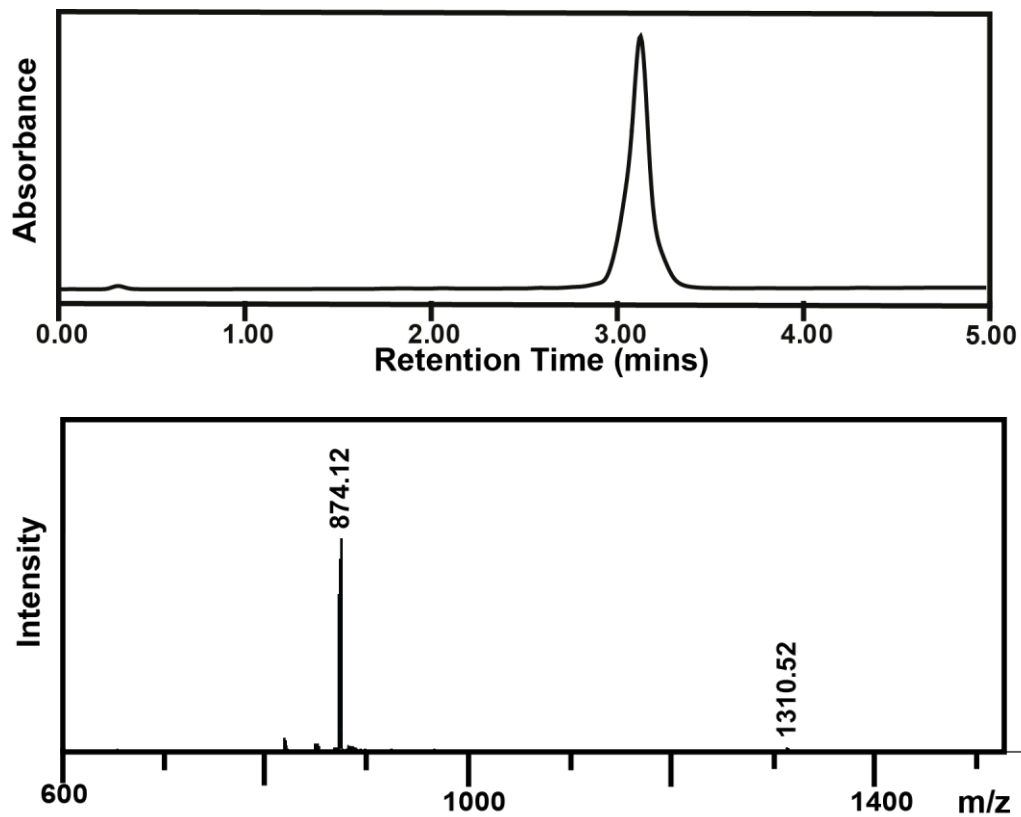
Figure 6.18 - MS Data shows $[M+3H]^{3+}$ at 874.12 and $[M+2H]^{2+}$ at 1310.52.

BIM DM
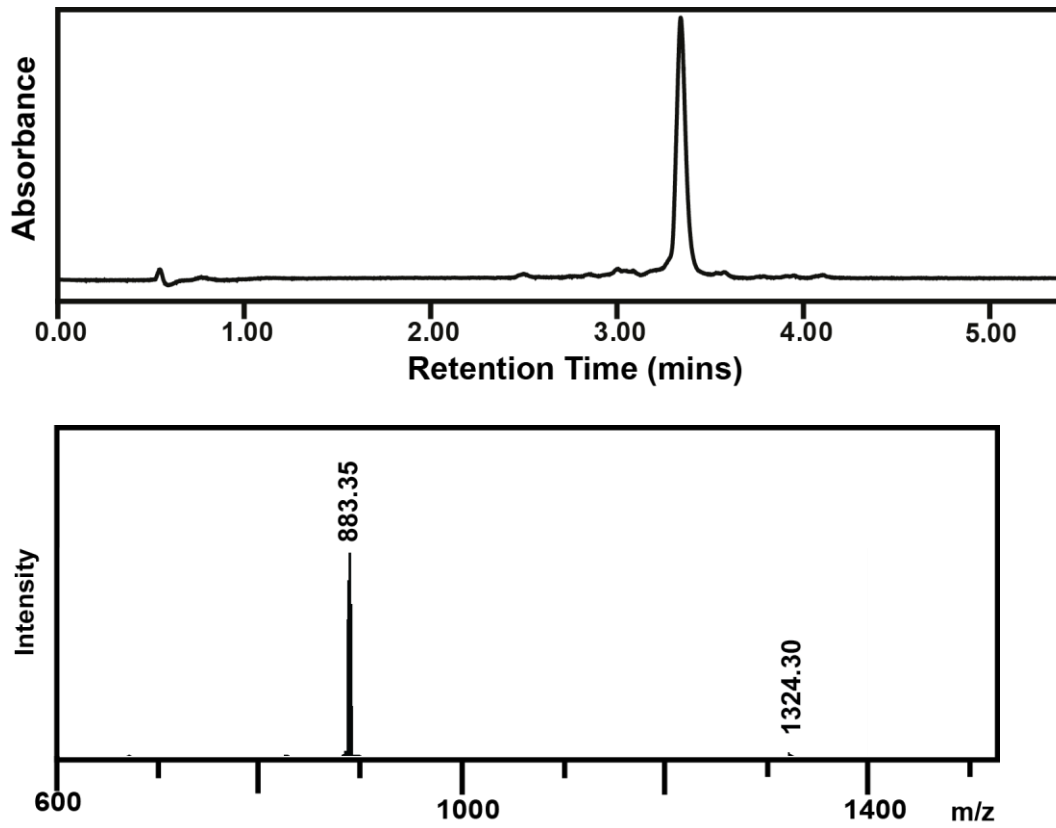
Figure 6.19 - MS Data shows [M+3H]³⁺ at 883.35 and [M+2H]²⁺ at 1324.30.

Im7 Peptide Series

Fragment 3
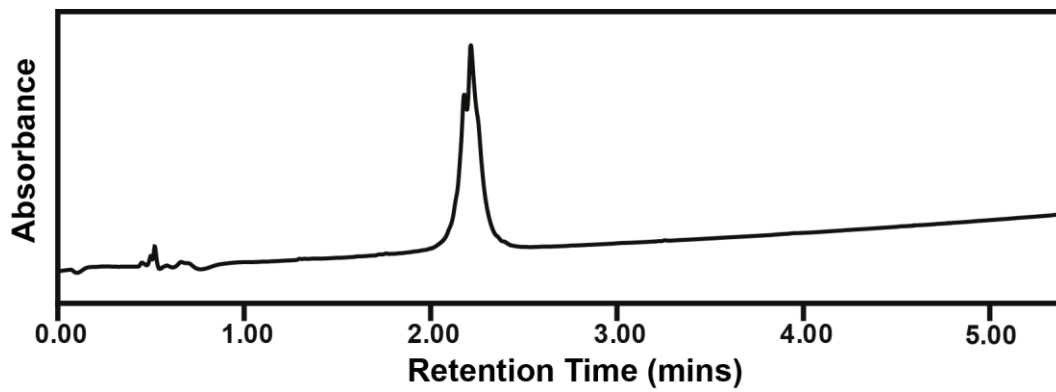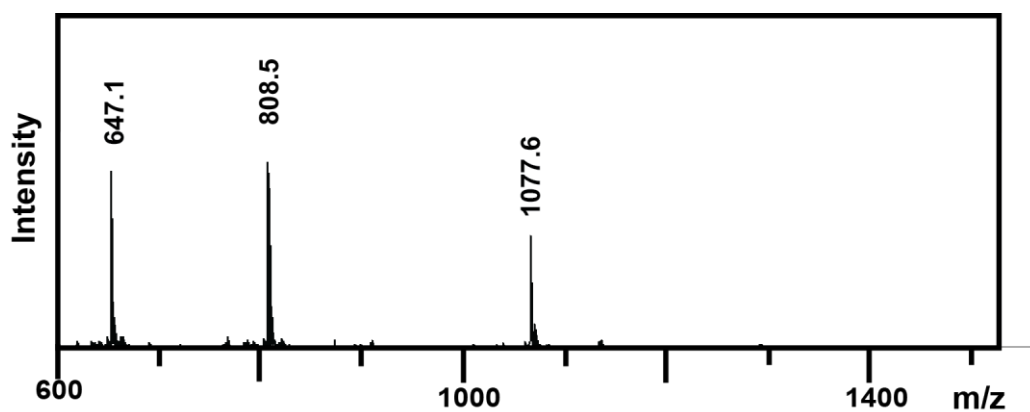
Figure 6.20 - MS Data shows the [M+5H]$^{5+}$ at 647.1,[M+4H]$^{4+}$ at 808.5 and [M+3H]$^{3+}$ at 1077.6.

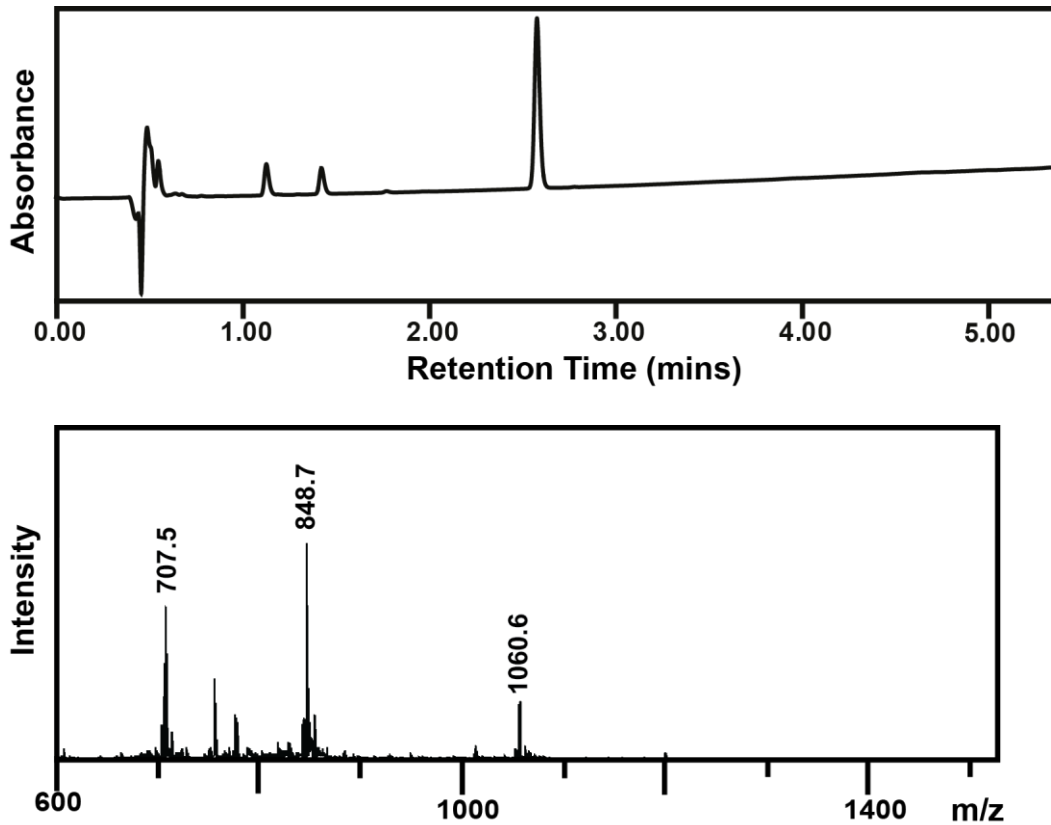## Fragment 2 C-terminal acid (crude trace)
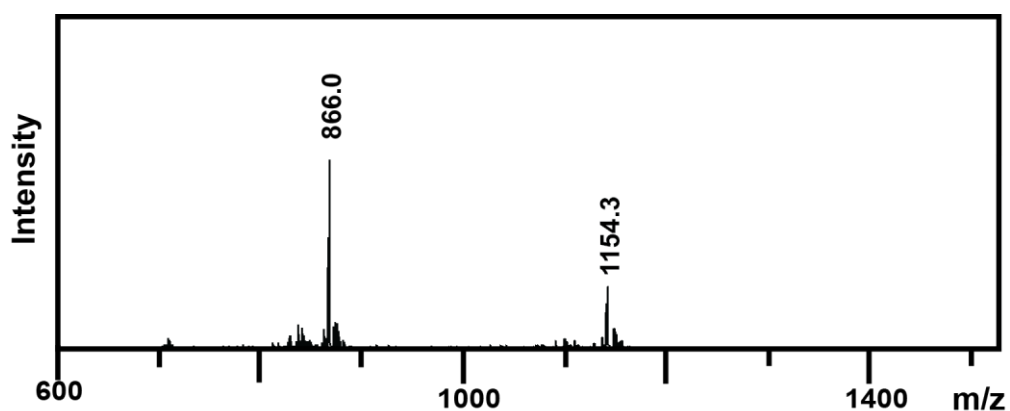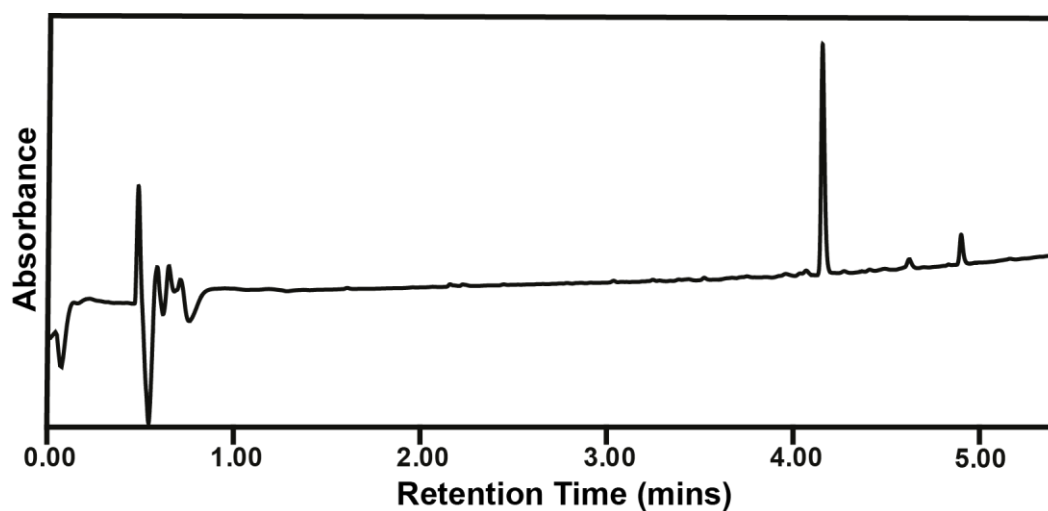
Figure 6.21 - The MS data was obtained after the deprotection of the side chains of the peptide with TFA, with the HPLC trace being the fully protected peptide. MS data displays [M+4H]$^{4+}$ at 866.0 and [M+3H]$^{3+}$ at 1154.3.

Im7 Fragment 2 C-terminal thioester
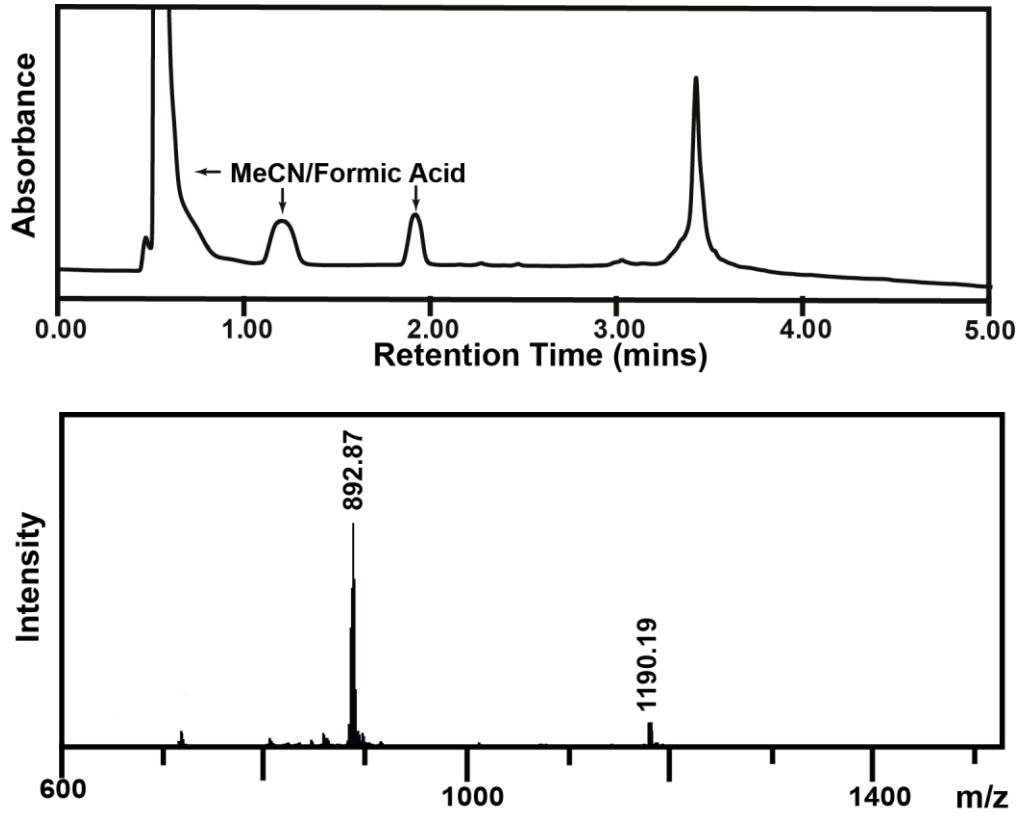
Figure 6.22 - MS data displays [M+4H]⁴⁺ at 892.87 and [M+3H]³⁺ at 1190.19.

Im7 C-terminal acid (crude)

Figure 6.23 - The MS data was obtained after the deprotection of the side chains of the peptide with TFA, with the HPLC trace being the fully protected peptide. MS data displays [M+6H]6+ at 707.5, [M+5H]5+ at 848.7 and [M+4H]4+ at 1060.6.

Im7 Fragment 1 C-terminal Nbz
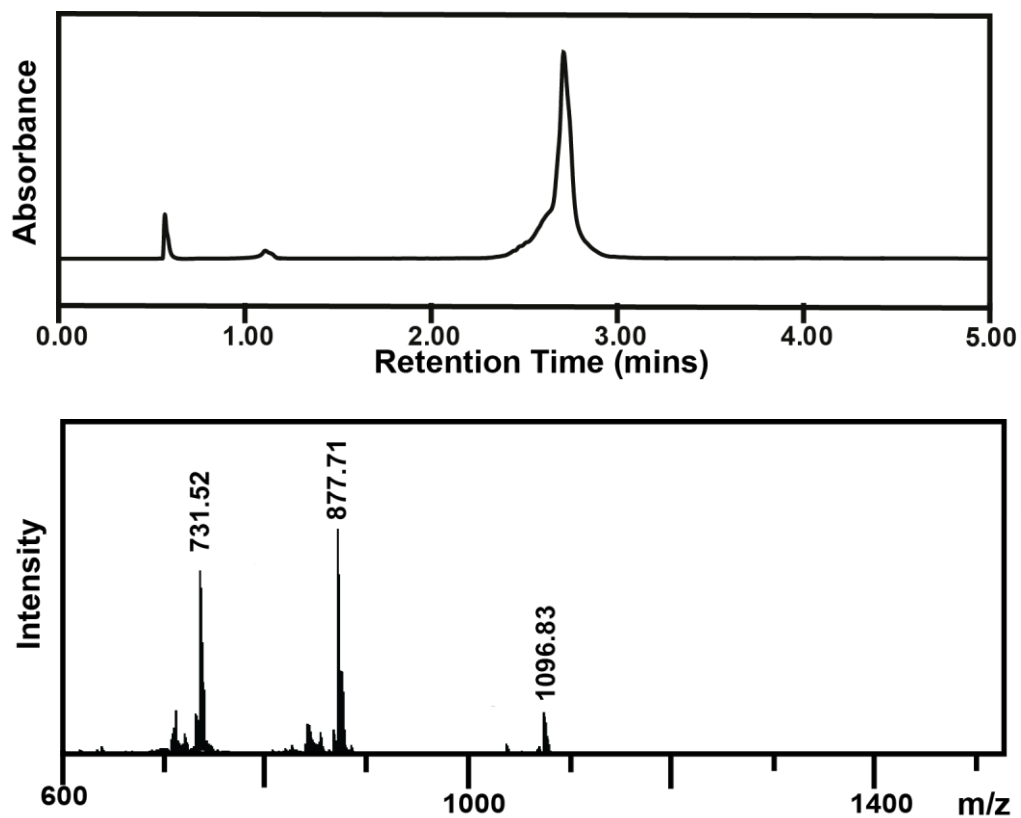
Figure 6.24 - MS data shows [M+5H]5+ at 731.52,[M+4H]4+ at 877.71 and [M+3H]3+ at 1096.83, with traces of the Nbz group hydrolysing during the MS - this is also visible on the HPLC trace.

Appendix II

6.1 Unstapled BID BH3 Peptide Biophysical Data

The unstapled BID BH3 peptides were assessed for their secondary structure in solution, enzymatic degradation resistance and inhibition potency of Bcl-x_L/BAK* (experimental procedures reported: 4.5).

The unstapled peptides generally possessed a random coil conformation in aqueous solution (30% acetonitrile in 40 mM phosphate buffer, pH 7.5) with low helical content, but the profile of the CD curve of BID DU appeared to be more helical than BID MU – suggesting that there is some helical induction of the peptide by the quaternary disubstituted amino acid. BID DU and MU were effective inhibitors of Bcl-x_L/BAK*, but their potencies were weaker than the BID WT and stapled BID peptides, which suggested that changing the native peptide sequence with olefinic amino acids is unfavourable to binding, but constraining the peptide mitigates this binding penalty. This was consistent with the stapled p53 investigation. The unstapled peptides also had a slight improvement of proteolytic resistance compared to BID WT, but this was less than the BID Aib peptide.

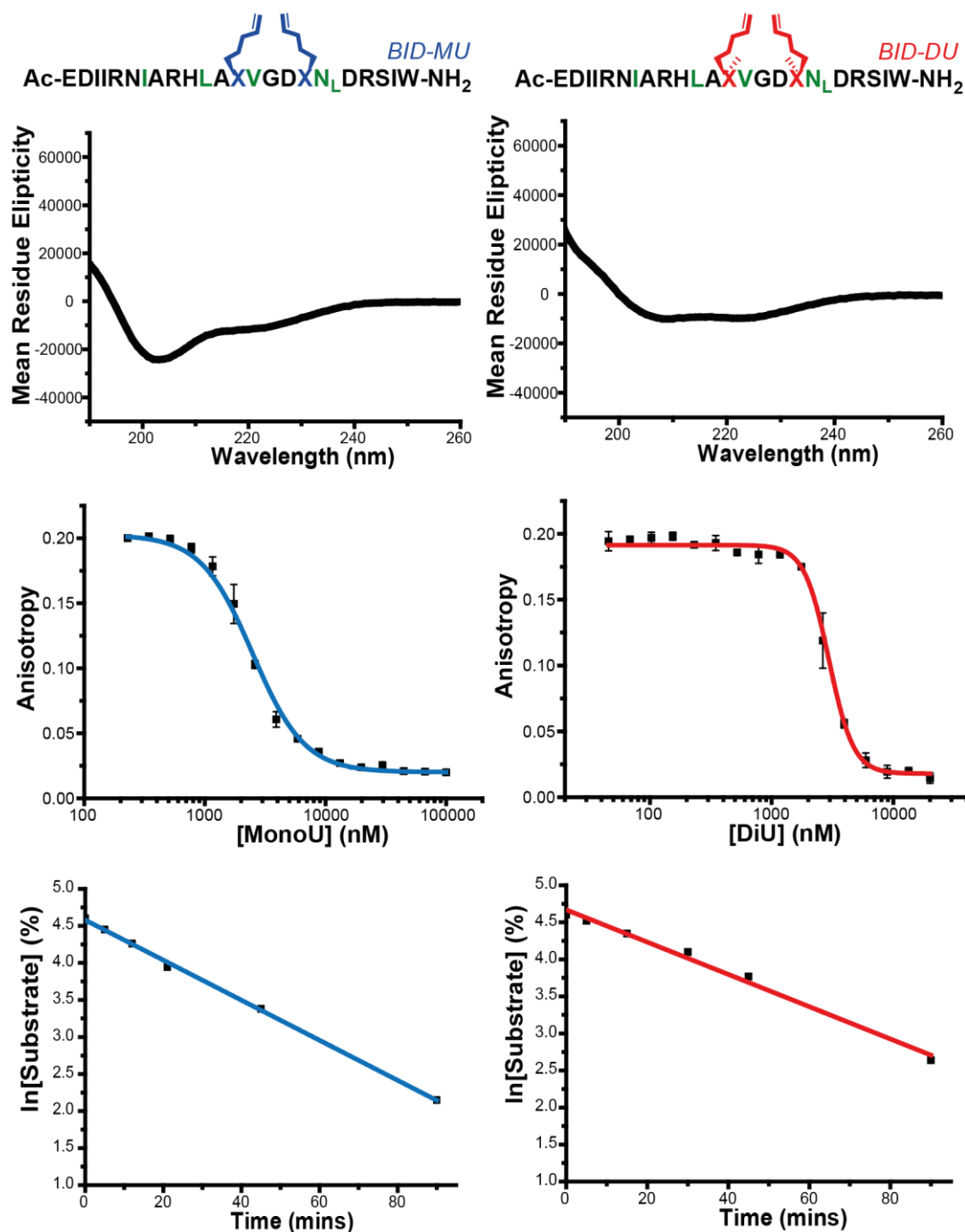| Peptide	% Helicity	IC$_{50}$ Bcl-x_L/BAK*	Trypsin t$_{1/2}$
BID MU	17	2.48 ± 0.11 µM	25.1 mins
BID DU	20	2.94 ± 0.10 µM	25.6 mins

Figure 6.25 – Circular Dichroism, Bcl-x$_L$/BAK* assay and proteolytic degradation data of the unstapled MU and DU BID BH3 peptides.

6.2 Additional Fluorescence Anisotropy Data

6.2.1 Complications in K$_i$ calculation

The fluorescence anisotropy assays have an intrinsic limitation that precludes the calculation of a dissociation constant or inhibition constant (K$_d$ or K$_i$) in competition mode. The assay does not occur in a two state equilibrium between

the free tracer/inhibitor or protein and protein-ligand complex. Additional contribution to anisotropy arise from homo-aggregates of the tracer (r_1, Figure 6.26 a) and hetero tracer-inhibitor aggregates (r_2, Figure 6.26 a). In the direct binding experiment, the contribution from r_1 is added to the theoretical minimum (r_0) to give a higher than expected experimental minimum (r_{min}, green curve, Figure 6.26 b).
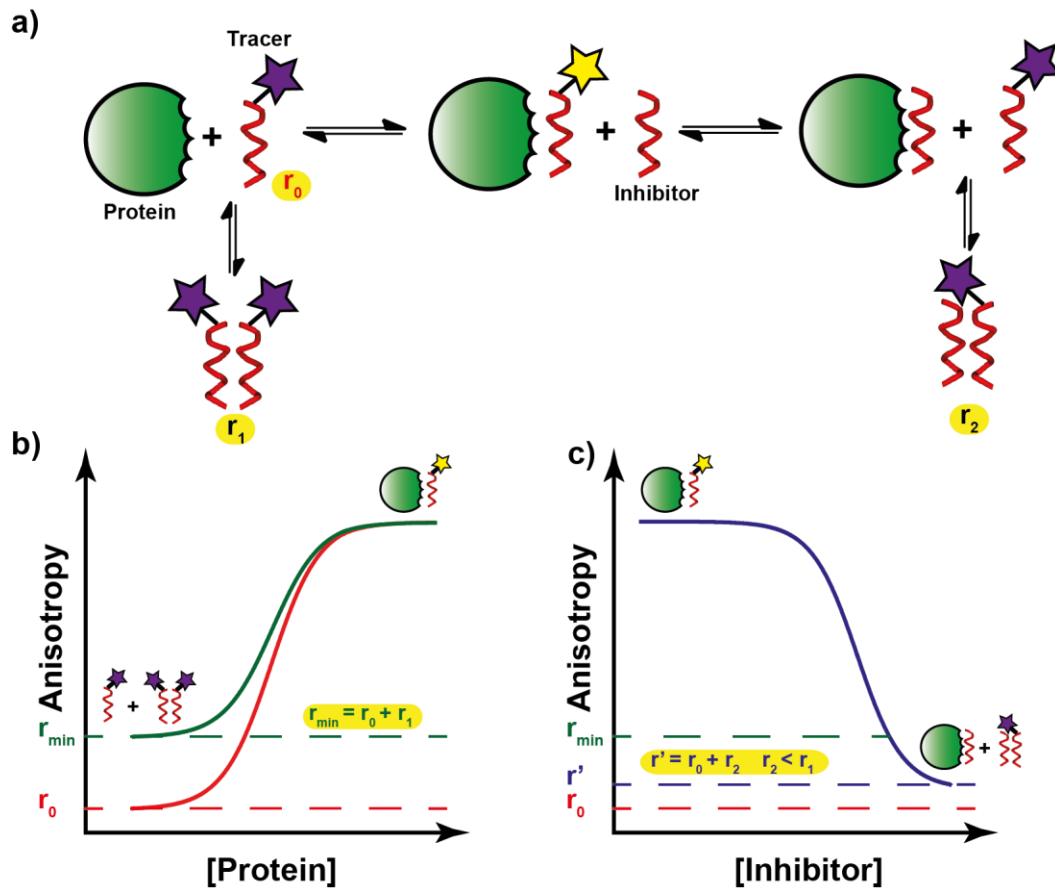
Figure 6.26 - Complex equilibria preclude K_d determination. a) Cartoon of the equilibria in the assay and highlighting the anisotropy contributions; b) Experimental (green) and theoretical (red) anisotropies in a direct binding experiment, which highlight the contribution of r_1 to r_{min}; c) anisotropy of the competition assay highlighting the r_0 and r_2 contributions to r'.

In competition mode, the anisotropy of hetero-aggregates (r_2) adds to the overall minimum r'. Since $r_2 < r_1$, the competition assay minimum r' differs from r_{min}, which precludes the correct determination of the anisotropy limits to calculate L_b (4.5.3.5) and therefore does not allow the determination of K_d.

6.2.2 Establishing Mcl-1/NoxaB* direct binding assays

The assay development of Mcl-1/NoxaB* was performed in collaboration with Dr. K. Long and V. Azzarito. To test inhibitors of Mcl-1 protein-protein interactions, a direct binding assay was established that avoided the complications of the long equilibration time that was experienced with the labelled BID and BAK peptides. NoxaB*, a 16mer BH3 peptide, required no prior addition of DMSO before its dilution into assay buffer. The protein titration experiment of Mcl-1 using 25 nM of NoxaB* afforded a K_d of 18.7 ± 0.9 nM, which is consistent with what has been previously reported.[6, 189] Unlike the BID* and BAK* BH3 peptides, NoxaB* required only 1 hour of incubation with Mcl-1 – where longer incubation times did not affect the observed anisotropy plateaux. In this experiment, deviation of the pH of the assay buffer from 7.0–8.0 abolished the binding of NoxaB* to Mcl-1.
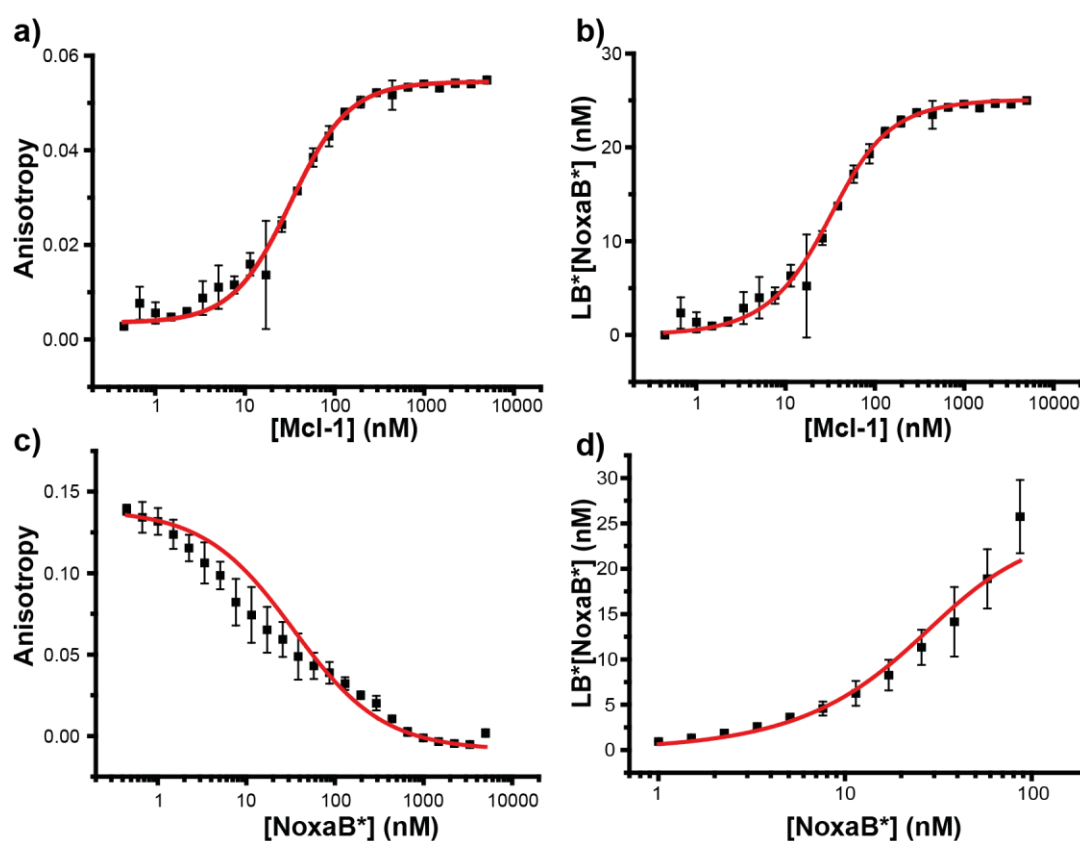
Figure 6.27 – Protein Titration of Mcl-l into NoxaB* displaying: a) Anisotropy change; b) K_d model curve. Peptide Titration of NoxaB* into Mcl-1 displaying c) Anisotropy change; d) K_d model curve.

The peptide titration afforded a K_d of 13.0 ± 2.29 nM but this experiment was complicated by the saturation of the plate reader detector at higher

concentrations of NoxaB* and increased noise at lower concentrations of NoxaB*. This direct binding experiment was transferred for the testing of inhibitors of Mcl-1/NoxaB*.

6.2.3 Testing of BAD, BAK and NoxaB peptides

The Wilson laboratory had previously synthesised other BH3 domains of proteins of the Bcl-2 family, which have selective binding to certain members of the Bcl-2 pro-apoptotic proteins. These BH3 peptides were tested against Mcl-1 and Bcl-x$_L$ to confirm their reported specificities. The assays were performed as described in 4.5.4.
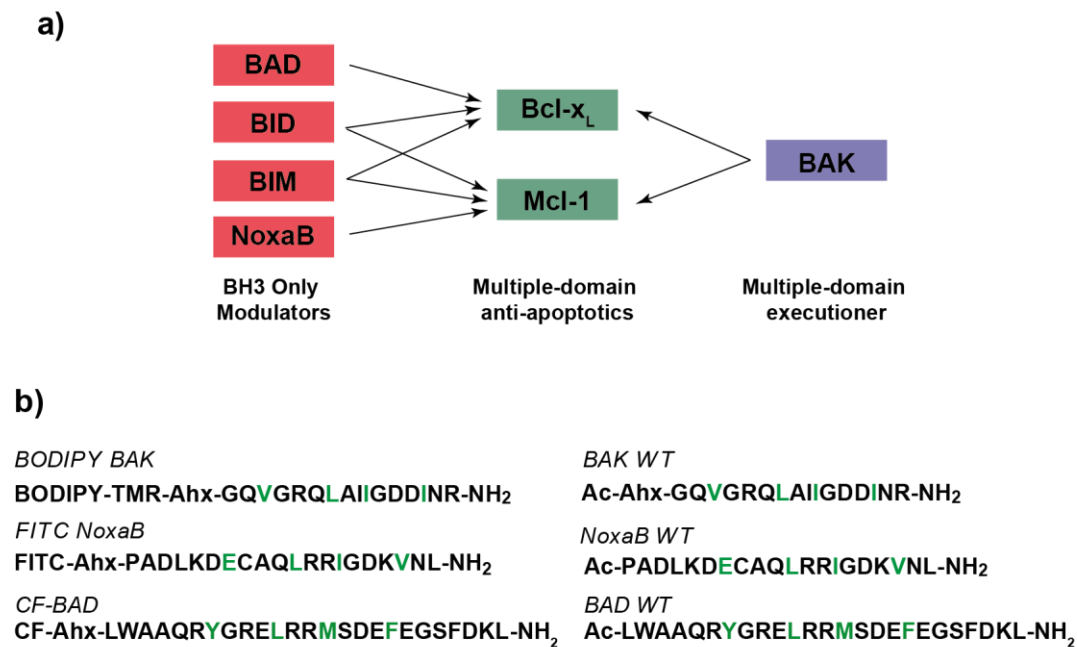
Figure 6.28 – a) Specificities of the BH3 protein family, including the pan-BH3 binding BID and BIM proteins; b) Sequences of the fluorescently labelled and unlabelled BAK, NoxaB and BAD BH3 peptides, with the key binding side chains coloured green.
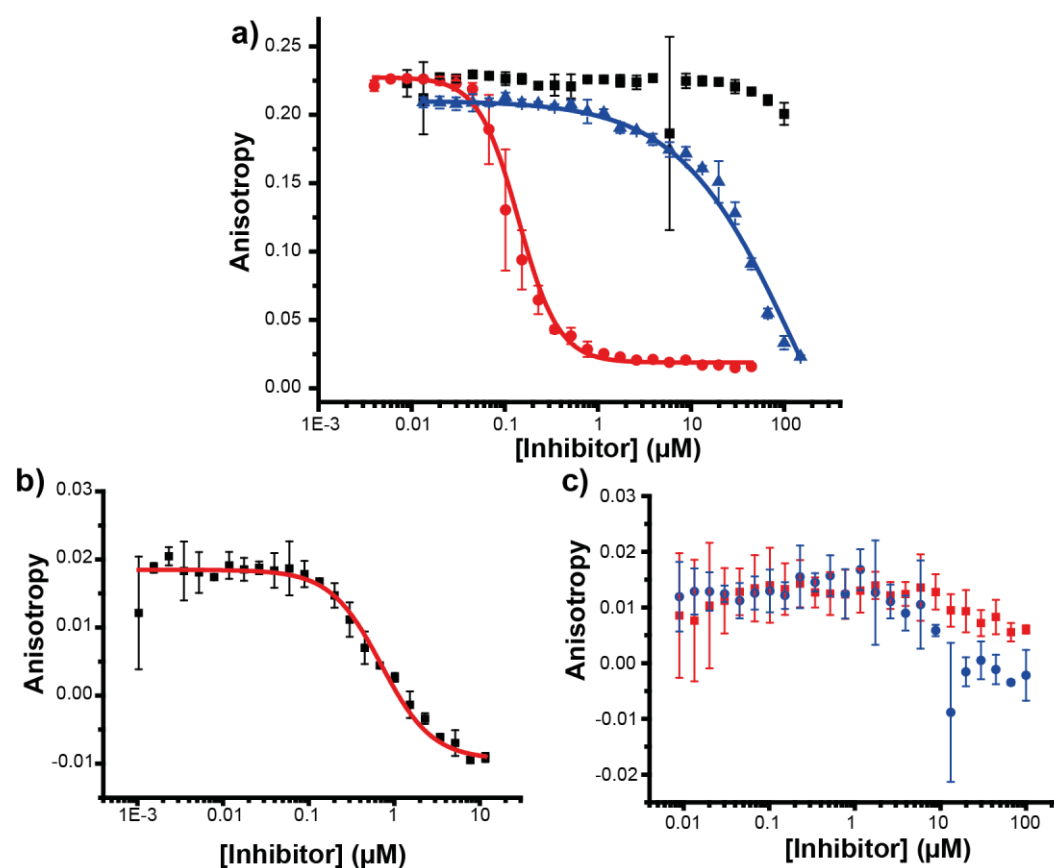
BH3 Peptide	IC$_{50}$ Bcl-x$_L$/BAK*	IC$_{50}$ Mcl-1/NoxaB*
NoxaB	No Inhibition	0.70 ± 0.03 μM
BAD	0.14 ± 0.01 μM	No Inhibition
BAK	> 50 μM	No Inhibition

Figure 6.29 – a) Competition assay curves for the inhibition of Bcl-x$_L$/BAK* with NoxaB (black), BAD (red) and BAK (blue); b) Competition curve of Mcl-1/NoxaB* inhibited by NoxaB and c) Assay results of the inhibition of Mcl-1/NoxaB* by BAK (blue) and BAD (red).

The competition assay results confirmed that BAD and NoxaB are selective for Bcl-x$_L$ and Mcl-1 respectively. The surprising result was the poor inhibition of Bcl-x$_L$/BAK* with unlabelled BAK, considering that BODIPY labelled BAK* binds to Bcl-x$_L$ with a K$_d$ of 4 nM (3.6.3.1). Also, BAK did not inhibit Mcl-1/NoxaB* despite literature precedent suggesting that the BAK protein is capable of binding to Mcl-1.

In the instances of the unlabelled peptides that did not inhibit a protein-protein interaction in the competition assays, a labelled analogue was used in direct binding assays.
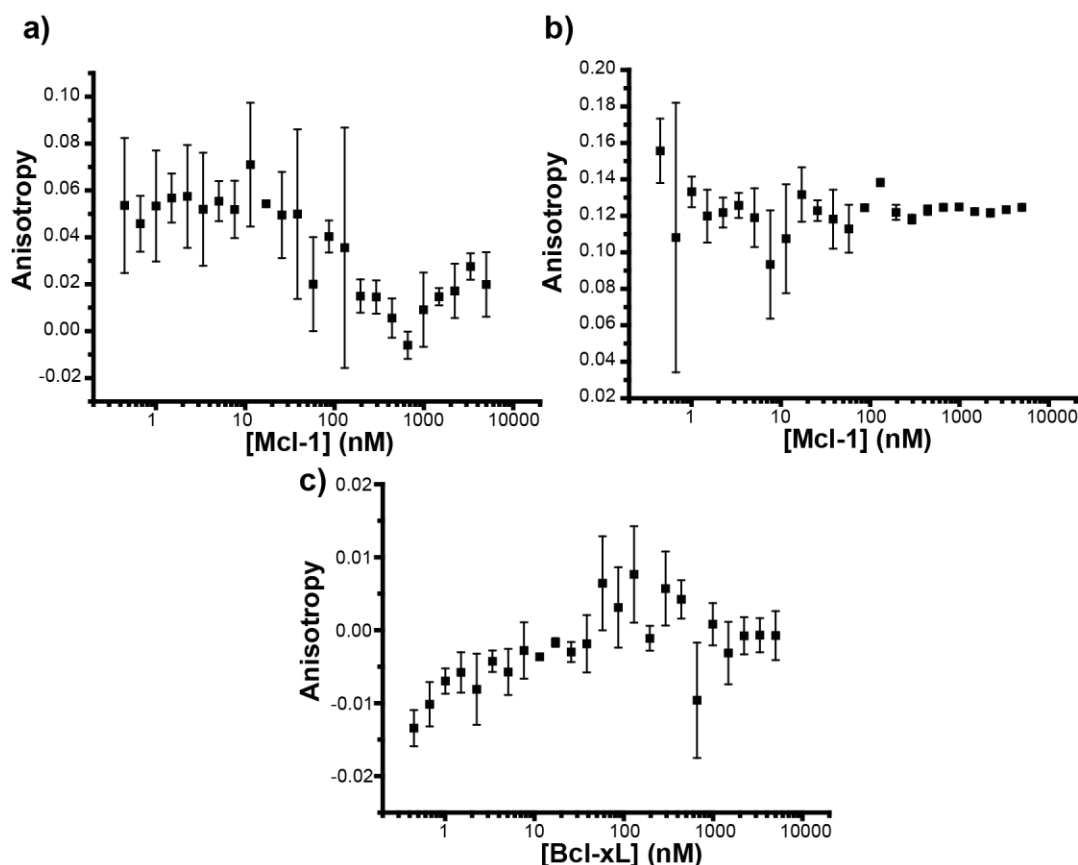
Figure 6.30 – Negative controls of a) CF-BAD* with Mcl-1; b) BODIPY-BAK* with Mcl-1 and c) FITC-NoxaB* with Bcl-x_L

The direct binding assays confirmed the selectivity profiles of NoxaB and BAD, whilst the labelled BAK* peptide did not bind to Mcl-1 in a similar result to the Mcl-1/NoxaB* competition assay with unlabelled BAK.

6.2.4 CF-BAD Direct Binding Assays

Direct binding assays were attempted with carboxy-fluorescein labelled BAD (CF-BAD), but assay development was hampered by the critical insolubility of the peptide. Assay stocks of CF-BAD at a 1 mM concentration required 20% DMSO to maintain a solution. Protein titrations performed in phosphate buffer did not show any change in anisotropy, which led to the change of assay buffer to Tris, which had proven successful for the labelled BID peptide series. The assay in Tris buffer gave some evidence of a transition in anisotropy, but turbidity of the solutions in the wells at higher concentrations of Bcl-x_L led to the anisotropy signal falling. Therefore, neither K_d nor EC_{50} were calculated for CF-BAD.
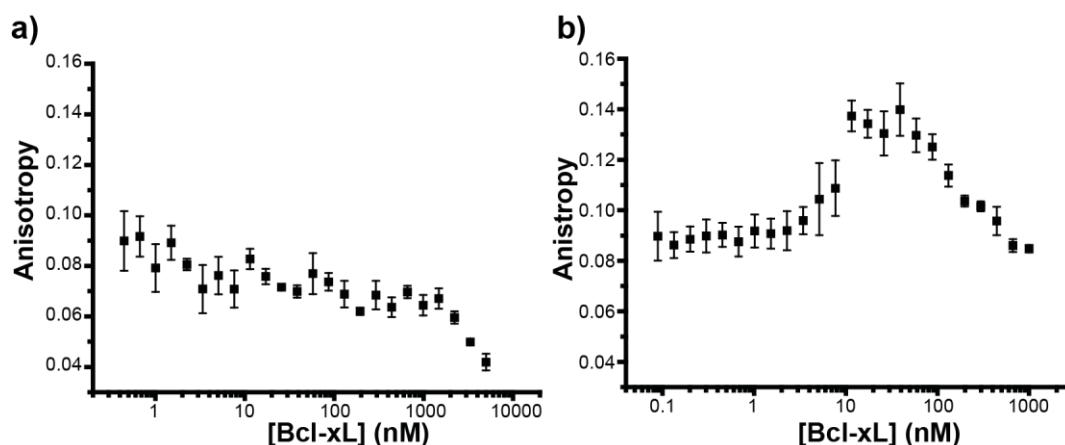
Figure 6.31 – Protein titration of Bcl-x_L into CF-BAD, with a) phosphate buffer (40 mM sodium phosphate, 200 mM NaCl, 0.02 mg ml^{-1} BSA, pH 7.50) and b) Tris buffer (50 mM Tris, 140 mM NaCl, pH 7.50).

6.2.5 FITC-BID Peptide Titration Experiments

As referred in 3.6.3 and 3.11, direct binding fluorescence anisotropy experiments are performed with two different titrations; protein and peptide titrations. Generally, the anisotropy minima and maxima of a ligand:protein interaction are extracted from the protein titration, which are transferred into the peptide titration to calculate K_d (4.5.3.5). However, the peptide titration is limited by the saturation of the plate reader detector at high concentrations of fluorophore and poor signal-to-noise ratio at low concentrations of fluorophore. As a result, the K_d values for the FITC labelled BID peptides and Mcl-1 or Bcl-x_L were calculated from the protein titration.

The protein concentration in the experiments was set at 100 nM, and the FITC labelled peptides were titrated from a concentration of 5 μM, with the experiment performed in Tris buffer. Plates were read after 2 h of incubation and rechecked after 18 h.

6.2.5.1 BID WT* Peptide Titrations

BID WT* demonstrated the problem with saturation and signal-to-noise in the Mcl-1 peptide titration, but a transition was observed and K_d calculated as 70.6 ± 15.0 nM (protein titration: 51 ± 19.9 nM). Against Bcl-x_L, there were insufficient data points to calculate an accurate K_d.
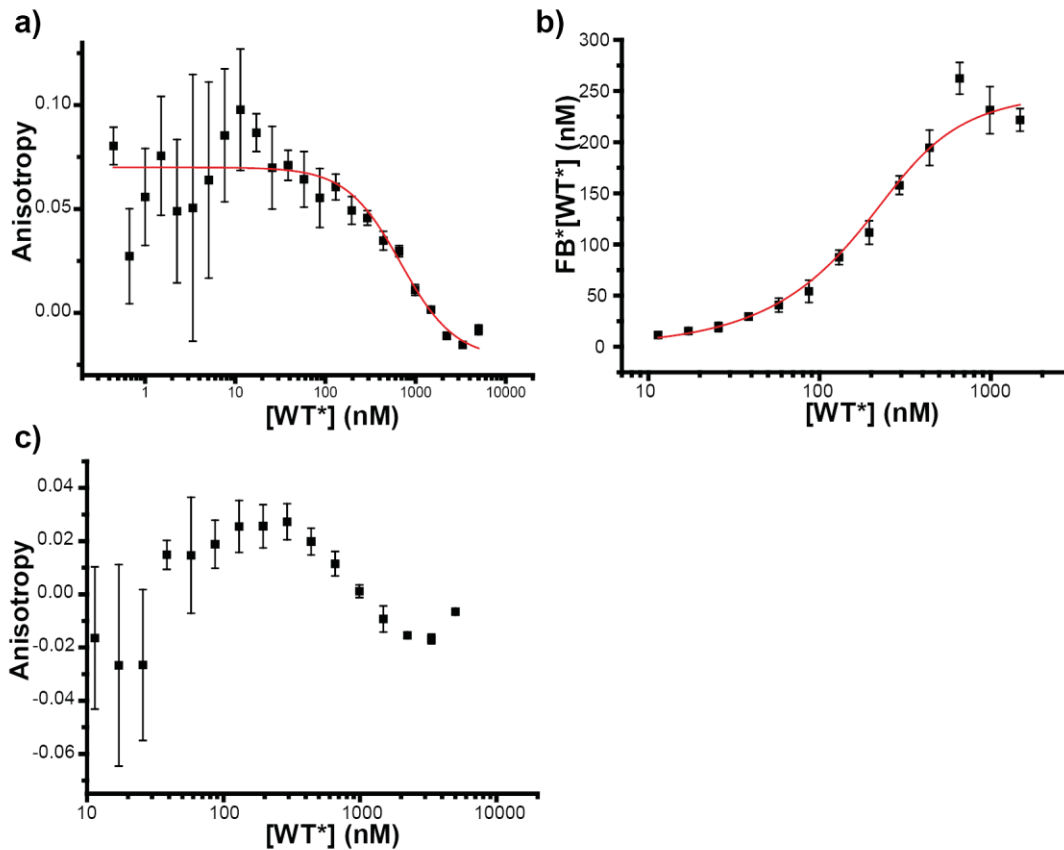
Figure 6.32 – a) Anisotropy and b) K_d data of BID WT*/Mcl-1 direct binding experiments; c) anisotropy of BID WT*/Bcl-x$_L$

6.2.5.2 BID Aib* Peptide Titrations

BID Aib* provided the best data for the peptide titration experiments with Mcl-1, with a clear transition observed and a K_d calculated at 15.4 ± 2.7 nM (protein titration: 66.2 ± 19 nM). Whilst the peptide titration with Bcl-x$_L$ has evidence of a change in anisotropy, the K_d model did not fit well, with a K_d calculated at 19 ± 17 nM (protein titration: 59.5 ± 11 nM).
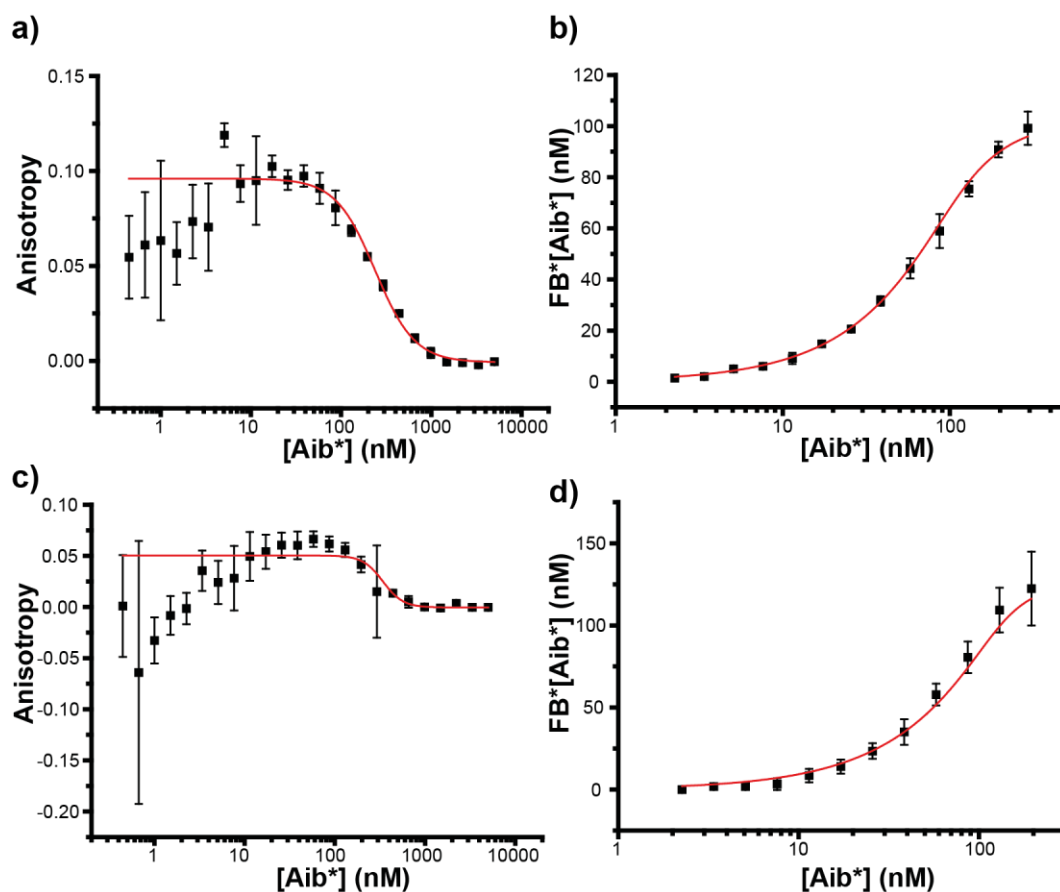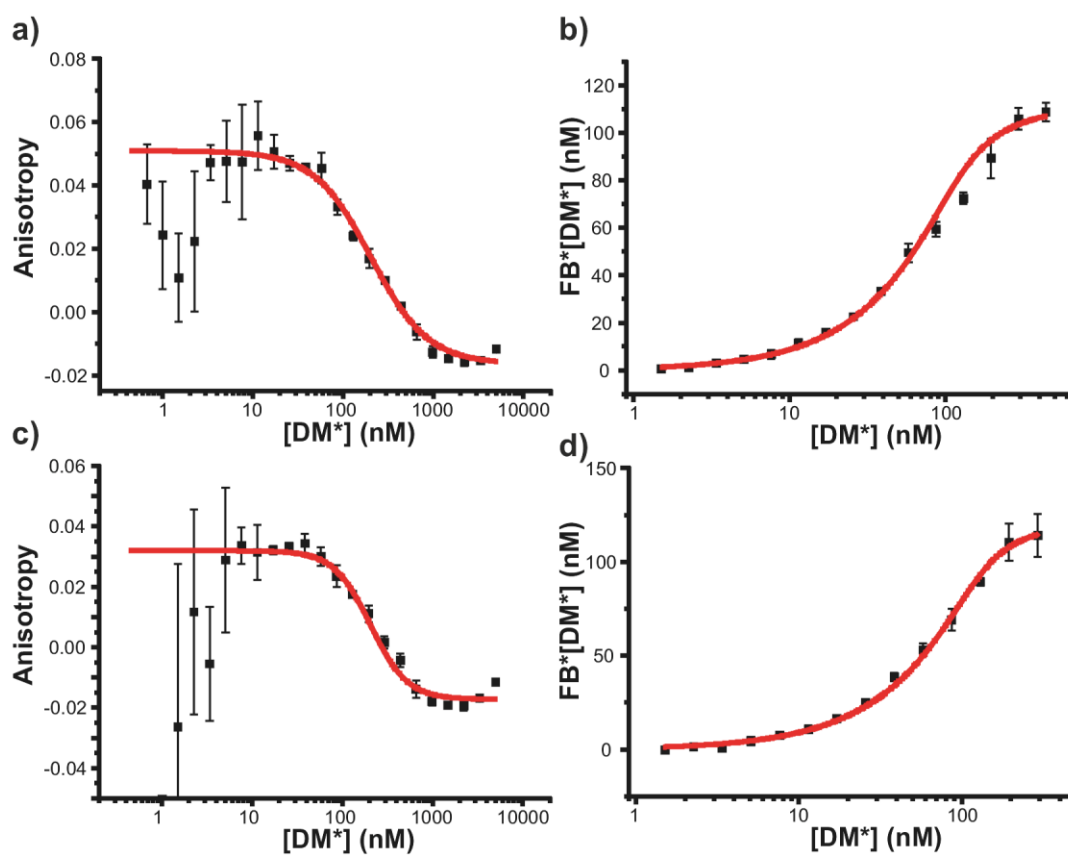
Figure 6.33 – a) Anisotropy and b) K_d data for the Mcl-1/BID Aib* peptide titration; c) anisotropy and d) K_d data for the Bcl-x_L/BID Aib* peptide titration.

6.2.5.3 BID DM* Peptide Titration Experiments

The peptide titration of BID DM* with Mcl-1 allowed a K_d of 17.2 ± 3.7 nM to be calculated (protein titration: 107 ± 23 nM) and 14.0 ± 2.7 nM with Bcl-x_L (protein titration: 168 ± 19 nM). Considering the large difference in the K_d values calculated between the protein and peptide titration, the K_d values from the protein titration were used in the discussions of the peptides, since the values of r_{max} and r_{min} differed between the protein and peptide titration.

Figure 6.34 – a) Anisotropy and b) K_d data for Mcl-1/BID DM* peptide titration; c) anisotropy and d) K_d data for the Bcl-x$_L$/BID DM* peptide titration.

6.2.5.4 BID MM* Peptide Titration

For BID MM*, there was no observed transition in the anisotropy data for either Mcl-1 or Bcl-x$_L$ which precludes the calculation of K_d. This particular peptide suffered from poor signal-to-noise below 100 nM, which is the expected region of K_d from the protein titration.
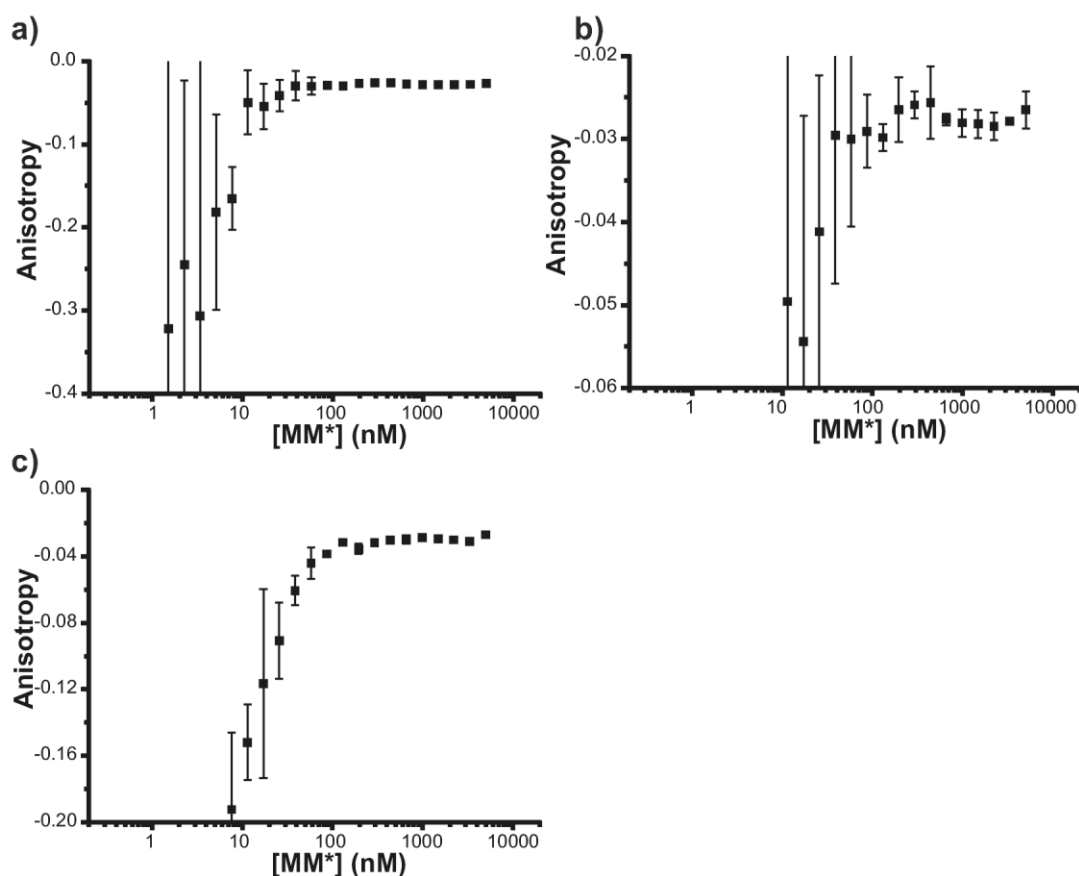
Figure 6.35 - a) Anisotropy of Mcl-1/BID MM* peptide titration. and b) expansion of the region beween 10-10000 nM; c) anisotropy of Bcl-x$_L$/BID MM* peptide titration.

6.2.6 Raw Anisotropies of FITC BID Protein Titrations

The anisotropies of the protein titrations of the FITC BID series (3.11.1.1 and 3.11.2) are included below. It was evident that the r_{max} and r_{min} obtained in the protein titration experiment were different to those from the peptide titration experiment, which rendered the two assays incompatible to calculate K_d together. Therefore, K_d was calculated from the protein titration data.
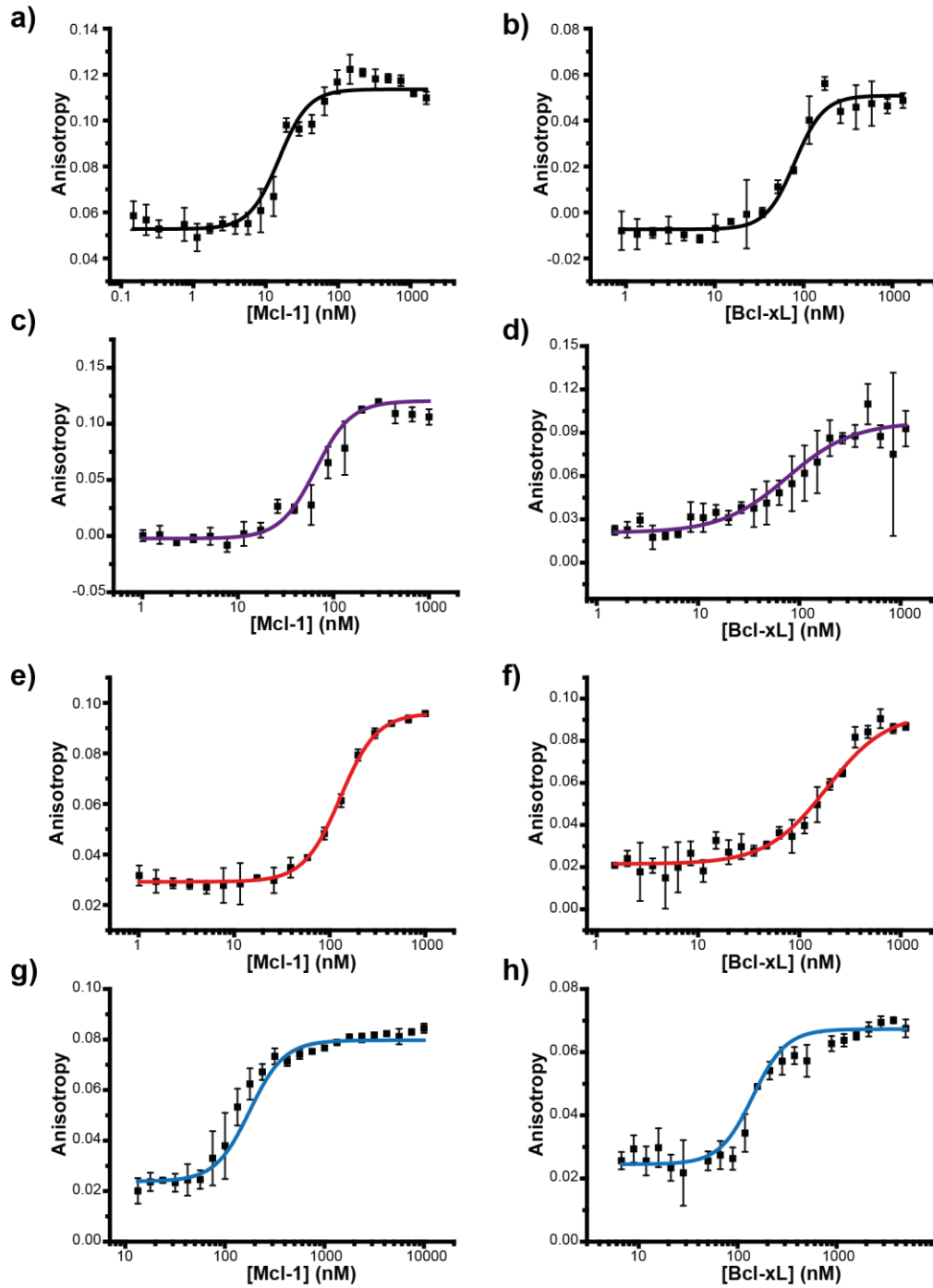
Figure 6.36 – Protein titration anisotropy curves for: a) BID WT*/Mcl-1; b) BID WT*/Bcl-xL; c) BID Aib*/Mcl-1; d) BID Aib*/Bcl-xL; e) BID DM*/Mcl-1; f) BID DM*/Bcl-xL; g) BID MM*/Mcl-1 and h) BID MM*/Bcl-xL.

Appendix III

Additional Biophysical Data

6.3 Thermal Ramping Circular Dichroism Data

The circular dichroism curves of BID WT, Aib, DU and MU are included below during the thermal ramping experiment (Figure 6.37). BID WT, MU and Aib displayed little change in their profiles at higher temperatures, which is not surprising considering that their CD profiles at 20 °C were predominantly random coil. At 20 °C, BID DU appeared to have a CD profile that suggested an α-helical conformation (6.1) but its % helicity was 20%. As the temperature of the measurement chamber increased, this apparent helical content did decay to a random coil profile, but, like the BID MM and BID DM peptides, the unfolding pathway was not cooperative.
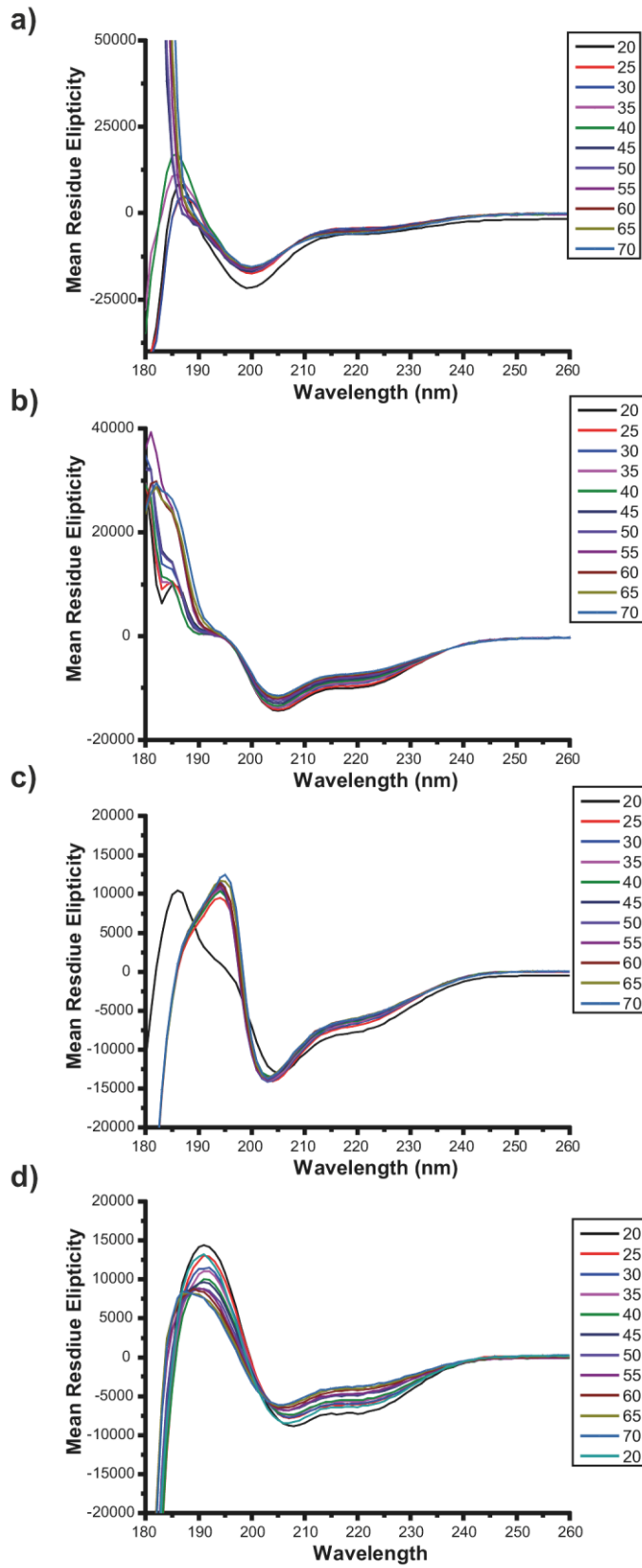
Figure 6.37 – Thermal unfolding curves for: a) BID WT, b) BID Aib, c) BID MU and d) BID DU.

6.4   Isothermal Titration Calorimetry (ITC)

ITC was attempted for BID DM, BID MM and BID WT*, following the conditions as described in 4.5.5. The precipitation of BID DM and BID MM in the syringe was responsible for the poor data observed, which was not improved by performing the experiment with peptide present in the cell and the protein in the syringe.
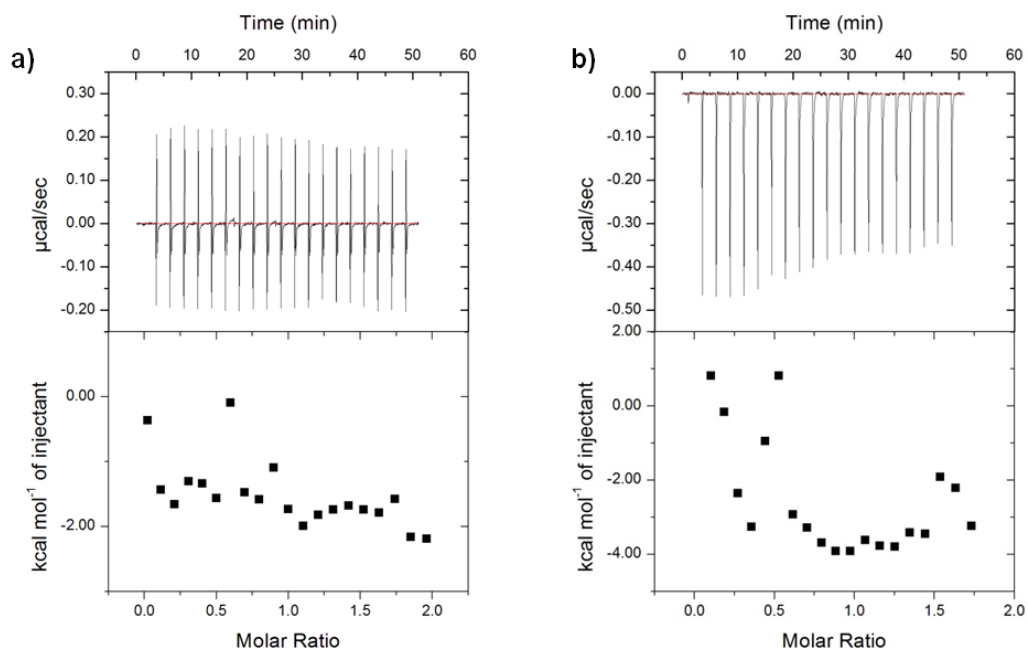

Figure 6.38 – ITC thermograms of BID MM (300 µM) with a) Mcl-1 (30 µM) and b) Bcl-x_L (35 µM).
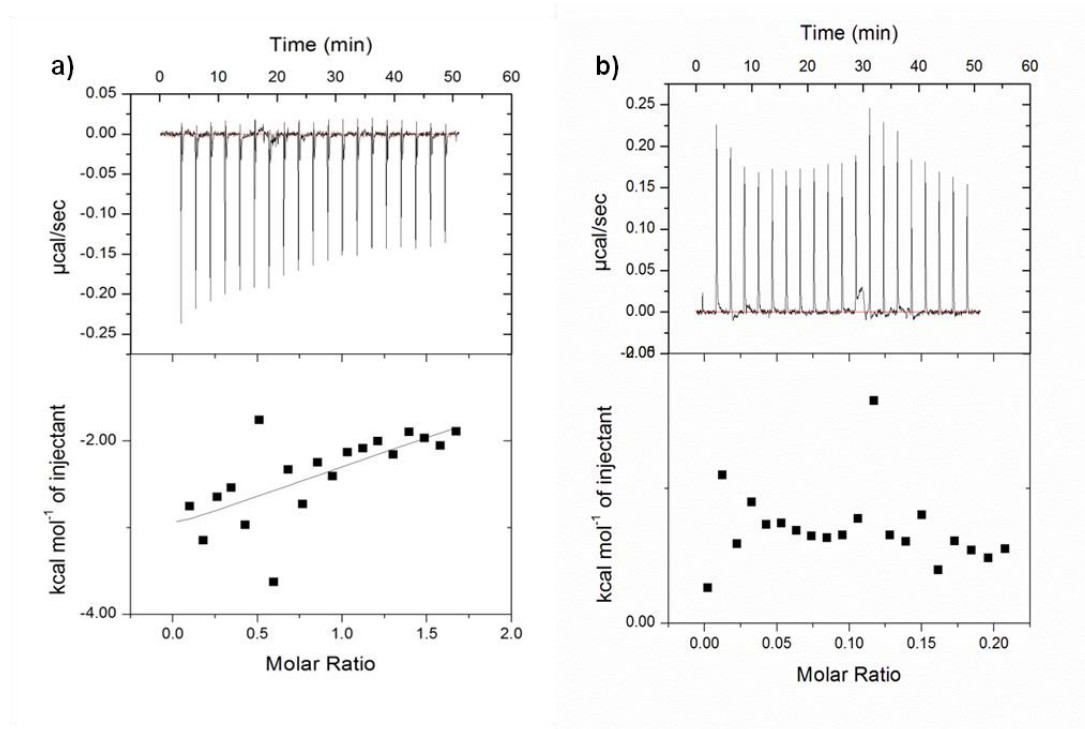
Figure 6.39 – ITC thermograms of BID DM (250 μM) with a) Mcl-1 (30 μM) and b) Bcl-x$_L$ (35 μM).
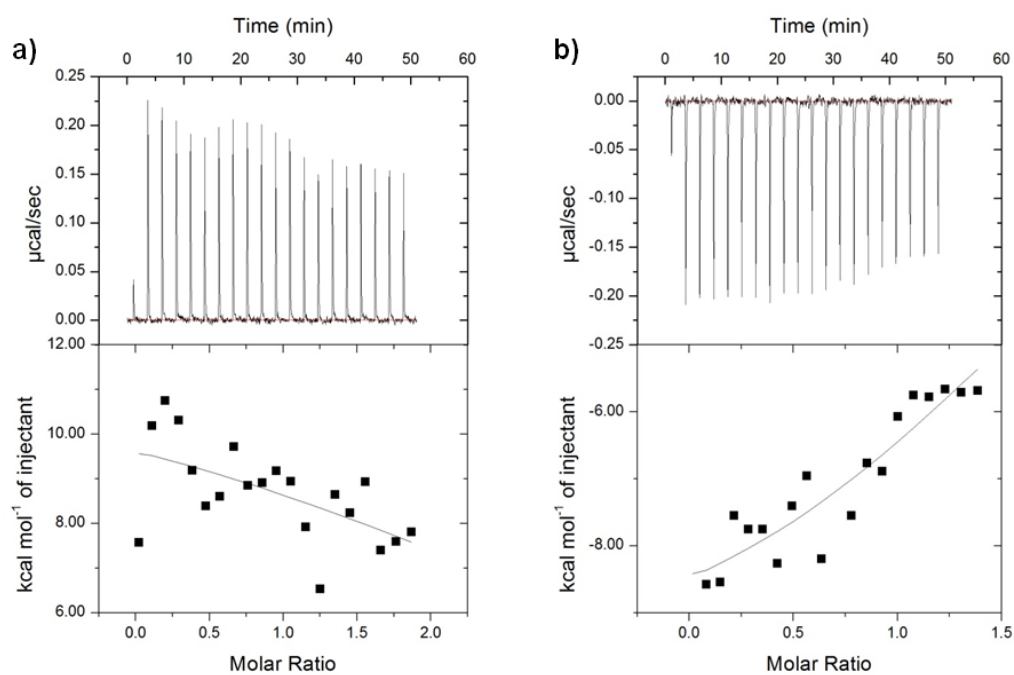
Figure 6.40 – ITC thermograms of BID WT* (300 μM) with a) Mcl-1 (30 μM) and b) Bcl-x$_L$ (30 μM)

Appendix IV

Protein Expression Data

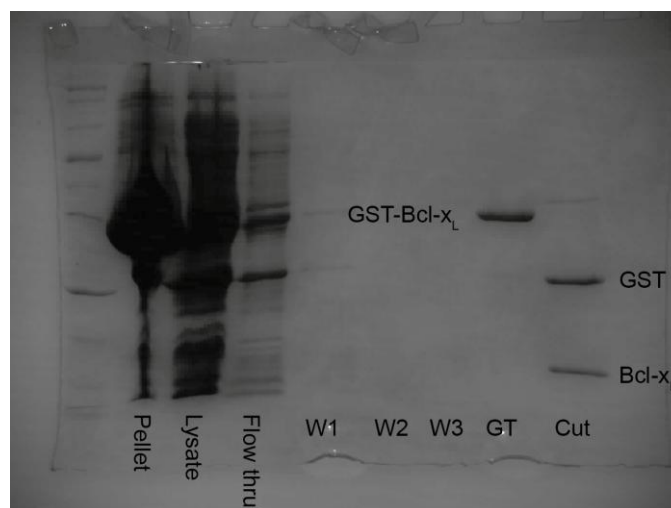To supplement sections 3.5.2 and 4.6

Figure 6.41 – SDS-PAGE Gel of the expressed GST-Bcl-x$_L$ (no loop); The flow through was the loading of the GST Superflow resin; W1 and W3 were 'low salt' washes (20 mM sodium phosphate pH 7.5, 140 mM NaCl, 1 mM DTT); W2 was a 'high salt' wash (20 mM sodium phosphate pH 7.5, 1 M NaCl, 1 mM DTT); GT was the elution with 20 mM reduced glutathione to afford GST-Bcl-x$_L$ fusion protein cleanly; 'cut' was the mixture after the use of PreScission Protease to remove the GST tag from Bcl-x$_L$.
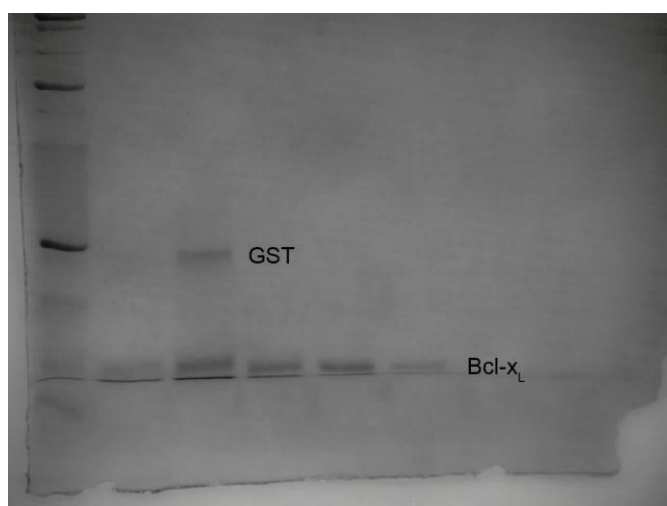

Figure 6.42 – SDS-PAGE Gel of the gel filtration column fractions of Bcl-x$_L$ 'no loop' protein after treatment with PreScission Protease

Appendix V

Additional *in cellulo* data

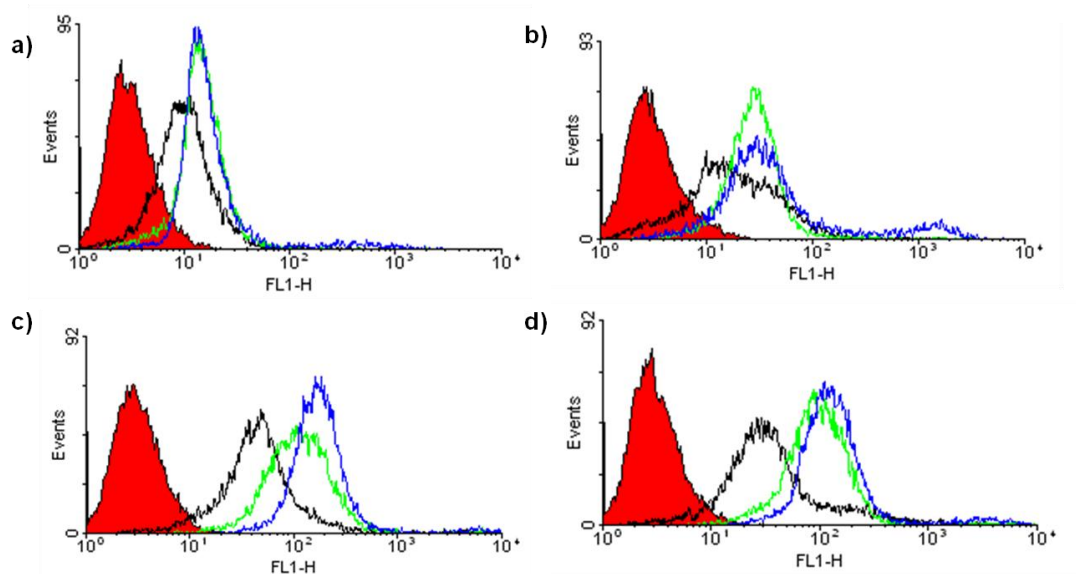The following data complements the findings described in 3.14.

Figure 6.43 - FACS analysis of paediatric glioblastoma cells treated with FITC-labelled BID peptides in serum-free media for a) BID WT*; b) BID Aib*; c) BID DM*; d) BID MM*. The curves represent DMSO vehicle (red), 2 h incubation (black), 4 h incubation (green) and 24 h incubation (blue).

SF188 paediatric glioblastoma cells were incubated with FITC-labelled WT and modified BID peptides for 2, 4 or 24 hours in serum-free media (10µM), followed by washing, digestion with trypsin and FACS analysis to assess cellular fluorescence. Cells treated with all FITC-labelled peptides displayed increased cellular fluorescence compared to cells treated with vehicle only (0.1% (v/v) DMSO) despite a 20 minute digestion with 1x trypsin at 37°C in order to reduce non-specific binding of peptides to cell surface proteins. However, cells treated with stapled derivatives did display increased cellular fluorescence compared to cells treated with BID WT*, particularly after 24 hours. As described in 3.14, confocal microscopy is required to validate cell penetration and localisation.
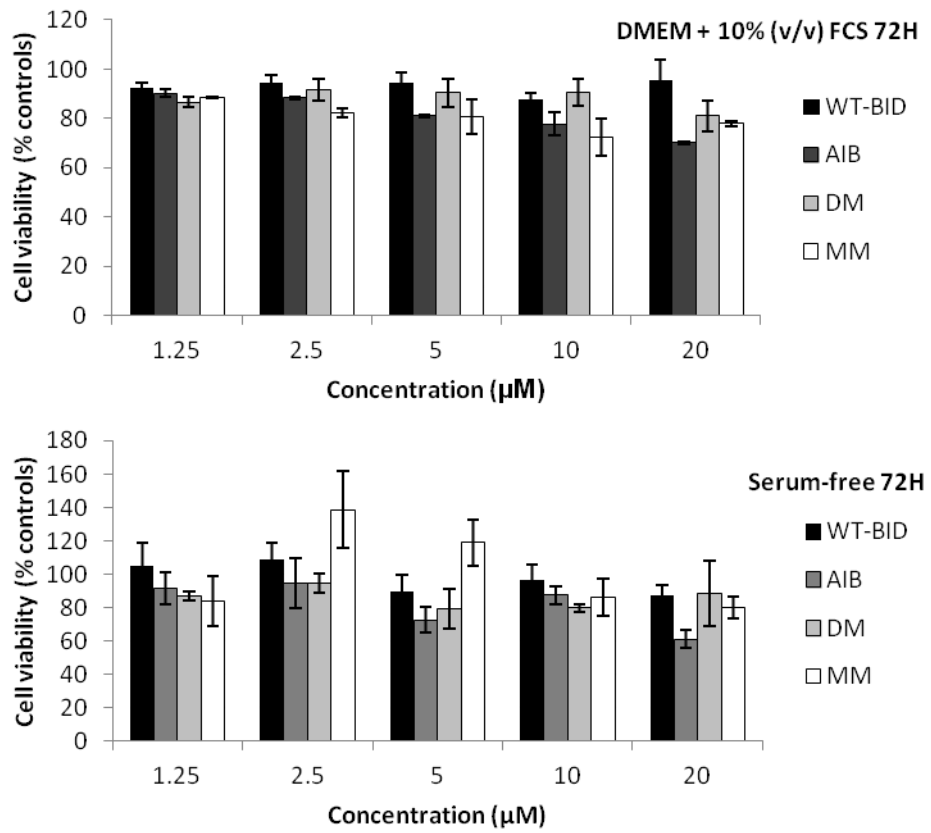
Figure 6.44 - Effect of unlabelled BID peptides on glioblastoma cell viability in serum containing (top) and serum-free media (bottom).

The stapled BID DM and BID MM peptides had a limited effect on cell viability, even after 72 hours and the complete withdrawal of serum treatment.

Appendix VI

6.5   X-ray Crystallographic Data

6.5.1 Alkylated Ni-Gly-BPB complex 46

The diffraction and structure solving was performed by Dr. C. Pask at the School of Chemistry X-ray service at the University of Leeds.

Empirical formula	C32H33N3NiO3
Formula weight	566.32
Temperature/K	99.9(3)
Crystal system	monoclinic
Space group	P21
a/Å	11.07980(8)
b/Å	21.99770(13)
c/Å	11.88015(9)
α/°	90.00
β/°	102.0025(7)
γ/°	90.00
Volume/Å3	2832.25(3)
Z	4
ρcalcmg/mm3	1.328
m/mm-1	1.284
F(000)	1192.0
Crystal size/mm3	0.15 × 0.07 × 0.04
Radiation	CuKα (λ = 1.54184)
2Θ range for data collection	7.6 to 133.2°
Index ranges	-13 ≤ h ≤ 12, -26 ≤ k ≤ 26, -14 ≤ l ≤ 14
Reflections collected	21899
Independent reflections	10002 [Rint = 0.0253, Rsigma = 0.0327]
Data/restraints/parameters	10002/1/693
Goodness-of-fit on F2	1.037
Final R indexes [I>=2σ (I)]	R1 = 0.0274, wR2 = 0.0688
Final R indexes [all data]	R1 = 0.0285, wR2 = 0.0696
Largest diff. peak/hole / e Å-3	0.36/-0.23
Flack parameter	-0.005(12)

6.5.2 BID MM in complex with Mcl-1

N.B. The optimisation of the resolved structure was still being performed at the time of writing.

The crystal growth and diffraction was performed by Dr. J. Miles. Structure solution was perfomed by Dr. J. Miles, Dr. T. Edwards and D. Monteiro. The Mcl-1 in complex with BID was at 12 mg mL^{-1}. The trays were stored at 4 °C. Crystals were optimised in a 1:1 drop of 18% PEG 20,000, 0.1 M Tris, pH 8.0, and the crystals were cryoprotected with 30% glycerol.

Diffraction data was collected from Diamond Light Source to 1.43 Å. The structure was solved using molecular replacement and the staple built as previously described in the literature.

Parameters:

- The unit cell dimensions are 80.83 Å, 37.020 Å and 56.920 Å.
- The angles are 90.0°, 90.0° and 90.0°.
- The space group is P 21 21 2.
- The R factor is 0.179 with an R free of 0.2072.
- The resolution is 1.43 Å.